U.S. DEPARTMENT OF COMMERCE
National Technical Information Service

PB-257 707

Radiative Effects of Pollutants on the Planetary Boundary Layer

Purdue Univ., Lafayette, Ind.

Prepared For
Environmental Sciences Research Lab.

July 1976

TECHNICAL REPORT DATA

(Please read Instructions on the reverse before completing)

1. REPORT NO.
EPA-600/4-76-039

2.

3. RECIPIENT'S ACCESSION NO.

4. TITLE AND SUBTITLE
RADIATIVE EFFECTS OF POLLUTANTS ON THE PLANETARY BOUNDARY LAYER

5. REPORT DATE
July 1976

6. PERFORMING ORGANIZATION CODE

7. AUTHOR(S)
A. Venkatram and R. Viskanta

8. PERFORMING ORGANIZATION REPORT NO.

9. PERFORMING ORGANIZATION NAME AND ADDRESS
School of Mechanical Engineering
Purdue University
West Lafayette, Indiana 47907

10. PROGRAM ELEMENT NO.
1AA009

11. CONTRACT/GRANT NO.
R803514

12. SPONSORING AGENCY NAME AND ADDRESS
Environmental Sciences Research Laboratory
Office of Research and Development
U.S. Environmental Protection Agency
Research Triangle Park, NC 27711

13. TYPE OF REPORT AND PERIOD COVERED
Interim

14. SPONSORING AGENCY CODE
EPA-ORD

15. SUPPLEMENTARY NOTES

16. ABSTRACT

The objective of this study was to gain a better understanding of the effects of pollutants on the thermal structure and pollutant dispersal in the planetary boundary layer. To this end numerical models of the boundary layer were constructed. Gaseous pollutants in the boundary layer were considered to absorb and emit thermal radiation, while aerosols were allowed to absorb and scatter solar energy.

First, a one-dimensional numerical model of the boundary layer was constructed. The model used the two-stream method for the computation of radiative fluxes, and a turbulent kinetic energy model to account for turbulence. A series of numerical experiments were performed to determine the role of pollutants in modifying thermal structure and pollutant dispersal in the boundary layer. The results showed that the predominant influence of gaseous and particulate pollutants on surface temperature was warming. Radiative participation by pollutants increased the stability of the surface layer during the day. During the night, the warmer surface temperatures caused the surface layer to become less stable.

The second phase of the study involved the construction of a two-dimensional numerical model to study the effects of pollutants on urban-rural differences in thermal structure and pollutant dispersal. The effects of pollutants on pollutant dispersal were found to be significant. At the source height (100 m) in the urban area, the pollutant concentration was reduced by as much as 13.5% during the night.

17. KEY WORDS AND DOCUMENT ANALYSIS

a. DESCRIPTORS	b. IDENTIFIERS/OPEN ENDED TERMS	c. COSATI Field/Group
*Air pollution		13B
*Boundary layer		20D
*Solar radiation		03B
*Thermal radiation		20M
*Mathematical models		12A

PRICES SUBJECT TO CHANGE

18. DISTRIBUTION STATEMENT
RELEASE TO PUBLIC

19. SECURITY CLASS *(This Report)*
UNCLASSIFIED

20. SECURITY CLASS *(This page)*
UNCLASSIFIED

21. NO. OF PAGES
262

22. PRICE
$9.00

EPA Form 2220-1 (9-73)

272162

PB 257 707

EPA-600/4-76-039
July 1976

Environmental Monitoring Series

UNITED STATES ENVIRONMENTAL PROTECTION AGENCY

REPRODUCED BY
NATIONAL TECHNICAL
INFORMATION SERVICE
U. S. DEPARTMENT OF COMMERCE
SPRINGFIELD, VA. 22161

RESEARCH REPORTING SERIES

Research reports of the Office of Research and Development, U.S. Environmental Protection Agency, have been grouped into five series. These five broad categories were established to facilitate further development and application of environmental technology. Elimination of traditional grouping was consciously planned to foster technology transfer and a maximum interface in related fields. The five series are:

1. Environmental Health Effects Research
2. Environmental Protection Technology
3. Ecological Research
4. Environmental Monitoring
5. Socioeconomic Environmental Studies

This report has been assigned to the ENVIRONMENTAL MONITORING series. This series describes research conducted to develop new or improved methods and instrumentation for the identification and quantification of environmental pollutants at the lowest conceivably significant concentrations. It also includes studies to determine the ambient concentrations of pollutants in the environment and/or the variance of pollutants as a function of time or meteorological factors.

This document is available to the public through the National Technical Information Service, Springfield, Virginia 22161.

EPA-600/4-76-039
July 1976

RADIATIVE EFFECTS OF POLLUTANTS ON THE PLANETARY BOUNDARY LAYER

by

A. Venkatram and R. Viskanta
School of Mechanical Engineering
Purdue University
West Lafayette, Indiana 47907

Grant No. R803514

Project Officer

James T. Peterson
Meteorology and Assessment Division
Environmental Sciences Research Laboratory
Research Triangle Park, North Carolina 27711

ENVIRONMENTAL SCIENCES RESEARCH LABORATORY
OFFICE OF RESEARCH AND DEVELOPMENT
U.S. ENVIRONMENTAL PROTECTION AGENCY
RESEARCH TRIANGLE PARK, NORTH CAROLINA 27711

DISCLAIMER

This report has been reviewed by the Environmental Sciences Research Laboratory, U.S. Environmental Protection Agency, and approved for publication. Approval does not signify that the contents necessarily reflect the views and policies of the U.S. Environmental Protection Agency, nor does mention of trade names or commercial products constitute endorsement or recommendation for use.

ABSTRACT

The objective of this study was to gain better understanding of the effects of pollutants on the thermal structure and pollutant dispersal in the planetary boundary layer. To this end numerical models of the boundary layer were constructed. Gaseous pollutants in the boundary layer were considered to absorb and emit thermal radiation, while aerosols were allowed to absorb and scatter solar energy. A series of numerical experiments were conducted for a variety of summer atmospheric conditions, and the modification of the temperature and concentration distributions by the radiatively participating pollutants was investigated.

The first part of the investigation consisted of the construction of a one-dimensional numerical model of the boundary layer. The model incorporated the two-stream method for the computation of radiative fluxes in the solar spectrum, and the turbulent kinetic energy model to account for turbulence. A series of numerical experiments were performed to determine the role of pollutants in modifying thermal structure and pollutant dispersal in the boundary layer. The results of the experiments showed that the predominant influence of gaseous and particulate pollutants on the surface temperature was one of warming. Under the conditions investigated the reduction of solar flux at the surface was not accompanied by a decrease in the surface temperature. The maximum predicted temperature rise was 2.8 C over a 45 hour period. Radiative participation by pollutants increased the stability of the surface layer during the day. This led to a decrease in the surface pollutant concentrations. During the night, the warmer surface temperatures caused the surface layer to become less stable which in turn increased surface pollutant concentrations. Elevated layers of pollutants were found to play an important role in modifying mixed layer growth. Solar participation generally hindered mixed layer growth while thermal participation helped the vertical expansion of the mixed layer.

The second phase of the study involved the construction of a two-dimensional numerical model to study the effects of pollutants on urban-rural differences in thermal structure and pollutant dispersal. Results of numerical experiments showed that radiative participation by pollutants increased the maximum urban heat island intensity by as much as 50%. Pollutants also induced temperature "crossover," the maximum of which was 0.3 C. The effects of pollutants on pollutant dispersal were found to be significant. At the source height (100 m) in the urban area, the pollutant concentration was reduced by as much as 13.5% during the night.

CONTENTS

LIST OF ILLUSTRATIONS viii

LIST OF TABLES xii

LIST OF ABBREVIATIONS AND SYMBOLS xv

ACKNOWLEDGMENT xviii

I. CONCLUSIONS 1

1.1 Conclusions of One-Dimensional Simulations 1
1.2 Conclusions of Two-Dimensional Simulations 3

II. RECOMMENDATIONS 5

2.1 Suggested Improvements in Modeling 5
2.2 Suggested Additional Simulations 6

III. DISCUSSION OF PROBLEM 8

3.1 Problem Area 8
3.2 Background 10

3.2.1 The Atmospheric Boundary Layer 10
3.2.2 Urban Heat Island Phenomenon 12
3.2.3 Effect of Pollutants on Thermal Structure 13

3.3 Objectives of This Study 15
3.4 Rationale 16
3.5 Scope of This Study 18

IV. FORMULATION OF PROBLEM 20

4.1 Physical Model 20
4.2 Formulation of Model Equations 22
4.3 Boundary Conditions 25
4.4 Parameterization of Urban-Rural Differences 30
4.5 One-Dimensional Model 31
4.6 Stability and Numerical Accuracy of the 1-D Momentum Equations 35
4.7 Numerical Scheme for Two-Dimensional Model 40

V. TURBULENCE MODELING 46

5.1 Introduction 46
5.2 The Eddy-Diffusivity Model 48
5.3 Atmospheric Turbulence Modeling 52
5.4 Kinetic Energy Turbulence Model 54
5.5 Mixing Length Model 59
5.6 The Equilibrium Layer 64
5.7 Turbulent Diffusivity for Two-Dimensional Model 65

VI. RADIATION MODEL 70

6.1 Introduction 70
6.2 The Radiative Transfer Equation 71
6.3 Radiative Transfer in the Solar Spectrum 76
6.4 Radiative Properties of Aerosols and Gaseous Absorbers in the Solar Spectrum 77
6.5 Two-Stream Equations 81
6.6 Band Models 86
6.7 Infrared Radiation Properties of Gases 89
6.8 Radiative Fluxes in the Thermal Spectrum 93

VII. RESULTS AND DISCUSSION: ONE-DIMENSIONAL MODEL 99

7.1 Introduction 99
7.2 Test Simulation 99

7.2.1 Initial Conditions and Parameters Used in Test Simulation 99
7.2.2 Results of Test Simulations 102

7.3 Radiative Effects of Pollutants 114

7.3.1 Introduction 114
7.3.2 Effect of Pollutants on Thermal Structure of Boundary Layer 116
7.3.3 Effect of Pollutants on the Earth-Boundary Layer System 126
7.3.4 Effect of Pollutants on Pollutant Dispersal . . . 131

7.4 Effect of Elevated Layers of Pollutants 134
7.5 Effect of Changing the Height of the Elevated Polluted Layer 152
7.6 Effect of Changing Aerosol Properties 169
7.7 Effect of Choice of Gaseous Pollutant 176

VIII. RESULTS AND DISCUSSION: TWO-DIMENSIONAL MODEL 177

8.1 Introduction 177
8.2 Initial Conditions and Surface Parameters 179

8.3 Effect of Pollutants on Thermal and Solar Fluxes 182
8.4 Effect of Radiative Participation on the Surface Temperatures of the Urban-Rural System 188
8.5 Effect of Radiative Participation by Pollutants on the Vertical Potential Temperatures Profile 196
8.6 Effect of Radiative Participation on the "Crossover" Effect 202
8.7 The Urban Heat Island and the Effects of Radiative Participation 208
8.8 Pollutant Distributions in the Urban-Rural System . . . 214
8.9 Effect of Radiative Participation by Pollutants on Pollutant Dispersal 220

REFERENCES 229

APPENDIX A: Calculation of Directly Transmitted and Diffuse Solar Radiation at the Top of the Atmospheric Layer 242

Table Page

7.11 Summary of Simulations with Elevated Layers 135

7.12 Comparison of Thermal Fluxes (in W/m^2) at the Surface (Elevated layer at 300 m) 141

7.13 Comparison of Solar Fluxes (in W/m^2) at Surface (Elevated layer at 300 m) 142

7.14 Comparison of Potential Temperatures (in K) at 1 m (Elevated layer at 300 m) 144

7.15 Comparison of Surface Temperatures (in K) of Simulation with Non-Participating (NP) Pollutants and Simulation with Solar Participation (SP) only (Elevated layer at 300 m) 145

7.16 Comparison of Temperatures (in K) at 1 m (Elevated Layer at 600 m) 161

7.17 Comparison of Solar Fluxes (in W/m^2) at Surface (Elevated Layer at 600 m). 163

7.18 Comparison of Thermal Fluxes (in W/m^2) at Surface (Elevated Layer at 600 m). 164

7.19 Comparison of Aerosol Concentrations (in μg/m^3) at 1 m (Elevated Layer at 600 m). 165

7.20 Comparison of Solar Fluxes (in W/m^2) and Temperature (in K) at 1 m (Elevated Layer at 1200 m). 168

7.21 Summary of Simulations Performed to Study the Effect of Aerosol Property Variation; r_s = 0.2, H = 01. 170

7.22 Comparison of Temperatures at 1 m to Study the Effect of Aerosol Parameter Variation 171

7.23 Comparison of Solar Fluxes at Surface to Study the Effect of Aerosol Parameter Variation. 172

8.1 List of Two-Dimensional Simulations 179

8.2 Grid Spacing, Surface Parameters and Pollutant Parameters. 181

8.3a Comparison of Incident Thermal and Solar Fluxes at the Surface (in W/m^2) for Simulations P and NP at x = 16 km (urban area) 183

Figure Page

7.11 Nighttime Potential Temperature Excess of Participating Simulation over Non-Participating Simulation 128

7.12 Effect of Radiative Participation on Earth-Atmosphere Albedo 130

7.13 Aerosol Concentration Profiles for Time 05:00 to 20:00 . . 132

7.14 Potential Temperature Profiles for Time 05:00 to 08:00 . . 136

7.15 Potential Temperature Profiles for Time 09:00 to 12:00 . . 137

7.16 Potential Temperature Profiles for Time 13:00 to 16:00 . . 138

7.17 Potential Temperature Profiles for Time 17:00 to 20:00 . . 139

7.18 Aerosol Concentration Profiles for Time 05:00 to 08:00 . . 147

7.19 Aerosol Concentration Profiles for Time 09:00 to 12:00 . . 148

7.20 Aerosol Concentration Profiles for Time 13:00 to 16:00 . . 149

7.21 Aerosol Concentration Profiles for Time 17:00 to 20:00 . . 150

7.22 Variation of Mixed Layer Height with Time Elevated Pollutant Layer at 300 m 151

7.23 Potential Temperature Profiles for Time 05:00 to 08:00 . . 153

7.24 Potential Temperature Profiles for Time 09:00 to 12:00 . . 154

7.25 Potential Temperature Profiles for Time 13:00 to 16:00 . . 155

7.26 Potential Temperature Profiles for Time 17:00 to 20:00 . . 156

7.27 Aerosol Concentration Profiles for Time 05:00 to 08:00 . . 157

7.28 Aerosol Concentration Profiles for Time 09:00 to 12:00 . . 158

7.29 Aerosol Concentration Profiles for Time 13:00 to 16:00 . . 159

7.30 Aerosol Concentration Profiles for Time 17:00 to 20:00 . . 160

7.31 Variation of Mixed Layer Height with Time Elevated Pollutant Layer at 600 m 167

7.32 Effect of Forward Scattering Factor on Earth-Boundary Layer Albedo of Second Day 174

Figure Page

7.33 Effect of Single Scattering Albedo on Earth-Boundary Layer Albedo of Second Day 175

8.1 Potential Temperature Isopleths at Time = 11:30 Hrs . . . 189

8.2 Potential Temperature Isopleths at Time = 15:30 Hrs . . . 190

8.3 Potential Temperature Isopleths at Time = 21:30 Hrs . . . 191

8.4 Potential Temperature Isopleths at Time = 01:30 Hrs . . . 192

8.5 Comparison of Surface Temperature Difference Between Participating and Non-Participating Simulations at Center of City 193

8.6 Surface Temperature Variation at x = 0 (Rural Beginning) . 195

8.7 Difference Between Temperature Profiles at Center of City (x = 16 Km) for Participating and Non-Participating Simulations (Time = 11:30, 1st Day) 197

8.8 Difference Between Temperature Profiles at Center of City (x = 16 Km) for Participating and Non-Participating Simulations (Time = 21:30, 1st Day) 198

8.9 Difference Between Temperature Profiles at Center of City (x = 16 Km) for Participating and Non-Participating Simulations (Time = 03:30, 2nd Day) 199

8.10 Difference Between Temperature Profiles at x = 0 for Participating and Non-Participating Simulations (Time = 11:30, 1st Day) 200

8.11 Difference Between Temperature Profiles at x = 0 for Participating and Non-Participating Simulations (Time = 21:30, 1st Day) 201

8.12 Difference Between Temperature Profiles of Urban Center and Rural Beginning for Participating and Non-Participating Simulations (Time = 11:30, 1st Day) 205

8.13 Difference Between Temperature Profiles of Urban Center and Rural Beginning for Participating and Non-Participating Simulations (Time = 21:30, 1st Day) 206

8.14 Difference Between Temperature Profiles of Urban Center and Rural Beginning for Participating and Non-Participating Simulations (Time = 03:30, 2nd Day) 207

Figure Page

8.15 Effect of Radiative Participation on the Urban Heat Island Effect. 210

8.16 Negative Heat Island Created by City 212

8.17 Effect of Surface Parameters on the Heat Island Effect 213

8.18 Aerosol Vertical Concentration Profiles at Center of City (x = 16 km) for Simulation NP. 215

8.19 Aerosol Vertical Concentration Profiles at Downwind of City (x = 24 km) for Simulation NP. 216

8.20 Variation of Aerosol Concentration with Time at x = 16 km for Simulation NP 218

LIST OF TABLES

Table Page

4.1 Comparison of Numerical Solutions of the Momentum Equations with Exact Solution 39

7.1 List of One-Dimensional Numerical Simulations 100

7.2 Vertical Grid Coordinates and Physical Properties and Parameters Used in Test Simulation. 101

7.3 Summary of Surface Parameters and Pollutant Properties Used in Simulations of Section 7.3. 115

7.4 Comparison of Thermal and Solar Fluxes at the Surface for Simulations with Participating (P) and Non-Participating (NP) Pollutants 117

7.5 Comparison of Potential Temperatures (in K) at 1 m and 100 m for Simulations with Participating (P) and Non-Participating (NP) Pollutants 119

7.6 Comparison of Surface Temperatures (in K) and Diffusivities (in m^2/s) at 10 m for Simulations with Participating (P) and Non-Participating (NP) Pollutants 120

7.7 Comparison of Terms in Energy Equation for Simulations with Participating (P) and Non-Participating (NP) Pollutants, Time is 12:00 hours of Second Day 123

7.8 Comparison of Energy Fluxes (in W/m^2) at the Surface for Simulations with Participating (P) and Non-Participating (NP) Pollutants 124

7.9 Comparison of Energy Fluxes (in W/m^2) at the Surface for Simulations with Participating (P) and Non-Participating (NP) Pollutants 125

7.10 Comparison of Aerosol Concentration (in $\mu g/m^3$) for Simulations with Participating (P) and Non-Participating (NP) Pollutants 133

Table		Page
7.11	Summary of Simulations with Elevated Layers	135
7.12	Comparison of Thermal Fluxes (in W/m^2) at the Surface (Elevated layer at 300 m)	141
7.13	Comparison of Solar Fluxes (in W/m^2) at Surface (Elevated layer at 300 m)	142
7.14	Comparison of Potential Temperatures (in K) at 1 m (Elevated layer at 300 m)	144
7.15	Comparison of Surface Temperatures (in K) of Simulation with Non-Participating (NP) Pollutants and Simulation with Solar Participation (SP) only (Elevated layer at 300 m)	145
7.16	Comparison of Temperatures (in K) at 1 m (Elevated Layer at 600 m)	161
7.17	Comparison of Solar Fluxes (in W/m^2) at Surface (Elevated Layer at 600 m).	163
7.18	Comparison of Thermal Fluxes (in W/m^2) at Surface (Elevated Layer at 600 m).	164
7.19	Comparison of Aerosol Concentrations (in μg/m^3) at 1 m (Elevated Layer at 600 m).	165
7.20	Comparison of Solar Fluxes (in W/m^2) and Temperature (in K) at 1 m (Elevated Layer at 1200 m).	168
7.21	Summary of Simulations Performed to Study the Effect of Aerosol Property Variation; $r_s = 0.2$, H = 01.	170
7.22	Comparison of Temperatures at 1 m to Study the Effect of Aerosol Parameter Variation	171
7.23	Comparison of Solar Fluxes at Surface to Study the Effect of Aerosol Parameter Variation.	172
8.1	List of Two-Dimensional Simulations	179
8.2	Grid Spacing, Surface Parameters and Pollutant Parameters.	181
8.3a	Comparison of Incident Thermal and Solar Fluxes at the Surface (in W/m^2) for Simulations P and NP at x = 16 km (urban area)	183

Table Page

8.3b Comparison of Total Radiation (Solar + Thermal) at $x = 16$ km for Simulations P and NP; Total Radiation in (W/m^2) 183

8.4 Comparison of Incident Thermal and Solar Fluxes at the Surface (in W/m^2) for Simulations P and NP at $x = 0$ km (Upwind Rural Area). 185

8.5 Comparison of Incident Thermal and Solar Fluxes at the Surface (in W/m^2) in Urban and Upwind Rural Areas for Simulation P 186

8.6 Comparison of Aeroxol Concentrations (in $\mu g/m^3$) at $z = 1$ m and $z = 100$ m at $x = 16$ km for Simulations P and NP 222

8.7 Comparison of Aerosol Concentrations (in $\mu g/m^3$) at $z = 100$ m at $x = 24$ km for Simulations P and NP 223

8.8 Comparison of Eddy Diffusivities (in m^2/s) at $z = 1$ m and $z = 100$ m for Simulations P and NP at $x = 16$ km . . . 225

8.9 Comparison of Eddy Diffusivities (in m^2/s) at $x = 16$ km for Simulations NP and P 227

LIST OF ABBREVIATIONS AND SYMBOLS

A	wide band absorptance
A_{wv}	fractional water vapor absorption
b	backward scattering factor
C	concentration
c_p	specific heat at constant pressure
c_v	specific heat at constant volume
E_b	blackbody emitted flux defined as πI_b
E_n	exponential integral of order n defined as

$$E_n(t) = \int_0 \mu^{n-2} \exp(-t/\mu)d\mu$$

F	radiative flux (solar or thermal) in +z or -z direction
F	total radiative flux in +z direction
f	Coreolis parameter or forward scattering factor
g	acceleration due to gravity
I	intensity of radiation
$I_{b\nu}$	Planck's function
h	thickness of equilibrium layer
H	Halstead moisture parameter or maximum model height
H^*	height of boundary layer in two-dimensional model
H_m	height of boundary layer in one-dimensional model
$\dot{H}_p$	anthropogenic heat production rate
K	turbulent eddy diffusivity
k	thermal conductivity or turbulent kinetic energy
L	horizontal extent of urban-rural system
L_H	latent heat of evaporation
L_o	Monin-Obukov length
M_{C_n}	surface pollutant source
p	pressure

$p(\mu'\to\mu)$	scattering phase function
P.B.L.	planetary boundary layer
p_ℓ	Legendre coefficient
P_ℓ	Legendre polynomial of order ℓ
Ri	gradient Richardson number, Eq. (5.3.1)
r	reflectance
$r(\mu'\to\mu)$	bidirectional reflectance
$\dot{S}_{C_n}$	volumetric pollutant source strength
T	thermodynamic temperature
t	time
u	horizontal velocity along x-axis
u_*	surface friction velocity
v	horizontal velocity along y-axis
w	vertical velocity along z-axis
x	horizontal coordinate or distance along urban-rural system
y	horizontal coordinate perpendicular to x
y_ℓ	water vapor path length
z	vertical coordinate
z_0	roughness length

Greek Letters

α	thermal diffusivity, $k/\rho C_p$
β	extinction coefficient ($\kappa + \sigma$)
γ_c	counter-gradient heat flux parameter
ε	emissivity, emittance
θ	potential temperature or zenith angle
κ	absorption coefficient or von Karman constant
λ	wavelength
μ	cosine of zenith angle of a beam of radiation
μ_0	cosine of solar zenith angle
ν	frequency
ρ	density
σ	scattering coefficient or Stefan-Boltzmann constant
τ	shear stress or optical depth

τ_o	optical thickness of P.B.L.
ϕ	azimuthal angle
ω	albedo for single scattering, σ/β

Subscripts

aer	aerosol
C_n	species
ν	frequency
g	geostrophic
H	heat
i	index denoting node along x-axis
j	index denoting node along y-axis
k	index denoting node along z-axis
M	momentum
o	surface value
s	solar or soil
t	thermal
w	water vapor

Superscripts

+	positive z direction
-	negative z direction
'	turbulent fluctuation

ACKNOWLEDGMENT

This research was supported by the Meteorology and Assessment Division, Environmental Protection Agency, under Environmental Protection Agency Grant Nos. R801102 and R803514. Computer facilities were made available by Purdue University Computing Center and the National Center for Atmospheric Research which is supported by the National Science Foundation.

The support of the project by the Environmental Protection Agency and the help provided by Dr. James T. Peterson, The Grant Project Officer, is acknowledged with sincere thanks.

Except for minor changes, this report constitutes the doctoral dissertation of Mr. A. Venkatram which was submitted to the Faculty of Purdue University in partial fulfillment of the degree of Doctor of Philosophy.

I. CONCLUSIONS

1.1 Conclusions of One-Dimensional Simulations

On the basis of the numerical simulations performed and the results obtained using the one-dimensional transport model it is concluded that:

1. The turbulence model was capable of reproducing important features of mixed layer formation. The counter-gradient heat flux parameter was necessary to model the collapse of turbulence during the night. The results of a test simulation using the turbulence model compared favorably with the O'Neill observations.
2. Pollutant aerosols reduced the solar flux at the surface by 15% on an average. Thermal participation by gaseous pollutants lead to an increase of the downward thermal radiation at the surface by about 10% at night. The magnitudes of the pollutant caused changes in solar and thermal fluxes at the surface were in good agreement with observations (Rouse, et al., 1973; Oke and Fuggle, 1972).
3. Absorption of solar radiation by aerosols increased the temperature of the boundary layer by as much as 0.5 C during a day. The absorption and emission of thermal radiation by gaseous pollutants lead to warming of the surface layer of the boundary layer, and cooling at higher levels.
4. Radiative participation by aerosols and gaseous pollutants lead to an increase in the surface temperature. The maximum temperature increase was 0.35 C during the day and 2.8 C during the night. The reduction of solar flux at the surface decreased the surface temperature by a maximum of 0.31 C during the first 8 hours of simulation. However, no temperature decrease was observed on the second day of simulation.

5. Solar energy absorption by aerosols increased the stability of the surface layer. This led to a decrease of surface pollutant concentrations during the day by a maximum of 7%. The significantly warmer surface temperatures during the night decreased the stability of the surface layer causing higher surface pollutant concentrations. The maximum increase was 18%. In presenting these conclusions it is important to reiterate that the pollutant source was elevated at 100 m.
6. Elevated layers of pollutants played a significant role in modifying mixed layer growth. Solar heating led to the formation of sharp inversions which hindered the vertical expansion of the mixed layer. Cooling induced by gaseous pollutants helped the growth of the mixed layer.
7. The height of the elevated pollutant layer was an important factor in determining the final height of the mixed layer. When the pollutant layer was placed at 300 m the mixed layer was able to penetrate the stable layer created by solar heating. However, when the pollutant layer was located at 600 m the inversion strength became large enough to prevent the mixed layer from penetrating the inversion.
8. In the process of creating a sharp inversion solar heating also led to the formation of an unstable layer above the inversion. Thus, when the mixed layer penetrated the inversion its growth thereafter was relatively rapid in the unstable layer above the inversion.
9. Elevated pollutant layers had a significant effect on pollutant dispersal as they affected the growth of the mixed layer. Dispersion was enhanced when the mixed layer height was large. On the other hand, a small mixed layer thickness was conducive to the buildup of pollutants near the surface.
10. Aerosol parameters were important in determining the effective albedo of the earth-boundary layer system. In general, an increase in single scattering albedo and backscattering factor led to an increase of the effective reflectance. The

effective albedo was most sensitive to the aerosol backscattering factor.

11. In most of the simulations, aerosols decreased the effective reflectance of the earth-boundary layer system at small zenith angles, and increased it at large zenith angles. Thus, aerosols had a warming influence in the hours around noon, and a net cooling effect around sunset and sunrise.

1.2 Conclusions of Two-Dimensional Simulations

On the basis of the preliminary results of the two-dimensional simulations it is concluded that:

1. The predominant effect of radiative participation by pollutants on the surface temperature is one of warming both in the rural as well as in the urban areas. The maximum pollutant induced temperature increase in the urban center was 1.86 C. When only aerosols were allowed to participate radiatively the reduction of solar flux at the surface caused a maximum temperature decrease of 0.3 C.
2. Radiative participation increased the nighttime urban heat island by a maximum of 50% in the early morning hours. Solar participation decreased the urban temperature excess during the day, while thermal participation increased the heat island intensity throughout the day.
3. Radiative participation by pollutants was an important contributing factor to the "crossover" effect. During the night, when no temperature crossover occurred in the simulation with non-participating pollutants, radiative cooling in the simulation with participating pollutants induced a temperature crossover of 0.3 C.
4. The predominant effect of radiative participation by pollutants on pollutant dispersal was that of decreasing pollutant concentrations in the boundary layer. In the urban area (x = 16 km) the maximum pollutant induced reduction occurred during the night and was 13.5% at the

source height and 8.2% at the surface. The rural decrease ($x = 24$ km) was 5.5% at 100 m and 7.5% at the surface. It is necessary to emphasize that the magnitudes of the pollutant induced concentration changes are largely dependent on the particular turbulence model used in the study. Definitive conclusions on the effects of pollutants on pollutant dispersal cannot be drawn without examining various turbulence models.

II. RECOMMENDATIONS

2.1 Suggested Improvements in Modeling

This investigation involved the modeling of a large number of physical processes. Although every attempt was made to model the physical processes as realistically as possible, the wide scope of this study gave rise to a number of suggestions for future research. Some of the problem areas which should receive attention are:

1. An improved mixing length model is needed. The self-similar profile used in this study does not account for the effect of local stability on the scale of turbulent eddies. This is unrealistic, and an improved procedure to calculate the mixing length is needed.
2. The solar radiation transfer model should be improved to account for the selective absorption by gases and aerosols. As a starting point the solar spectrum can be divided into two regions taking advantage of the fact that water vapor absorbs mainly in the region, 1-4 μm. This division of the solar spectrum should be kept to the minimum to prevent computational requirements from becoming excessive.
3. A procedure should be incorporated into the thermal radiation model to account for the absorption and emission of a combination of pollutant gases. A realistic pollutant model should include the most important pollutants found in the atmosphere. The incorporation of such a model necessarily involves a procedure to account for the overlap between the pollutant gas bands. As narrow band models are time consuming, it is necessary to modify wide band models to account for overlap.

4. Radiative transfer in the polluted urban atmosphere is at least two-dimensional and very complicated. Some simple approximate yet mathematically and numerically tractable analysis must be developed to account for two-dimensional effects.
5. A simple model must be developed to handle the transport of water in the soil layer. The currently available (Eagleson, 1970) soil transport models involve considerable data handling and cannot be readily incorporated into a numerical model. A soil transport model in combination with a physically realistic procedure to account for evapotranspiration at the air-soil interface is needed because latent transport may be a significant fraction of the net energy transfer at the earth's surface.
6. An improved procedure to solve the two-dimensional conservation equations must be developed. Possible improvements are the use of a staggered grid system and the incorporation of a conservative Arakawa scheme. This might solve the problems encountered in the attempt to incorporate the turbulent kinetic energy model into the two-dimensional numerical model.
7. As the location of pollutant sources determines whether radiative participation by pollutants increases or decreases surface pollutant concentrations it is necessary to develop a realistic pollutant emission model. The model should account for the space (elevated or surface based) as well as time (source strengths and time variation) distributions of pollutant sources.

2.2 Suggested Additional Simulations

An analysis of the results of the numerical simulations showed that a greater understanding of the problem could be obtained by performing a number of additional simulations. Specifically, the following numerical studies should be conducted:

1. Sensitivity studies should focus attention on the role of surface parameters in determining the effect of radiative participation on the surface temperature. The results of this study indicate that the effect of the reduction of solar flux at the surface on the surface temperature is dependent on the surface evaporation rate. Other studies (Mitchell, 1971; Wang and Domoto, 1974) also show that radiative effects are related to the surface albedo and the surface moisture. It is clear that additional simulations would provide valuable insight into these effects.
2. Numerical experiments must be conducted to investigate the effect of various outflow boundary conditions (downstream) on the temperature, velocity and species distributions.
3. Simulations must be performed to determine the relative importance of urban-rural surface parameters in producing the heat island and the crossover effect.
4. Simulations must be performed to examine the role of the turbulence model in determining pollutant induced changes of pollutant dispersal. This can be accomplished by performing a series of simulations with identical initial conditions but with different turbulence models. Some of the suggested turbulence models are surface layer similarity formulations (Businger, 1973), Richardson number correlations (Pandolfo, et al., 1971), turbulent kinetic energy models (Launder and Spalding, 1974), second-order models (Donaldson, 1973), and simplified sub-grid scale model (Orlanski, et al., 1974). As atmospheric turbulence is still incompletely understood, only conclusions based on results of simulations which examine the effect of the choice of the turbulence model will find acceptance.

III. DISCUSSION OF PROBLEM

3.1 Problem Area

The rapid increase in industrialization and urbanization over the past few decades has been accompanied by relatively significant changes in the climate in and around urban locales. This inadvertent climate modification has been evidenced by observations (Chandler, 1965; Summers, 1966; Oke and East, 1971; Oke, 1972) of urban-rural differences of various aspects of climate such as temperature, humidity, visiblity, radiation, wind and precipitation. One of the better known features of the urban environment is the so-called heat island effect which is associated with the existence of warmer surface temperatures in the urban regions than in the surrounding rural environs. The heat island effect is also related to the differences in the thermal structures between urban and rural areas. Recent observations (Bornstein, 1968; Clarke, 1969) show that while fewer surface inversions occur over cities than over rural areas, weak elevated inversions occur at a greater frequency over urban areas. It is generally accepted that the heat island is primarily caused by the differences in the urban-rural surface characteristics such as thermal properties, surface moisture, surface albedo, roughness, and heat sources. While these differences can be used to explain thermal effects at the surface, they cannot be directly related to the formation of elevated inversions. It has been suggested (Bornstein, 1968) that these inversions could be caused by the radiative effects of pollutant layers. Recent theoretical studies by Atwater (1970) and Bergstrom (1972) in addition to lending some credence to the theory show that pollutants can contribute significantly to the heat island effect.

A qualitative explanation of the process of weather modification by air pollutants is fairly simple. Particulates in the atmosphere absorb and scatter the incoming solar radiation leading to a reduction in the solar energy reaching the earth and thus a cooling. However, Mitchell (1971) has recently shown that while stratospheric aerosols do lead to a cooling, slightly-absorbing aerosols in the troposphere may serve to increase surface temperatures. Other pollutants, such as CO_2, which are relatively opaque to long-wave thermal radiation, can produce a "greenhouse" effect leading to an increase in surface temperatures. This simple explanation of the effect of anthropogenic pollutants on the climate is clearly more relevant to the global scale than to the small scales of an urban area. The microclimate of an urban area is determined by the energetics and the dynamics of the planetary boundary layer, the evolution of which is largely controlled by turbulence. Thus, estimates of the effects of the pollutants on the climate have to be based on studies which account for the interaction of turbulence and radiation, both of which are extremely complex phenomena. There have been relatively few studies on the radiative effect of pollutants on a local scale (Atwater, 1970, 1972, 1974; Pandolfo et al., 1971; Zdunkowski and Mcquage, 1972; Bergstrom and Viskanta, 1973), but the results indicate that the effects can be substantial within a period of a few days. However, the models used in these studies were relatively crude, and the results obtained can at best be considered tentative. Considerably more research effort is needed before short and long-term effects of pollutants can be estimated.

Thermal modification by pollutants is just one of the many effects of urbanization on the atmospheric structure of the city and the rural surroundings. Although observational data can provide information on the urban microclimate, it cannot be utilized in determining the causative factors of the atmospheric structure of the urban area. An understanding of the various effects of urbanization can be obtained only by isolating possible causative factors, and studying their effects by varying them one at a time. Such a procedure is not practical from the point of view of an observational program as it is not possible to manipulate the urban environment. One technique which can be employed to help fill this observational gap is numerical simulation. A numerical model describes the dynamics and thermodynamics of a city in terms of differential equations (conservation laws) and boundary conditions. It is through these boundary conditions that city parameters such as tall buildings, heat production by the city and pollutant emission are described. The main advantage of numerical simulation lies in its ability to predict the effect of changes of initial and boundary conditions on the planetary boundary layer variables. Thus, a numerical model can serve as an invaluable tool in determining the effects of urban changes such as urban renewal, park development, industrial siting and freeway location. Numerical simulation can also provide guidance for observational programs by determining the relative importance of atmospheric variables. This information can help to minimize redundancy in the field program. Observational programs, in turn, can provide invaluable feedback for improvement of the numerical model.

3.2 Background

3.2.1 The Atmospheric Boundary Layer

As the winds created by the rotation of the earth blow over the surface of the globe, they maintain a layer of "frictional influence," or atmospheric boundary layer. The boundary layer is turbulent, and extends to heights of the order of one kilometer. The large scale flow or the free atmosphere receives much of its heat and virtually all of its water vapor through the turbulent transfer processes in the boundary layer. The turbulent activity in the boundary layer is also responsible for the transfer of kinetic energy from the atmosphere to the boundary layer. Since, as much as one-half of the atmosphere's loss of kinetic energy occurs in the boundary layer, the turbulent motion in the boundary layer has an appreciable influence on the evolution of weather systems (Tennekes, 1974).

As man lives inside the boundary layer, his interaction with the transport processes of the boundary layer determines the quality of his daily environment. Pollutant and heat wastes injected into the boundary layer are dispersed vertically by turbulent mixing and horizontally by the wind. Thus, the primary variables of micrometeorology are the wind velocity vector and the boundary layer height which essentially determines the extent of vertical mixing.

The boundary-layer thickness varies from about a few tens of meters on calm nights to about two thousands meters on sunny summer afternoons (Tennekes, 1974). This variation in the boundary layer thickness is caused primarily by the effects of vertical heat transfer on turbulent motion. During the day, upward heat transfer enhances turbulent activity which is responsible for the entrainment of the stable nonturbulent layer which caps the boundary layer. During the night, the downward heat transfer caused by the cooling of the earth's surface, suppresses turbulence and the boundary layer rapidly decreases in height. In relatively rare situations with negligible heat transfer the boundary layer thickness is determined by the shear stress at the surface and the local rate of the earth's rotation.

During the day, the thermally enhanced turbulent mixing of the boundary layer is so effective that the vertical distribution of boundary layer variables such as potential temperature, moisture, pollutants and wind is more or less uniform through most of the boundary layer. For this reason, meteorologists refer to the boundary layer as the "mixed" layer. The distinctive structure of the mixed layer has allowed the construction of simple models (Leahey and Friend, 1971; Tennekes, 1973; Carson, 1973) to predict the variation of the mixed layer height during the day. Considering their simplicity, these models have had remarkable success (Tennekes and Ulden, 1974; Leahey and Friend, 1971) in forecasting mixed layer heights. However, these forecasts are necessarily short-term (12 hours), and considerably more sophisticated models are required to predict the diurnal variation of the boundary layer.

3.2.2 Urban Heat Island Phenomenon

One of the better known features of urban climatology is the existence of higher temperatures in the urban area than in the rural surroundings. This phenomenon, known as the urban heat island effect, has been documented for over a century (Howard, 1833). Howard's measurements showed that the urban temperature excess was greatest at night, when it amounted to 2.0 C. During the day, the heat island effect was found to be negative with the city being 0.15 C cooler than the surrounding countryside. But on the average, the city was found to be warmer than the countryside by about 1 C. These results are similar to those of more modern investigations (Chandler, 1962).

Several mechanisms have been suggested to explain the formation of the heat island. Howard (1833) attributed the urban temperature excess to anthropogenic heat production. Recent observations (SMIC, 1971; Bornstein, 1968) show that the anthropogenic heat production term may dominate the other energy sources during the winter months, and may be as large as 2½ times the solar input. Bornstein (1968) and Chandler (1961) have also emphasized the importance of reduced evaporation rates in urban areas. They argue that as less energy is required for evaporation, there is excess solar energy to heat up the urban surface. It is also believed (Mitchell, 1961) that the higher thermal conductivities and heat capacities of paving materials and buildings of the city, allow more energy to be stored in the "surface" layer of the city than in that of the countryside during the day. This additional stored energy which is released during the night creates the excess in the urban temperature. The smaller urban albedos (Craig and Lowry, 1972) can contribute to the daytime heat island effect. During the day, the higher eddy diffusivities (Bowne and Ball, 1970) associated with the rough surface (tall buildings) of the city tend to counteract heat island causative factors. However, the higher levels of turbulence can lead to a reduction of the city's ventilation by "breaking" the wind. Kratzer (1956) and more recently Fuggle and Oke (1968) have attributed the heat island to the blanketing effect of atmospheric pollutants. It is argued that layers of pollutants absorb radiation during the day, and re-emit thermal radiation during the night. This increased downward thermal radiation results in the observed nocturnal temperature excess.

From the preceding discussion, it is clear that the urban heat island is the result of a complex set of interacting physical processes. Over recent years, a better understanding of the heat island phenomena has been obtained by supporting observations with numerical modeling studies such as those of Myrup (1969), Tag (1969), McElroy (1971), Pandolfo (1971), and Nappo (1972). As the physical processes involved in the formation of the heat island are exceedingly complex and incompletely understood, these models are necessarily simple. However, they have provided valuable insight into the relative significance of the factors responsible for the urban temperature excess.

The magnitude of the heat island effect is important from the point of view of practical applications such as the design of human comfort systems and urban planning. Thus, the need for "quick" estimates of the urban-rural temperature difference has given rise to a number of empirical studies which attempt to correlate the urban temperature excess with urban parameters such as population, wind speed, cloud cover, etc. Some of the more successful correlations are due to Ludwig (1970), and Oke (1972, 1973).

3.2.3 Effect of Pollutants on Thermal Structure

Observations show that there are distinct differences between the vertical temperature profile of the city and that of the surrounding rural area. The tower measurements of Munn and Stewart (1965) made over southern Ontario indicated higher percentages of inversion-free nights at the urban sites. Bornstein (1968) studying New York's thermal structure, found that while the rural sites exhibited a greater frequency of surface inversions, a greater number of elevated inversions occurred over the city. He also observed that while city temperatures were generally higher than those over the countryside up to heights around 300 meters, a temperature crossover effect occurred around 400 meters where temperatures were generally lower than those of the surrounding area. This finding is similar to those of Duckworth and Sandberg (1954). More recently, Rouse, et al. (1973) observed sharp elevated inversions over a polluted industrial area in Hamilton, Ontario. These inversions were strongly developed in the morning, weakened in the hours around noon, and strengthened towards the evening.

The described features of the urban thermal structure are believed to be caused by the radiative participation of pollutants (Sheppard, 1958; Atwater, 1970; Bergstrom and Viskanta, 1972). It is argued that the increased nocturnal thermal radiation associated with the cooling of pollutant layers, heats up the earth's surface thus preventing the formation of a surface radiation inversion. On the other hand, the cooling of elevated pollutant layers may be responsible for the temperature "crossover" effect and the formation of elevated inversions.

There have been relatively few theoretical investigations on the effect of pollutants on the thermal structure. Using a one-dimensional radiative-conductive model Atwater (1970) showed that the cooling due to layers of pollutants could cause elevated inversions. Bergstrom and Viskanta (1972) studied the effect of pollutants using a one-dimensional model which accounted for turbulence effects through semi-empirical eddy diffusivity correlations. Their results indicated that pollutants could be responsible for the destruction of the nocturnal surface inversion. They also showed the formation of elevated inversions due to pollutant induced cooling. Utilizing a boundary layer model developed by Pandolfo (1971), Atwater has investigated the thermal changes induced by pollutants. He concluded from his results that the major effect of pollutants was to cause the delay of the onset of unstable conditions after sunrise.

Most one-dimensional simulation (Atwater, 1970; Bergstrom and Viskanta, 1972; Zdunkowski and McQuage, 1972) studies show that pollutants may contribute significantly to the heat island effect.

However, more realistic investigations based on two-dimensional models seem to downplay the importance of pollutants as a causatory factor of the urban temperature excess. Atwater's (1974) results show that pollutants are only a minor factor in the formation of the urban heat island. The more recent two-dimensional study of Viskanta, et al. (1975) shows that under certain conditions radiative participation can in fact reduce the urban-rural temperature difference. This result is significant in that it contradicts other studies. From the preceding discussion it is evident that considerably more research is required before a satisfactory understanding of the effects of pollutants on the thermal structure is obtained.

3.3 Objectives of this Study

The primary objective of the study is to enhance understanding of the effects of pollutants on the urban environment. Specifically, the research program proposed to determine the role of pollutants in modifying the thermal structure which, in turn, affects pollutant dispersal. Particular attention will be paid to the interaction of pollutants with the stable layer. To this end, the net effect of the most important pollutants on radiative flux and its divergence, temperature, concentrations, and flow fields will be predicted.

The specific aims of this study are:

1) Construction of a physically realistic radiative transfer model in the urban boundary layer in which gaseous and particulate pollutants are present.
2) Construction of a turbulence model capable of representing turbulent transport effects over a wide range of atmospheric conditions.
3) Development of a one-dimensional transport model for simulating the thermal structure and dispersion in an urban atmosphere.
4) Simulation of a variety of atmospheric situations using the one-dimensional transport model to study the effect of pollutants on the urban climate.

5) Development of an unsteady two-dimensional transport model to study the effect of pollutants on urban-rural climatic differences.

Some of the questions this study will address itself to are:

1) Under what meteorological conditions is radiative transfer important enough to compete with turbulent transport?
2) What should the pollutant concentration be in order to affect the thermal structure and pollutant dispersion?
3) How do the radiatively participating pollutants affect the height of the mixed layer during the day?
4) Does the variation of the pollutant concentration with height (i.e., sharp concentration gradients) contribute to the formation of an elevated stable layer?
5) How do pollutants affect the stability of the inversion? Do they stabilize the inversion or do they accelerate the breakup of the inversion?
6) What role do pollutants play during the formation of surface inversions at night?

These questions relate to the effect of pollutants on the thermal structure and pollutant dispersal. In addition to these questions, the research program hopes to shed some understanding about the structure of the mixed layer and its interaction with the inversion.

3.4 Rationale

After presenting the objectives of this study it is necessary to answer the following question to justify the research effort: Apart from the academic interest in the effects of pollutants, what is the practical importance of the slight modification of thermal structure the radiative participation of pollutants may be able to cause? The key to answering this question can be found in the nature of atmospheric turbulence. The planetary boundary layer is turbulent, and except for a shallow layer next to the earth's surface, the turbulence in the boundary layer is thermally controlled. During the day, the negative potential temperature gradients in the atmosphere are responsible for the production of turbulent kinetic energy, and during the night the slight positive potential temperature gradients inhibit turbulence. These potential temperature gradients which are so effective in promoting or suppressing turbulent activity are typically of the order of a few degrees per kilometer. In view of this, it is easy to see the significance of the small changes in temperature pollutants can produce. These temperature changes become all the more important when pollutant effects are localized, i.e. temperature changes over small vertical distances producing large potential temperature gradients.

With the background provided by the discussion of the preceding paragraph it is easy to see the importance of the possible thermal effects of pollutants in the practical tasks of (1) forecasting of pollution episodes, (2) calculation of pollutant dispersion, (3) prediction of thermal structure of a city. The turbulent planetary boundary layer serves as a conduit through which the city flushes out its pollutant and heat wastes. Since the atmospheric variables such as temperature, wind speed and pollutant distribution are nearly uniform (mixed) inside the boundary layer, fairly accurate estimates of the pollutant concentration and the temperature can be obtained from a knowledge of the wind velocity, boundary layer height, and the sources of heat and pollutant emissions (Tennekes, 1974). The variables which can be possibly affected by pollutants are the wind and the boundary layer height. Pollutants may modify the wind by altering the turbulent intensity. Clearly this effect will be important during the night when turbulent transport does not overwhelmingly dominate radiative transfer. Pollutant induced changes of a few degrees at the earth's surface could also change the stability of the surface layer quite drastically. As turbulent activity during the night is confined to the surface layer, this alteration of stability could affect the intensity of vertical mixing and thus pollutant dispersal. During daytime, the vertical expansion of the boundary layer is limited by a capping inversion. Clearly, the rate of growth of the boundary layer is dependent on the stability of the inversion. As there is no turbulent activity inside the inversion, pollutant induced heating or cooling can cause dramatic changes in the stability of the inversion. Thus, elevated layers of pollutants inside the inversion can play a significant role in controlling boundary layer height, one of the most important variables of micrometeorology (Tennekes, 1974).

It is clear that the radiative participation of pollutants can affect thermal structure and pollutant dispersal through the feedback mechanisms described in the preceding paragraph. It is desirable therefore to understand these feedback mechanisms and obtain estimates of pollutant caused thermal changes. If numerical simulations show that the radiative interaction of gaseous and particulate pollutants with solar and atmospheric radiation is important, the inclusion of radiative transfer in air quality simulation models (AWSM) may become mandatory.

3.5 Scope of this Study

This section discusses the improvements made by this study over previous investigations of the effect of radiative participation by pollutants on local climate. The specific contributions of this study are listed below:

1) A relatively sophisticated turbulence model was developed and incorporated into the dynamic numerical model. All previous studies (Atwater, 1970, 1972, 1975; Pandolfo et al., 1971; Zdunkowski and McQuage, 1972; Bergstrom and Viskanta, 1973; Viskanta, Bergstrom and Johnson, 1975) of the radiative effects of pollutants have utilized relatively crude turbulence models. As the thermal structure of the boundary layer is determined by the interaction between radiation and turbulence, it is unrealistic to emphasize the role of radiation at the cost of that of turbulence. Bergstrom and Viskanta (1972) and Viskanta, Bergstrom and Johnson (1975) have used sophisticated radiation models in combination with relatively simple turbulence models to study changes induced by pollutants. In view of the importance of

turbulence, it is clear that the results of such studies have to be viewed with a degree of skepticism. Even partial understanding of the effects of pollutants can only be obtained by using radiation and turbulence models which are representative of the relative importance of the two physical processes.

2) A simple solar radiation model based on the two-flux method was developed and incorporated into the numerical model. The radiation model although relatively crude compared to that of Bergstrom and Viskanta (1972) affords substantial savings in computer time without introducing unacceptable idealizations. The model accounts for absorption and scattering of solar radiation in a consistent manner, and it represents an improvement over the radiation model developed by Atwater (1971). Atwater's treatment of scattering can at best be considered "fairly approximate." Furthermore, his assumption of extinction coefficients being independent of pollutant concentrations ignores the importance of the distribution of pollutants in determining the heating rates. The model used in this study trades a degree of sophistication for considerable flexibility in the variation of aerosol parameters such as forward scattering factor and single scattering albedo.
3) As the turbulence model was able to reproduce important features of mixed layer formation, it was possible to study the radiative effects of pollutants on the growth of the mixed layer. A number of simulations were performed to determine the role of elevated layers of pollutants in modifying mixed layer growth. No such studies appear to have been conducted to date.
4) The simulations have investigated the effects of radiative participation by pollutants on the effective albedo of the earth-boundary layer system. The effective albedo is an important parameter which determines the total energy absorbed in the system. Workers (Atwater, 1970, 1972, 1974; Bergstrom and Viskanta, 1973; Pandolfo, et al., 1971) who have coupled the dynamics of the boundary layer with the influences of air pollutants have not studied this important effect.

IV. FORMULATION OF PROBLEM

4.1 Physical Model

A schematic diagram of the earth-atmosphere system being considered in this study is shown in Figure 4.1. The physical model consists of four layers: (1) the free atmosphere where the atmospheric variables are determined by the large scale flow [as the simulation time scale of the model is relatively small (48 hours), the free atmospheric variables can be assumed to be unaffected by the flow in the boundary layer]; (2) the "polluted" atmosphere in which the atmospheric variables such as velocities, temperature and pollutant concentrations are functions of space and time, and change in response to varying boundary conditions primarily at the lower boundary (earth-air interface) and at the upper boundary (free atmosphere); (3) the soil layer in which the temperature is a function of depth and time only; and (4) the lithosphere in which the temperature is constant over the time scale of simulation.

The urban parameters such as anthropogenic heat sources, surface albedo and emittance, thermal diffusivity and conductivity of the soil, roughness height, and surface and/or elevated pollutant sources are prescribed functions of the horizontal distance along the urban-rural complex. The variation in topography is not accounted for, i.e., except for the roughness variation the terrain is assumed to be uniform.

The forcing function of the model is the time dependent solar irradiation. Incoming short-wave solar radiation heats up the earth's surface during the daytime; a part of this radiation is absorbed and scattered in the polluted atmosphere. The solar energy absorbed at the air-soil interface is partly transferred to the atmosphere and the soil by conduction. Another part of the energy is used for evaporating water, and the remaining energy is reradiated as longwave

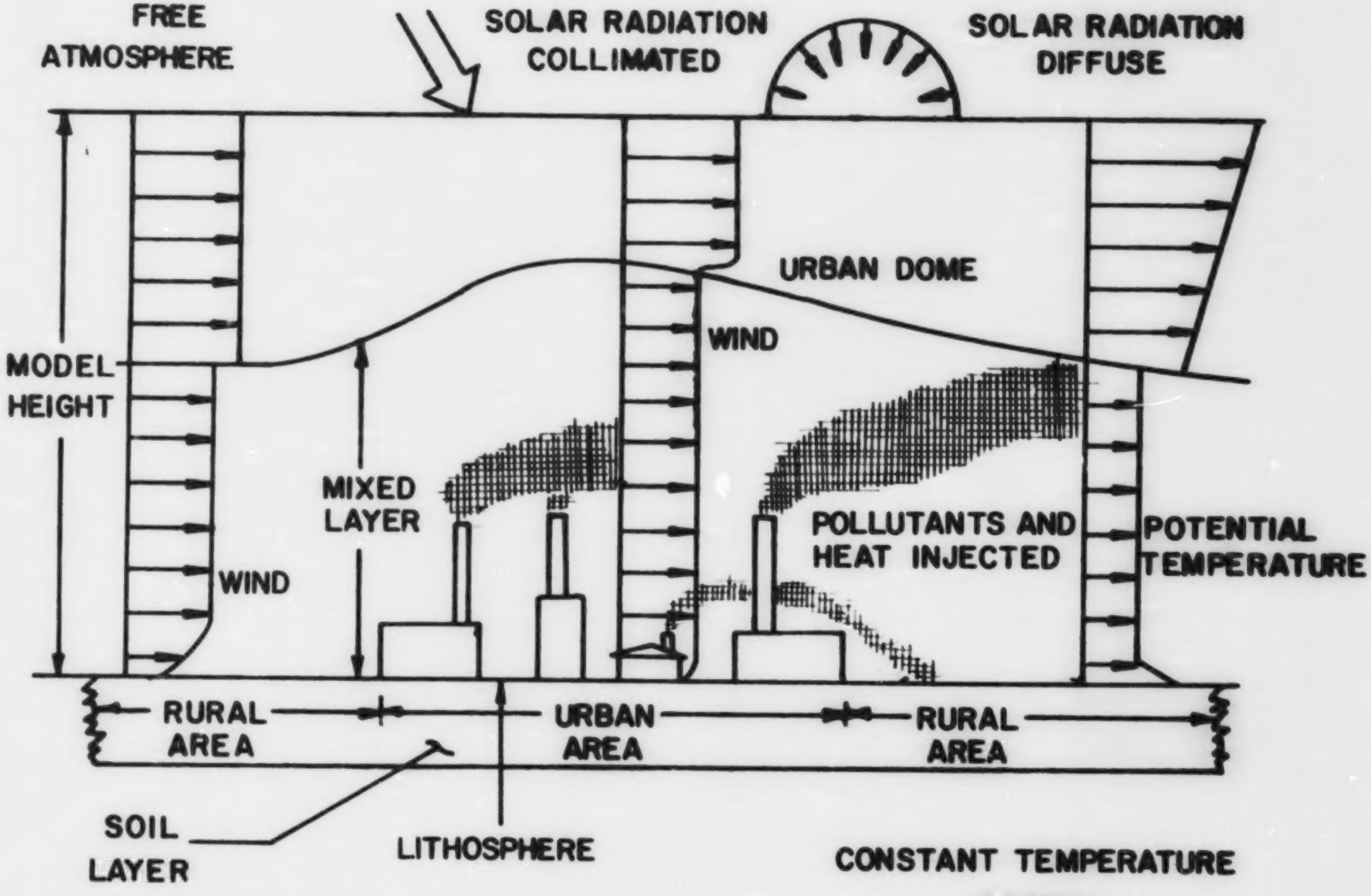
FREE ATMOSPHERE
SOLAR RADIATION COLLIMATED
SOLAR RADIATION DIFFUSE
MODEL HEIGHT
URBAN DOME
WIND
MIXED LAYER
POLLUTANTS AND HEAT INJECTED
POTENTIAL TEMPERATURE
WIND
RURAL AREA
URBAN AREA
RURAL AREA
SOIL LAYER
LITHOSPHERE
CONSTANT TEMPERATURE REGION

Figure 4.1 Schematic of Earth-Atmosphere System

thermal radiation. The distribution of energy in the atmosphere is accomplished through convection, radiation and turbulent diffusion. The atmosphere also emits thermal radiation part of which is absorbed at the air-soil interface. During the night, the earth's surface cools in the absence of solar irradiation. Thus, the soil-atmosphere system goes through a diurnal cycle of heating during the day, and cooling during the night. These variations in air temperature and thermal stratification, in turn, affect the velocity, moisture and pollutant concentration fields through changes in intensity of turbulent mixing.

4.2 Formulation of Model Equations

In deriving the conservation equations the following assumptions are made:

1) The transport processes are two-dimensional, i.e., all the variables are functions only of the vertical co-ordinate z and one horizontal co-ordinate x, and are independent of the co-ordinate y. Clearly, the assumption of two-dimensionality is not very realistic in view of the fact that turbulence is a three dimensional phenomenon. However, this model does not attempt to resolve turbulent motion; turbulence effects are parameterized with the turbulent diffusivity. Thus, this assumption depends on whether the urban-rural system can be considered to be one-dimensional, i.e., the urban-rural characteristics vary only along the x-co-ordinate. It is clear that realistic city parameters would vary in two dimensions giving rise to three-dimensional flow effects. Although it is not clear how important three-dimensional circulation patterns are, it is felt that the two-dimensional model is capable of providing understanding of the most important urban effects. The inclusion of the third dimension in addition to increasing the complexity of the problem would have increased the computer time as well as storage by a few orders of magnitude.

2) Atmosphere is hydrostatic. This approximation has been used in several heat island studies (Estoque, 1963; Estoque and Bhumralkar,

1969) and is valid when the horizontal scales are much larger than the vertical scales. It allows the calculation of the pressure distribution from a knowledge of the temperature distribution.

3) The Boussinesq approximations are applicable to the boundary layer. The approximations can be summarized by the statements: 1) Density fluctuations result principally from thermal effects rather than pressure effects, and 2) density variations in the mass and momentum conservation equations may be neglected except when they are coupled to the gravitational acceleration in the buoyancy force. Spiegel and Veronis (1960) have shown that the Boussinesq approximations are valid when the fluid layer under consideration is confined to a thickness which is much smaller than the minimum of the scale heights of the atmospheric variables. Furthermore, it is necessary that the motion-induced fluctuations do not exceed, in order of magnitude, the static variations of the variables. The conditions mentioned are satisfied in the atmospheric boundary layer. An important consequence of the approximations is that the continuity equation reduces to the incompressible form. This together with the hydrostatic assumption, allows the calculation of the vertical velocity from the continuity equation.

4) The viscous dissipation term in the energy balance can be neglected. It can be easily shown (Spiegel and Veronis, 1960) that this assumption is valid at the relatively low velocities found in the atmosphere.

5) In applying the equation of radiative transfer to the planetary boundary layer, the atmosphere is considered to be horizontally homogeneous--the radiation model is one-dimensional. As an accurate solution of the one-dimensional transfer equation requires substantial computer time, it would be impractical and presently unwarranted in terms of computer time and storage to use a two-dimensional radiation model.

6) Energy transfer in the soil layer is one-dimensional. As the horizontal temperature gradients are much smaller than the vertical temperature gradients, conduction in the horizontal direction

can be neglected in comparison to that in the vertical direction; the energy equation reduces to the one-dimensional diffusion equation.

With the preceding assumptions the governing equations can be written as (Estoque, 1973)

Planetary Boundary Layer

x-momentum:

$$\frac{\partial u}{\partial t} + u\frac{\partial u}{\partial x} + w\frac{\partial u}{\partial z} = fv - \frac{1}{\rho}\frac{\partial p}{\partial x} + \frac{1}{\rho}\frac{\partial \tau_x}{\partial z} + \frac{\partial}{\partial x}\left(K_x\frac{\partial u}{\partial x}\right) \qquad (4.2.1a)$$

y-momentum:

$$\frac{\partial v}{\partial t} + u\frac{\partial v}{\partial x} + w\frac{\partial v}{\partial z} = -fu - \frac{1}{\rho}\frac{\partial p}{\partial y} + \frac{1}{\rho}\frac{\partial \tau_y}{\partial z} + \frac{\partial}{\partial x}\left(K_x\frac{\partial v}{\partial x}\right) \qquad (4.2.1b)$$

Continuity:

$$\frac{\partial u}{\partial x} + \frac{\partial w}{\partial z} = 0 \qquad (4.2.1c)$$

Energy:

$$\frac{\partial \theta}{\partial t} + u\frac{\partial \theta}{\partial x} + w\frac{\partial \theta}{\partial z} = -\frac{\partial F_\theta}{\partial z} + \frac{\partial}{\partial x}\left(K_x\frac{\partial \theta}{\partial x}\right) + S_\theta \qquad (4.2.1d)$$

Water Vapor:

$$\frac{\partial C_w}{\partial t} + u\frac{\partial C_w}{\partial x} + w\frac{\partial C_w}{\partial z} = \frac{\partial}{\partial z}\left(K_M\frac{\partial C_w}{\partial z}\right) + \frac{\partial}{\partial x}\left(K_x\frac{\partial C_w}{\partial x}\right) + \dot{C}_w \qquad (4.2.1e)$$

Pollutant Concentration (Species):

$$\frac{\partial C_n}{\partial t} + u\frac{\partial C_n}{\partial x} + w\frac{\partial C_n}{\partial z} = -\frac{\partial F_{C_n}}{\partial z} + \frac{\partial}{\partial x}\left(K_x\frac{\partial C_n}{\partial x}\right) + \dot{S}_{C_n};$$

$$n = 1, 2, \ldots, N \qquad (4.2.1f)$$

Hydrostatic Equilibrium (z-momentum):

$$\frac{\partial p}{\partial z} = -\rho g \qquad (4.2.1g)$$

Equation of state:

$$p = \rho RT \tag{4.2.1h}$$

Soil Layer

Energy equation:

$$\frac{\partial T_s}{\partial t} = \alpha_s \frac{\partial^2 T_s}{\partial z^2} \tag{4.2.1i}$$

In Eqs. (4.2.1a) and (4.2.1b) τ_x and τ_y are the turbulent momentum fluxes, F_θ and F_{c_n} are the turbulent heat and pollutant fluxes, respectively, S_θ and S_{c_n} are the internal sources of heat and pollutants, and $\dot{C}_w$ is the volumetric rate of water vapor generation. The turbulent fluxes and the source term in the energy equation are given by,

$$\tau_x = \rho K_M \,\partial u/\partial z \tag{4.2.2a}$$

$$\tau_y = \rho K_M \,\partial v/\partial z \tag{4.2.2b}$$

$$F_\theta = -K_H(\partial\theta/\partial z - \gamma_c) \tag{4.2.2c}$$

$$F_{c_n} = -K_c \,\partial C_n/\partial z \tag{4.2.2d}$$

$$S_\theta = -(p_0/p)^{R/c_p} \frac{\partial F}{\partial z} + \dot{H}_p \tag{4.2.2e}$$

In Eq. (4.2.2c), γ_c is a small positive quantity which accounts for the countergradient heat flow often observed in the atmosphere. On the basis of Telford and Warner's observations (1966), Deardorff recommends a value of 0.7×10^{-3} K/m for γ_c.

4.3 Boundary Conditions

The boundary conditions are specified at the top and bottom of the atmospheric layer under consideration. At this point it is necessary to distinguish between the top of the atmospheric layer and the top of the boundary layer. The top of the atmospheric layer is the height of the last vertical grid point which is placed around 2 km. The top of the planetary boundary layer, on the other hand, is a function of space and time, and varies from a minimum of about 200 meters to a maximum of about 1500 meters. The definition of the boundary layer height will be discussed in following sections. It is appropriate to mention here that the top of the atmospheric layer serves as a maximum bound on the height of the boundary layer.

At the earth's surface ($z = z_0$) the boundary conditions are:

$$u = v = w = 0 \tag{4.3.1a}$$

$$T = T_0(x,t) \tag{4.3.1b}$$

$$C_w = C_{w_0}(x,t) \tag{4.3.1c}$$

$$C_n = C_{n_0}(x,t) \tag{4.3.1d}$$

The ground temperature $T_0(x,t)$ is calculated from an energy balance at the earth's surface,

$$F_1 - F_2 + F_3 - F_4 - F_5 - F_6 = 0 \tag{4.3.2}$$

where

F_1 - thermal (longwave) emission from the ground

F_2 - atmospheric eddy transfer of sensible and latent heat

F_3 - soil heat flux

F_4 - atmospheric thermal radiation flux due to water vapor, carbon dioxide, and pollutant gases and aerosols

F_5 - incident solar radiation flux absorbed at the surface

F_6 - anthropogenic heat flux

The expressions for the fluxes can be written as

$$F_1 = \varepsilon_t \sigma T_o^4 \qquad (4.3.3a)$$

$$F_2 = \rho_a c_{pa} K_H \left[\frac{\partial\theta}{\partial z} - \gamma_c\right]_o + L_H K_c \left.\frac{\partial C_w}{\partial z}\right|_o \qquad (4.3.3b)$$

$$F_3 = -k_s \left.\frac{\partial T_s}{\partial z}\right|_o \qquad (4.3.3c)$$

$$F_4 = \varepsilon_t F_t^-(0) \qquad (4.3.3d)$$

$$F_5 = (1 - r_s)\, F_s^-(0) \qquad (4.3.3e)$$

The surface water vapor concentration is calculated by postulating that the ratio of the actual evaporation rate to the potential evaporation rate is a constant (Halstead, et al., 1957). Then, assuming that the water vapor potential causing evaporation can be represented by the difference in water vapor concentrations between the surface and the first grid point one can write

$$H = [C_w(z_1) - C_{wo}]/[C_w(z_1) - C_{wsat}] \qquad (3.3.5)$$

where $C_w(z_1)$ is the water vapor concentration at the first grid point, and C_{wsat} is the water vapor concentration at the surface for saturation conditions. The ratio of the actual evaporate rate to the potential evaporation rate, H, is called the Halstead moisture parameter and ranges from unity for evaporation over water to zero for dry soil.

It should be pointed out that the modeling of evaporation by way of the Halstead moisture parameter is at best a very rough approximation to the actual physical process of evapotranspiration. This approach completely ignores the important role the soil plays in controlling the rate of evaporation; it assumes that the soil offers no resistance to the water which is transported through it and which eventually evaporates at the soil-air interface. Also, the Halstead moisture parameter approximation does not allow for the drying out of the soil. This model for evaporation was used only because other simple models are not significantly better. Manabe's (1969) model assumes that there is a finite amount of water in the soil. This water is depleted as evaporation takes place at a rate proportional to the amount of water left in the soil. Although this approach allows for the drying out of the soil, it also ignores soil resistance. Although more detailed models for predicting evaporation from the earth's surface are available (Philips, 1957), their applicability to the problem under consideration is limited because the heterogeneity of the urban soil layer does not allow calculation of "average" soil properties such as permeability, moisture potential, etc.

The surface pollutant concentration is given by specifying the pollutant source M_{C_n} as follows

$$M_{C_n} = -K_c \, \partial C_n/\partial z \quad \text{at} \quad z = 0 \quad . \tag{4.3.6}$$

Elevated pollutant sources are modeled by source terms $\dot{S}_{C_n}$ in the pollutant species equations.

At the bottom of the soil layer the temperature is taken to be a constant

$$T_s(x,z,t) = \text{constant} \quad \text{at} \quad z = -z_\Delta \tag{4.3.7}$$

The boundary conditions at the top of the atmospheric layer (z = H) are specified by requiring the values of the atmospheric variables to remain constant, i.e.,

$$u = u_g \tag{4.3.8a}$$

$$v = v_g \tag{4.3.8b}$$

$$\theta = \theta_g \tag{4.3.8c}$$

$$C_w = C_{wg} \tag{4.3.8d}$$

$$C_n = C_{ng} \tag{4.3.8e}$$

Boundary conditions (4.3.8) are consistent with the notion the variables u_g, v_g, θ_g, C_{wg} and C_{ng} associated with the large scale weather system do not vary significantly over the time scale of simulation.

In the free atmosphere the flow is assumed to be geostrophic so that the pressure gradients at z = H can be replaced by

$$\left.\frac{\partial p}{\partial x}\right|_H = \rho f v_g \tag{4.3.9a}$$

$$\left.\frac{\partial p}{\partial y}\right|_H = -\rho f u_g \tag{4.3.9b}$$

As the boundary layer does not extend to heights greater than 2000 m, the geostrophic balance at z = H is not affected by boundary layer turbulence.

Since $[\partial p/\partial x]_H$ is a constant, the pressure along x at z = H is given by

$$p(x,H) = p(0,H) + \left[\frac{\partial p}{\partial x}\right]_H x \tag{4.3.10}$$

where p(0,H) is specified.

The lateral boundary conditions were assumed to be periodic in the x-direction, i.e., the atmospheric variables have the same values at the beginning and the end of the urban-rural system. Physically, the boundary condition means that at distances far enough from the urban area the atmospheric variables attain values which are not significantly different from those at large distances upwind of the urban complex. Clearly, the formulation of the periodic boundary condition assumes that there are sinks of energy and pollutants between the end of the urban area and the end of the rural area.

The imposition of periodic boundary conditions forces pollutant concentrations to build up over the urban rural system. Although this situation might be unrealistic in general, it represents stagnating conditions during which pollution episodes occur. As the earth-atmosphere interface can absorb momentum as well as energy, the velocity and temperature yields are not expected to be affected by the conservation effects periodic boundary conditions tend to introduce. Thus, the numerical scheme accounts for advection effects on the velocity and temperature fields and at the same time avoids the difficulties associated with inflow and outflow boundary conditions (Roache, 1972). It should be mentioned that Orlanski, et al. (1974) have studied heat island formation using a model with periodic boundary conditions.

The upstream variables are calculated from the one-dimensional conservation equations. Then, the downstream variables are updated by

$$\psi_d (L,z) = \psi_u(0,z) \tag{4.3.11}$$

where ψ_d and ψ_u represent the downstream and upstream variables respectively, and $x = L$ denotes the end of the urban-rural system.

The specification of the initial conditions will be discussed in a later section. With suitable initial conditions and the boundary conditions described in the preceding paragraphs, the formulation of the problem will be complete when the eddy diffusivities and the divergence of the radiative flux are known. The computation of eddy diffusivities and the radiative fluxes will be discussed in detail in chapters describing the turbulence and the radiation models used in this study.

4.4 Parameterization of Urban-Rural Differences

From the point of view of the numerical model it is necessary to describe the difference between the urban and rural areas in terms of parameters. The roughness height is used to parameterize the variation of the height of structures in the urban-rural system. The tall buildings in the urban area are associated with relatively large values of roughness length. Since the roughness length serves as the mixing length for the calculation of the turbulent kinetic energy at the surface, a larger roughness length would predict a larger generation of turbulent kinetic energy. This increased turbulent kinetic energy would be reflected as larger diffusivities which would be responsible for the slowing of the wind velocities over the urban area.

The dryness of the urban area relative to that of the rural area is modeled in terms of smaller values of the Halstead moisture parameter. As there were no studies to guide the selection of the moisture parameters, values were fixed by numerical experimentation.

Although cities are constructed with materials which are lighter (Bray, et al., 1966) in the solar spectrum than the foliage and soil of the surrounding countryside, the trapping effect of buildings can lead to an overall lower solar albedo for the urban area (Craig and Lowry, 1972). This study assumed that the albedo of the urban area was lower than that of the rural area.

As the urban area is the main source of pollutants and heat, it was assumed that the heat and pollutant sources were distributed only in the urban area. The pollutant sources were elevated and their strength was allowed to vary sinusoidally, increasing during the day, and decreasing after nightfall.

The values and the distribution of the urban-rural parameters can be found in Chapter VIII.

4.5 One-Dimensional Model

An examination of the objectives of this investigation showed that it was possible to achieve some of them with a one-dimensional model. As the major emphasis of the one-dimensional simulations was on the radiative effects of pollutants, there was some justification in assuming that the atmosphere is horizontally homogeneous. Pollutants are most likely to have the greatest effect on the thermal structure through radiative participation when convective motions are small--stagnating high pressure centers with light winds. Thus, the simulations performed with a horizontally homogeneous (1-D) model would represent situations in which pollutants would play a significant role in determining the thermal structure.

The highly nonlinear nature of the governing differential equations raised the possibility of errors being introduced by the numerical scheme used to solve them. It is well known (Roache, 1972) that the presence of the nonlinear advective terms in the two-dimensional equations can lead to serious difficulties in the construction of a satisfactory numerical method. Even if the method is stable, there is always the possibility of numerical errors becoming as large as physical effects. On the other hand, one-dimensional numerical schemes are relatively simple, and can be "checked out" with no difficulty. Thus, it was felt that the relatively error-free one-dimensional numerical method was better suited to investigate radiative effects whose magnitudes are usually very small.

In this section, the one-dimensional model equations will be presented, and the special numerical techniques used in their solution will be described.

The one-dimensional model equations are:

x-momentum:

$$\frac{\partial u}{\partial t} = \frac{\partial}{\partial z}\left(K_M \frac{\partial u}{\partial z}\right) + f(v - v_g) \qquad (4.5.1)$$

y-momentum:

$$\frac{\partial v}{\partial t} = \frac{\partial}{\partial z}\left(K_M \frac{\partial v}{\partial z}\right) - f(u - u_g) \qquad (4.5.2)$$

Energy:

$$\frac{\partial \theta}{\partial t} = \frac{\partial}{\partial z}\left[K_H \left(\frac{\partial \theta}{\partial z} - \gamma_c\right)\right] - \frac{1}{\rho c_p}\left(\frac{p_o}{p}\right)^{R/c_p} \frac{\partial F}{\partial z} \qquad (4.5.3)$$

Species (Pollutants and Water vapor):

$$\frac{\partial C_n}{\partial t} = \frac{\partial}{\partial z}\left(K_c \frac{\partial C_n}{\partial z}\right) + \dot{S}_{C_n}, \quad n = 1, 2, \ldots, N \qquad (4.5.4)$$

The rest of the equations and the boundary conditions remain unchanged from the two-dimensional model.

Equations (4.2.1) and (4.2.2) can be combined into one equation by defining a complex variable w*

$$w^* = (u - u_g) + i(v - v_g) \tag{4.5.5}$$

Multiplying Eq. (3.5.2) by i, and adding Eq. (3.5.2) one obtains a single equation for w*

$$\frac{\partial w^*}{\partial t} + ifw^* = \frac{\partial}{\partial z}\left(K_M \frac{\partial w^*}{\partial z}\right) \tag{4.5.6}$$

At first glance, it seems that the introduction of w* would simplify the computational process considerably. However, it should be noticed that the numerical solution of w* involves complex arithmetic; the mathematical operations required are not much different from that needed in the solution of the two Eqs. (4.5.1) and (4.5.2). The main advantage of defining w* is the programming simplicity it affords. Furthermore, it will be shown later that the implicit finite difference equation for the linearized form of Eq. (4.5.6) is unconditionally stable.

Further, programming facility can be obtained by combining the aerosol and gas concentrations into a single complex variable. The special form of the boundary conditions for the potential temperature and the water vapor concentration did not allow a similar conversion into a complex variable.

The finite difference approximations employed in the numerical solution of the one-dimensional model equations can be illustrated by considering the following equation

$$\frac{\partial \phi}{\partial t} = \frac{\partial}{\partial z}\left(K \frac{\partial \phi}{\partial z}\right) + S_\phi \tag{4.5.7}$$

where ϕ represents the variables of the model, and S_ϕ denotes terms containing first order derivatives. Then, the finite difference approximations for the terms in Eq. (3.5.7) can be written as

$$\frac{\partial\phi}{\partial t} \approx \left(\phi_j^{n+1} - \phi_j^n\right)/\Delta t \qquad (4.5.8a)$$

$$\frac{\partial}{\partial z}\left(K\frac{\partial\phi}{\partial z}\right) \approx \frac{2}{\left(z_{j+1} - z_{j-1}\right)}\left[\frac{K_1\left(\phi_{j+1}^{n+1} - \phi_j^{n+1}\right)}{\left(z_{j+1} - z_j\right)} - \frac{K_2\left(\phi_j^{n+1} - \phi_{j-1}^{n+1}\right)}{\left(z_j - z_{j-1}\right)}\right] \qquad (4.5.8b)$$

In the above approximations j denotes the j-th grid point counted vertically upwards, and n denotes n-th time step. Thus, ϕ_j^n represents the value of the variable ϕ at the n-th time step and located at the j-th vertical grid point. Further

$$K_1 \equiv (K_{j+1} + K_j)/2 \qquad (4.5.9a)$$

and

$$K_2 \equiv (K_j + K_{j-1})/2 \qquad (4.5.9b)$$

The first derivative terms in ϕ are represented as

$$\frac{\partial\phi}{\partial z} \approx a_1(\phi_{j+1} - \phi_j) + a_2(\phi_j - \phi_{j-1}) \qquad (4.5.10)$$

where

$$a_1 = \frac{(z_j - z_{j-1})}{(z_{j+1} - z_j)(z_{j+1} - z_{j-1})} \qquad (4.5.11a)$$

$$a_2 = \frac{(z_{j+1} - z_j)}{(z_j - z_{j-1})(z_{j+1} - z_{j-1})} \qquad (4.5.11b)$$

It is noted that the finite difference scheme is first order accurate in time, and second order in space. A second order accurate scheme in time was initially used but abandoned when it was found that the solution oscillated. It can be easily shown (Roache, 1972) that the finite difference method used in this study is unconditionally stable when the eddy diffusivity is a constant. However, it should be stated that no definite conclusions about the stability of the system can be drawn when the eddy diffusivity is an arbitrary function of space and time. The presence of nonlinear source terms in the diffusion equation can also complicate convergence and stability studies.

The application of the finite difference approximations at the grid points results in a tridiagonal matrix which can be very efficiently solved using the Thomas algorithm (Rosenberg, 1969).

4.6 Stability and Numerical Accuracy of the 1-D Momentum Equations

An examination of the momentum equations (4.5.1) and (4.5.2) shows that a finite difference representation of the equations would contain the source terms, $f(v - v_g)$ and $-f(u - u_g)$. As these source terms have to be considered to remain constant over the time step of integration, it is not possible to ensure stability for large time steps. One solution to this problem of stability is to introduce the complex variable w^* as has been done in Eq. (4.5.6). It will be theoretically shown in this section that the finite difference representation of Eq. (4.5.6) is unconditionally stable. Also, as a check on the stability and the convergence of the numerical scheme, the classical Ekman layer solution will be compared against the steady state numerical solution of the finite difference equation for w^*. This examination of the momentum equations will help to validate the numerical schemes used in the solution of the other model equations which are all similar in form to the momentum equations.

The linearized form of Eq. (4.5.6) can be written as

$$\frac{\partial w^*}{\partial t} + ifw^* = K \frac{\partial^2 w^*}{\partial z^2} \qquad (4.6.1)$$

The insertion of the finite difference approximations of Section 4.1 into Eq. (4.2.1) results in

$$w_j^{n+1} - w_j^n + ifw_j^{n+1}\Delta t = a\Delta t(w_{j+1}^{n+1} - w_j^{n+1})$$
$$-b\Delta t(w_j^{n+1} - w_{j-1}^{n+1}) \qquad (4.6.2)$$

The stars (*) have been dropped for convenience, and a and b are given by

$$a \equiv 2K/[(z_{j+1} - z_j)(z_{j+1} - z_{j-1})] \qquad (4.6.3a)$$

$$b \equiv 2K/[(z_j - z_{j-1})(z_{j+1} - z_{j-1})] \qquad (4.6.3b)$$

Rearranging Eq. (3.2.2) one obtains

$$w_j^{n+1}(1 + if\Delta t + a\Delta t + b\Delta t) - a\Delta tw_{j+1}^{n+1} - b\Delta tw_{j-1}^{n+1} = w_j^n \qquad (4.6.4)$$

For simplicity it is assumed that the distances between the grid points are equal. The stability analysis for unequal grid spacing involves a great deal of algebra; but it can be proved that the system is still unconditionally stable. The results of a numerical experiment will lend additional justification to this statement.

Decomposing w into a Fourier series, one can write each mode of the series as

$$w_j^{n+1} = \tilde{w}^{n+1} e^{ik_z j\Delta z} \qquad (4.6.5a)$$

$$w_{j+1}^{n+1} = \tilde{w}^{n+1} e^{ik_z (j+1)\Delta z} \qquad (4.6.5b)$$

$$w_{j-1}^{n+1} = \tilde{w}^{n+1} e^{ik_z (j-1)\Delta z} \qquad (4.6.5c)$$

$$w_j^n = \tilde{w}^n e^{ik_z \Delta z} \qquad (4.6.5d)$$

where Δz is the vertical grid spacing, and w^{n+1} and w^n are the complex amplitudes corresponding to the wavenumber k_z at the $(n+1)^{th}$ and n^{th} time step respectively.

Substituting Eqs. (4.6.5) into Eq. (4.6.4) one obtains

$$\tilde{w}^{n+1}[(1 + if\Delta t + 2a\Delta t) - a\Delta t(e^{i\theta} + e^{-i\theta})] = \tilde{w}^n \tag{4.6.6}$$

where

$$\theta \equiv ik_z\Delta z \tag{4.6.7}$$

Then,

$$\tilde{w}^{n+1}/\tilde{w}^n = 1/[1 + if\Delta t + 2a\Delta t(1 - \cos\theta)] \tag{4.6.8}$$

The amplication factor G is given by

$$G = 1/[1 + if\Delta t + 2a\Delta t(1 - \cos\theta)] \tag{4.6.9}$$

Then, to prove that the system is unconditionally stable, it is required to show that the amplitude of G is less than or equal to unity for all values of θ. It is easily seen that this condition is satisfied, as the minimum value (modulus) of the denominator of the amplification factor is greater than unity.

As a final check on the stability of the system, a numerical experiment was conducted. The analytical solution of the following problem was used as a basis for comparison against the numerical solution of Eq. (4.5.6).

The differential equation under consideration was

$$\frac{\partial w^*}{\partial t} + ifw^* = K\frac{\partial^2 w^*}{\partial z^2} \tag{4.6.6}$$

and the boundary conditions were chosen to be

$$w^* = -(u_g + iv_g); \quad z = 0 \tag{4.6.11a}$$

$$w^* = 0 \quad ; \quad z = h \tag{4.6.11b}$$

It is easy to see that in terms of the u and v velocities, boundary conditions (4.6.11a) and (4.6.11b) reduce to

$$u = v = 0; \quad z = 0 \qquad (4.6.11c)$$

$$u = u_g,\ v = v_g; \quad z = h \qquad (4.6.11d)$$

The solution of Eq. (4.5.6) with B.C's (4.6.11a) and (4.6.11b) is straightforward and is given by

$$\begin{aligned} u - u_g = \Big\{ & (-u_g \cos az + v_g \sin az)e^{-a(z+2h)} \\ & + (u_g \cos a(2h - z) - v_g \sin a(2h - z))e^{-a(z+2h)} \\ & + (u_g \cos a(z - 2h) - v_g \sin a(z - 2h))e^{a(z-2h)} \\ & + (-u_g \cos az - v_g \sin az)e^{-az}\Big\}/D \end{aligned} \qquad (4.6.12a)$$

$$\begin{aligned} v - v_g = \Big\{ & (-u_g \sin az - v_g \cos az)e^{-a(4h-z)} \\ & + (u_g \sin a(2h-z) + v_g \cos a(2h-z))e^{-a(z+2h)} \\ & + (u_g \sin a(z - 2h) + v_g \cos a(z - 2h))e^{a(z-2h)} \\ & + (u_g \sin az - v_g \cos az)e^{-az}\Big\}/D \end{aligned} \qquad (4.6.12b)$$

where

$$D \equiv e^{-4ah} - -2e^{-2ah} \cos 2ah + 1 \qquad (4.6.13a)$$

$$a \equiv \sqrt{f/2K} \qquad (4.6.13b)$$

The solution has been expressed in terms of u and v to facilitate comparison with the numerical solution.

Table 4.1 Comparison of Numerical Solutions of the Momentum Equations with Exact Solution

Vertical Height z (m)	Exact Solution		Numerical Solution Δt = 150 s		Numerical Solution Δt = 300 s	
	u	v	u	v	u	v
0	0	0	0	0	0	0
1.0	.00349	.01903	.00346	.01905	.00346	.01905
5.0	.01762	.09493	.01744	.09500	.01744	.09500
10.0	.03562	.18929	.03526	.18942	.03526	.18942
20.0	.07271	.37629	.07199	.37654	.07199	.37654
30.0	.11125	.56099	.11017	.56137	.11017	.56137
40.0	.15118	.74341	.14975	.74391	.14975	.74391
50.0	.19248	.92355	.19069	.92418	.19069	.92418
100.0	.41822	1.79043	.41535	1.79150	.41535	1.79150
200.0	.95241	3.35880	.95135	3.35940	.95135	3.35940
300.0	1.57119	4.71573	1.57158	4.71572	1.57158	4.71572
400.0	2.24740	5.87357	2.24890	5.87294	2.24890	5.87284
500.0	2.95785	6.84579	2.96017	6.84432	2.96017	6.84432
600.0	3.68309	7.64657	3.68597	7.64438	3.68597	7.64438
700.0	4.40706	8.29039	4.41028	8.28755	4.41028	8.28755
800.0	5.11688	8.79171	5.12026	8.78829	5.12026	8.78829
900.0	5.80248	9.16470	5.80588	9.16083	5.80588	9.16083
1000.0	6.45640	9.42307	6.45970	9.41886	6.45970	9.41886
1100.0	7.07342	9.57989	7.07655	9.57546	7.07655	9.57546
1200.0	7.65041	9.64749	7.65330	9.64298	7.65330	9.64298
1300.0	8.18599	9.63741	8.18859	9.63294	8.18859	9.63294
1400.0	8.68035	9.56036	8.68264	9.55606	8.68264	9.55606
1500.0	9.13500	9.42623	9.13698	9.42221	9.13698	9.42221
1600.0	9.55261	9.24412	9.55429	9.24047	9.55429	9.24047
1700.0	9.93682	9.02238	9.93819	9.01921	9.93819	9.01921
1800.0	10.29205	8.76872	10.29313	8.76608	10.29313	8.76608
1900.0	10.62335	8.49023	10.62415	8.48820	10.62415	8.48820
2000.0	10.93629	8.19356	10.93681	8.19218	10.93681	8.19218
2100.0	11.23678	7.88498	11.23704	7.88428	11.23704	7.88428
2200.0	11.53100	7.57050	11.53100	7.57050	11.53100	7.57050

The parameters chosen for the numerical experiment were,

$$f = 10^{-4}\ \mathrm{sec}^{-1};\ K = 50\ \mathrm{m}^2/\mathrm{sec};\ h = 2200\ \mathrm{m};$$

$$u_g = 11.531\ \mathrm{m/sec};\ v_g = 7.5705\ \mathrm{m/sec} \qquad (4.6.14)$$

The velocities were initialized with arbitrary logarithmic profiles, and the transient numerical solution was allowed to approach steady state. Three time steps were used: Δt = 75 s, 150 s and 300 s. All the three solutions converged to the same steady state solution (to the fifth decimal place) within fifty interations. The results of the numerical experiments are presented in Table 4.1. In addition to showing the stability of the system (nonlinear grid spacing) the results also reveal the accuracy of the numerical scheme. It is seen that the numerical scheme is accurate to within 1.1 percent of the analytical solution. The maximum error occurs at the third grid point (5 m) where the small velocities and the relatively large gradients are most likely to give rise to errors. It is felt that this error is well within the acceptable limits for this type of study in which trends rather than numerically precise results are more significant.

4.7 Numerical Scheme for Two-Dimensional Model

The two-dimensional model equations can be represented by the following general form:

$$\frac{D\phi}{Dt} \equiv \frac{\partial\phi}{\partial t} + u\frac{\partial\phi}{\partial x} + w\frac{\partial\phi}{\partial z} = \frac{\partial}{\partial z}\left(K_z\frac{\partial\phi}{\partial z}\right) + \frac{\partial}{\partial x}\left(K_x\frac{\partial\phi}{\partial x}\right) + S(\phi) \qquad (4.7.1)$$

where ϕ represents the model variables.

As the accuracy of the results of a numerical investigation are determined by the numerical method used, the selection of a suitable numerical technique is very important. A number of numerical methods for solving equations of the type presented above are available in the literature (Roache, 1972; Rosenberg, 1969). These methods can be classified into two broad categories, implicit and explicit. Explicit methods are "one step" methods in which a variable is advanced to a new time level using only information from the previous time step. Thus, the updating of a variable involves the solution of a linear algebraic equation with one unknown, and the computational requirement is very small. Explicit methods can be made very accurate, and at the same time they can be designed to obey important conservation laws (Roache, 1972). It is clear that the utility of a numerical method is limited if it does not conserve quantities like kinetic energy and momentum. From a numerical viewpoint, it is important to use a conservative method to avoid nonlinear advective instability (Lilly, 1965). In order to take advantage of these desirable features of explicit methods, certain stringent restrictions have to be placed on the time steps and the grid spacing to keep the solution stable. These restrictions are functions of the nonlinear coefficients in the differential equations, and although in principal it is possible, it is not always practical to use time steps and grid spacing determined by the stability condition of the particular explicit numerical method. In addition to being variable (as they are dependent on the time varying coefficients), time steps can become so small that the total number of computational steps required to integrate a variable over a time interval can become large enough to make computer time requirements prohibitive.

Implicit schemes approximate the advective and the diffusion terms in the conservation equations in terms of the variables at the new step. Thus, it is necessary to solve a system of algebraic equations to obtain the values of the variables at the new time step. It is clear that implicit methods are computationally more complex than explicit methods; however, most implicit schemes are unconditionally stable and thus for a given grid size it is possible to use time steps which are large enough to make the total computer time smaller than that required for an explicit scheme. It should be mentioned that implicit schemes are not conservative, and considerably more numerical complexity is required to obtain the degree of accuracy of an explicit scheme.

Experimentation with several explicit methods showed that it was impractical from the point of view of computer time to use the time steps required by the stability conditions. Thus, implicit techniques were examined, and the method selected is based on the time-splitting method due to Marchuk (1965). The familiar alternating direction finite-difference method (Roache, 1972) was not used because the explicit differencing of the terms during each half time step gave rise to oscillations with large time steps. On the other hand, the implicit differencing of the time-split equations kept the solution stable for relatively large time intervals. Essentially, time-splitting consists of "splitting" the integration of a two-dimensional (or three-dimensional) differential equation into one-dimensional steps. Then, the steps involved in the integration of Eq. (4.4.1) are represented by

$$\frac{\partial \phi}{\partial t} + u \frac{\partial \phi}{\partial x} = \frac{\partial}{\partial x}\left(K_x \frac{\partial \phi}{\partial x}\right) \tag{4.7.2a}$$

$$\frac{\partial \phi}{\partial t} + w \frac{\partial \phi}{\partial z} = \frac{\partial}{\partial z}\left(K_z \frac{\partial \phi}{\partial z}\right) + S(\phi) \tag{4.7.2b}$$

Equation (4.7.2a) is solved first, and the solution obtained serves as an input to Eq. (4.7.2b). The result of the integration of Eqs. (4.7.2a) and (4.7.2b) is the final solution; no meaning is attached to the intermediate solution. The validity of these operations is intuitively clear; theoretical justification can be found in the paper by Marchuk (1965).

It is noticed that Eqs. (4.4.2a) and (4.4.2b) can be solved using implicit finite-difference schemes. The finite-difference representation of Eq. (4.4.2a) can be written as

$$\frac{\phi_{i,j}^{n+1} - \phi_{i,j}^{n}}{\Delta t} + \left(u \frac{\partial \phi}{\partial x}\right)_{i,j}^{n+1} = \left[\frac{\partial}{\partial x}\left(K_x \frac{\partial \phi}{\partial x}\right)\right]_{i,j}^{n+1} \tag{4.7.3}$$

where $\phi^n_{i,j}$ represents the value of ϕ located at (x_i, z_j, t_n), and

$$\left(u \frac{\partial\phi}{\partial x}\right)^{n+1}_{i,j} = \left(u_{1i}\ \phi^{n+1}_{i,j} - u_{2i}\ \phi^{n+1}_{i-1,j}\right)/\Delta x \tag{4.7.4a}$$

$$u_{1i} \equiv \left(u^n_{i+1,j} + u^n_{i,j}\right)/2 \tag{4.7.4b}$$

$$u_{2i} \equiv \left(u^n_{i-1,j} + u^n_{i,j}\right)/2 \tag{4.7.4c}$$

The finite-difference analog for the diffusion term, $\frac{\partial}{\partial x}\,[(K_x \frac{\partial\phi}{\partial x})]$, can be written in the same manner as that for the term $\frac{\partial}{\partial z}\,[(K_z \frac{\partial\phi}{\partial z})]$ which has already been described before.

The method used to finite-difference the advective term $u\ \partial\phi/\partial x$ was motivated by a conservative explicit scheme for the advection equation. It is noticed that the finite-difference method is second order accurate in space, and first order in time.

With the exception of the term $w\ \partial\phi/\partial z$, the finite-difference analogs of the terms of Eq. (4.7.2b) have already been discussed in Section (4.5). The advective term $w\ \partial\phi/\partial z$ can be written as

$$w\ \partial\phi/\partial z \simeq \bar{w}\left[a\left(\phi^{n+1}_{i,j+1} - \phi^{n+1}_{i,j}\right) + b\left(\phi^{n+1}_{i,j} - \phi^{n+1}_{i,j-1}\right)\right] \tag{4.7.5}$$

where

$$\bar{w} \equiv \left(w^n_{i,j+1} + w^n_{i,j} + w^n_{i,j-1}\right)/3 \tag{4.7.6a}$$

and

$$a \equiv (z_j - z_{j-1})/[(z_{j+1} - z_{j-1})(z_{j+1} - z_j)] \tag{4.7.6b}$$

$$b \equiv (z_{j+1} - z_j)/[(z_{j+1} - z_{j-1})(z_j - z_{j-1})] \tag{4.7.6c}$$

It should be noted that the scheme given by Eq. (4.7.5) is second order accurate in space.

The set of finite-difference equations for Eqs. (4.7.2a) can be represented by tridiagonal matrices which can very efficiently be solved using the Thomas Algorithm (Rosenberg, 1969)

The finite-difference approximations used to calculate the vertical velocity and the pressure are

$$w_{i,j+1} = w_{i,j} - \left[\left(\frac{\partial u}{\partial x}\right)_{i,j} + \left(\frac{\partial u}{\partial x}\right)_{i,j+1}\right](z_{j+1} - z_j)/2 \qquad (4.7.7)$$

where

$$\left(\frac{\partial u}{\partial x}\right)_{i,j} \simeq (u_{i,j} - u_{i-1,j})/\Delta x \qquad (4.7.8a)$$

$$\left(\frac{\partial u}{\partial x}\right)_{i,j+1} \simeq (u_{i,j+1} - u_{i-1,j+1})/\Delta x \qquad (4.7.8b)$$

and

$$p_{i,j-1} = \left\{p_{i,j}^{R/c_p} + \left(g p_{0,i}^{R/c_p} \Big/ 2c_p\right)\left[1/\theta_{i,j} + 1/\theta_{i,j-1}\right]\left[z_j - z_{j-1}\right]\right\}^{c_p/R} \qquad (4.7.9)$$

It is noted from Eq. (4.7.7) that the vertical velocity is computed by integrating the continuity equation in the direction of increasing z (increasing j). The condition that the vertical velocity is zero at the air-soil interface translates into

$$w_{i,1} = 0; \quad i = 1, 2, \ldots, N \qquad (4.7.10)$$

where N is the number of grid points along the x-direction.

The pressure is computed by integrating the hydrostatic equation in the direction of decreasing z. In Eq. (4.7.9) $p_{0,i}$ is the pressure at the top of the atmospheric layer corresponding to the location x_i.

Equidistant grid-spacing was used in the x-direction. As the vertical gradients of the atmospheric variables are larger near the air-soil interface than those at greater heights, it was necessary to use a non-linear grid-spacing in the vertical (z) direction to provide good resolution; the grid-spacing was small near the interface and became larger away from the ground. The details of the grid system can be found in Chapter VII.

V. TURBULENCE MODELING

5.1 Introduction

The most difficult problem associated with the numerical modeling of the planetary boundary layer is finding a satisfactory method to simulate the effects of turbulence. Over the past few years, there has been considerable interest in atmospheric turbulence, and the active research in the field has produced a multitude of turbulence models. The state-of-the-art has been excellently surveyed in the papers by Reynolds (1974a), Mellor and associates (1973), and Lumley and Khajeh-Nouri (1974). The currently available turbulence models are described in the following paragraphs.

Eddy-diffusivity or mixing length models express the transport of a variable as the product of the gradient of the variable and an eddy diffusivity. This model which was proposed independently by G. I. Taylor and L. Prandtl is based upon kinetic theory concepts, and draws an analogy between the irregular motion of molecules in a fluid and the less uncorrelated motion of turbulent "eddies." Then, the eddy diffusivity is expressed as the product of a velocity characterizing the turbulent motion and a mixing length which corresponds to the mean free path in kinetic theory. Although the serious shortcomings of the kinetic theory analogy have been recognized, mixing length models have found widespread use mainly because of their simplicity and their surprising success in treating a wide variety of turbulent flows. It should be pointed out that in flows characterized by a single length scale, the mathematical formulation (not the physical model) of the mixing length model can even attain a certain degree of respectability. This reinterpretation of the model under certain conditions will be discussed in more detail in a later section.

Higher order models bypass the concept of eddy diffusivity and attempt to calculate the second moments of turbulent fluctuations directly. Thus, there is no necessity to express the second moments of fluctuating quantities (Reynolds stresses, etc.) in terms of the mean field. Basically, the models attempt to formulate differential equations for the moments. These differential equations, in addition to containing the required moments contain moments of higher order. It is possible to construct differential equations for each of the higher order moments, but an attempt to continue this process of formulating differential equations will result in an infinite set of equations which cannot be solved. Thus, it is necessary to "truncate" the differential equations at a certain stage and express the higher order moments as functions of moments of lesser degree. For example, the third order moments occurring in the equations for the Reynolds stresses would be functions of second moments like the Reynolds stresses, heat flux, etc. Thus, the classical closure problem consists of constructing "suitable" functions for the higher order moments. These functions (functionals to be exact) have to obey certain physical and mathematical constraints. In fact, most of the present research on higher order models (Lumley and Khajeh-Nouri, 1974; Reynolds, 1974b) has concentrated on methods to systematically construct these functionals.

Most of the working higher order models (Donaldson, 1973; Wyngaard, et al., 1974) are second order, and their success in modeling turbulent flows seems to lend credence to the basic philosophy of higher order modeling which states that the less critical is the closure approximation the higher the degree of the turbulent moment it is applied to.

Direct numerical simulation of turbulence utilizes the fact that the Navier-Stokes equations can be used to simulate turbulence if the numerical technique can resolve scales comparable to those of the dissipative eddies. Most of the direct simulation studies (Orszag and Patterson, 1972; Fox and Lilly, 1972) have used Fourier decomposition techniques and attempt to have their small wavelengths of the order of the turbulence microscale of the flow. The range of wave numbers necessary to simulate the flow becomes larger as the Reynolds number increases; thus, such an approach becomes rapidly impractical from the point of view of computer core requirements as well as cost as the Reynolds number increases (Fox and Lilly, 1972). An alternative approach to direct simulation of turbulent is the so-called sub-grid scale modeling (Deardorff, 1974) which takes advantage of the existence of a wide inertial subrange in high Reynolds number flows. Then, it is possible to choose a "practical" grid size which lies within the inertial subrange without putting too much strain on computer core requirements. The motion below the grid scale is modeled making use of the fact that in the inertial subrange the spectral energy flux is equal to the dissipation, and the precise nature of the postulated dissipative mechanism does not influence the large scales of the motion (Tennekes and Lumley, 1972). Direct numerical simulation techniques suffer from the disadvantage that one calculation is not sufficient; each calculation is a realization in an ensemble and a sufficient number of independent runs must be made to obtain stable statistics. Thus, such simulations tend to use up a great deal of computer time, and it is not practical to incorporate direct numerical simulation of turbulence into numerical models of the planetary boundary layer. However, it should be emphasized that direct numerical simulation of turbulence has provided valuable insight into the nature of turbulence.

5.2 The Eddy-Diffusivity Model

Before describing the kinetic energy model for turbulence, the concept of eddy diffusivity will be discussed in some detail to provide justification for the utilization of a modified eddy diffusivity in this study. The eddy diffusivity model can be best explained by considering the Reynolds stress tensor $-\overline{u_i u_j}$. The model would give,

$$-\overline{u_i' u_j'} = K(u_{i,j} + u_{j,i}) \qquad (5.2.1)$$

It is easy to see that the above equation is a direct counterpart of the laminar Newtonian stress law with K the eddy diffusivity replacing ν the kinematic viscosity. The implications of the above formulations are discussed in great detail in the book by Tennekes and Lumley (1972) and in the review paper by Reynolds (1974a) and need not be repeated here. It is sufficient to reiterate that the physical basis for the eddy diffusivity concept is incorrect in most of the details. In spite of its shortcomings, the model has been widely used because of its simplicity and its surprising success in treating a wide variety of turbulent flows.

From equation (5.2.1) it can be seen that K has to be of the form,

$$K = cv\ell \tag{5.2.2}$$

where v is a velocity characterizing the turbulent motion, ℓ is the so-called mixing length and c is a constant. Substituting (5.2.2) in (5.2.1) one obtains,

$$\overline{-u_i'u_j'} = cv\ell(u_{i,j} + u_{j,i}) \tag{5.2.3}$$

To be specific, consider the case, i = 1, j = 2 and $u_{2,1} = 0$. Then, (5.2.3) becomes

$$\overline{-u_1'u_2'} = cv\ell\ u_{1,2} \tag{5.2.4}$$

By associating ℓ with the size of the large turbulent eddies which cause most of the transport, it is possible to justify Eq. (5.2.4) without resorting to kinetic theory concepts. If it is accepted that the larger turbulent eddies derive their energy directly by the straining action of the mean flow, one would expect the time scale of the mean flow to be of the same order as the time scale of the large eddies. Then,

$$v/\ell = c_1|u_{1,2}| \tag{5.2.5}$$

or

$$v = c_1\ell|u_{1,2}| \tag{5.2.6}$$

In most turbulent flows u_1' and u_2' are of the same order of magnitude: u_1' and $u_2' = O(v)$. Then, one can write,

$$\overline{-u_1'u_2'} = c_{12}v^2 \tag{5.2.7}$$

where c_{12} is an undetermined constant. Substituting (5.2.6) into (5.2.7) one gets

$$\overline{-u_1'u_2'} = c_1^2c_{12}\ell|u_{1,2}|u_{1,2} \tag{5.2.8}$$

Equation (5.2.8) is the one originally proposed by Prandtl. If the correlation between u_1' and u_2' is good, and the straining of the eddies is an effective mechanism, the coefficients c_1 and c_{12} should be of order 1. From (5.2.8) it is easy to see that the eddy diffusivity can be expressed as

$$K = c\ell^2|u_{1,2}| \tag{5.2.9}$$

and the fluctuating velocity v can be written as

$$v = \ell|u_{1,2}| \tag{5.2.10}$$

The preceding arguments to derive (5.2.9) imply that the turbulence is in equilibrium with the mean flow; the dynamics of larger eddies are controlled by the mean flow. Thus, the model would predict small eddy diffusivities in regions of small shear. However, there are situations, especially in atmospheric flows, in which small velocity gradients are associated with large momentum transport. Clearly, such situations make the physical basis for the eddy diffusivity concept even less firm. One partial solution to the problem is to use a turbulent velocity scale which is less sensitive to the mean gradients, and the natural alternative velocity scale is the square root of the turbulent kinetic energy k. Then, the eddy diffusivity becomes

$$K = ck^{\frac{1}{2}}\ell \qquad (5.2.11)$$

By allowing the kinetic energy to evolve it is possible to have large turbulent kinetic energies in regions of small shear. Thus, the above formulation allows for large fluxes even when the mean gradients are small.

The mixing length ℓ is the most elusive variable in the eddy diffusivity model. For turbulent flows bounded by solid surfaces, the mixing length is taken to be

$$\ell = \kappa z \qquad (5.2.12)$$

where κ is the von Karman constant and z is the distance from the solid surface. Equation (5.2.12) was the form suggested by Prandtl and was used in derivation of the "law of the wall" (Cebeci and Smith, 1974) which has been experimentally verified. The basic idea of using the distance from the solid surface as the mixing length has remained unchanged ever since Prandtl first put it forward in 1926. Various investigators have suggested improvements to the model mainly to increase the accuracy of their predictions. Details of ingenious mixing length models for a wide variety of engineering flows can be found in the book by Cebeci and Smith (1974). The mixing length model which has found widespread use in atmospheric modeling is that due to Blackadar (1962). The model assumes that the mixing length increases linearly with height near the earth's surface and reaches an asymptotic value at greater heights. The equation for the model is

$$\ell = \kappa z/(1 + \kappa z/\lambda) \qquad (5.2.13)$$

The asymptotic mixing length λ is related to the height of the planetary boundary layer. The formulation given by (5.2.13) is based on experimental findings (Rossby and Montgomery, 1935) which indicates that ℓ ceases to increase with height at upper levels. Furthermore, it incorporates the physically realistic idea that ℓ should not exceed a fixed fraction of the boundary layer height. Other mixing length models which are similar to Blackadar's have been suggested by Ohmstede and Appleby (1964) and Lettau (1962). The more recent turbulence models (Launder and Spalding, 1972) do not specify the mixing length but allow it to evolve with the mean field through a differential equation. This approach which is more physically acceptable than the arbitrary specification of the mixing length has certain disadvantages which will be discussed in a later section.

5.3 Atmospheric Turbulence Modeling

The language of atmospheric turbulence differs in many details from that of engineering turbulence because the effects of thermal stratification are considerably more important in the planetary boundary layer. In contrast to engineering turbulent flows in which turbulence is maintained by velocity gradients (eddy diffusivity ideas are more applicable), atmospheric turbulence is mainly produced by buoyancy. The effects of wind shear are felt only in a shallow layer next to the earth's surface.

The effect of stratification on the turbulence in the boundary layer is traditionally described with the aid of the Richardson number which is defined as

$$Ri = \frac{g}{T}\frac{\partial\theta}{\partial z} \Big/ \left\{ \left(\frac{\partial u}{\partial z}\right)^2 + \left(\frac{\partial v}{\partial z}\right)^2 \right\} \qquad (5.3.1)$$

The definition of the Richardson number assumes that only the vertical velocity and temperature gradients are significant in determining the turbulence characteristics. This assumption is valid in the atmospheric boundary layer in which horizontal gradients are usually very small compared to vertical gradients. A positive Richardson number implies stable conditions in which turbulence produced by shear is being converted into potential energy by the positive potential temperature gradient. A negative Richardson number, on the other hand, would mean that buoyancy is aiding shear in producing turbulence. The significance of the preceding statements will become clear when the turbulent kinetic energy equations are examined in a later section.

The eddy diffusivity used in atmospheric turbulence modeling is expressed as follows (Estoque, 1963),

$$K = \ell^2 \left|\frac{\partial u}{\partial z}\right| f(Ri) \qquad (5.3.2)$$

where f is a function of the Richardson number. The function f has been derived using semi-empirical arguments, and investigators (Estoque, 1963; Pandolfo, 1966) have had success in deriving velocity and temperature profiles in the surface layer using these functions. An alternative approach to surface layer modeling is that advanced by the Soviet school (Moin and Yaglom, 1971). It postulates that the wind and temperature profiles are universal when they are non-dimensionalized using the proper scales. In the diabatic surface layer, u_* the friction velocity serves as the velocity scale, and the temperature and the vertical distance are scaled by the parameters defined below,

$$\theta_{*_0} = -\overline{(\theta' w')}_0 / \kappa u_* \qquad (5.3.3)$$

and

$$L_0 = u_*^2 T / g\kappa^2 \theta_{*_0} \qquad (5.3.4)$$

where $\overline{(\theta' w')}_0$ is the surface heat flux, κ is the von Karman constant, T is the mean temperature of the surface layer and g is the acceleration due to gravity. The temperature scale is θ_{*_0}, and L_0, which is the Monin-Obuknov length, serves as the length scale. The physical interpretation of the Monin-Obukhov length will be discussed later.

Then, it is postulated that the temperature and wind profiles can be expressed as,

$$\frac{\kappa z}{u_*}\frac{du}{dz} = \phi_m\left(\frac{z}{L_0}\right) \tag{5.3.5}$$

$$\frac{z}{\theta_{*_0}}\frac{d\theta}{dz} = \phi_h\left(\frac{z}{L_0}\right) \tag{5.3.6}$$

Experimental observations (Businger, et al., 1971) show that the non-dimensional velocity and temperature profiles can indeed be described by universal functions which depend upon the stability (the direction of the heat flux) of the surface layer. A discussion of the stability functions can be found in the book by Monin and Yaglom (1971). The turbulent layer above the surface layer is not as well understood, and there is considerable controversy surrounding the selection of scaling variables. However, a series of numerical experiments by Deardorff (1972; 1974) indicate that it is possible to find velocity and length scales in the well mixed boundary layer. It is not yet clear whether it is possible to find scaling parameters for the stable boundary layer.

Over the past few years, several models (Carson, 1973; Deardorff, 1972; Tennekes, 1973) have been proposed to predict the evolution of the well-mixed boundary layer. These models parameterize the boundary layer and do not attempt to predict the detailed turbulence structure. Although this approach is the most natural one to predict the important boundary layer variables, such as mixed layer height and boundary layer potential temperature, it suffers from the disadvantage that it can predict only the gross features and cannot treat local temperature changes caused by heat sources or radiative heating or cooling. As the object of this investigation is to study the effect of pollutants on the thermal structure, it is necessary to use a turbulence model which will enable one to resolve localized cooling or heating. The model adopted in this study is described in the next section.

5.4 Kinetic Energy Turbulence Model

Most of the models which have attempted to treat the important physical processes in the boundary layer have used semi-empirical

Richardson number correlations to calculate eddy diffusivities. These models have had a degree of success in treating shear dominated turbulence but predict imprecise eddy diffusivities in regions with small wind shears. These inaccurate predictions can give rise to incorrect physical effects. The limitations of the semi-empirical eddy diffusivity correlations have been clearly recognized, and recent papers by Shir and Bornstein (1974) and P. A. Taylor (1974) discuss the need for improved models for turbulence. Recently, Wyngaard et al. (1974) have demonstrated that for some special cases it is computationally feasible in terms of time and money to incorporate "higher" order turbulence models in numerical models of the planetary boundary layer. Their 1-D model requires 10 minutes on the CDC-6600 for a twenty-four hour simulation. It is suspected that inclusion of radiation, surface energy balances, horizontal variation of surface parameters advection and other effects which would be required for a realistic boundary layer model would require considerably more than ten minutes computer time (CDC-6600) if turbulence models like that of Wyngaard, et al. are utilized.

It is believed that the kinetic energy turbulence model represents the best compromise between the simplistic semiempirical Richardson number correlations and the computationally cumbersome "higher" order models. The kinetic energy model has been developed and utilized by Spalding and his co-workers (1969) to model a wide variety of engineering flows. Peterson (1969) has applied the model to the problem of the modification of planetary boundary layer by roughness changes under neutral conditions. Delage (1974) has applied the model to the nocturnal atmospheric boundary layer, and Lykosov (1972) has studied the diurnal variation of the boundary layer using a kinetic energy turbulence model. These and other studies indicate that the kinetic energy model is indeed an improvement over the Richardson number correlation approach. In view of this, it was decided to incorporate the turbulent kinetic energy model in the present investigation.

The turbulent kinetic energy equation is presented below. The details of the derivation can be found in books on turbulence (Monin and Yaglom, 1971; Cebeci and Smith, 1974). The equation after making the usual closure assumptions is

$$\frac{Dk}{Dt} = \frac{\partial}{\partial z}\left(k^{\frac{1}{2}}\,\ell\,\frac{\partial k}{\partial z}\right) - \overline{u'w'}\,\frac{\partial u}{\partial z} - \overline{v'w'}\,\frac{\partial v}{\partial z} + \frac{g}{T}\,\overline{w'\theta'} - \varepsilon \qquad (5.4.1)$$

where

$$k = \frac{1}{2}\,\overline{u_i u_i} \qquad (5.4.2)$$

ℓ is the mixing length, $\overline{-u'w'}$ is the shear stress in the x-direction, $\overline{-v'w'}$ is the shear stress in the y-direction, and $\overline{w'\theta'}$ the upward heat flux.

The term Dk/Dt represents the rate of change of kinetic energy and in expanded form reads

$$\frac{Dk}{Dt} = \frac{\partial k}{\partial t} + u_i\,\frac{\partial k}{\partial x_i} \qquad (5.4.3)$$

The term $\partial/\partial z(k^{\frac{1}{2}}\ \ell\ k/\partial z)$ accounts for the diffusion of turbulent kinetic energy. The terms $\overline{-u'w'}\ \partial u/\partial z$ and $\overline{-v'w'}\ \partial v/\partial z$ represent production of turbulent energy by mean shear, and the term $g\ \overline{w'\theta'}/T$ accounts for buoyancy production of turbulent kinetic energy. The term ε is the viscous dissipation of turbulent energy. As all of the available experimental evidence indicated that the dissipation of the large scale eddies ε can be written as

$$\varepsilon = C_D k^{\frac{3}{2}}/\ell \qquad (5.4.4)$$

where C_D has to be determined experimentally $C_D = 0.09$ is the commonly accepted value (Launder and Spalding, 1972).

Invoking the eddy diffusivity concept one can express the second moments in Eq. (5.4.1) as

$$\overline{-u'w'} = K_M\,\frac{\partial u}{\partial z} \qquad (5.4.5a)$$

$$\overline{-v'w'} = K_M\,\frac{\partial v}{\partial z} \qquad (5.4.5b)$$

$$-\overline{w'\theta'} = K_H\left(\frac{\partial \theta}{\partial z} - \gamma_c\right) \qquad (5.4.5c)$$

where K_M is the eddy diffusivity for momentum and K_H is the eddy diffusivity for heat. This study assumes that K_H/K_M is 1.35 which is the value observed under neutral conditions (Businger, 1972). Although K_H is observed to be greater than 1.35 K_M under unstable conditions, no attempt was made to model the variation of eddy diffusivity ratio with stability. It should be mentioned that, as yet, there is no satisfactory theory to predict the diffusivity ratio.

Then, one can write

$$K_M = k^{\frac{1}{2}}\ell \tag{5.4.6}$$

and

$$K_H = \alpha k^{\frac{1}{2}}\ell \tag{5.4.7}$$

where $\alpha = 1.35$ ($\alpha = K_H/K_M = 1.35$). With Eqs. (5.4.4) through (5.4.7) Eq. (5.4.1) can be rewritten as,

$$\frac{Dk}{Dt} = \frac{\partial}{\partial z}\left(k^{\frac{1}{2}}\ell\ \frac{\partial k}{\partial z}\right) + k^{\frac{1}{2}}\ell\left[\left(\frac{\partial u}{\partial z}\right)^2 + \left(\frac{\partial u}{\partial z}\right)^2 + \left(\frac{\partial v}{\partial z}\right)^2\right.$$

$$\left. - \frac{\alpha g}{T}\left(\frac{\partial\theta}{\partial z} - \gamma_c\right)\right] - C_D\ k^{\frac{3}{2}}/\ell \tag{5.4.8}$$

In the surface layer, experimental observations indicate that the production of turbulence is matched by dissipation. If this is taken into consideration Eq. (5.4.8) would read,

$$k^{\frac{1}{2}}\ell\left[\left(\frac{\partial u}{\partial z}\right)^2 + \left(\frac{\partial v}{\partial z}\right)^2 - \frac{\alpha g}{T}\left(\frac{\partial\theta}{\partial z} - \gamma_c\right)\right] = C_D k^{\frac{3}{2}}/\ell \tag{5.4.9}$$

or

$$k = \frac{\ell^2}{C_D}\left[\left(\frac{\partial u}{\partial z}\right)^2 + \left(\frac{\partial v}{\partial z}\right)^2\right](1 - \alpha Ri) \tag{5.4.10}$$

where Ri, the Richardson number, is defined as

$$Ri = \frac{\alpha g}{T}\left(\frac{\partial\theta}{\partial z} - \gamma_c\right) / \left[\left(\frac{\partial u}{\partial z}\right)^2 + \left(\frac{\partial v}{\partial z}\right)^2\right] \tag{5.4.11}$$

This definition is a slightly modified form of that expressed by (5.3.1).

From Eq. (5.4.10) it is easy to see that k becomes negative if $Ri > 1/\alpha$. A physical interpretation of the solution for k given by Eq. (5.4.10) is that turbulence can exist only if the Richardson number is less than a critical Richardson number given by

$$Ri_{cr} = 1/\alpha \tag{5.4.12}$$

There is still considerable controversy over the value of Ri_{cr}, and it is not even entirely clear that a clearly defined critical Richardson number even exists (Monin and Yaglom, 1971). However, experimental evidence suggests that true turbulence cannot exist in flows with Richardson number greater than 0.25 (Webb, 1970).

As the Monin-Obuknov length serves as a length scale under stable conditions, it is useful to derive the important length from the turbulent kinetic energy equation. Equating the shear production term to the buoyancy production term, and using the experimentally verified approximation of the constancy of fluxes in the surface layer, one obtains from Eq. (5.4.1)

$$\frac{u_\star^3}{\kappa z_h} = -\frac{\alpha g}{T}(\overline{w'\theta'})_0 \tag{5.4.13}$$

where z_h is the height at which turbulence production is matched by dissipation and where the x-axis is directed along the direction of surface shear, and $\partial u/\partial z$ has been replaced by $u_\star/\kappa z_h$.

The surface friction velocity $u_\star$ is defined by

$$u_\star^2 = \overline{-u'w'} \tag{5.4.14}$$

Then in terms of the definition given by (5.3.3) for $\theta_\star$, one obtains from (5.4.13)

$$z_h = L_0/\alpha \tag{5.4.15}$$

Thus, from Eq. (5.4.15) it is easy to see that L_0, the Monin-Obukhov length, represents the height below which one would expect turbulence production to be dominated by shear effects. Above heights of the order of L_0 buoyancy would play the major role in producing turbulence. Under stable conditions L_0 is a positive quantity and it can be shown quite easily that the size of the dominant eddies scale with the Monin-Obukhov length (Monin and Yaglom, 1971).

5.5 Mixing Length Model

Before Eq. (5.4.8) can be solved one has to have a formulation for the mixing length ℓ. Near the surface ($z = 0$) ℓ is known to behave like $\ell = C_D^{1/4} \kappa z$. The calculation of the mixing length above the surface layer is a problem still under consideration. The mixing length can either be specified or calculated from a differential equation for ℓ or a related quantity such as the dissipation rate. The latter procedure has been used with a great deal of success by Spalding and his co-workers at Imperial College (1969). More recently, Wyngaard, et al. (1974) have used a dissipation rate equation to compute the time scale of their turbulence equations. Lykosov (1972) used a modified from of von Karman formulation for the mixing length. Delage (1974) has used a prescription which is similar to that proposed by Deardorff (1972). Delage's formulation, which is applicable only to the nocturnal boundary layer, makes use of the fact that above the surface layer the dominant eddies scale with the Monin-Obukhov length under stable conditions. The expressions due to Blackadar (1962), Appleby (1964) and Lettau (1962) have already been discussed. The unknown which appears in most of the mixing length formulations is the asymptotic mixing length which is a fraction of the boundary layer height. Traditionally, the boundary layer height was taken to be a fraction of the length scale formed with the friction velocity u_*, and the Coriolis parameter f. The asymptotic mixing length λ would be written as

$$\lambda = C\, u_*/f \qquad (5.5.16)$$

The effects of stratification on λ are taken into account by writing

$$\lambda = C(u_*/f)\ g(\mu) \tag{5.5.17}$$

where g is a function of the stratification parameter μ given by

$$\mu = \kappa u_*/(fL_0) \tag{5.5.18}$$

Implicit in the formulation given by (5.5.17) is that surface fluxes control the height of the boundary layer, and that the atmosphere is neutrally stratified above the surface layer. Observations, however, show the turbulent planetary boundary layer is capped by a stable layer. Thus, the vertical expansion of the boundary layer is clearly controlled by the stability of the air aloft. Then, the boundary layer height can only be calculated from the internal structure of the boundary layer. Numerical experiments by Deardorff (1974) show that u_*/f cannot be used as a scaling parameter under unstable conditions, and the height of the mixed layer is the relevant scale. This seems to indicate that, at least, under unstable conditions the maximum mixing length should be related to the mixed layer height. However, under stable conditions, formulae like (5.5.17) might be applicable (Businger and Arya, 1974) because the turbulent region is confined to the layer next to the surface making it possible for the surface fluxes to control the boundary layer height.

For the purposes of this investigation, it was decided to prescribe the mixing length rather than use the dissipation rate equation which is still in the process of development. Initially, Blackadar's (1963) expression for the mixing length was utilized. The asymptotic mixing length was related to the mixed layer height through the equation

$$\lambda = 0.1\ H_m \tag{5.5.19a}$$

where H_m is the mixed layer height. H_m was defined as the height at which the turbulent kinetic energy reached an arbitrarily small value ($= 10^{-6}$ m^2/sec^2). At the outset, it is clear that Blackadar's mixing length model has an undesirable feature in that the mixing length increases monotonically throughout the boundary layer. Although it allows for a gradual leveling off of the mixing length, the relatively large mixing lengths tend to amplify small instabilities in the capping inversion above the boundary layer. This can give rise to two maxima in the eddy diffusivity profiles as illustrated in Figure 5.1. As the mixing length is associated with the dominant scale of turbulent motion, a model which predicts large mixing lengths in regions in which there is little or no turbulent activity, is physically unrealistic. Clearly, a mixing length formulation should allow for a decrease of the mixing length in the upper part of the boundary layer.

Recent experimental (Kalmykov, et al., 1975; Deardorff, 1974) studies show that the mixing length does indeed decrease towards the edge of the boundary layer. Kalmykov, et al. (1975) conducted an extensive study of the behavior of the mixing length in a variety of shear dominated flows. From their large volume of experimental data, they concluded that the mixing length profiles are self-similar and can be well represented by the following expression:

$$\bar{\ell} = C_D^{1/4} \kappa \eta (1 - \eta)/(1 + \eta) \qquad (5.5.19b)$$

where

$$\bar{\ell} = \ell/H_m \qquad (5.5.20a)$$

$$\eta = z/H_m \qquad (5.5.20b)$$

and C_D is the dissipation constant, and κ is the von Karman constant. Equation (5.5.19b) predicts that $\bar{\ell}$ increases linearly near the surface, reaches a maximum of about 0.04 at $\eta = 0.5$, and decreases to a value of 0 at the edge of the boundary layer. This study does provide some basis for the construction of the mixing length model. However, the results cannot be directly applied to the study of this research because of the significant differences between shear dominated flows and those controlled by thermal stratification. Deardorff's numerical modeling study of the convective boundary layer shows a mixing length

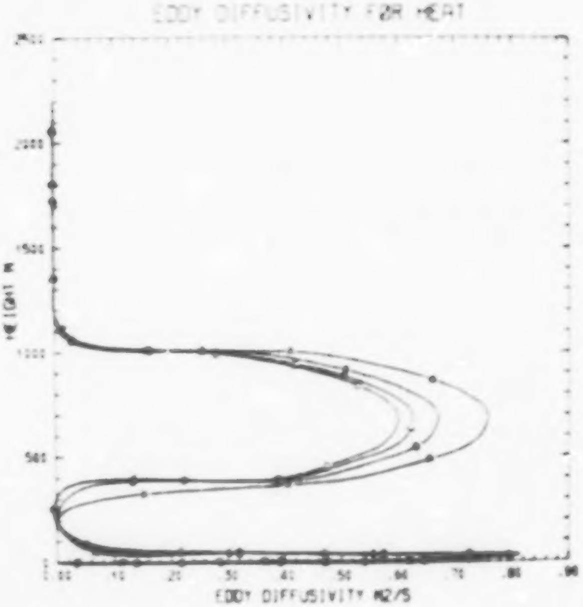

Figure 5.1 Eddy Diffusivity Profiles with Blackadar's Formulation. Simulation is for Time 19:00 to 22:00 Hours. A, B, C, D Represent Profiles at 1 Hour Intervals.

behavior similar to that of the investigation of Kalmykov, et al. However, the mixing lengths are considerably larger as gravity controlled convection tends to elongate turbulent eddies in the vertical direction. The mixing length $\overline{\ell}$ reaches a maximum of about 0.072 at $\eta = 0.5$ and decreases to a value of around 0.0405 at $\eta = 1.0$. The rather large value of $\overline{\ell}$ at $\eta = 1.0$ is associated with gravity waves rather than true turbulence. It is clear that Deardorff's results have greater applicability to the study under consideration.

The mixing length model used in this investigation was constructed to incorporate the most important features of the results described in the preceding paragraph. To summarize, the mixing length model possessed the following characteristics:

$$\ell = C_D^{1/4} \kappa z \quad \text{near} \quad z = 0 \tag{5.5.21a}$$

$$\ell = 0.8\ C_D\ H_m; \quad z = H_m/2 \tag{5.5.21b}$$

$$\ell = 0.1\ C_D\ H_m; \quad z = H_m \tag{5.5.21c}$$

The value of $0.8\ C_D\ H_m$ for ℓ at $H_m/2$ was obtained from Deardorff's study. Since H_m was taken as the height at which there was virtually no turbulence, ℓ was assumed to have the small value of $0.1\ C_D\ H_m$. The larger value obtained by Deardorff was associated with gravity waves rather than turbulence. The magnitude of $0.1\ C_D\ H_m$ used in this study is based on the observation that the overshoot of convective elements at the top of the boundary layer is approximately ten percent of the boundary layer height. The mixing length at the edge of the boundary layer is not critical as it is associated with small values of turbulent kinetic energy.

A fourth order polynomial was utilized in the formulation of the mixing length distribution. In addition to being able to satisfy the required boundary conditions, a fourth order polynomial permits flexibility in the choice of the magnitudes of the mixing lengths at the middle and at the top of the boundary layer. The dimensionless mixing length $\overline{\ell}$ can be then written as

$$\bar{\ell} = a\eta + b\eta^2 + c\eta^3 + d\eta^4 \qquad (5.5.22)$$

It should be mentioned that polynomials have been used before (Fedyayevsky, 1936; Sherstyuk, 1969) to describe mixing length behavior. The coefficients a, b, c, and d are determined by applying the boundary conditions (5.5.21). Implicit in Eq. (5.5.22) is the assumption that the mixing length profile is self-similar. Justification for this assumption is provided by Kalmykov, et al. (1975). Furthermore, Deardorff (1972, 1974) in his investigations shows that the height of the boundary layer serves as a scaling height for atmospheric variables during convective conditions. Above $z = H_m$ the mixing length was assumed to decrease linearly to zero at the maximum model height around 2000 meters.

5.6 The Equilibrium Layer

As the turbulent time scales are very small near the earth's surface, very short time steps would have to be utilized in the numerical solution of the turbulent kinetic energy equation. The small length scales associated with the turbulent eddies give rise to relatively large (compared to the other terms in the turbulent kinetic energy equation) dissipation rates. Thus, the time step used in the numerical solution of the kinetic energy equation had to be made small enough to prevent the dissipation rate, which remains constant over the time interval, from driving the turbulent kinetic energy to a physically unrealistic negative value. However, small time steps made the computational costs excessive; the way around this problem was to take advantage of the near equality of the production and dissipation of turbulent kinetic energy in the surface layer (Tennekes and Lumley, 1972). Also, the time rate of change of kinetic energy is almost two orders of magnitude smaller than the other terms (Lenschow, 1974). Using these observations about the surface layer the turbulent kinetic equation can be written as,

$$k^{\frac{1}{2}}\ell\left[\left(\frac{\partial u}{\partial z}\right)^2 + \left(\frac{\partial v}{\partial z}\right)^2 - \frac{\alpha g}{T}\left(\frac{\partial \theta}{\partial z} - \gamma_c\right)\right] - \frac{C_D k^{\frac{3}{2}}}{\ell} = 0 \qquad (5.6.1)$$

Then, the surface layer in which Eq. (5.6.1) is valid is called the equilibrium layer in this study--the production and dissipation of turbulent kinetic energy are in equilibrium. The equilibrium layer is similar to the constant flux layer used by boundary layer modelers (Estoque, 1963; Sasamori, 1970; Bornstein, 1972). Both the constant flux layer and the equilibrium layer are based on the principle of quasi-stationarity--negligible time lag between a physical change and the forcing causing the change. In fact, one would expect the thickness of the equilibrium layer to be of the same order of magnitude as that of the constant flux layer. Based on Estoque's (1963) value for the constant flux layer, the thickness of the equilibrium layer was chosen to be 50 meters.

Equation (5.6.1) can be solved for the turbulent kinetic energy k,

$$k = \frac{\ell^2}{C_D}\left[\left(\frac{\partial u}{\partial z}\right)^2 + \left(\frac{\partial v}{\partial z}\right)^2 - \frac{\alpha g}{T}\left(\frac{\partial \theta}{\partial z} - \gamma_c\right)\right] \qquad (5.6.2)$$

Once k is known from Eq. (5.6.2) K_H and K_M can be computed from Eqs. (5.4.6) and (5.4.7).

5.7 Turbulent Diffusivity for Two-Dimensional Model

Initially, the turbulence model described in the preceding sections was incorporated into a one-dimensional transport model which was then successfully utilized in simulating a variety of boundary layer events. An attempt to incorporate the turbulence model based on the turbulent kinetic energy equation into the two-dimensional urban transport model gave rise to instability problems with the numerical scheme, and after considerable experimentation it was decided to use a simpler scheme to compute the turbulent diffusivities above the equilibrium layer.

The generally accepted behavior (Estoque, 1963; Deardorff, 1967; Bornstein, 1972) of the eddy diffusivity can be summarized as follows.

The eddy diffusivity increases near the ground reaching a maximum a few hundred meters from the surface, and then decreases to a small value at the top of the planetary boundary layer. Based on this behavior numerical modelers (Estoque, 1963; Wu, 1965; Deardorff, 1967; O'Brien, 1970) have suggested a variety of eddy diffusivity models. Estoque (1963) assumed that the eddy diffusivity decreased linearly from a maximum at the top of the surface layer to zero at the top of the boundary layer, Deardorff (1967) used an empirical formulation but accounted for the experimentally observed (Telford and Warner, 1964) counter gradient flux. Wu (1965) used the formulation given by Eq. (5.4.9) but modified the mixing length to account for its gradual leveling off at great heights. O'Brien (1970) assumed that the eddy diffusivity profile could be fitted with a cubic polynomial. Pandolfo, et al. (1963) extended surface layer based Richardson number correlations for the eddy diffusivity to the entire boundary layer. It should be pointed out that the described methods to calculate the diffusivity profiles are semi-empirical in nature, and are used only because better techniques such as higher-order modeling (Donaldson, 1973) and subgrid scale modeling (Deardorff, 1974) are computationally cumbersome and at this stage cannot be incorporated into practical boundary layer models.

Eddy diffusivities based on local Richardson numbers are accurate only in regions of strong positive wind shear (Shir and Bornstein, 1974). Thus, in the region above the equilibrium layer, where the velocity as well as the temperature gradients are small, it is necessary to use a technique which is not dependent on the Richardson number. The natural alternative is to specify the eddy diffusivity profile as has been done by several investigators (Estoque, 1963; O'Brien, 1970). It is not clear why an arbitrary specification of the eddy diffusivity profile is preferable to imprecise eddy diffusivity values obtained from Richardson number correlations until it is pointed out that the numerical differentiation involved in the computation of the Richardson number gives rise to large errors in regions in which velocity and temperature gradients are small. These errors in turn lead to unrealistically jagged eddy diffusivity profiles as evidenced by Pandolfo's (1971) results. Furthermore, Richardson number correlations for the eddy diffusivity are based on the equilibrium assumption (production equals dissipation of turbulence) which is clearly not valid above the surface layer (Lenschow, 1973). From the preceding discussion it should be clear that the specification of the eddy diffusivity profile is not more empirical than the use of Richardson number correlations; the main advantage of the specification of the profile is the numerical facility it affords.

This study utilized the O'Brien (1970) cubic polynomial to specify the vertical eddy diffusivity profile. The O'Brien model ensures the continuity of the slope of the eddy diffusivity profile at the top of the equilibrium layer, and it also allows the eddy diffusivity to reach a maximum above the height of the equilibrium layer. These physically realistic features of the O'Brien model are not found in the models due to Estoque (1963) and McPherson (1968). It should be mentioned that Sasamori (1970) and Bornstein (1972) have incorporated the O'Brien diffusivity distribution into their "successful" boundary layer models.

The O'Brien formulation assumes that the following are known:

$$K(H^*),\quad (\partial K/\partial z)_{H^*},\quad K(h),\quad (\partial K/\partial z)_h$$

where H^* is the height of the boundary layer, h is height of the equilibrium layer, and K is the eddy diffusivity. If it is assumed that the variation of K at H^* is zero, then the eddy diffusivity distribution can be written as,

$$\begin{aligned} K(z) = K(H^*) + \left(\frac{z - H^*}{H^* - h}\right)^2 \Bigg\{ & K(h) - K(H^*) \\ & + (z - h)\left[\left(\frac{\partial k}{\partial z}\right)_h + \frac{2[K(h) - K(H^*)]}{H^* - h}\right]\Bigg\} \end{aligned} \tag{5.7.1}$$

Equation (5.7.1) yields parabolic curves, as predicted by Blackadar (1962), Lettau (1962), and Lettau and Dabberdt (1970), and as observed at night by Elliot (1964).

Sasamori (1970) assumed that h was a function of the eddy diffusivity near the ground, but used a fixed value for H^*; Bornstein (1972) fixed the values of both h and H^*. In these above mentioned studies h refers to the height of the layer near the surface in which the fluxes (momentum, heat and mass) can be considered to be constant with height. As has been discussed in the preceding section, this investigation defines h as the thickness of the surface layer in which it is assumed that the production and dissipation of turbulence are in balance. It is clear from both definitions that h should be a function of the turbulence characteristics of the surface, and a realistic model should account for the variation of h with time. Sasamori (1970) has suggested a method to compute h from the internal characteristics of the surface layer; however, the method has not yet been widely accepted, and most boundary layer modelers (Estoque, 1972; Wagner and Yu, 1972; Bornstein, 1972) have chosen to fix the value of h. In view of these considerations it was decided to use a constant value of 50 meters for h (Estoque, 1963).

The boundary layer thickness H^* is a function of space and time (Tennekes, 1974), and it can vary from a few tens of meters on clear nights with light winds to about two thousand meters on sunny summer afternoons. The boundary layer is identified with the turbulent region next to the earth's surface, and the details of the formation of the boundary layer or the mixed layer have already been discussed in a preceding chapter. In the one-dimensional model, the turbulent kinetic energy distribution was used to define the boundary layer thickness. For the reasons given before the turbulent kinetic energy equation was not solved in the two-dimensional model and it was necessary to use an alternative definition for the boundary layer thickness. As the mixed layer is usually capped by a stable layer in which there is virtually no turbulence, the boundary layer thickness was defined as the height at which the potential temperature gradient exceeded an arbitrary positive value which was large enough to suppress turbulent activity. Implicit in this definition of the boundary layer thickness is the assumption that shear effects are of secondary importance compared to thermal effects and it is only necessary to have a large enough potential temperature gradient to inhibit turbulent activity. Clearly, this assumption cannot be justified when the boundary layer is growing and is confined to the high shear region next to the earth's surface, or when the upward heat flux is small (Monin-Obukov length is large). Thus, it would seem that a better definition for the boundary layer thickness would involve some sort of Richardson number criterion. However, as has been discussed before, the numerical computation of the Richardson number presents problems which have not yet been resolved. Thus, for the purposes of this study it was decided to use the simpler potential temperature gradient criterion to define the boundary layer thickness. Then, the mixed layer height was defined as the lowest level at which $\partial\theta/\partial z$ exceeded 4 C Km^{-1}, a value suggested by Deardorff (1967).

As the region above the boundary layer is not turbulent, the eddy diffusivity is assumed to be zero above $z = H^*$. The error introduced by neglecting the molecular diffusivity is negligible over the time scale of simulation.

The eddy diffusivity below $z = h$ is computed from turbulence equilibrium considerations, and the term $(\partial K/\partial z)h$ is calculated using a first order finite difference scheme.

VI. RADIATION MODEL

6.1 Introduction

The spectrum of atmospheric radiation can be divided into two fairly distinct regions. Most of the radiation emitted by the sun and reaching the earth is confined to the spectral region between 0.3 μm to 4 μm, while the energy emitted by the earth atmosphere system lies between 4 μm to 100 μm. The spectrum of solar radiation is very close to the spectral distribution of the energy emitted by a blackbody at approximately 6000 K. Similarly, the earth atmosphere system can in effect be replaced by a blackbody at 245 K.

The principal absorbers of solar radiation are water vapor in the troposphere and ozone in the stratosphere. Water vapor absorbs primarily in the near infrared region, $0.7\ \mu m \leq \lambda \leq 4\ \mu m$, while ozone is effective in the ultraviolet ($\lambda \leq 0.35\ \mu m$) and in the visual range ($0.5\ \mu m \leq \lambda \leq 0.7\ \mu m$). In addition to being absorbed, solar radiation is scattered by gas molecules (Rayleigh scattered) and aerosols (Mie scattered).

In the thermal part of the spectrum, the principal absorbers are water vapor and carbon dioxide. Water vapor has strong bands centered at 2.7 μm and 6.3 μm, and a rotational band extending from 20 μm to 100 μm under standard atmospheric conditions. Carbon dioxide absorbs strongly in bands centered at 2.7 μm, 4.3 μm and 14.8 μm. Ozone has a band centered at 9.6 μm. The 8 μm to 12 μm region, which is referred to as the atmospheric window, is relatively transparent, and it is in this region that the presence of pollutant absorption bands is important.

Most of the ultraviolet region ($\lambda \leq 0.35\ \mu m$) of the solar spectrum is absorbed by stratospheric ozone when the solar energy reaches the top of the atmospheric boundary layer which usually extends to heights around 2 kilometers. Inside the boundary layer, the short-wavelength solar energy is scattered by gases and natural and man-made aerosols. It is also absorbed by water vapor and pollutant gases such as NO_2. Solar energy is also absorbed to a smaller extent by aerosols. Thermal radiation is absorbed and emitted by water vapor, carbon dioxide, and pollutant gases such as carbon monoxide and ammonia. Aerosols in addition to absorbing can also scatter thermal radiation. At the surface of the earth, solar radiation is absorbed and reflected diffusely while thermal radiation is reflected, emitted, and absorbed diffusely. Figure 6.1 schematically illustrates the interaction of atmospheric radiation with the planetary boundary layer.

6.2 The Radiative Transfer Equation

The equation of radiative transfer expresses the conservation of radiant energy in terms of the change of intensity of a pencil of radiation traversing an absorbing, emitting, and scattering medium. The derivation of the equation of transfer can be found in standard works on radiative transfer (Chandrasekhar, 1960, for example) and it is sufficient to present the equation,

$$\mu \frac{\partial I_\nu(z,\mu,\phi)}{\partial z} = -\beta_\nu(z) I_\nu(z,\mu,\phi) + \kappa_\nu(z) I_{b\nu}(z) + \frac{\sigma_\nu(z)}{4\pi} \int_{\mu'} \int_{\phi'} p_\nu(z,\mu',\phi' \rightarrow \mu,\phi) I_\nu(z,\mu',\phi') d\mu' d\phi' \qquad (6.2.1)$$

where $I_\nu(z,\mu,\phi)$ is the intensity of the pencil of radiation at a point defined by the spherical coordinates z,μ,ϕ. The equation then states that the change of intensity (the term on the left) of the beam of radiation is caused by the processes signified by the terms on the right of the equation. The term $-\beta_\nu(z)I_\nu(z,\mu,\phi)$ accounts for the extinction of radiation by scattering and absorption; $\beta_\nu(z)$ is called the extinction coefficient and is the sum of the absorption coefficient $\kappa_\nu(z)$ and the scattering coefficient $\sigma_\nu(z)$. The term $\kappa_\nu(z)I_{b\nu}(z)$ accounts for the increase of the intensity by the emission of the medium and the term

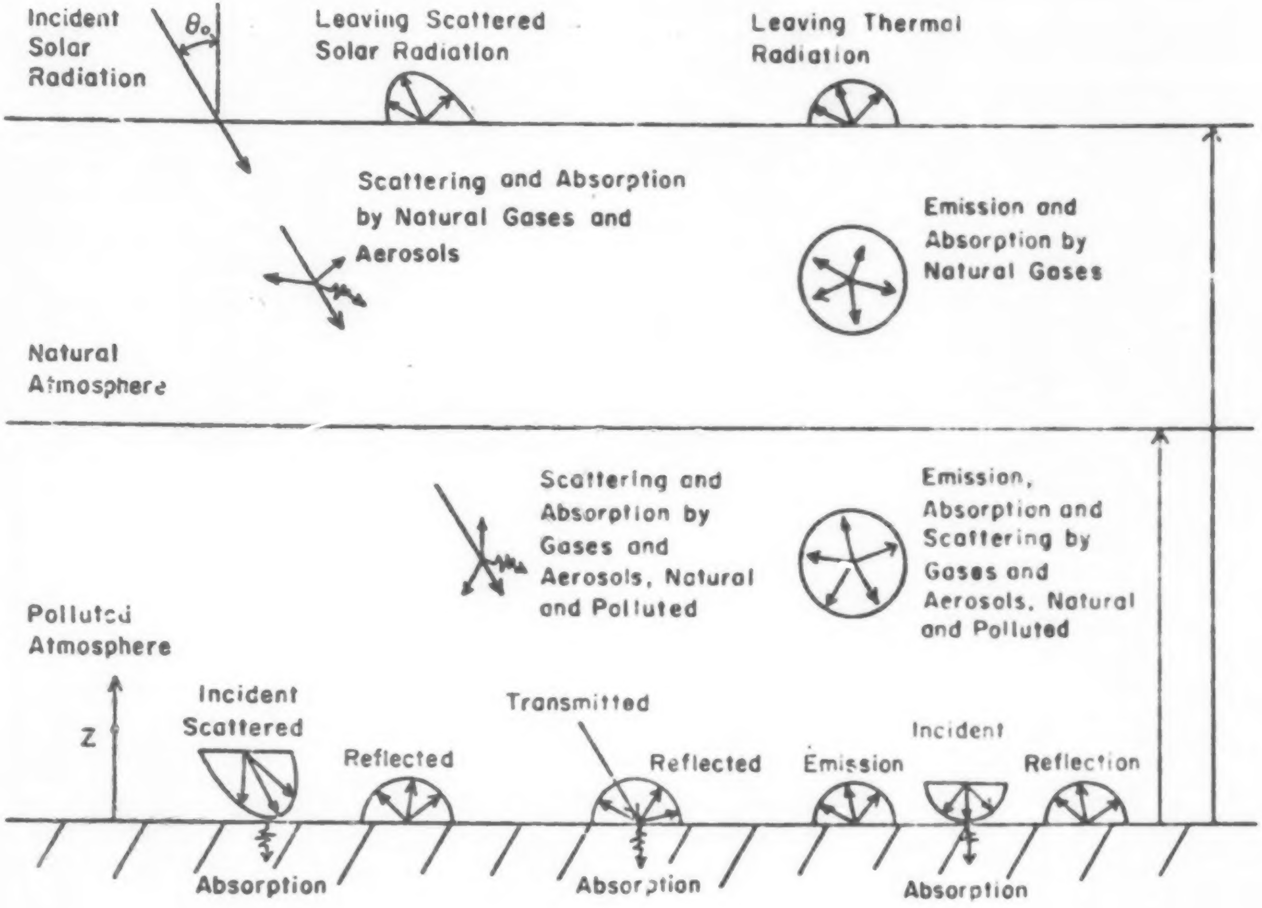
Incident
Solar
Radiation
θ_o
Leaving Scattered
Solar Radiation
Leaving Thermal
Radiation
Scattering and Absorption
by Natural Gases and
Aerosols
Emission and
Absorption by
Natural Gases
Natural
Atmosphere
Scattering and
Absorption by
Gases and
Aerosols, Natural
and Polluted
Emission,
Absorption and
Scattering by
Gases and
Aerosols, Natural
and Polluted
Polluted
Atmosphere
Z
Incident
Scattered
Reflected
Transmitted
Reflected
Emission
Incident
Reflection
Absorption
Absorption
Absorption

Figure 6.1 Physical Model for Thermal and Solar Radiation

$$\frac{\sigma_\nu(z)}{4\pi}\int_{\mu'}\int_{\phi'} p_\nu(z,\mu',\phi' \rightarrow \mu,\phi) I_\nu(z,\mu',\phi') d\mu' d\phi'$$

accounts for the contribution of radiant energy to the beam by scattering. The scattering phase function $p_\nu(z,\mu',\phi' \rightarrow \mu,\phi)$ represents the fraction of energy scattered from a pencil of radiation propagating in the direction μ',ϕ' into the solid angle centered around the direction μ,ϕ. In writing Eq. (6.2.1) is it assumed that the radiative transfer is quasisteady, the index of refraction of the medium is unity, and the atmosphere is in local thermodynamic equilibrium. The coordinate system used in formulating Eq. (6.2.1) is illustrated in Figure 6.2.

Equation (6.2.1) is a nonhomogeneous integro-differential equation and its solution presents formidable mathematical difficulties. Additional complexities arise in attempting to characterize a medium which scatters and absorbs radiation. A number of techniques have been utilized to solve the equation of transfer, and descriptions of these models can be found in books by Goody (1964) and Kondratyev (1969). An excellent summary of methods applicable to a scattering atmosphere can be found in a report published by the Radiation Commission of the I.A.M.A.P. (1974).

In applying the equation of transfer to the atmosphere, it is assumed that the atmosphere is horizontally homogeneous. This assumption is based on two considerations which are:

1. Computational simplicity: A 2-D or 3-D radiative transfer model would require excessive computational effort. The significance of this statement becomes clear when one notes that an accurate solution of the 1-D radiative transfer equation requires substantial computer time.
2. The approximate horizontal homogeneity of the boundary layer: Over the horizontal scales (~20 km) of interest the gradients of the atmospheric variables are small compared to the vertical gradients. Therefore, there is some justification in considering the atmosphere to be horizontally homogeneous. An approximate method to handle horizontal inhomogeneity

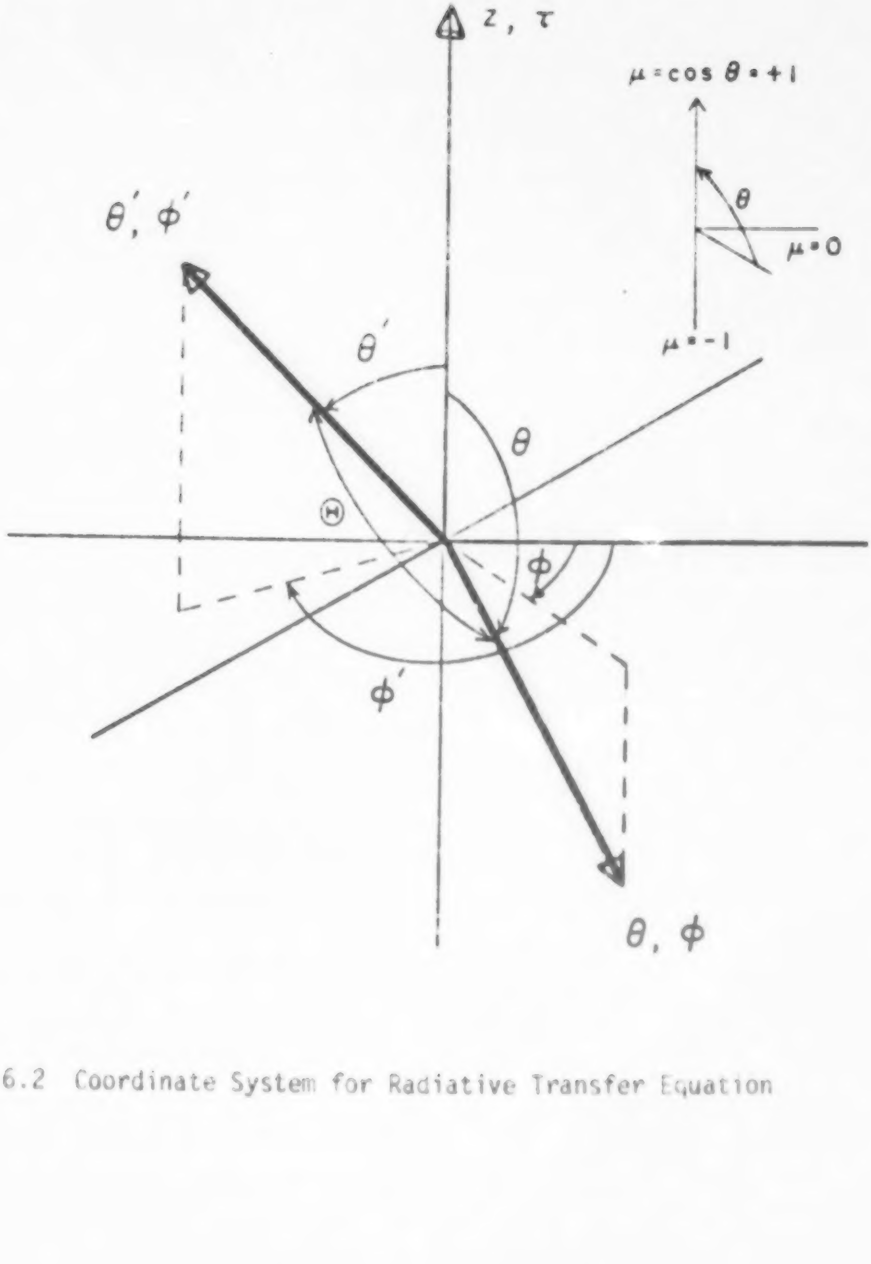
z, τ
μ = cos θ = +1
θ
μ = 0
μ = -1
θ′, ϕ′
θ′
θ
Θ
ϕ
ϕ′
θ, ϕ

Figure 6.2 Coordinate System for Radiative Transfer Equation

would be to compute the 1-D radiative fluxes along horizontal locations and use interpolation to compute fluxes at intermediate points.

Using the assumption of horizontal homogeneity Eq. (6.2.1) can be written as

$$\mu \frac{dI_\nu}{dz} = -\beta_\nu(z) I_\nu(z,\mu) + \kappa_\nu(z) I_{b\nu}(z) + \frac{\sigma_\nu(z)}{2} \int_{-1}^{+1} p_\nu(z,\mu' \rightarrow \mu) I_\nu(z,\mu') d\mu' \tag{6.2.2}$$

In writing Eq. (6.2.2) it has been assumed that the phase function as well as the intensity has been averaged over the azimuthal angle ϕ.

This equation can be more conveniently expressed by defining the following quantities. The optical thickness τ_ν at the frequency ν is given by

$$\tau_\nu(z) = \int_0^z \beta_\nu(x) dx \tag{6.2.3a}$$

and the single scattering albedo ω_ν is defined by

$$\omega_\nu(z) = \sigma_\nu(z)/\beta_\nu(z) = \sigma_\nu(z)/[\kappa_\nu(z) + \sigma_\nu(z)] \tag{6.2.3b}$$

Using the definitions given by Eqs. (6.2.3a) and (6.2.3b), Eq. (6.2.2) can be written as

$$\mu \frac{dI_\nu(\tau_\nu,\mu)}{d\tau_\nu} = -I_\nu(\tau_\nu,\mu) + (1 - \omega_\nu) I_{b\nu}(\tau_\nu) + \frac{\omega_\nu}{2} \int_{-1}^{+1} p_\nu(\mu' \rightarrow \mu) I_\nu(\tau_\nu,\mu') d\mu' \tag{6.2.4}$$

The radiative energy flux F_ν across a plane at height z is defined by

$$F_\nu = 2\pi \int_{-1}^{+1} I_\nu(\mu) \mu d\mu \tag{6.2.5}$$

The fact that the atmospheric radiation spectrum can be divided into two distinct regions can be advantageously utilized in solving Eq. (6.2.4). In the solar spectrum, extending from 0.3 μm to 4.0 μm, emission can be safely neglected, and in the thermal spectrum (4.0 μm to 100 μm) scattering can be assumed to be negligible. The former assumption is based on the fact that most of the emission occurs in the thermal spectrum, and the latter on the fact that aerosols, which cause most of the scattering, do not interact with long-wave terrestrial radiation. Also, the effect of larger aerosol (~1 μm), which can interact with thermal radiation, is negligible because larger aerosols are found in small numbers (Peterson, et al., 1969).

6.3 Radiative Transfer in the Solar Spectrum

In the solar spectrum, the emission term in the radiative transfer equation can be neglected and Eq. (6.2.4) reduces to

$$\mu \frac{dI_\nu}{d\tau_\nu} = -I_\nu + \frac{\omega_\nu}{2} \int_{-1}^{+1} p_\nu(\mu' \rightarrow \mu) I_\nu(\tau_\nu, \mu') d\mu' \qquad (6.3.1)$$

For convenience in writing the equation the dependence of I_ν on μ and τ_ν has been dropped. Even in its relatively simplified form, Eq. (6.3.1) presents mathematical difficulties, and except for the simplest scattering phase functions, it does not permit an analytic solution and numerical methods have to be resorted to. Any satisfactory solution of the equation would entail computation of the radiative fluxes over small wavelength intervals in order to account for the strong absorption in certain narrow wavelength bands. This computational process is costly and cumbersome, and several approximate methods have been suggested to reduce the numerical effort. The methods usually involve one of the two approximations: (1) discretization of the angular distribution of the radiation intensity examples of which are provided by the six-stream method of Chu and Churchill (1955), the Eddington approximation used by Pitts (1954), the Chandrasekhar approximation (1960), modified two-stream method by Sagan and Pollack (1967), and the spherical harmonic approximation used by Canosa and

Panafiel (1973); (2) approximating the scattering phase function by a simpler mathematically tractable function examples of which are provided by the small angle approximation due to Romanova (1962) and the delta function approximation due to Potter (1970).

The scope of this study did not permit detailed calculation of the radiative fluxes; considerations of computational efficiency played the major role in the choice of the technique to calculate the fluxes. The detailed radiation model due to Bergstrom (1972) which was available for use in this research program was not selected because it required computer time which was excessive from the point of view of this study. An examination of other available methods showed that the so-called two-stream method met the requirement of computational convenience without introducing unacceptable idealizations. As the name implies, the method approximates the angular distribution of intensity by two intensities, one of which characterizes the radiation field in the forward direction and the other, the backward direction. Also, the phase function is parameterized by introducing the forward and the backward scattering factors which are the fractions of the radiative flux scattered in the forward and backward directions, respectively. These statements will become clear when the two-stream equations are derived. The two-stream method has been used by Sagan and Pollack (1967) to study scattering in Venusian clouds, and by Rasool and Schneider (1971) to study the effect of aerosols on global climate. More recently, Wang and Domoto (1974) have adapted the method to treat nongray gaseous absorption with multiple scattering in the planetary atmosphere.

6.4 Radiative Properties of Aerosols and Gaseous Absorbers in the Solar Spectrum

As radiative transfer was just one of the several physical processes modeled in this investigation, it was necessary to use a radiation model which would be simple and at the same time yield relatively accurate estimates of the radiative fluxes. The adoption of the two-stream approximation leads to a reduction of computational effort only if the properties of the radiative participants are parameterized. From the point of view of storage as well as computer time, it is necessary to avoid detailed integrations over wavelength. For reasons which will be discussed later, aerosols allow parameterization of properties. Gaseous absorbers such as NO_2 and SO_2, on the other hand, have to be accounted on a wavelength basis because their strong absorption precludes mean property representations. Thus, it was found convenient to assume that aerosols and water vapor were the only participants in the solar spectrum. This emphasis on aerosols is not unrealistic especially in view of recent studies (Rasool and Schneider, 1971; Mitchell, 1971; McCormick and Ludwig, 1967; Braslau and Dave, 1973; Landsberg, 1970; Wang and Domoto, 1974; Kondratyev, et al., 1974) which indicate that aerosols can play a major role in determining the radiation balance of the earth-atmosphere system.

It is assumed that radiative properties of aerosols can be represented by spectrally averaged quantities. This assumption is based on a recent study by Bergstrom (1971) which shows that the absorption and scattering coefficients of slightly absorbing aerosols (10% carbon content) vary very slightly in the wavelength interval, $0.3\ \mu m \leq \lambda \leq 1.0\ \mu m$, a region which contains 70% of the solar radiation. Furthermore, as aerosols are predominantly scatterers, the spectral distribution of the solar radiation is not as drastically altered as it would have been by strong absorption bands, and there is justification in defining mean radiative properties weighted with respect to the solar spectral distribution. A number of studies (Rasool and Schneider, 1971; Atwater, 1970) have also used representative values for the radiative properties of aerosols in calculating the solar fluxes.

In estimating the optical path due to the water vapor, the nonlinearity of the absorption of the water vapor bands has to be taken into account. Relatively large amounts of water vapor inside the boundary layer do not cause significant heating because most of the energy in the important water vapor bands is absorbed in the region above the planetary boundary layer. Thus, a large increase in water vapor path length is accompanied by a proportionately much smaller increase in absorption.

In order to avoid lengthy computations involving wavelength integration, a parameterized expression (Lacis and Hansen, 1974) for water vapor absorption has been used to calculate the effective water vapor optical thickness. For a cloud-free atmosphere, Lacis and Hansen (1974) use the following expression to compute the absorption by water vapor in the ℓ-th layer of the atmosphere:

$$A_{\ell,wv} = \mu_o \pi F_o \left\{ A_{wv}(y_\ell + 1) - A_{wv}(y_\ell) + R_g [A_{wv}(y_\ell^*) - A_{wv}(y_{\ell+1}^*)] \right\} \tag{6.4.1}$$

where πF_o is the solar constant, μ_o is the cosine of the solar zenith angle, R_g is the ground albedo, y_ℓ is the effective water vapor amount traversed by the direct solar beam in reaching the ℓ-th layer, y_ℓ^* is the effective water vapor path traversed by the reflected radiation in reaching the ℓ-th layer from below, and A_{wv} is an empirical function of ℓ-th; $A_{wv}(y_\ell)$ gives the fraction of energy absorbed in a layer of effective water vapor thickness y_ℓ. This study utilizes the function $A_{wv}(y_\ell)$ suggested by Yamamoto (1962) which is given by

$$A_{wv}(y) = 2.9y/[(1 + 141.5y)^{0.635} + 5.925y)] \tag{6.4.2}$$

where y has the units of cm of precipitable water vapor.

In order to utilize Eq. (6.4.2) to calculate an effective thickness required in the two flux formulation, consider a beam of solar radiation traversing a layer ℓ. The energy absorbed in this layer A_E, is then given by,

$$A_E = \pi F_o \mu_o [A_{wv}(y_{\ell+1}/\mu_o) - A_{wv}(y_\ell/\mu_o)] \tag{6.4.3}$$

where y_ℓ is the effective path length measured vertically downwards from the top of the atmosphere. Assuming that the layer can be represented by an incremental optical thickness $\Delta\tau$, one can write

$$[1 - A_{wv}(y_\ell/\mu_0)][1 - \exp(-\Delta\tau/\mu_0)] = A_{wv}(y_{\ell+1}/\mu_0) - A_{wv}(y_\ell/\mu_0) \qquad (6.4.4)$$

Then,

$$\Delta\tau = -\mu_0 \ln[1 - (A_{wv}(y_{\ell+1}/\mu_0) - A_{wv}(y_\ell/\mu_0))/(1 - A_{wv}(y_\ell/\mu_0)] \qquad (6.4.5)$$

There is some ambiguity in the definition of the incremental optical thickness given by (4.4.5). Optical thicknesses can be computed for the radiation reaching the layer from below, and for the scattered radiation. Thus, it is possible to associate several optical thicknesses with the same layer. This is inconvenient and it is necessary to choose a "dominant" optical thickness. Assuming that most of the solar energy is contained in the direct beam, the optical thickness was defined by considering the absorption of the direct beam. Equation (6.4.5) defines the "direct beam" optical thikcness. Clearly, it is desirable to have a definition based on scattered radiation to handle cases when the zenith angle is large (early morning and evening) and most of the solar radiation is diffuse. However, it is not practical to use two different optical thicknesses. Also, as the magnitude of the diffuse radiation is small, the computation of the optical thickness at large zenith angles is not critical.

Empirical methods (Paily, et al., 1974) were used to compute the direct and diffuse radiation at the top of the boundary layer. Though empirical, these methods have been tested thoroughly and given accurate estimates of the total fluxes. Thus, the basic method to compute the radiative fluxes in the solar spectrum consisted of two steps: (1) compute scattered (diffuse) and directly transmitted solar fluxes at the top of the planetary boundary layer using empirical methods, and (2) compute radiative fluxes in the boundary layer using the more accurate two-flux method. The fluxes computed in step 1 serve as boundary conditions for the calculation in step 2.

6.5 Two-Stream Equations

The two-stream equations can be derived by considering the radiative transfer equation in the form,

$$\mu \frac{dI}{d\tau} = -I + \frac{\omega}{2} \int_{-1}^{+1} p(\mu' \rightarrow \mu) I(\tau,\mu') d\mu' \qquad (6.5.1)$$

The dependence of the intensity on the frequency ν has been dropped on the basis of the mean property assumption discussed in the preceding section.

The boundary conditions for Eq. (6.5.1) can be written as,

$$I(0,\mu) = 2 \int_{0}^{1} r_s(-\mu' \rightarrow \mu) I(0,-\mu')\mu' d\mu' \ ; \quad \mu > 0 \qquad (6.5.2a)$$

and

$$I(\tau_0,\mu) = S\delta[\mu - (-\mu_0)] + I_d \ ; \quad \mu > 0 \qquad (6.5.2b)$$

where r_s is the mean bi-directional reflectance of the earth's surface, μ_0 is the optical thickness of the boundary layer, S is the direct beam component (at zenith angle $\cos^{-1} \mu_0$) of the solar radiation at the top of the boundary layer and I_d is intensity of the diffuse component. Then, Eq. (6.5.2a) states that the intensity of the radiation traveling in $+\mu$ direction is the sum of the contributions from the beams of radiation reflected at the surface. Equation (6.5.2b) states that the source of radiation at the top of the boundary layer consists of the direct and the diffuse components of solar radiation.

To aid in the solution of Eq. (6.5.1) the scattering phase function is expressed as a finite series of Legendre polynomials

$$p(\tau,\mu' \rightarrow \mu) = \sum_{\ell=0}^{N} p_\ell(\tau) P_\ell(\mu) P_\ell(\mu') \qquad (6.5.3)$$

where $P_\ell(\mu)$ is a Legendre polynomial of order ℓ. Details of the derivation of Eq. (6.5.3) can be found in the book by Chandrasekhar (1960).

Substitution of Eq. (6.5.3) into Eq. (6.5.1) yields

$$\mu \frac{dI}{d\tau} = -I + \frac{\omega}{2} \sum_{\ell=0}^{N} p_\ell(\tau) \int_{-1}^{+1} P_\ell(\mu) P_\ell(\mu') I(\tau,\mu') d\mu' \qquad (6.5.4)$$

To simplify the application of the boundary condition (6.5.2b) the directly transmitted solar radiation is subtracted from the mean intensity I which is then redefined by

$$\tilde{I}(\tau,\mu) = I(\tau,\mu) - S\delta[\mu - (-\mu_0)]e^{(\tau_0-\tau)/\mu} \qquad (6.5.5)$$

Substitution of (6.5.5) in (6.5.4) results in

$$\mu \frac{d\tilde{I}}{d\tau} = -\tilde{I}(\tau,\mu) + \frac{\omega}{2} \sum_{\ell=0}^{N} p_\ell P_\ell(\mu) \int_{-1}^{+1} \tilde{I}(\tau,\mu') P_\ell(\mu') d\mu'$$

$$+ \frac{\omega}{2} S e^{(\tau_0-\tau)/\mu} \sum_{\ell=0}^{N} p_\ell P_\ell(\mu) P_\ell(-\mu_0) \qquad (6.5.6)$$

The two-stream approximation can be introduced by considering the integral F given by

$$F = \int_{-1}^{+1} \tilde{I}(\tau,\mu)\mu d\mu \qquad (6.5.7a)$$

Using a two-point Gaussian quadrature formula, F can be expressed as

$$F = (I^+ - I^-)/\sqrt{3} \qquad (6.5.7b)$$

Thus, I^+ represents the intensity radiation traveling in $+\mu$ ($= 1/\sqrt{3}$) direction, and I^-, that of the radiation traveling in the $-\mu$ ($= -1/\sqrt{3}$) direction.

The two-stream equations are obtained by multiplying Eq. (6.5.6) by $d\mu$ and $\mu d\mu$, respectively, and integrating over μ from +1 to -1,

$$\frac{1}{\sqrt{3}}\frac{dI^+}{d\tau} = (f\omega - 1)I^- + b\omega I^- + \frac{\omega}{2}S[1 - \sqrt{3}(1 - 2b)\mu_o]e^{-(\tau_o-\tau)/\mu_o} \tag{6.5.8a}$$

$$-\frac{1}{\sqrt{3}}\frac{dI^-}{d\tau} = (f\omega - 1)I^- + b\omega I^+ + \frac{\omega}{2}S[1 + \sqrt{3}(1 - 2b)\omega_o]e^{-(\tau_o-\tau)/\mu_o} \tag{6.5.8b}$$

where I^+ and I^- have been defined by Eq. (6.5.7b). The backscattering factor, b, and the forward scattering factor, f, are defined by the equations

$$2b = 1 - \frac{1}{2}\int_{-1}^{+1} P(\mu)\mu d\mu \tag{6.5.9a}$$

$$f = 1 - b \tag{6.5.9b}$$

Then, assuming that the earth's surfacc reflects diffusely, the boundary conditions can be expressed in terms of I^+ and I^-

$$I^+(0) = r_s\left[I^-(0) + \sqrt{3}\,\mu_o S e^{-\tau_o/\mu_o}\right] \tag{6.5.10a}$$

and

$$I^-(\tau_o) = I_d \tag{6.5.10b}$$

Even with the simplifications afforded by the two-flux approximation it is not possible to obtain analytic solutions for Eqs. (6.5.8) because ω, f, and b are functions of the optical depth. It should be mentioned, however, that Wang and Domoto (1974) have obtained an approximate solution to the two-flux equations using a perturbation technique.

In order to facilitate an analytic solution of the two-stream equations it is assumed that the radiative properties of the constituents of the planetary boundary layer can be represented by a mean single scattering albedo, and a mean forward scattering factor which are defined by the following equation

$$\bar{\omega} = (\tau_R + \omega\tau_A)/(\tau_R + \tau_A + \tau_G) \tag{6.5.11}$$

where $\bar{\omega}$ is the mean single scattering albedo, ω is the aerosol single scattering albedo, τ_A is the aerosol optical thickness, τ_R is the Rayleigh optical thickness, and τ_G is the optical thickness of the absorbing gas.

The mean forward scattering factor $\bar{f}$ is defined by

$$\bar{f} = (f\tau_A + f_R\tau_R)/(\tau_A + \tau_R) \tag{6.5.12}$$

where f is aerosol forward scattering factor, and f_R is the Rayleigh forward scattering factor ($f_R = 0.5$).

With the assumptions described in preceding paragraphs, Eqs. (6.5.8) reduce to a pair of coupled linear differential equations, and the solution is straightforward

$$I^+(\tau) = \alpha_1\beta_1 e^{\alpha\tau} + \alpha_2\beta_2 e^{-\alpha\tau} + C_1 e^{-(\tau_o-\tau)/\mu_o} \tag{6.5.13a}$$

$$I^-(\tau) = \beta_1 e^{\alpha\tau} + \beta_2 e^{-\alpha\tau} + C_2 e^{-(\tau_o-\tau)/\mu_o} \tag{6.5.13b}$$

where

$$\alpha = \sqrt{3}[(1 - \bar{\omega}\,\bar{f})^2 - (\bar{\omega}\,\bar{b})^2]^{\frac{1}{2}} \tag{6.5.14a}$$

$$\alpha_1 = \sqrt{3}\,\bar{\omega}\,\bar{b}/(\sqrt{3}(1 - \bar{\omega}\,\bar{f}) + \alpha) \tag{6.5.14b}$$

$$\alpha_2 = \sqrt{3}\,\bar{\omega}\,\bar{b}/(\sqrt{3}(1 - \bar{\omega}\,\bar{f}) - \alpha) \tag{6.5.14c}$$

where

$$\bar{b} = 1 - \bar{f} \tag{6.5.14d}$$

Before defining β_1, β_2, C_1 and C_2 it is convenient to define the intermediate quantities,

$$b_2 = \sqrt{3}\,\bar{\omega}\,\bar{b} \tag{6.5.15a}$$

$$S_1 = \sqrt{3}(1 - \sqrt{3}(1 - 2\bar{b})\mu_0)\bar{\omega}S/2 \tag{6.5.15b}$$

$$S_2 = \sqrt{3}(1 + \sqrt{3}(1 - 2\bar{b})\mu_0)\bar{\omega}S/2 \tag{6.5.15c}$$

$$a = \sqrt{3}(1 - \bar{\omega}\,\bar{f}) \tag{6.5.15d}$$

$$d_1 = a - 1/\mu_0^2 - b_2^2 \tag{6.5.15e}$$

$$d_2 = (\alpha_1 - r_s)e^{-\alpha\tau_0} - (\alpha_2 - r_s)e^{\alpha\tau_0} \tag{6.5.15f}$$

$$t_1 = (\rho C_2 - C_1 + r_s\sqrt{3}\,\mu_0 S)e^{-(\tau_0/\mu_0+\alpha\tau_0)} - (I_d - C_2)(\alpha_2 - r_s) \tag{6.5.15g}$$

$$t_2 = (\alpha_2 - r_s)(I_d - C_2) - (r_s C_2 - C_1 + r_s\sqrt{3}\,\mu_0 S)e^{-(\alpha\tau_0-\tau_0/\mu_0)} \tag{6.5.15h}$$

Then,

$$C_1 = [S_1(a - 1/\mu_0) + S_2 b_2]/d_1 \tag{6.5.16a}$$

$$C_2 = [S_2(a + 1/\mu_0) + S_1 b_2]/d_1 \tag{6.5.16b}$$

$$\beta_1 = t_1/d_2 \tag{6.5.16c}$$

$$\beta_2 = t_2/d_2 \tag{6.5.16d}$$

Then, in terms of F^+ and F^-, the radiative flux F is given by

$$F = 2\pi\int_{-1}^{+1} I(\tau,\mu)\mu d\mu = 2\pi\int_{-1}^{+1}\left\{\tilde{I}(\tau,\mu) + S\delta[\mu - (-\mu_0)]e^{(\tau_0-\tau)/\mu}\right\}\mu d\mu$$

$$= \frac{2\pi}{\sqrt{3}}[I^+ - I^-] - 2\pi\mu_0 S e^{-(\tau_0-\tau)/\mu_0} \tag{6.5.17}$$

The divergence of the solar radiative flux can be written as

$$\frac{dF}{d\tau} = 2\pi[\alpha\beta_1 e^{\alpha\tau}(\alpha_1 - 1) + \alpha\beta_2 e^{-\alpha\tau}(1 - \alpha_2)$$

$$+ e^{-(\tau_0-\tau)/\mu_0}(C_1 - C_2)/\mu_0]/\sqrt{3} - 2\pi\mu_0 S e^{-(\tau_0-\tau)/\mu_0} \Big/ \mu_0 \tag{6.5.18}$$

6.6 Band Models

Infrared absorption and emission of thermal radiation is a consequence of coupled vibrational and rotational energy transitions. As these transitions occur at discrete frequencies the absorption spectra of polyatomic gases tend to be discontinuous. Figure 6.3 illustrates the absorption spectrum of carbon dioxide, and it can be seen that absorption occurs in fairly distinct bands which are separated by regions in which negligible absorption occurs. The location of a particular band is determined by the associated vibrational transition, while the "lines" in the band are governed by rotational transitions which accompany the vibrational transition. Thus, a typical infrared spectrum would consist of a few bands each of which would consist of hundreds of lines.

Although modern spectroscopy can resolve detailed line structure, it is impractical to do line by line calculations to compute radiative fluxes routinely. The alternative to this type of exact calculation is to utilize band models. Before proceeding on the subject of band models, it is convenient to define the band absorptance or the effective bandwidth

$$A = \int_{\Delta\nu} [1 - \exp(-\kappa_\nu L)]d(\nu - \nu_0) \tag{6.6.1}$$

where A is the band absorptance of a homogeneous layer of gas of thickness L, and ν_0 is the center of the interval of integration $\Delta\nu$,

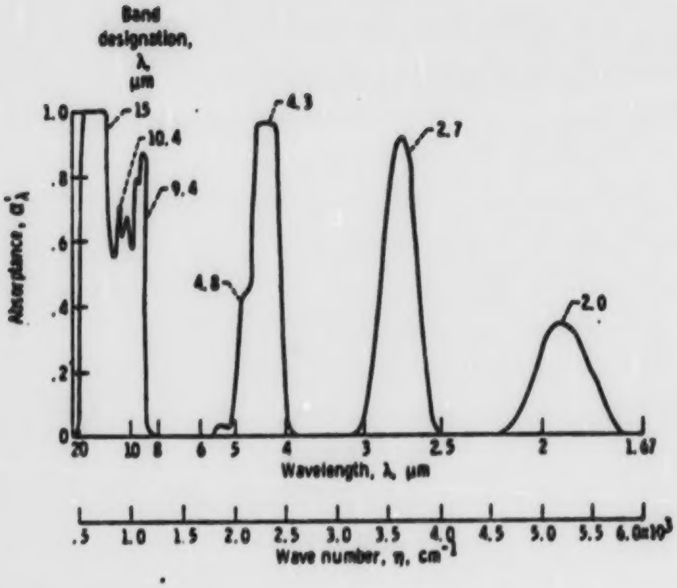

Figure 6.3 Low-Resolution Spectrum of Absorption Bands for CO_2 Gas at 830 K, 10 atm, and for Path Length Through Gas of 38.8 cm (Siegel, R., and Howell, J. R.: 1972, Thermal Radiation Heat Transfer, McGraw-Hill Book Company, New York, 814 pp, pg 406)

and κ_ν is the monochromatic absorption coefficient. Physically, A represents the effective bandwidth over which the emitted radiation can be considered to be black. The integrand $[1 - \exp(-\kappa_\nu L)]$, by itself, is the fraction of energy absorbed at a frequency ν from a beam of radiation in traversing a distance L through a homogeneous gas. These two different physically interpretations are a direct result of Kirchoff's law, and suggest that A can be associated with either the emission or the absorption of radiation: band absorptance suggestive of absorption and effective bandwidth suggestive of emission.

The construction of a band model involves postulating the structure of the lines in the bands in terms of line parameters. Based on the line postulate an expression for the band absorptance is derived, and the unknown line parameters are determined by correlating experimental absorptance data with the theoretically obtained expression. The line structure assumptions determine the particular band model. Some of these band models are the Elsasser regular band model, the statistical Mayer-Goody model, Random Elsasser band model, and the Quasi-Random band model (Tiwari, 1975). The application of any model to a particular case depends upon the nature of the absorbing-emitting molecule. While a model may provide excellent correlation with experimental data for linear molecules, it might fail to do so for asymmetric and spherical top molecules.

Before describing the model used in this investigation, it is necessary to discuss the difference between narrow and wide band models. A narrow band model results when $\Delta\nu$, the interval of integration, is of the order of spacing of the lines. Then, the narrow band absorptance can be expressed in terms of mean line parameters which are the mean half-width, the mean line spacing, and the mean line intensity (the integral of the absorption coefficient over the line width). The transition from the narrow band model to the wide band model is made by calculating the band absorptance over the entire band after making plausible assumptions about the variation of the mean line parameters over the band. The nature of the assumptions determines the particular wide band model. The models mentioned in the previous paragraphs are narrow band models while some of the wide band models are the box model due to Penner (1959) and the exponential wide band model due to Edwards (1964, 1967).

The preceding paragraphs provide a very brief description of band models. More details can be found in excellent summary papers by Tien (1968), Cess and Tiwari (1972), and Tiwari (1975).

6.7 Infrared Radiation Properties of Gases

It should be clear from the previous section that the definition of band absorptance is strictly applicable only to a homogeneous gas layer. Thus, in order to utilize the concept of band absorptance in the computation of radiative fluxes in an inhomogeneous atmosphere, it is necessary to use a method which "corrects" for the inhomogeneity. One such method is the Curtis-Godson approximation which essentially replaces an inhomogeneous layer by a "radiatively" equivalent homogeneous layer enabling the use of narrow band models. An alternative to this technique is to use emissivities. The concept of emissivity as it is used by meteorologists (Brooks, 1950; Sasamori, 1968; Eliott and Stevens, 1961; Atwater, 1970) is empirical in nature; it associates an emissivity with a gas layer, and the effects of inhomogeneity are taken into account by using empirically determined pressure and temperature correction factors. Rodgers (1966) has shown that the emissivity approximation is capable of the same order of accuracy as the more exact methods (for example, the diffuse approximate due to Rodgers and Walshaw, 1966), but only if used in an empirical rather than a theoretical manner. Emissivities must be fitted to calculated or accurately measured atmospheric fluxes rather than directly to spectral data obtained in the laboratory.

As the principle behind the emissivity approximation is now well enough established for most meteorological purposes, this study utilized empirical emissivities wherever possible. For water vapor, the emissivity correlations derived by Atwater (1970) from Kuhn's (1963) emission data were used. It should be mentioned that Kuhn's data are based on measured atmospheric fluxes. Also, as the effects of carbon dioxide overlap with water vapor at 15 μm have been subtracted out, the use of Kuhn's data avoids the problem of overlap. For carbon dioxide the emissivity correlation proposed by Shekter (1950) and subsequently revised by Kondratyev (1969) was used. As emissivity correlations are not available for common pollutant gases such as ammonia, carbon monoxide and ethylene, it was necessary to use wide band absorptances to define an effective emissivity given by

$$\varepsilon_{\varepsilon f}(u) = \sum_i E_{b\nu_i}(T_{ef}) A_i(ru, T_{ef}, P_{ef})/T_{ef} \qquad (6.7.1)$$

where i refers to a band, $E_{b\nu_i}$ is the blackbody emitted flux at the center of the band, u is the mass length, σ is the Stefan-Boltzmann constant, and r is the diffusivity factor, the meaning of which will be explained later. The effective pressure P_{ef} is defined by

$$P_{ef} = \frac{1}{u} \int_0^u P(t)dt \qquad (6.7.2)$$

and T_{ef} is the temperature corresponding to P_{ef}. Equation (6.7.2) has been used by Jurica (1970), and is based on the Curtis-Godson approximation.

The technique implied by Eq. (6.7.2) to correct the temperature and pressure variation is empirical, and has been used in this study because it is simple compared to the more rigorous methods (Chan and Tien, 1969; Edwards and Morizumi, 1970), and Jurica (1970) has had some success in using the method. It should be pointed out that the definition of emissivity given by Eq. (6.7.1) has meaning only when applied to a homogeneous gas layer. Rodgers (1966) has shown that it is not possible to define a unique emissivity when an inhomogeneous gas is being considered--the upward and the downward fluxes require different emissivities to make the definitions of the emissivities compatible with the radiative transfer equation. It should be reiterated that the concept of emissivity does not "fall out" of the radiative transfer equations, but can be very useful when treated in an empirical manner. It is felt that in the absence of empirically derived emissivities for the pollutant gases there is justification in using Eq. (6.7.1) to provide estimates for the emissivities.

The Edwards exponential wide band model was used to calculate the effective emissivities of the pollutant gases. This choice of a wide band model was based on two considerations. Firstly, the Edwards model has enjoyed considerable success in correlating band absorptance data; secondly, its utilization allows the incorporation of band absorptance correlations which can be expressed as single explicit functions of the path length (Tien and Lowder, 1966; Goody and Belton, 1967; Cess and Tiwari, 1972).

The exponential wide band model assumes that the mean line intensity is an exponentially decaying function of the wave number. Then, utilizing the narrow statistical band model, the expression for the band absorptance can be integrated over the bandwidth. The band absorptance can be then written as

$$A = A(C_1, C_2, C_3, \beta, X) \tag{6.7.3a}$$

where

$$\beta = \frac{C_2^2 P_e}{4C_1C_3} \tag{6.7.3b}$$

$$X = \rho L \tag{6.7.3c}$$

and L is the thickness of the homogeneous gas layer, ρ is the density and P_e is an effective pressure which takes pressure broadening by other gases into account. C_1, C_2, and C_3 are functions of temperature and characterize the structure of the band. A summary of the functions C_1, C_2, and C_3 for a number of gases can be found in papers by Edwards (1964a, 1964b) and in the review paper by Tien (1968). In the original formulation due to Edwards, different pathlength ranges involved the utilization of different functional forms of A. As it is desirable to have a single explicit expression for the band absorptance for the whole path length range, researchers (Tien and Lowder, 1966; Cess and Tiwari, 1972) have suggested single continuous correlations for the band absorptance. One such formulation is that due to Tien and Lowder (1966) and has been used in this study. The band absorptance is given by

$$\bar{A}(u,t) = \ln\{uf_2(t)[(u + 1)/(u + af_2(t))] + 1\} \tag{6.7.4}$$

where

$$\bar{A} \equiv A/C_3$$
$$u \equiv (C_1/C_3)X \tag{6.7.5}$$
$$t \equiv (C_2^2/4C_1C_3)p$$

and

$$f_2(t) = 2.94[1 - \exp(-2.60t)] \tag{6.7.6}$$

As has been mentioned before, gaseous pollutants are important only when they absorb in the atmospheric window extending from 8 μm to 12 μm. Thus, a representative pollutant has to meet the requirement of being a strong absorber in the atmospheric window region. An examination of the absorption properties of a number of pollutant gases showed that ammonia was the best candidate for a representative pollutant. Ammonia has its strongest band (at 300 K) centered at 10.5 μm, and it absorbs very strongly in the entire window region. Also, ammonia seems to be becoming an increasingly important air pollutant since it is associated with the presence of a large population (Ludwig et al., 1969). The importance of ammonia as a pollutant has motivated a number of studies on the infrared properties of the gas (France and Williams, 1966; Walsh, 1969). Recently (1973) Tien has correlated the France-Williams (1966) data to yield the wide-band parameters which were used in this study. In addition to ammonia, this investigation has also used sulphur dioxide, carbon monoxide, and methane as possible pollutants. The wide band parameters for carbon monoxide and methane were taken from the review paper by Tien (1968), and those for sulphur dioxide from a more recent paper by Chan and Tien (1971).

An alternative to using a single gas as a representative pollutant is to use a combination of gases which together cover the entire window region. One such combination could consist of SO_2 and C_2H_4. C_2H_4 absorbs strongly in the 9 to 12 μm region and SO_2 absorbs in the range 7 to 9 μm. The proportion of the gases in the mixture can be adjusted to produce the desired absorption properties.

6.8 Radiative Fluxes in the Thermal Spectrum

In the thermal spectrum, scattering can be neglected and the radiative transfer equation reduces to

$$\mu \frac{dI_\nu(\tau_\nu,\mu)}{d\tau_\nu} = -I_\nu(\tau_\nu,\mu) + I_{b\nu}(\tau_\nu) \qquad (6.8.1)$$

The boundary conditions are

$$I_\nu^+(0,\mu) = \varepsilon I_{b\nu}(0) + 2(1-\varepsilon)\int_0^1 I_\nu^-(0,\mu')\mu' d\mu' \qquad (6.8.2a)$$

$$I_\nu^-(\tau_{0\nu},\mu) = 0 \qquad (6.8.2b)$$

where it has been assumed that the earth's surface is a diffuse emitter. In this equation $\tau_{0\nu}$ is the effective optical thickness of the earth's atmosphere, and

$$I^+(\tau_\nu,\mu) \equiv I(\tau_\nu,\mu); \quad \mu > 0 \qquad (6.8.3a)$$

$$I^-(\tau_\nu,\mu) \equiv I(\tau_\nu,\mu); \quad \mu < 0 \qquad (6.8.3b)$$

Boundary condition (6.8.2a) states that at the earth's surface, the source of radiation consists of the radiation emitted by the ground and the reflected radiation. Boundary condition (6.8.2b) states that there is no thermal source at the top of the atmosphere.

The solution to Eq. (6.8.1) with boundary conditions (6.8.2) can be readily written as (Viskanta, 1966)

$$I_\nu^+(\tau_\nu,\mu) = I_\nu^+(0,\mu)e^{-\tau_\nu/\mu} + \int_0^{\tau_\nu} I_{b\nu}(t)e^{-(\tau_\nu-t)/\mu}\,dt/\mu, \quad \mu > 0 \tag{6.8.4a}$$

$$I_\nu^-(\tau_\nu,\mu) = \int_{\tau_\nu}^{\tau_{o\nu}} I_{b\nu}(t)e^{-(t-\tau_\nu)/\mu}\,dt/\mu \quad , \mu < 0 \tag{6.8.4b}$$

The radiative flux $F_\nu(\tau_\nu)$ can be expressed as

$$\begin{aligned} F_\nu(\tau_\nu) &= 2\pi\int_{-1}^{+1} I_\nu(\tau_\nu,\mu)\mu d\mu \\ &= 2\pi\int_0^1 I_\nu(\tau_\nu,\mu)\mu d\mu + 2\pi\int_{-1}^0 I_\nu(\tau_\nu,\mu)\mu d\mu \\ &= 2\pi\int_0^1 I_\nu^+(\tau_\nu,\mu)\mu d\mu + 2\pi\int_0^1 I_\nu^-(\tau_\nu,\mu)\mu d\mu = F_\nu^+ - F_\nu^- \end{aligned} \tag{6.8.5}$$

where

$$F_\nu^+ = 2\pi\int_0^1 I_\nu^+(\tau_\nu,\mu)\mu d\mu \tag{6.8.6a}$$

$$F_\nu^- = -2\pi\int_0^1 I_\nu^-(\tau_\nu,\mu)\mu d\mu \tag{6.8.6b}$$

Substituting Eqs. (6.8.4) into Eq. (6.8.6) yields

$$\begin{aligned} F_\nu^+(\tau_\nu) &= E_3(\tau_\nu)[2\varepsilon E_{b\nu}(0) + 2(1-\varepsilon)F_\nu^-(0)] \\ &\quad + 2\int_0^{\tau_\nu} E_{b\nu}(t)\frac{d}{dt}E_3[\tau_\nu - t]dt \end{aligned} \tag{6.8.7a}$$

$$F^-(\tau) = 2\int_{\tau_\nu}^{\tau_{o\nu}} E_{b\nu}(t)\frac{d}{dt}E_3[t-\tau_\nu]dt \tag{6.8.7b}$$

where $E_n(t)$ is the exponential integral function, and $E_{b\nu}$ is the blackbody emitted flux.

Then, the total (integrated over the spectrum) fluxes can be written as

$$F^+(a) = \int_0^\infty F_\nu^+(\tau_\nu)d\nu = 2\varepsilon \int_0^\infty E_{b\nu}(0)E_3(\tau_\nu)d\nu$$
$$+ \int_0^\infty 2(1 - \varepsilon)F_\nu(0)E_3(\tau_\nu)d\nu$$
$$+ 2 \int_0^\infty\int_{\tau_\nu}^{\tau_0} E_{b\nu}(t) \frac{d}{dt} E_3[\tau_\nu - t]dtd\nu \tag{6.8.8a}$$

and

$$F^-(z) = \int_0^\infty 2 \int_{\tau_\nu}^{\tau_{0\nu}} E_{b\nu}(t) \frac{d}{dt} E_3[t - \tau_\nu]dtd\nu \tag{6.8.8b}$$

Recalling the definition of τ_ν,

$$\tau_\nu(z) \equiv \int_0^z \kappa_\nu(z)dz \tag{6.8.8c}$$

it is noticed that it is not possible to interchange the order of integration in Eqs. (6.8.8a) and (6.8.8b) unless the gaseous layer under consideration is homogeneous, i.e., $\kappa_\nu \neq \kappa_\nu(z)$. Thus, a precise computation of fluxes in an inhomogeneous layer would involve line by line integrations along the path followed by integration over the wave numbers. Clearly, such a method is impractical, and it is necessary to use an alternative procedure such as the Curtis-Goodson approximation described in the preceding section. Before considering an inhomogeneous layer, it is convenient to examine the computation of fluxes in a homogeneous gas layer. The application of Eqs. (6.8.8a) and (6.8.8b) to a homogeneous layer yields

$$F^+(z) = \int_0^\infty [\varepsilon E_{b\nu}(0) + (1 - \varepsilon)F_\nu^-(0)]2E_3(\kappa_\nu z)d\nu$$
$$+ \int_0^z\int_0^\infty E_{b\nu}(\xi) \frac{d}{d\xi} 2E_3[\kappa_\nu(z - \xi)]d\nu d\xi \tag{6.8.9a}$$

and

$$F^-(z) = \int_z^h\int_0^\infty E_{b\nu}(\xi)\,\frac{d}{d\xi}\,2E_3[\kappa_\nu(\xi - z)]\,d\nu\,d\xi \qquad (6.8.9b)$$

where h is the effective thickness of the atmosphere. In meteorological application (Goody, 1964) $E_3(t)$ is approximated by

$$E_3(t) = \frac{1}{2}\exp(-rt) \quad \text{with} \quad r = 1.66 \qquad (6.8.10)$$

Using Eq. (4.8.10) with the assumption that the widths of absorption bands are small compared to the entire thermal spectrum (so that $E_{b\nu}$ in a band can be replaced by the value at the center of the band) Eqs. (6.8.9) can be written as

$$F^+(z) = \sum_i [\varepsilon E_{b\nu_i} + (1 - \varepsilon)F^-_{\nu i}(0)][\Delta\nu_i - A_i(rz)]$$

$$+ \sum_j \varepsilon E_{b\nu_j}\Delta\nu_j + \int_0^z \sum_i E_{b\nu_i}(\xi)A_i'[r(z - \xi)]\,d\xi \qquad (6.8.11a)$$

and

$$F^-(z) = \int_z^h \sum_i E_{b\nu_i}(\xi)A_i'[r(\xi - z)]\,d\xi \qquad (6.8.11b)$$

where

$$A(t) = \int_{\Delta\nu} [1 - \exp(-\kappa_\nu t)]\,d\nu \qquad (6.8.12a)$$

and

$$A'(t) = \partial A(t)/\partial t \qquad (6.8.12b)$$

and i refers to the absorption bands of the gas, and j denotes the bands in which no absorption occurs; $E_{b\nu_i}$ is the blackbody emitted flux at the center of the i-th band.

It is seen that the fluxes in a homogeneous layer can be expressed in terms of band absorptances which have been experimentally correlated.

For meteorological applications, the earth's surface is assumed to be black (Goody, 1964), and Eqs. (6.8.11) reduce to

$$F^{+}(z) = \sigma T_s^4 - \sum_i E_{b\nu_i} A_i(rz) + \int_0^z \sum_i E_{b\nu_i}(\xi) A_i'[r(z - \xi)]d\xi \tag{6.8.13a}$$

and

$$F^{-}(z) = \int_z^h \sum_i E_{b\nu_i}(\xi) A_i'[r(\xi - z)]d\xi \tag{6.8.13b}$$

The introduction of the emissivity given by Eq. (4.7.1) into Eqs. (4.8.13a) and (4.18.13b) yields

$$F^{+}(z) = \sigma T_s^4[1 - \varepsilon(z)] + \int_0^z \sigma T^4(\xi) \frac{\partial \varepsilon(z - \xi)}{\partial \xi} d\xi \tag{6.8.14a}$$

and

$$F^{-}(z) = \int_z^h \sigma T^4(\xi) \frac{\partial \varepsilon(\xi - z)}{\partial \xi} d\xi \tag{6.8.14b}$$

where T_s is the temperature of the ground.

Equations (6.18.14a) and (6.8.14b) are the form of the radiative transfer equations employed in meteorological investigations. It is clear that this simple form results only when the gas layer under consideration is homogeneous. However, the approach used by meteorologists assumes that the same equations apply to an inhomogeneous atmosphere if the emissivity is corrected for inhomogeneity. Although this approach is empirical, its success in computing fluxes has proved it to be a very useful alternative to laborious narrow band calculations (with the Curtis-Godson approximation).

This study used Eqs. (6.8.14a) and (6.8.14b) to compute the infrared fluxes. The numerical scheme adopted was similar to the ones used by Jurica (1970) and other meteorologists (e.g., Atwater, 1966). The thermal fluxes are evaluated by dividing the atmosphere into a number of homogeneous sublayers and the upward flux F^+ and the downward flux F^- are given by the equations

$$F^-(z_i) = \sum_{n=i+1}^{N} \sigma T_n^4 \Delta\varepsilon_n \tag{6.8.15a}$$

$$F^+(z_i) = \sum_{n=2}^{i} \sigma T_n^4 \Delta\varepsilon_n + \sigma T_s^4[1 - \varepsilon(z_i)] \tag{6.8.15b}$$

where N is the number of layers the atmosphere has been divided into and the incremental emissivity $\Delta\varepsilon$ is defined by

$$\Delta\varepsilon_n \equiv \varepsilon(|z_n - z_i|) - \varepsilon(|z_{n-1} - z_i|) \tag{6.8.16}$$

Then, the net thermal flux F_t is given by

$$F(z_i) = F^+(z_i) - F^-(z_i) \tag{6.8.17}$$

The emissivity ε is evaluated at an effective temperature and pressure defined by Eq. (6.7.2).

VII. RESULTS AND DISCUSSION: ONE-DIMENSIONAL MODEL

7.1 Introduction

This chapter will present and discuss the numerical simulations performed with the unsteady one-dimensional models. To gain a degree of confidence in the turbulence model, the results of a test simulation were compared against typical observations of the O'Neill Study (Lettau and Davidson, 1957). The comparison emphasized the numerical reproduction of important physical features rather than accurate predictions. As the purpose of this study was to understand physical trends, no attempt was made to "adjust" the parameters of the model to actually reproduce observations. The relative success of a number of simple boundary layer models (Estoque, 1963; Deardorff, 1967, Sasamori, 1970) in producing results which compare very well with observations indicates that such an adjustment of parameters is possible.

The one-dimensional simulations emphasized the effects of pollutants on thermal structure and pollutant dispersal. The role of elevated as well as surface layers of aerosols and pollutants in modifying vertical temperature and concentration profiles was investigated. The sensitivity studies focused attention on the effect of varying aerosol parameters and pollutant gases. A list of the one-dimensional simulations is presented in Table 7.1.

7.2 Test Simulation

7.2.1 Initial Conditions and Parameters Used in Test Simulation

A non-uniform grid system was used in the one-dimensional simulations. The reasons for the smaller grid spacing near the earth's surface have already been discussed. Table 7.2 presents the vertical

Table 7.1 List of One-Dimensional Numerical Simulations

Section	Ref:	Radiative Participation	Gaseous Pollutant	Aerosol Properties			Elevated Layer Height
				ω	f	β_{ex} $m^2/\mu g$	
7.3	NP	None	--	--	--	--	--
7.3	P	Thermal & Solar	NH_3	0.90	0.85	10^{-6}	--
7.4	NP	None	--	--	--	--	300
7.4	P	Thermal & Solar	NH_3	0.90	0.85	10^{-6}	300
7.4	SP	Solar	--	0.90	0.85	10^{-6}	300
7.4	TP	Thermal	NH_3	--	--	--	300
7.4	NP	None	--	--	--	--	600
7.4	P	Thermal & Solar	NH_3	0.90	0.85	10^{-6}	600
7.4	SP	Solar	--	0.90	0.85	10^{-6}	600
7.4	TP	Thermal	NH_3	--	--	--	600
7.4	SP	Solar	--	0.90	0.85	10^{-6}	1200
7.5	1	None	--	--	--	--	--
7.5	2	Solar	--	0.80	0.85	5×10^{-7}	--
7.5	3	Solar	--	0.99	0.85	5×10^{-7}	--
7.5	4	Solar	--	0.90	0.85	5×10^{-7}	--
7.5	5	Solar	--	0.90	0.50	5×10^{-7}	--

Table 7.2 Vertical Grid Coordinates and Physical Properties and Parameters Used in Test Simulation

a) Atmospheric Coordinates

j	1	2	3	4	5	6	7	8	9	10	11	12	13	14	15
z(m)	0	1.0	5.0	10.0	20.0	30.0	40.0	50.0	100.0	200.0	300.0	400.0	500.0	600.0	700.0
j	16	17	18	19	20	21	22	23	24	25	26	27	28	29	30
z(m)	800.0	900.0	1000.0	1100.0	1200.0	1300.0	1400.0	1500.0	1600.0	1700.0	1800.0	1900.0	2000.0	2100.0	2200.0

b) Soil Coordinates

j	1	2	3	4	5	6
z(m)	0	0.01	0.05	0.1	0.3	0.5

c) Physical Properties and Parameters

$k_s = 2.0$ W/m·C

$\rho_s = 1.5 \times 10^3$ Kg/m^3

$c_{ps} = 1.0 \times 10^3$ J/Kg C

$r_s = 0.16$

$\epsilon_t = 0.95$

Solar Declination = 11°

Surface temperature = 300.5 K

Coreolis Parameter $f = 10^{-4}$ sec^{-1}

Latitude = 42.5 · N

$u_g = 11.53$ m/s

$v_g = 7.52$ m/s

$z_o = 0.01$ m

$H = 0.01$

grid coordinates and the physical properties and parameters utilized in the study.

The test simulation was started at 05:00, and the initial conditions were representative of early morning atmospheric conditions during the period August-September, 1953 over the flat prairies at O'Neill, Nebraska. Specifically, the potential temperature profile was based on Carson's (1973) comments. Carson has made a detailed study of the O'Neill profiles (Lettau and Davidson, 1957) and concludes that the typical early morning profile is characterized by two gradients. The nocturnally established surface inversion is typically about 400 m deep and has a gradient of about 18×10^{-3} K/m. The layer above it, extending to about 2 Km, has a typical gradient of about 6×10^{-3} K/m. Thus, using this information, an initial potential temperature profile was constructed after assuming an appropriate surface temperature. The initial surface temperature and velocity profile corresponded to August 25th of the O'Neill observations. The water vapor was assumed to be uniformly distributed with a concentration of 1.5 $\mathrm{gm/m^3}$. The soil temperature was taken to be uniform at the surface temperature over the depth of the soil layer. The upper atmospheric data were taken from McClatchey, et al. (1972). The time step used in the simulation was 75 s.

7.2.2 Results of Test Simulations

In this section, the test simulation will be discussed in detail. The results will be compared against observational data of the O'Neill Study (Lettau and Davidson, 1957). To ascertain the validity of the turbulence model, the results will be discussed with reference to other recent boundary layer studies such as those of Orlanski, et al. (1974) and Lykosov (1972). As Lykosov (1972) also used a turbulent kinetic energy model, special emphasis will be placed on his results.

Figures 7.1 to 7.3 illustrate the evolution of the potential temperature and eddy diffusivity over a twenty-four hour period. They show that the model can reproduce important features of mixed layer formation. The nocturnal surface based inversion is rapidly

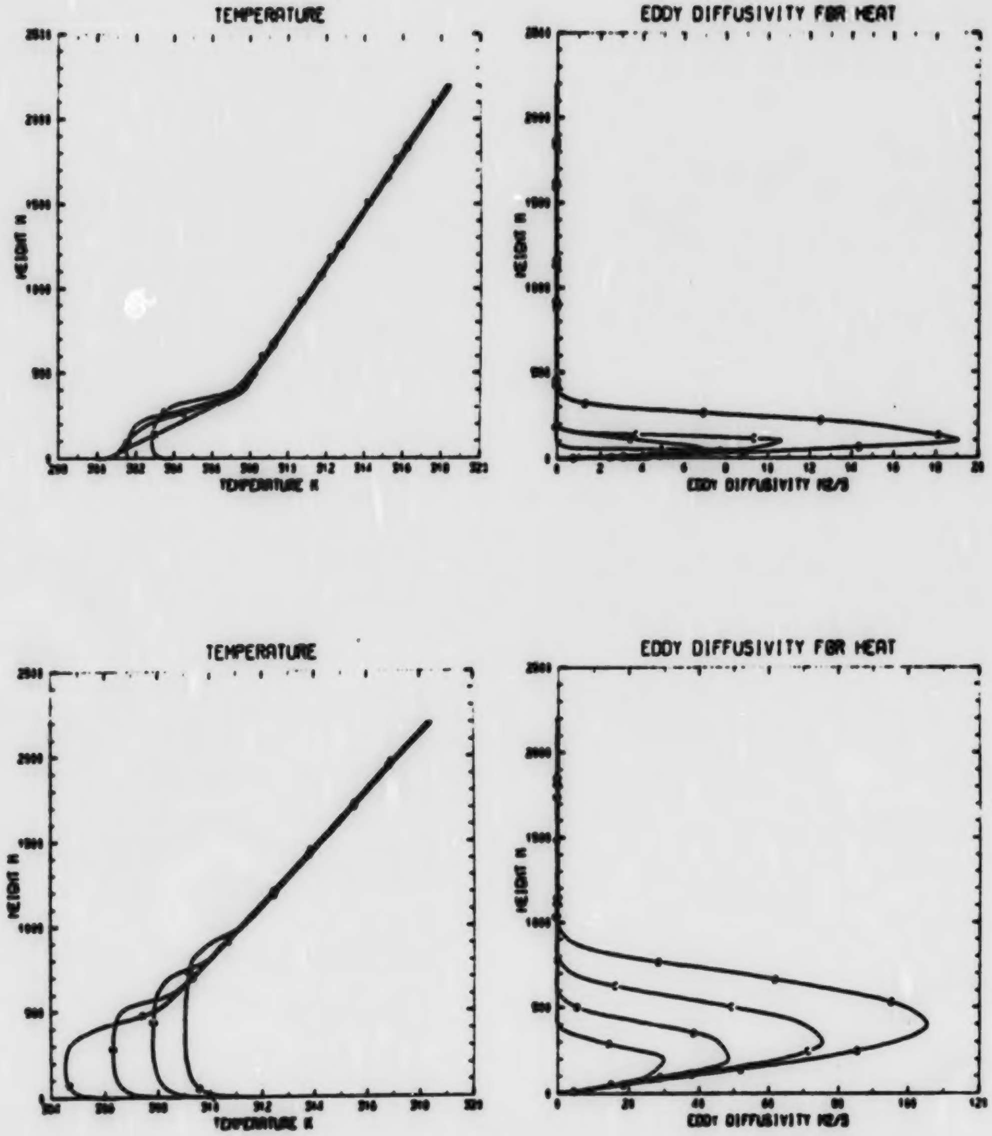

Figure 7.1 Potential Temperature and Eddy Diffusivity Profiles at 1 hour Intervals. A, B, C, and D Represent Profiles in Chronological Order. Top Row is for Time 05:00 to 08:00 and Bottom Row is for Time 09:00 to 12:00.

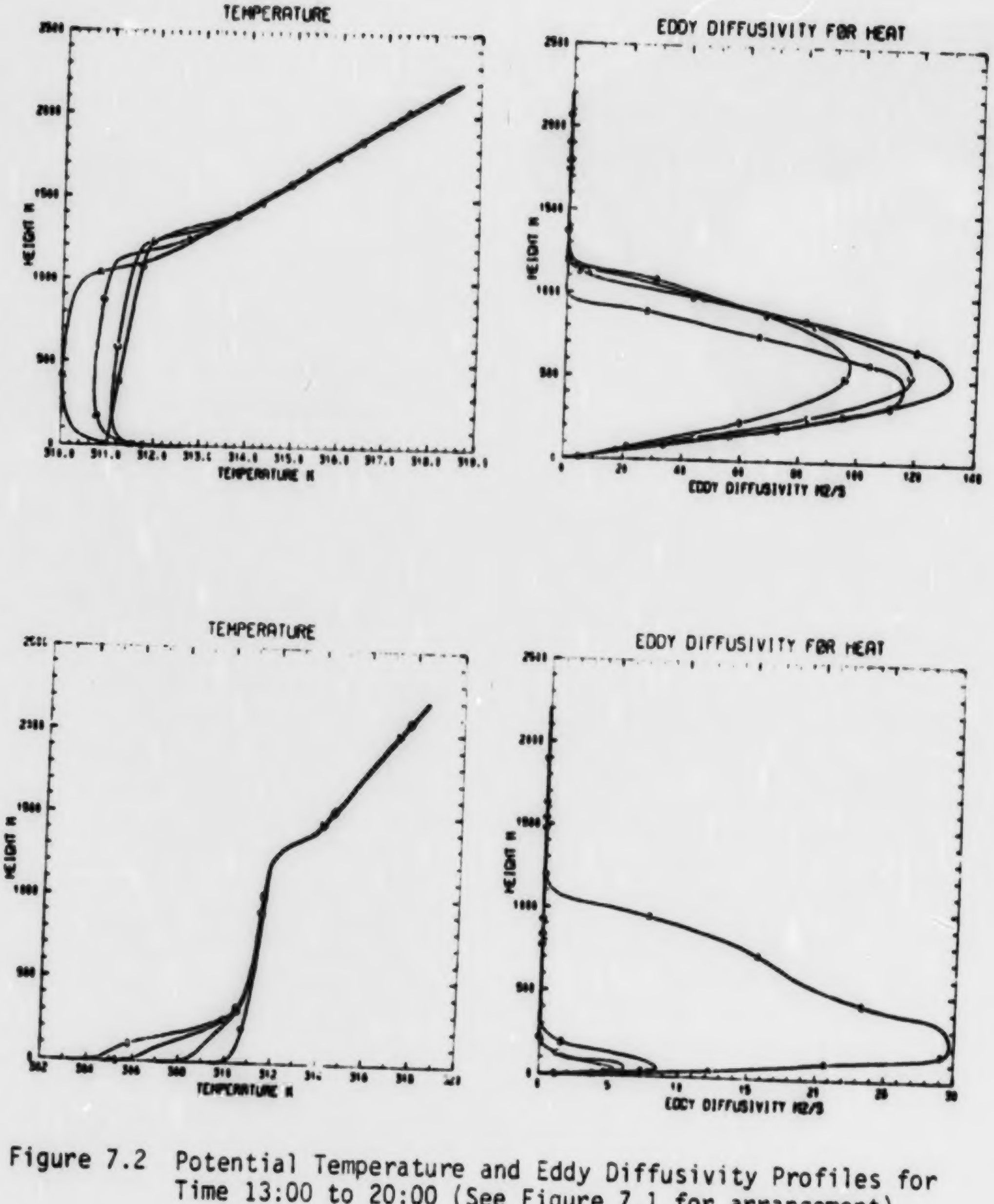

Figure 7.2 Potential Temperature and Eddy Diffusivity Profiles for Time 13:00 to 20:00 (See Figure 7.1 for arrangement).

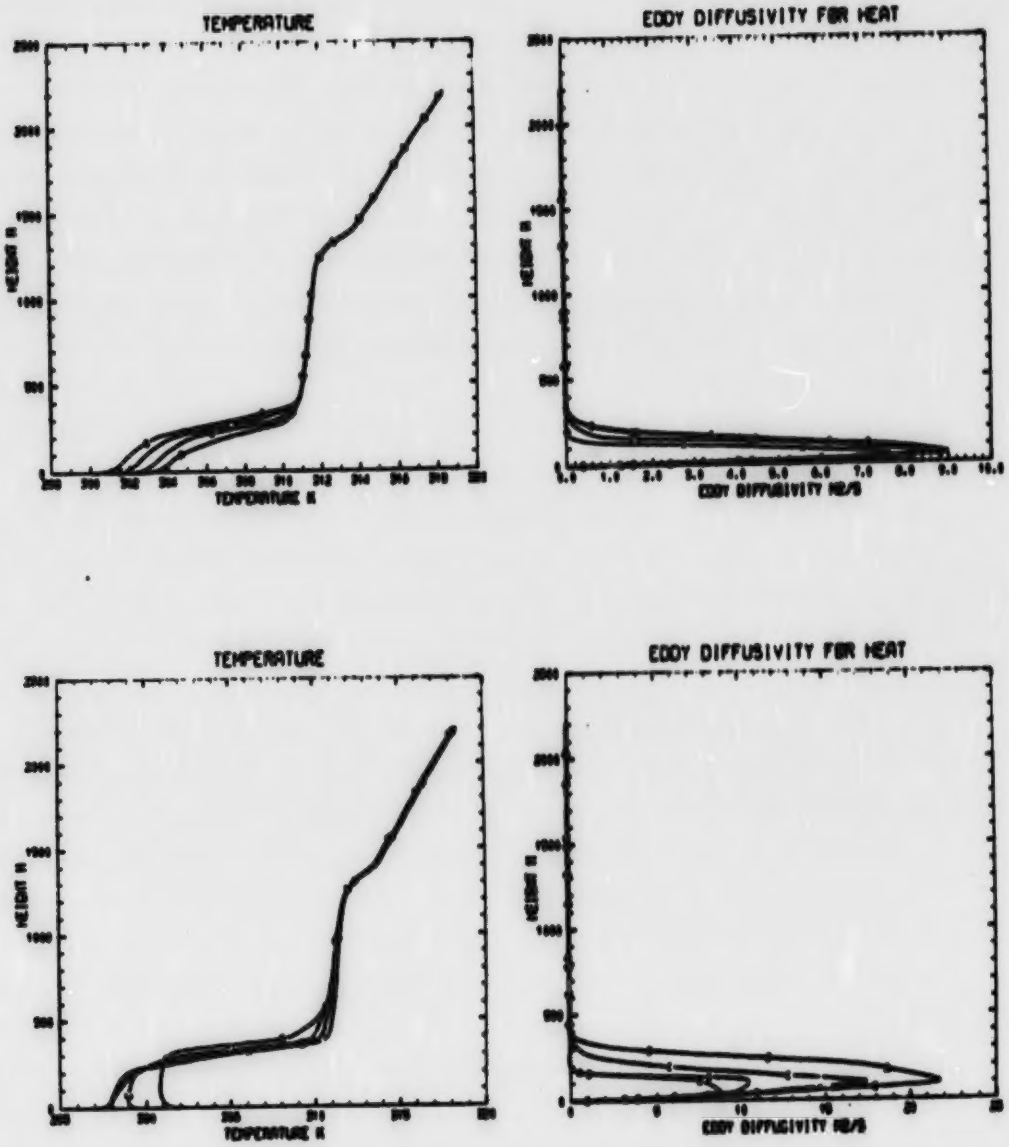

Figure 7.3 Potential Temperature and Eddy Diffusivity Profiles for Time 21:00 to 04:00 (See Figure 7.1 for arrangement).

eroded away as the sun heats up the earth's surface. It is noted that, in agreement with Carson's observations (1973), the stronger surface inversion which is about 400 m deep is eroded from below in about 4 hours. The mixed layer grows more rapidly against the smaller resistance of the stable layer above the nocturnally established surface inversion, and reaches a maximum height of around 1300 meters in ten hours (15:00). This agrees fairly well with the O'Neill observations of August 25, 1953 as illustrated in Figure 7.4. The observed initial inversion rise is more rapid than that predicted. This discrepancy could be associated with the uncertainty in the initial conditions and surface parameters.

The predicted temperature profiles are in qualitative agreement with observations (Lettau and Davidson, 1957; Clarke, et al., 1971). The daytime profile is characterized by a shallow superadiabatic layer extending to less than 100 m, and the mixed layer above it has a slightly stable gradient indicative of a countergradient heat flux. The turbulent mixed layer is capped by a sharp inversion which has a typical strength of 1.5 K.

The eddy diffusivity profiles show the increase in turbulent activity as the mixed layer grows. The eddy diffusivity increases in the lower portion of the mixed layer, reaches a maximum at heights around half of the boundary layer thickness, and decreases to zero at the edge of the boundary layer. The largest values of eddy diffusivity occur during the day and are of the order of 100 m^2/sec which is in agreement with other investigations (Orlanski, et al., 1974; Deardorff, 1967).

The evening and nighttime potential temperature and eddy diffusivity profiles exhibit some interesting features. In about two hours after the surface starts cooling at around 14:00 hours, turbulence is virtually extinguished in the bulk of the boundary layer. This is indicated by the rapid decrease in the mixed layer height and the collapse of the eddy diffusivity profiles. This unusual behavior of the nocturnal boundary layer has been observed experimentally by Kaimal, et al. (1975) in Minnesota, and has also been theoretically predicted by

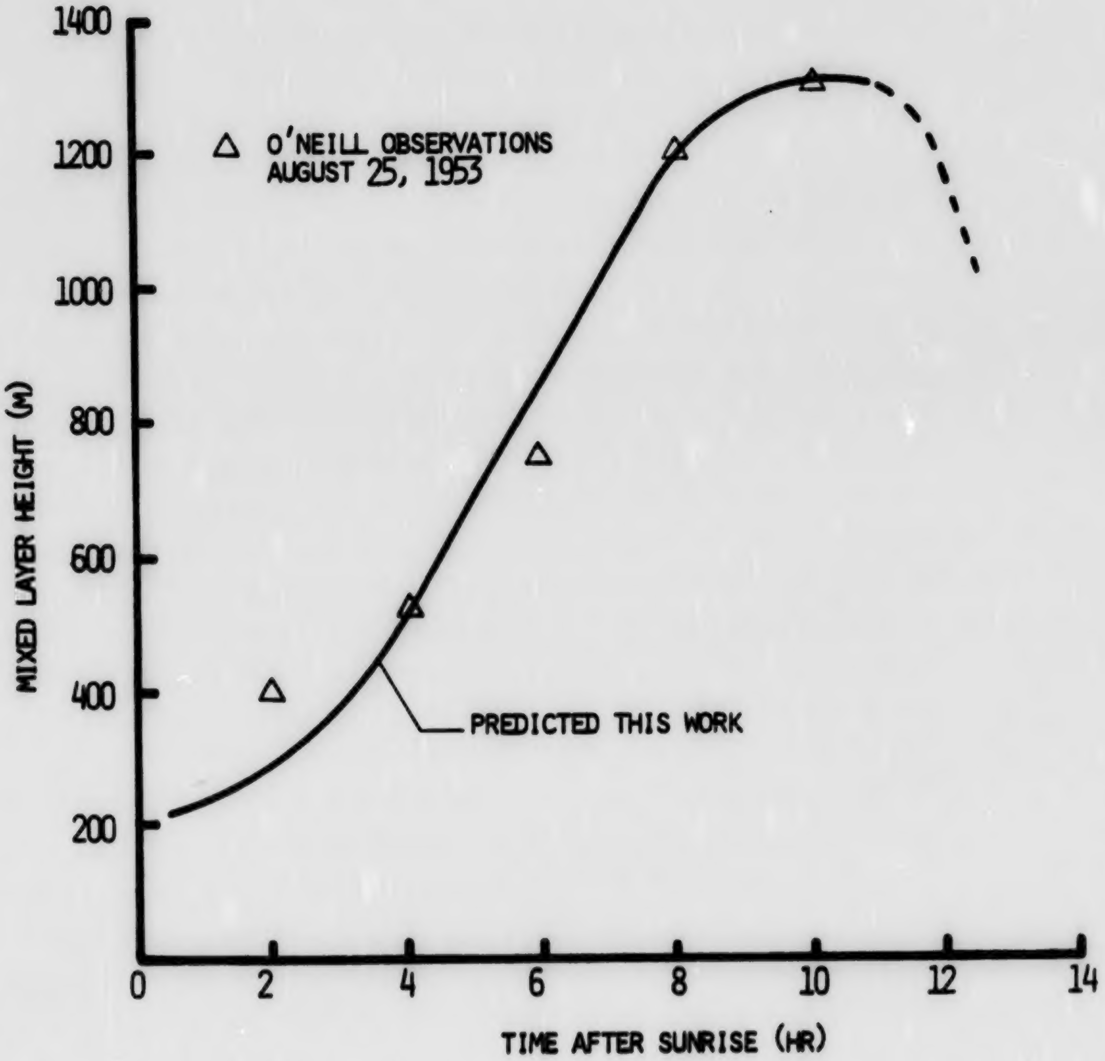

Figure 7.4 Comparison of Mixed Layer Heights

Orlanski, et al. (1975). The typical boundary layer variation of the O'Neill Study is illustrated in Figure 7.5. The discontinuities in the boundary layer depth near sunrise and sunset are indicative of the sharp changes in turbulent activity associated with high surface cooling rates. It is interesting to note that the model used in this study predicted this physical phenomenon only when the counter-gradient parameter was included in the energy equation. Otherwise, the mixed layer continued to grow even after sunset. The importance of the counter-gradient flux seems to indicate that the upward transport of heat during the day is caused by surface generated buoyant plumes penetrating the weakly stable mixed layer. The turbulence in the mixed layer being associated with buoyant parcels is extinguished as soon as the surface cools and stops producing buoyant plumes. The numerical model of this study predicted negligibly small nocturnal boundary layers. Although there is not enough observational data to disprove the validity of this result, it was necessary to set a minimum value of 200 meters for the nighttime boundary layer to prevent the formation of unrealistically large surface inversions. The value of 200 meters was based on the Wangara data (Clarke, et al., 1971) which indicated that the nocturnal boundary layer varied from around 150 meters to 250 meters (Melgarejo and Deardorff, 1974) in height. Admittedly, this treatment of the boundary layer is empirical; however, there is no satisfactory theory for the stable boundary layer and the scope of this study did not permit a further investigation of the problem.

Figure 7.6 shows the potential temperature variation at 50 m over a simulation period of 12 hrs. It is seen that the temperature variation shows reasonably good agreement with the O'Neill observations.

Figures 7.7 and 7.8 reproduce some results obtained by Lykosov (1972). It is evident that the results show some noticeable differences from those of this study. According to Lykosov's model, the mixed layer height varies by a factor of about two, from 600 meters in the night to about 1200 meters in the day. This study shows the boundary layer height varying by a factor of about six, from 200

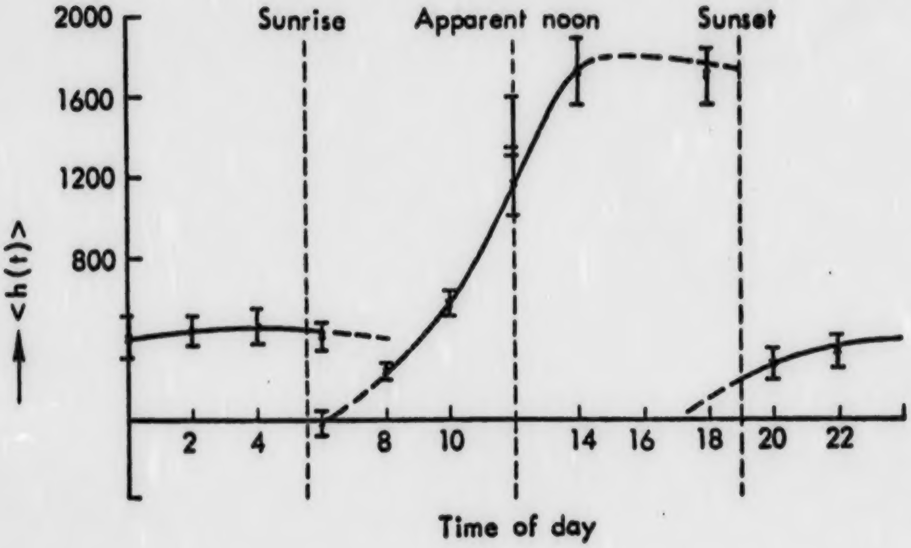

Figure 7.5 The Mean Boundary Layer Thickness <h(t)>, Deduced for the O'Neill Data and Plotted with Standard Errors as Functions of Time of Day, t, in Mean Solar Time (Carson, 1973).

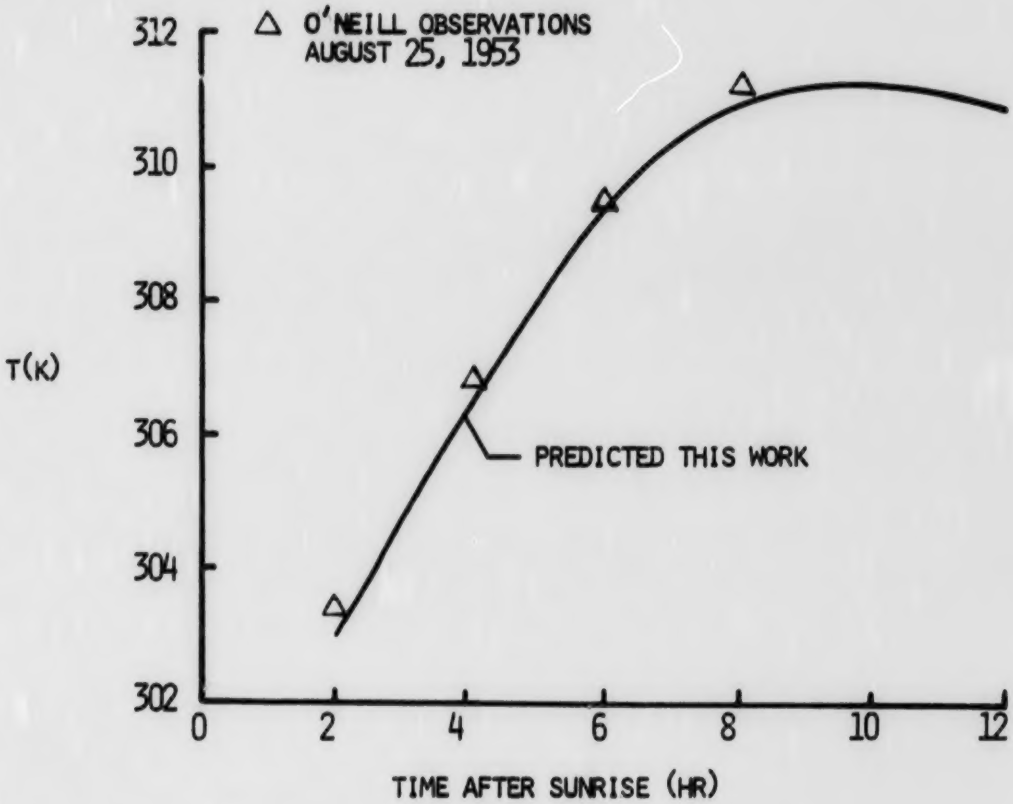

Figure 7.6 Comparison of Temperature Variation at 50 M

meters in the night to about 1300 meters in the afternoon. This wider variation of the mixed layer height agrees more closely with observations (Clarke, et al., 1971). Although the observations indicate that weak turbulence may extend to greater heights than the nocturnal boundary layer, turbulent activity above the boundary layer cannot be as large as that predicted by Lykosov. It is clear from Figure 7.7 that the surface inversions extend to heights of 600 meters indicating that the turbulence does not decay as rapidly as it should above the typical nocturnal boundary layer height of 200 meters.

There is a significant difference between the eddy diffusivity profiles predicted by Lykosov and those obtained in this study. Figure 7.8 shows that the heights at which the turbulent exchange coefficient attains a maximum are around 100 meters during the course of a diurnal cycle. On the other hand, this study predicts a very wide variation of the height at which the eddy diffusivity becomes a maximum, and as the height is approximately half the mixed layer thickness it is dependent on the variation of the mixed layer thickness.

The test simulation has shown that the model predictions are reasonably consistent with observational as well as theoretical studies. It is felt that a detailed investigation of the effect of initial conditions as well as surface parameters will help to improve the capabilities of the model.

As an additional test of the turbulence model, a numerical experiment was conducted to study stress profiles in a neutral boundary layer. The potential temperature was assumed to be uniform in the boundary layer, and the velocity field was initialized with an arbitrary logarithmic profile. The unsteady momentum equations were used to obtain the steady state stress profiles by allowing the time dependent solutions to approach steady state. The absence of thermal stratification made it possible to use a simple mixing length model which was similar to that suggested by Blackadar (1962). As the boundary layer height scales with u_*/f under neutral conditions, ℓ was assumed to be given by

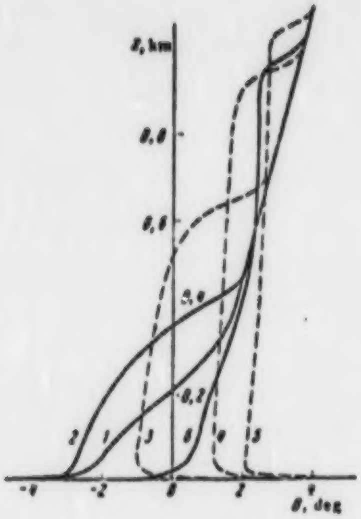

Figure 7.7 Profiles of the Potential Temperature $\Theta(z) = (\gamma_a - \gamma)z + \nu(z)$ for various hours of the day: (1) 2; (2) 6; (3) 10; (4) 14; (5) 18; (6) 22 h (Lykosov, 1972). (ν is Eddy Diffusivity)

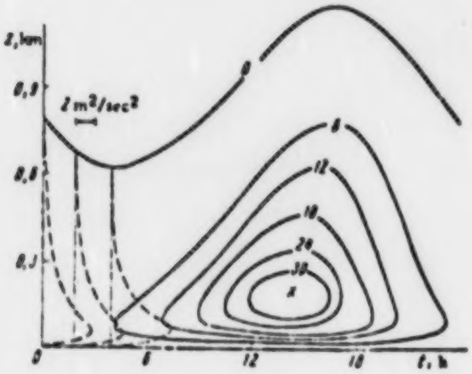

Figure 7.8 Isopleths of the Turbulent Exchange Coefficient ν. The Dashed Lines are Profiles of ν for Three Times of Day (0, 2, and 4 hrs) (Lykosov, 1972).

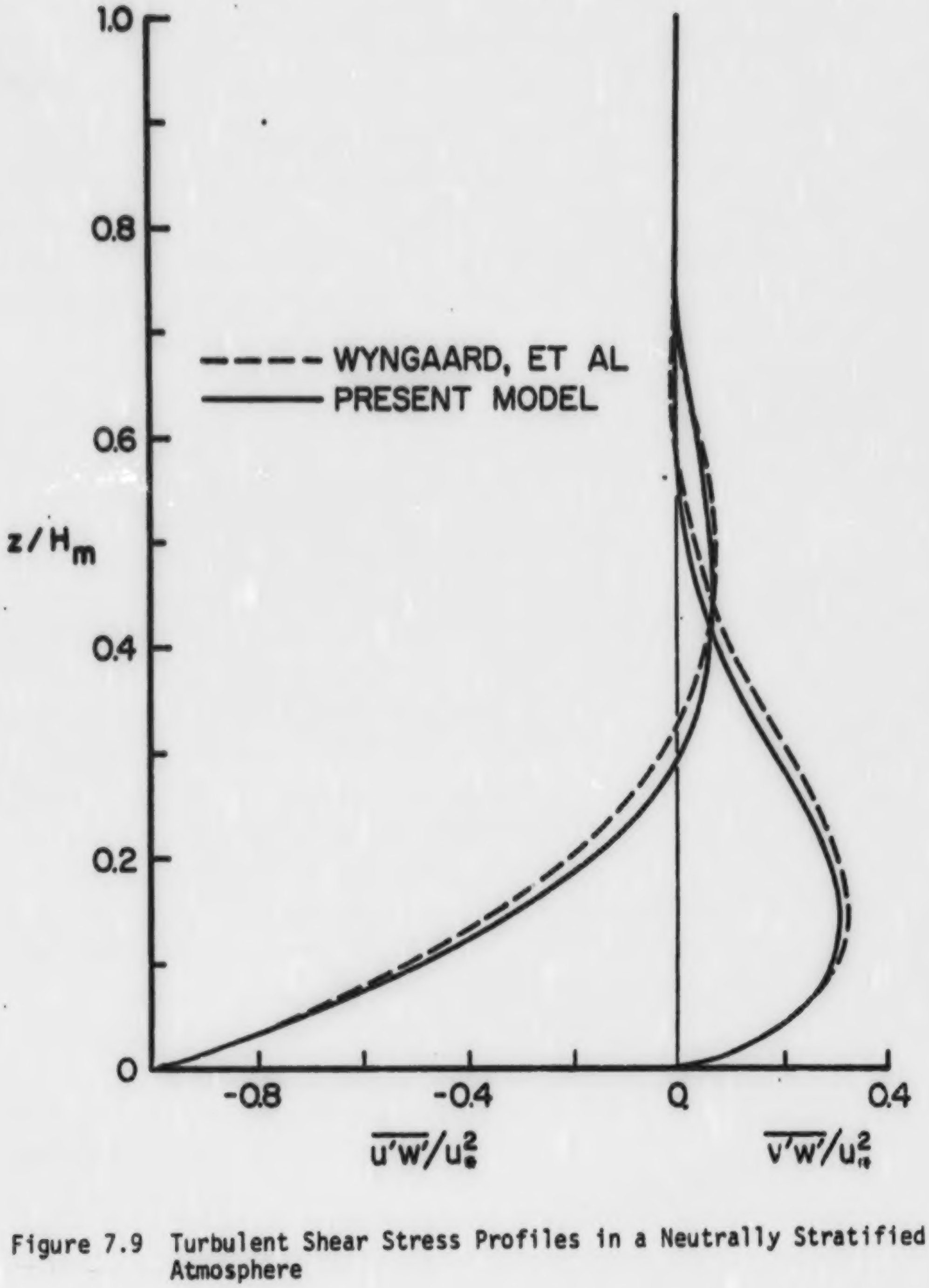

Figure 7.9 Turbulent Shear Stress Profiles in a Neutrally Stratified Atmosphere

$$\ell = C_D^{1/4} \kappa(z + z_0)/(1 + C_D^{1/4} \kappa(z + z_0)/\ell_0) \qquad (7.3.1)$$

where

$$\ell_0 = 0.009\ C_D^{1/4} u_*/f \qquad (7.3.2)$$

Figure 7.9 shows the stress profiles obtained. It is seen that they compare remarkably well with the results from a considerably more complicated turbulence model formulated by Wyngaard, et al. (1974). However, the velocity defect profiles did not agree as well with those of Wyngaard, et al. Further adjustment of the constant in the formula for ℓ_0 will be necessary for improved agreement.

7.3 Radiative Effects of Pollutants

7.3.1 Introduction

This section will describe the numerical simulations performed to investigate the radiative effects of gaseous and particulate pollutants on the thermal structure and pollutant dispersal in the planetary boundary layer. As pollution episodes occur when the winds are low, the initial velocities were taken to be one fourth of those used in the test simulation. The initial temperature structure (temperature gradients) was identical to that of the test simulation. Since the purpose of the simulations was to study the effects of pollutants on the planetary boundary layer as a whole, it was decided to use surface parameters which were not exclusive to the urban area. The surface parameters used are based on those suggested by Pandolfo, et al. (1971) and are presented in Table 7.3

The aerosol parameters are based on the calculations of Hansen and Pollack (1970). The aerosol extinction coefficient was chosen so that with the average mass loadings obtained in the simulations the optical thickness in the solar spectrum would be in the range 0.1 to 0.2. These values of optical thickness are based on the measurements of Herman, Browning and Curran (1971) which place the mean atmospheric optical thickness in the visible spectrum around 0.1. The single scattering albedo of 0.90 corresponds to a slightly

Table 7.3 Summary of Surface Parameters and Pollutant Properties Used in Simulations of Section 7.3

a) Surface Parameters

k_s = 2.0 W/m/c

ρ_s = 1.5 × 10^3 kg/m^3

c_{ps} = 1.0 × 10^3 J/kg/c

r_s = 0.2

ε_t = 1.0

H = 0.1

Z_o = 0.01 m

u_g = 2.88 m/s

v_g = 1.88 m/s

Surface Temperature = 285 K

Height of Elevated Source = 100 m

$S_h = 0.05\ |\sin(\pi t/24)|$ μgm/m^3/s (Aerosol and gas)

Latitude = 42.5°N

Solar Declination = 11°N

b) Aerosol Properties

$\beta_{ex} = 10^{-6}$ m^2/μgm

f = 0.85

ω = 0.90

absorbing aerosol--the amounts of backscatter and absorption are equal in a layer of an optical thickness of 0.5. As ammonia absorbs strongly in the 8-12 μm region, it was used as a representative pollutant. Aerosol properties are also listed in Table 7.3.

The pollutant source was assumed to be elevated in order to model industrial emissions which are the most important pollutant sources. It is noted that the source is allowed to vary during the course of the day. The source strength increases during the day, reaches a peak 12 hours after sunrise and decreases during the night. This variation of the pollutant source is a simple representation of industrial emission during the course of the day (Roberts, et al., 1971). The lack of data and the objectives of this study did not warrant a more detailed treatment of pollutant emissions.

Two numerical simulations were conducted; in the first one the pollutants were taken to be non-participating, and in the second one the pollutants (aerosol and gas) were allowed to participate radiatively. As a large number of variables are involved in the simulations, it is impractical to present all the numerical results of the experiments. Only some selected results which are relevant to the understanding of the radiative effects of pollutants are presented. It is noted that most of the results are given in tabular form in order to emphasize the very small differences between the variables of the non-participating simulation and those of participating simulation.

7.3.2 Effect of Pollutants on Thermal Structure of Boundary Layer

Table 7.4 illustrates the effect of radiative participation of pollutants on the thermal and solar fluxes at the surface. It is seen that aerosols decrease the solar flux at the surface by as much as 25% at large zenith angles (17:00 of second day). At small zenith angles the attenuation of solar flux is around 5% (11:00 of second day). The average attenuation of about 15% agrees well with recent observations by Rouse, et al. (1973) over Hamilton, Ontario. Thermal

Table 7.4 Comparison of Thermal and Solar Fluxes at the Surface for Simulations with Participating (P) and Non-Participating (NP) Pollutants

	Solar Flux (W/m^2)			Thermal Flux (W/m^2)		
Time	NP	P	NP-P	NP	P	NP-P
07:00	237.60	216.2	21.4	294.0	294.3	- 0.3
09:00	550.4	532.8	17.6	305.7	308.6	- 2.9
11:00	738.5	726.4	12.1	320.3	327.6	- 7.3
13:00	734.9	720.5	14.4	331.9	344.1	-12.2
15:00	543.0	516.6	26.4	337.2	353.8	-16.6
17:00	233.5	198.4	35.1	336.0	356.0	-20.0
19:00	0	0	0	328.0	351.3	-23.3
21:00	0	0	0	321.1	348.2	-27.1
23:00	0	0	0	316.5	346.7	-30.2
01:00	0	0	0	313.3	345.5	-32.2
03:00	0	0	0	310.6	344.3	-33.7
05:00	0	0	0	308.2	342.8	-34.6
07:00	233.5	184.9	48.6	311.6	345.2	-33.6
09:00	540.0	491.8	48.2	329.0	362.4	-33.4
11:00	725.2	687.9	37.3	344.3	379.7	-35.4
13:00	722.2	682.0	40.2	351.6	388.4	-36.8
15:00	534.1	477.2	56.9	354.7	393.7	-39.0
17:00	229.8	172.6	57.2	352.3	392.7	-40.4
19:00	0	0	0	343.3	386.6	-43.3
21:00	0	0	0	336.2	382.4	-46.2
23:00	0	0	0	331.2	380.2	-49.0
01:00	0	0	0	327.7	378.6	-50.9
03:00	0	0	0	324.6	377.1	-52.5

participation by ammonia increases the downward thermal flux by a maximum of about 16% at 03:00 of the second day. The average increase of about 10% is consistent with observations made by Oke and Fuggle (1972) who measured an increase in the downward thermal flux of approximately 10 percent in Montreal, Canada.

Table 7.5 lists the potential temperatures for the simulations. It is seen that during the first 4 hours (7:00 to 11:00) the potential temperature at 1 m is slightly lower for the participating simulation than for the non-participating simulation. An examination of Table 7.6 shows that during the first day the surface temperature for simulation P is cooler due to the decrease in solar flux. After 19:00 of the first day the surface temperature as well as the temperature at 1 m is warmer for the simulation with participating pollutants for the remaining period of simulation. The temperature excess reaches a maximum of 3.25 C at the surface at 03:00 of the second day. During the night, the substantial increase of downward thermal flux by the participating pollutants leads to an increase of the surface temperature. However, during the day the increase in solar attenuation is not accompanied by a decrease in surface temperature. The surface temperature for the simulation with participating pollutants is about 0.15 C on an average higher than that with non-participating pollutants during the second day. An explanation for this apparent anomaly will be provided in the next paragraph. It is noted that while solar absorption causes a slight increase in potential temperature (~0.18 C) at 100 m, the large concentration of pollutants at the source located at 100 m leads to cooling at night. The temperatures in the boundary layer are higher on the second day than those of the first day because the thermal structure at the beginning of the second day is considerably different from that initially. It is clear that periodicity in the thermal structure variation can be obtained by adjusting the initial conditions. However, there is no necessity to force the temperature (or velocity) field to repeat itself 24 hours later because experimental observations (Clarke, et al., 1971) do not exhibit "precise" cyclic behavior.

Table 7.5 Comparison of Potential Temperatures (in K) at 1 m and 100 m for Simulations with Participating (P) and Non-participating (NP) Pollutants

	z = 1 m			z = 100 m		
Time	NP	P	NP-P	NP	P	NP-P
07:00	285.54	285.23	0.31	286.42	286.50	-0.08
09:00	290.62	290.37	0.25	288.63	288.48	0.15
11:00	294.66	294.59	0.07	291.86	291.83	0.03
13:00	296.63	296.69	-0.06	294.04	294.16	-0.12
15:00	296.48	296.54	-0.06	295.06	295.24	-0.18
17:00	294.36	294.31	0.05	295.00	295.13	-0.13
19:00	290.60	291.02	-0.42	294.71	294.76	-0.05
21:00	288.61	289.28	-0.67	294.71	294.76	-0.05
23:00	287.19	288.25	-1.06	294.50	294.41	0.09
01:00	286.14	287.46	-1.32	294.03	293.91	0.12
03:00	285.23	286.82	-1.59	293.57	293.38	0.19
05:00	284.41	286.27	-1.86	293.07	292.85	0.22
07:00	287.79	288.82	-1.03	292.09	291.70	0.39
09:00	294.40	294.88	-0.48	292.72	293.33	-0.61
11:00	298.04	298.30	-0.26	295.58	296.03	-0.45
13:00	299.05	299.39	-0.35	296.83	297.35	-0.52
15:00	298.60	298.88	-0.28	297.45	298.02	-0.57
17:00	296.46	296.66	-0.20	297.75	297.75	-0.03
19:00	292.72	293.72	-1.00	296.94	297.34	-0.40
21:00	290.73	292.14	-1.41	296.93	297.31	-0.38
23:00	289.27	291.19	-1.92	296.76	296.92	-0.16
01:00	288.17	290.46	-2.29	296.30	296.41	-0.11
03:00	287.16	289.87	-2.71	295.88	295.87	0.01

Table 7.6 Comparison of Surface Temperatures (in K) and Diffusivities (in m^2/s) at 10 m for Simulations with Participating (P) and Non-Participating (NP) Pollutants

Time	Surface Temperature NP	Surface Temperature P	Diffusivity of Heat NP	Diffusivity of Heat P
07:00	285.76	285.39	0.90	0.83
09:00	291.75	291.45	1.48	1.46
11:00	296.23	296.13	1.72	1.70
13:00	289.01	298.03	1.75	1.73
15:00	297.18	297.17	1.58	1.56
17:00	294.14	294.05	1.10	1.01
19:00	289.95	290.44	0.43	0.48
21:00	288.10	288.89	0.59	0.60
23:00	286.81	287.92	0.55	0.59
01:00	285.81	287.17	0.56	0.59
03:00	284.93	286.56	0.56	0.60
05:00	284.12	286.03	0.58	0.61
07:00	288.06	289.03	0.89	0.91
09:00	295.43	295.80	1.34	1.33
11:00	299.36	299.48	1.70	1.71
13:00	300.16	300.41	1.77	1.74
15:00	299.15	299.29	1.59	1.54
17:00	296.20	296.39	1.06	0.83
19:00	292.05	293.17	0.40	0.48
21:00	290.21	291.75	0.58	0.52
23:00	288.89	290.87	0.55	0.60
01:00	287.82	290.19	0.55	0.60
03:00	286.84	290.19	0.56	0.60

This study indicates that the predominant effect of aerosols is that of warming of the earth-boundary layer system. Aerosols decrease the solar flux reaching the earth's surface, an effect which, at first glance, would tend to decrease the surface temperature. However, a more careful examination of the surface energy balance shows that the reduction of solar flux need not be accompanied by a decrease in the surface temperature. It is seen from Tables 7.4 and 7.8 that the evaporative flux is a large fraction of the incoming solar plus thermal fluxes. As a relatively small fraction of the solar radiation contributes to sensible heating, the surface temperature is not very sensitive to changes in the incident flux. Thus, if all other physical processes, such as surface turbulence, were unaffected by aerosols, a decrease in the solar flux would cause a relatively small decrease in the surface temperature in order to bring the surface energy fluxes into balance. However, the readjustment of the surface energy balance can be accomplished by changes of the temperature of the surface air layer, and these changes would be sufficient to offset the small decrease in surface temperature which would be necessary otherwise. The results of this study show that the aerosols by absorbing solar radiation in the surface layer cause the necessary change in the thermal structure of the layer next to the earth's surface to prevent the decrease in the surface temperature. By direct absorption of solar radiation aerosols lead to an increase in the temperature of the surface air layer. This temperature increase causes two effects which are equivalent to the reduction in surface temperature. First, the higher temperature above the surface decreases the upward turbulent heat flux by decreasing the temperature gradient causing the heat flux. The reduction in the unstable temperature gradient decreases the eddy diffusivity of heat of the surface layer which in turn decreases the turbulent heat flux.

An examination of Table 7.8 shows that the total downward flux (solar plus thermal) is altered very slightly by radiative participation of pollutants. The reduction in solar flux (see Table 7.4) is almost matched in magnitude by the increase in downward thermal flux. This result is consistent with measurements by Rouse, et al. (1974) over Hamilton, Ontario. Thus, the relative insensitivity of the surface temperature to the reduction in the incident radiation together with the small decrease in the total downward radiation allows the surface temperature to be determined primarily by the aerosol induced heating of the surface layer.

The effectiveness of the heating caused by absorption of solar radiation by aerosols is evident from Table 7.7 which compares the solar heating term against the turbulent heating term in the energy equation. It is seen that radiative participation by aerosols increases the solar heating term by a factor of three. Furthermore, at some heights the magnitude of the solar heating term is almost the same as that of the turbulent heating term.

The effect of radiative participation by aerosols on the stability of the surface layer is evident from Table 7.6. During the day, the diffusivity at 10 m is decreased by radiative participation. During the night, the increase in the thermal radiation and the accompanying increase in surface temperature causes the surface layer to be less stable. This effect is reflected in the increase of turbulent diffusivities during the night as shown in Table 7.6.

The modification of surface fluxes by radiative participation is clearly indicated in Tables 7.8 and 7.9. It is seen that the daytime turbulent fluxes are reduced due to radiative participation. The reasons for this have already been considered. Although the stability of the surface layer is decreased by radiative participation during the night the substantially higher temperatures at the surface lead to a reduction of the downward turbulent fluxes. The soil fluxes are smaller with radiative participation than without because the higher soil temperatures allow less energy to flow into the soil layer during the day, and the higher surface temperatures during the night reduce the energy transported towards the surface. The evaporative fluxes are higher for simulation P than for simulation NP because the higher surface temperatures increase the saturation water vapor pressure at the surface and thus the concentration.

Table 7.7 Comparison of Terms in Energy Equation for Simulations with Participating (P) and Non-Participating (NP) Pollutants, Time is 12:00 hours of Second Day.

	$-\frac{\partial F_s}{\partial z}\frac{1}{\rho c_p} \times 10^5$(K/s)		$\frac{\partial}{\partial z}[K_H(\frac{\partial\theta}{\partial z} - \gamma_c)] \times 10^5$(K/s)	
z(m)	NP	P	NP	P
1	5.0	12.0	68.0	62.0
5	4.0	12.0	11.0	10.0
10.0	4.0	12.0	18.0	15.0
20.0	4.0	12.0	25.0	22.0
30.0	4.0	12.0	29.0	27.0
50.0	4.0	12.0	35.0	32.0
100.0	4.0	12.0	38.0	35.0
200.0	4.0	11.0	38.0	35.0
300.0	4.0	11.0	35.0	33.0
400.0	4.0	11.0	29.0	27.0

Table 7.8 Comparison of Energy Fluxes (in W/m²) at the Surface for Simulations with Participating (P) and Non-participating (NP) Pollutants

	Solar Plus Thermal		Latent	
Time	NP	P	NP	P
07:00	531.6	510.5	74.9	70.9
09:00	856.1	841.4	176.2	171.1
11:00	1058.7	1054.0	274.4	269.4
13:00	1066.7	1064.6	322.0	320.9
15:00	880.2	870.4	284.5	282.0
17:00	569.5	554.5	168.2	156.8
19:00	327.7	361.3	35.3	39.0
21:00	321.1	348.2	19.3	20.3
23:00	316.5	346.7	6.9	12.3
01:00	313.3	345.5	1.1	6.7
03:00	310.6	344.3	0	3.7
05:00	308.2	342.8	0	1.8
07:00	545.1	530.1	28.2	14.0
09:00	869.0	854.2	137.3	140.2
11:00	1069.5	1067.6	288.7	309.5
13:00	1073.8	1070.4	345.1	353.6
15:00	888.8	870.9	295.9	297.9
17:00	582.1	565.3	163.7	136.3
19:00	343.3	386.6	31.0	40.1
21:00	336.2	382.1	15.3	21.1
23:00	331.2	380.2	2.7	12.8
01:00	327.7	378.6	0	7.1
03:00	324.6	377.1	0	4.0

Table 7.9 Comparison of Energy Fluxes (in W/m²) at the Surface for Simulations with Participating (P) and Non-participating (NP) Pollutants

	Soil Flux		Turbulent Flux	
Time	NP	P	NP	P
07:00	- 64.0	- 52.9	- 14.1	- 10.3
09:00	-164.2	-161.9	-104.0	- 98.3
11:00	-182.8	-187.7	-164.0	-159.7
13:00	-145.2	-148.8	-151.8	-147.0
15:00	- 78.0	- 78.3	- 75.7	- 68.1
17:00	- 2.6	- 3.0	20.0	22.8
19:00	74.0	60.2	33.0	30.5
21:00	58.2	44.4	30.4	22.4
23:00	50.1	34.4	23.8	20.6
01:00	45.5	29.1	20.5	17.5
03:00	44.0	25.7	18.9	15.8
05:00	43.0	23.6	18.1	14.8
07:00	-107.0	- 90.9	- 18.8	- 14.0
09:00	-214.4	-202.8	- 84.0	- 75.8
11:00	-185.4	-172.8	-139.4	-128.8
13:00	-138.2	-137.0	-130.0	-117.5
15:00	- 77.8	- 73.8	- 61.2	- 44.6
17:00	- 5.5	- 11.9	23.1	20.4
19:00	67.5	43.2	32.2	28.7
21:00	50.2	27.4	30.7	21.9
23:00	42.4	18.8	23.8	19.4
01:00	40.1	13.7	21.0	16.7
03:00	39.2	10.5	19.8	15.2

The effect of pollutant participation on the thermal structure is evident from Figures 7.10 and 7.11. Direct solar energy absorption by aerosols increases the temperature of the boundary layer by about 0.1 C on the first day, and about 0.55 C on the second day of simulation. These higher temperatures persist during the night as seen in Figure 7.11. The nocturnal surface temperature is about 2 C higher at 05:00 of the second day and about 2.8 C higher at 21:00 on the same day. This excess temperature is caused by the increase in downward thermal radiation due to gaseous pollutants. It is seen that in the vicinity of the elevated source at 100 m, the high pollutant concentrations cause a small degree of cooling.

7.3.3 Effect of Pollutants on the Earth-Boundary Layer System

The effective solar reflectance or albedo of the earth-boundary layer system can be used to determine the overall effects of pollutants participating in the solar spectrum. If the addition of pollutants is accompanied by a decrease in albedo the resultant effect is one of warming, and an increase in albedo caused by pollutants would lead to a relative cooling of the earth-boundary layer system. It is clear that while aerosol and water vapor absorption tend to decrease the albedo, aerosol and Rayleigh scattering tend to increase the albedo. Figure 7.12 illustrates the effect of aerosol participation on the effective albedo of the earth-boundary layer system. It is seen that the albedo reaches a minimum at solar noon and increases with zenith angle. This result is consistent with the findings of Bergstrom and Viskanta (1973). The albedo with non-participating pollutants is lower than the assumed surface albedo of 0.2 because water vapor absorption in the boundary layer dominates Rayleigh scattering (Lacis and Hansen, 1974) under clear skies. It is noted that aerosol participation increases the effective albedo at large zenith angles. This increase is caused by two factors. As the aerosols used in this study scatter predominantly in the forward direction ($f = 0.85$) backscattering becomes important only when the optical path length is

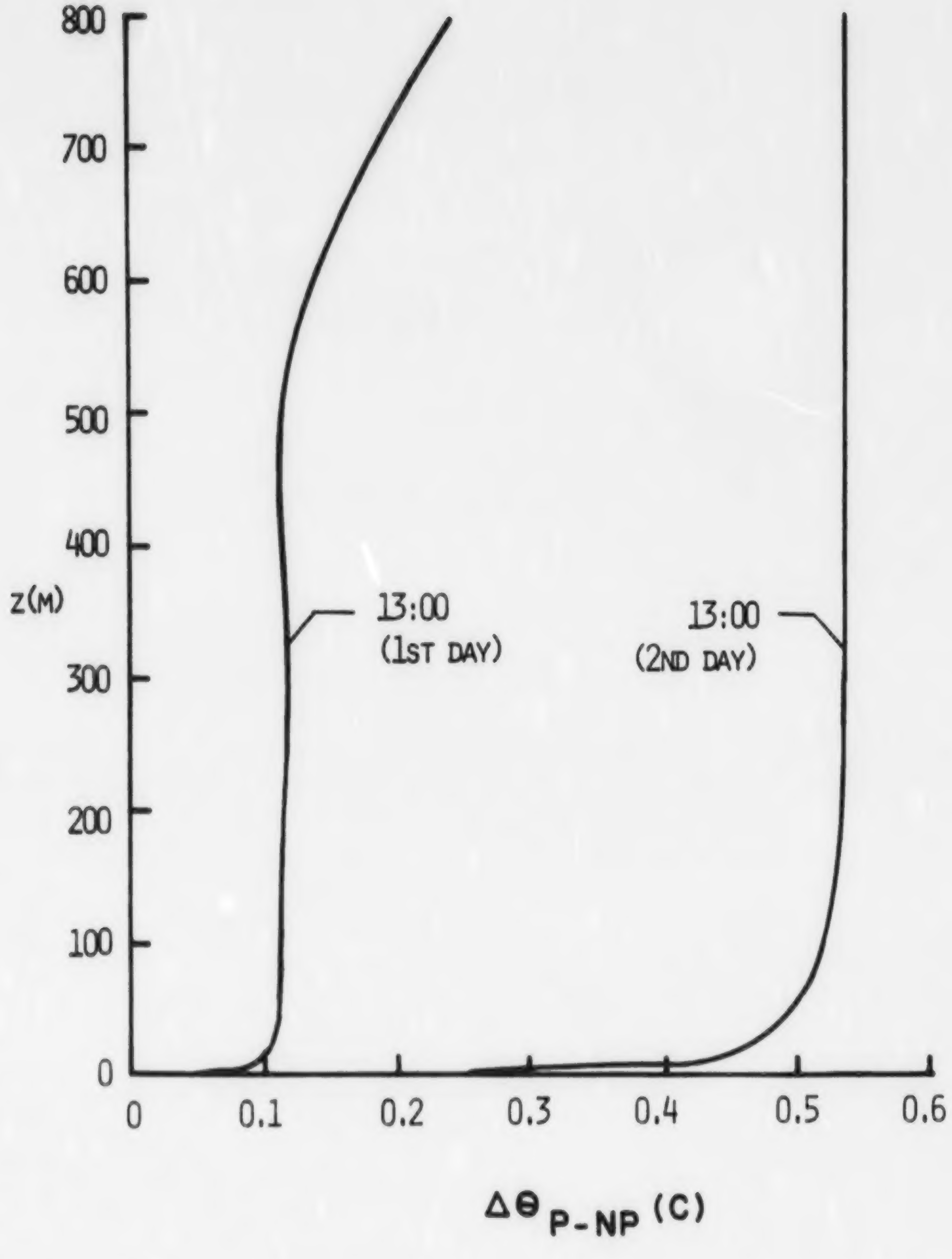

Figure 7.10 Daytime Potential Temperature Excess of Participating Simulation over Non-Participating Simulation

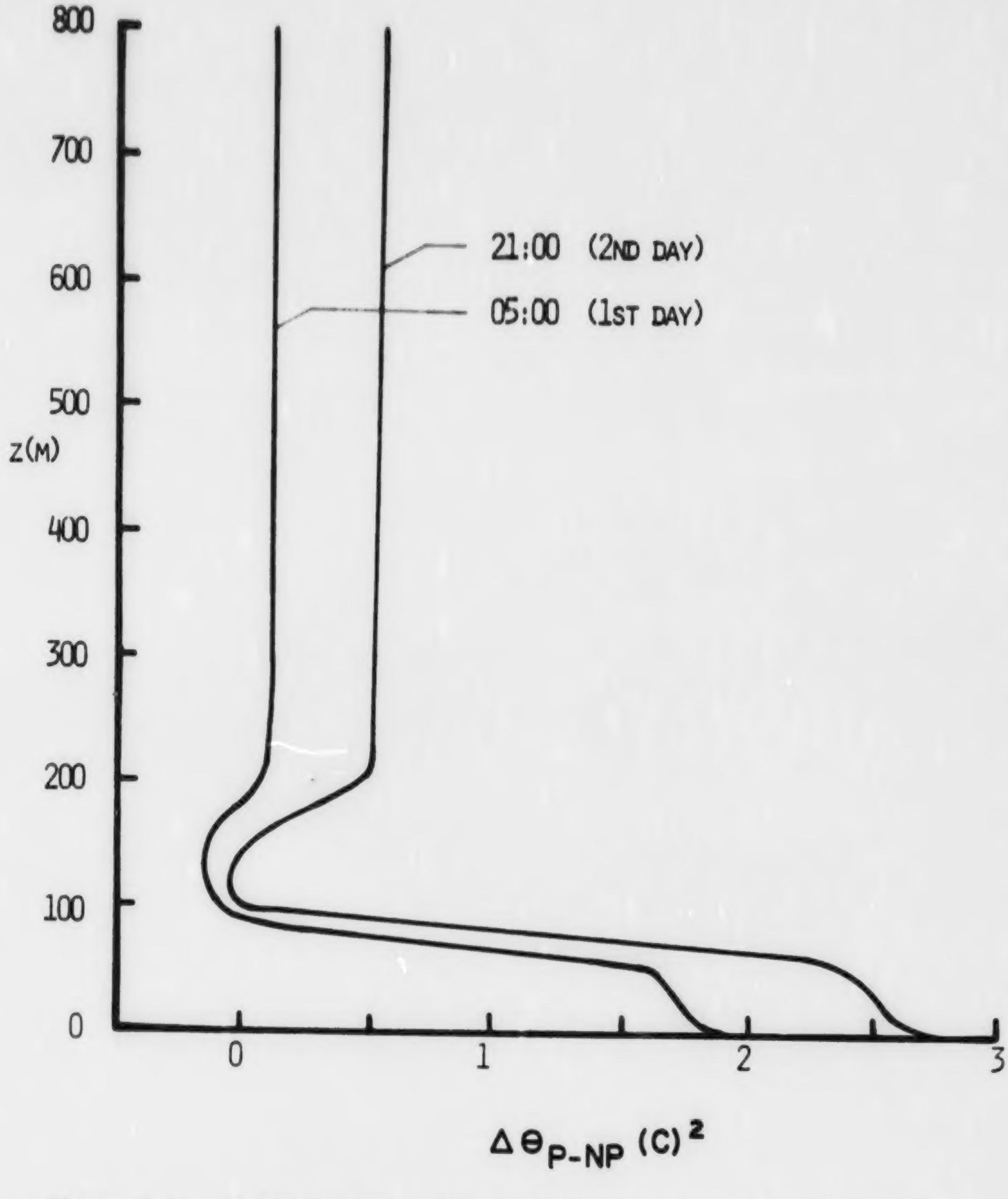

Figure 7.11 Nighttime Potential Temperature Excess of Participating Simulation over Non-Participating Simulation

large. Furthermore, as the increase in the zenith angle is accompanied by an increase in the water vapor path length above the boundary layer, the incremental water vapor absorption in the boundary layer is decreased. At low zenith angles around noon aerosol absorption of solar radiation leads to a decrease in the effective reflectance as seen in Figure 7.12. An important consequence of this decrease in albedo is the net heating of the earth-boundary layer system during the hours around noon. As 60% of the total solar energy available during a day is incident on the earth-atmosphere system during the period denoted by AB in Figure 7.12, the warming effect of aerosols can be significant. The effect of this warming on the surface temperature is dependent on the proportions of latent and sensible heating at the surface as well as amount of convective contact between the aerosol layer and the surface.

It is interesting to compare the results of this study with those of similar investigations (Bergstrom and Viskanta, 1973; Atwater, 1975). Bergstrom and Viskanta (1973) as well as Atwater (1975) while predicting warmer atmospheric temperatures find that solar attenuation caused by aerosols leads to a decrease in the surface temperature. Bergstrom and Viskanta (1973) show that the aerosol cooling effect on the surface can be as large as 2 C over a period of two days. It is evident from the discussion of the preceding paragraphs that the effect of aerosol induced boundary layer warming on the surface temperature is dependent on the degree of solar attenuation as well as the surface parameters. Bergstrom and Viskanta used relatively high pollutant mass loadings which lead to a greater reduction of the solar fluxes (12% at solar noon). As they neglected evaporation, the surface temperature was sensitive to this reduction in solar flux, and consequently their surface temperature was decreased. Thus, it is clear that it is not possible to draw any conclusions on the effect of aerosols on the surface temperature without qualifying the conclusions with statements about surface parameters, radiative properties of pollutants, concentration and distribution of pollutants, latitude and time of the season.

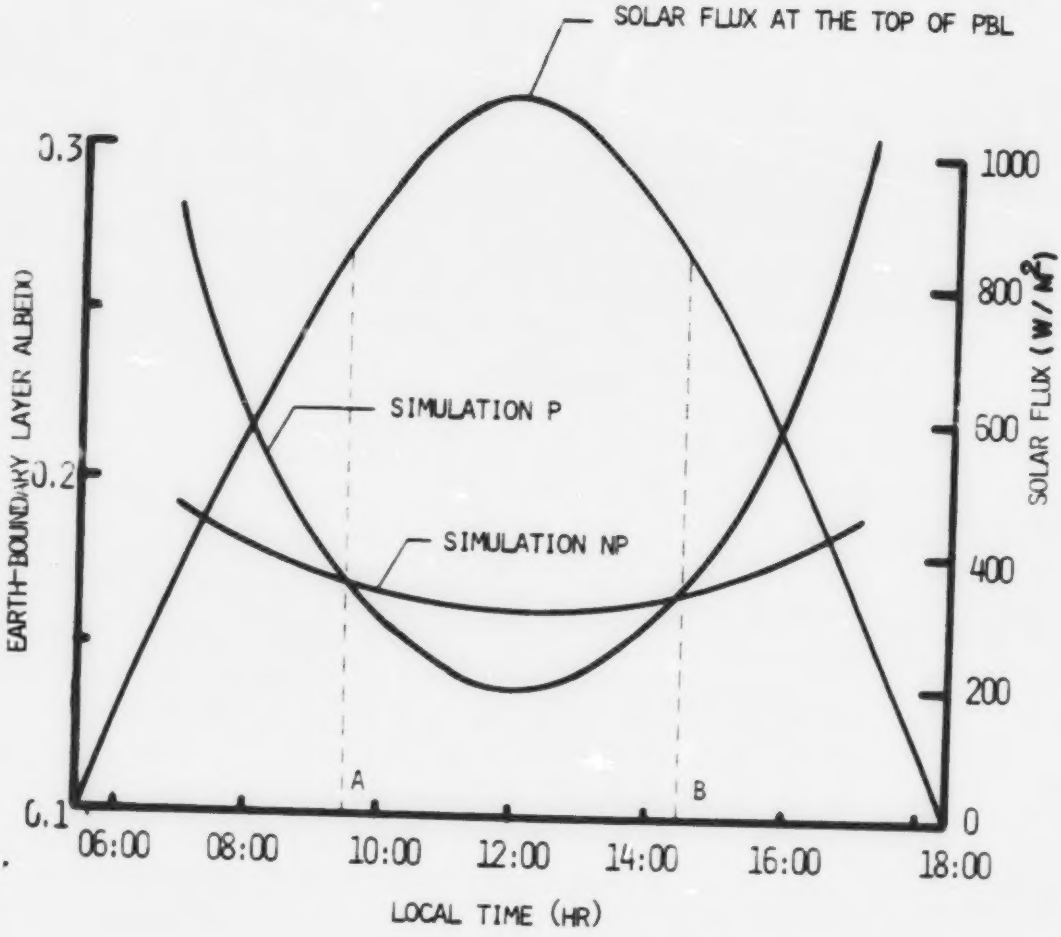

Figure 7.12 Effect of Radiative Participation on Earth-Atmosphere Albedo

7.3.4 Effect of Pollutants on Pollutant Dispersal

Figure 7.13 shows the evaluation of the aerosol concentration profiles over a period of 16 hours. The figure has been presented primarily to illustrate the effect of introducing pollutants into the boundary layer from an elevated source. It can be seen that the aerosol concentration reaches a maximum at the source and decreases above and below the source height of 100 m. During the day the aerosol concentration is almost uniform through the boundary layer. The stability of the nocturnal boundary layer leads to large (~700 μg / m³) aerosol concentrations at the source. As turbulent activity is confined to the lowest 200 m, pollutants injected from the source accumulate in the surface layer. Increased vertical mixing in the nocturnal boundary layer only serves to transfer pollutants from the source to the ground. The relevance of this statement will become clear when the effects of pollutants on pollutant dispersal are discussed in the next paragraph.

Solar heating due to aerosols during the day decreases the instability of the surface layer, and the increase in the thermal radiation during the night tends to decrease the stability of the surface layer. Thus, radiative participation by pollutants decreases the amount of pollutants transported from the source to the surface during the day, and increases the amount transported during the night. These effects are evident from an examination of Table 7.10. With pollutant participation the aerosol concentration is lower by a maximum of about 64 μg / m³ (7%) during the day. The effects of pollutants on pollutant dispersal are more significant during the nighttime. Radiative pollutant participation increases the aerosol concentration at 1 m by as much as 90 μg / m³ (18%). At 200 m the aerosol concentration is lower with pollutant participation than without. The higher surface temperatures caused by pollutants lead to increased vertical mixing and lower pollutant concentrations at 200 m.

Radiative participation by pollutants did not affect the growth of the mixed layer to an appreciable extent in the simulations

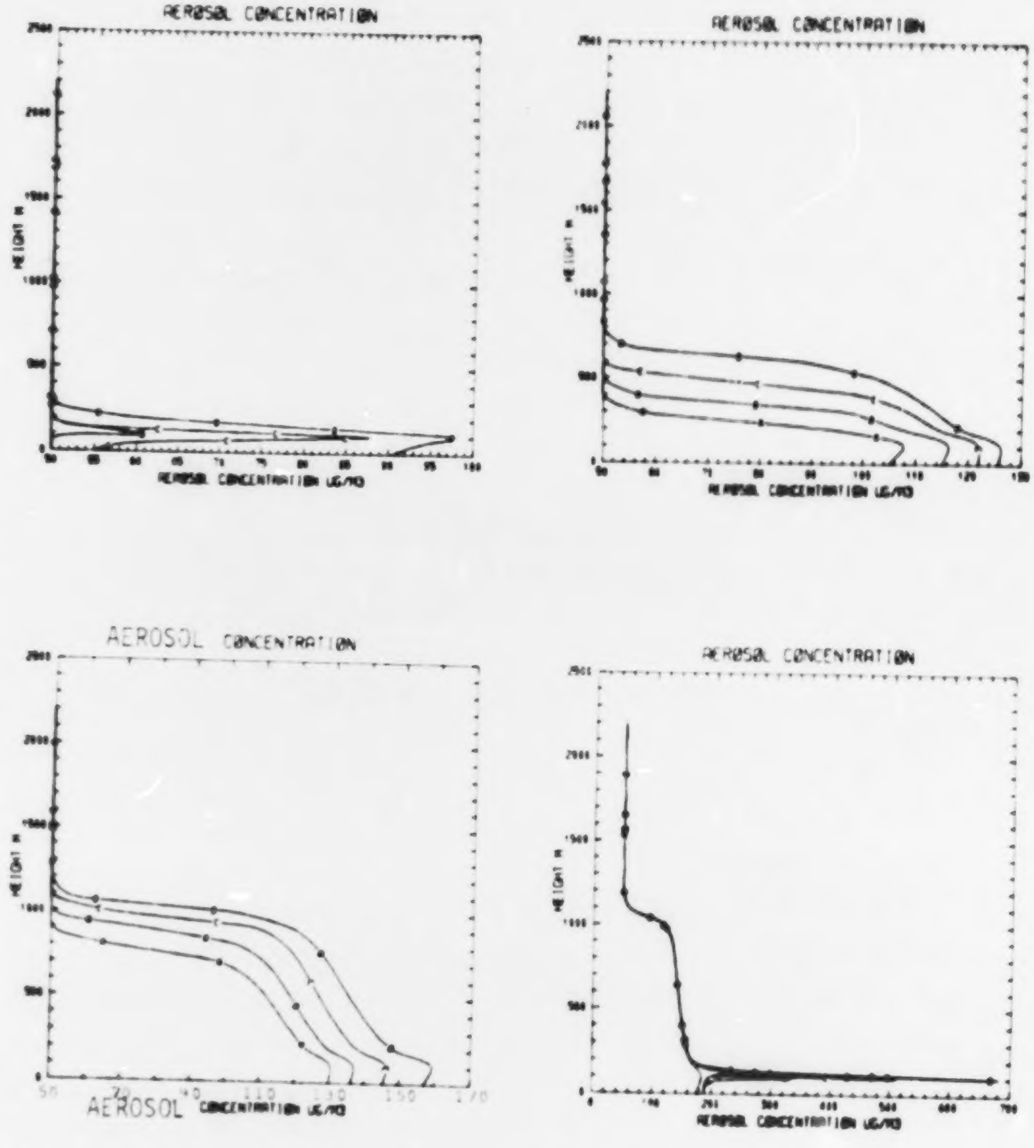

Figure 7.13 Aerosol Concentration Profiles for Time 05:00 to 20:00. Top Row is for Time (Left to Right) 05:00 to 08:00 and Bottom Row is for Time 09:00 to 12:00.

Table 7.10 Comparison of Aerosol Concentration (in μg/m³) for Simulations with Participating (P) and Non-participating (NP) Pollutants

	z = 1 m			z = 200 m		
Time	NP	P	NP-P	NP	P	NP-P
07:00	55.0	53.4	1.6	50.3	50.1	0.2
09:00	105.0	106.4	- 1.4	95.0	94.5	0.5
11:00	122.0	124.6	- 2.6	115.0	117.3	- 2.3
13:00	130.0	131.4	- 1.4	123.5	124.7	- 1.2
15:00	145.3	146.0	- 0.7	138.3	138.9	- 0.6
17:00	175.3	177.5	- 2.2	163.7	164.3	- 0.6
19:00	188.3	188.4	- 0.1	165.7	164.1	1.6
21:00	188.6	188.7	- 0.1	165.7	164.1	1.6
23:00	208.3	238.8	-30.5	165.7	164.1	1.6
01:00	275.8	322.4	-46.6	165.7	164.1	1.6
03:00	344.7	407.5	-62.8	165.7	164.1	1.6
05:00	407.3	487.3	-80.0	165.7	164.1	1.6
07:00	504.4	593.5	-89.1	167.5	165.4	1.1
09:00	805.1	780.6	24.5	487.0	437.5	49.5
11:00	414.5	350.1	64.4	377.0	321.5	55.5
13:00	298.6	280.5	18.1	289.4	272.0	17.4
15:00	292.8	277.6	15.2	284.5	268.9	15.6
17:00	315.3	302.5	12.8	301.2	281.3	19.9
19:00	330.9	322.5	8.4	300.5	282.0	18.5
21:00	331.8	323.7	8.1	300.5	282.0	18.5
23:00	347.9	385.9	-38.0	300.5	282.0	18.5
01:00	414.2	476.6	-62.4	300.5	282.0	18.5
03:00	477.5	568.8	-91.3	300.5	282.0	18.5

described in this section. However, radiative participation was found to be very important in determining the mixed layer height when pollutant layers were situated at heights above the surface. The simulations investigating these effects are described in the next section.

7.4 Effect of Elevated Layers of Pollutants

Pollutants which are vertically dispersed when the mixed layer grows during the day, can form elevated layers when the boundary layer contracts around sunset. Elevated pollutant layers could also result from the emission of pollutants from tall smokestacks which can be as high as 320 m (Cole and Lyons, 1972). As these elevated layers are associated with stable regions (above the mixed layer) where turbulence is inhibited, their radiative participation can lead to a significant modification of the thermal structure of the stable layer. Since the stability of the inversion capping the mixed layer controls the growth of the mixed layer, elevated pollutant layers can affect pollutant dispersal and fumigation as well as the temperature of the mixed layer.

In this section, the simulations performed to investigate the effect of elevated pollutant layers will be discussed. The pollutant parameters are based on those calculated by Hansen and Pollack (1970) for typical aerosols. Table 7.11 summarizes the particulars of the simulations and the pollutant parameters used. The pollutant layers were chosen to be 300 m thick and the maximum pollutant concentration was taken to be 400 $\mu g / m^3$. The relatively large value of 400 $\mu g / m^3$ was used to highlight radiative effects. The vertical distribution of pollutants within the elevated layer is shown in the initial profiles for the pollutant concentrations.

The first set of simulations were performed with the lower edge of the pollutant layer located at 300 m. The results of four different simulations are shown in Figures 7.14 to 7.17. These figures illustrate the evolution of the potential temperature profiles over a 16 hour period. The temperature profiles of simulation NP

Table 7.11 Summary of Simulations with Elevated Layers

a) Aerosol Parameters

$$\beta_{ex} = 10^{-6} \frac{m^2}{\mu g}$$

$$f = 0.85$$

$$\omega = 0.90$$

b) Pollutant gas: NH_3 (Ammonia)

c) Simulations:

NP - No participation by gaseous pollutants (thermal) and aerosols (solar)

P - Participation by gaseous pollutants and aerosols

SP - Participation by aerosols only

TP - Participation by gaseous pollutants only

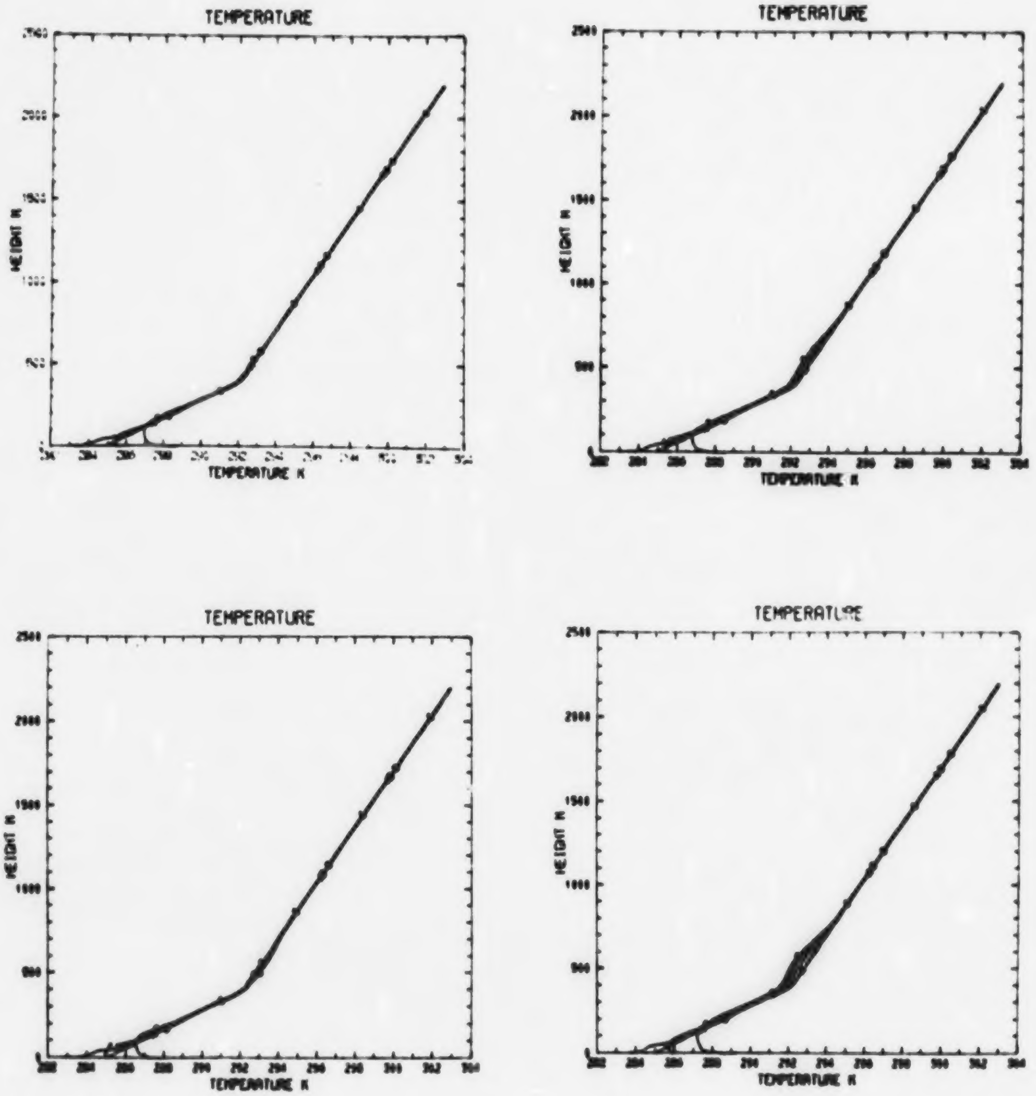

Figure 7.14 Potential Temperature Profiles for Time 05:00 to 08:00. Top Left is Simulation NP, Top Right is Simulation P, Bottom Left is Simulation SP and Bottom Right is Simulation TP. Elevated Pollutant Layer at 300 m.

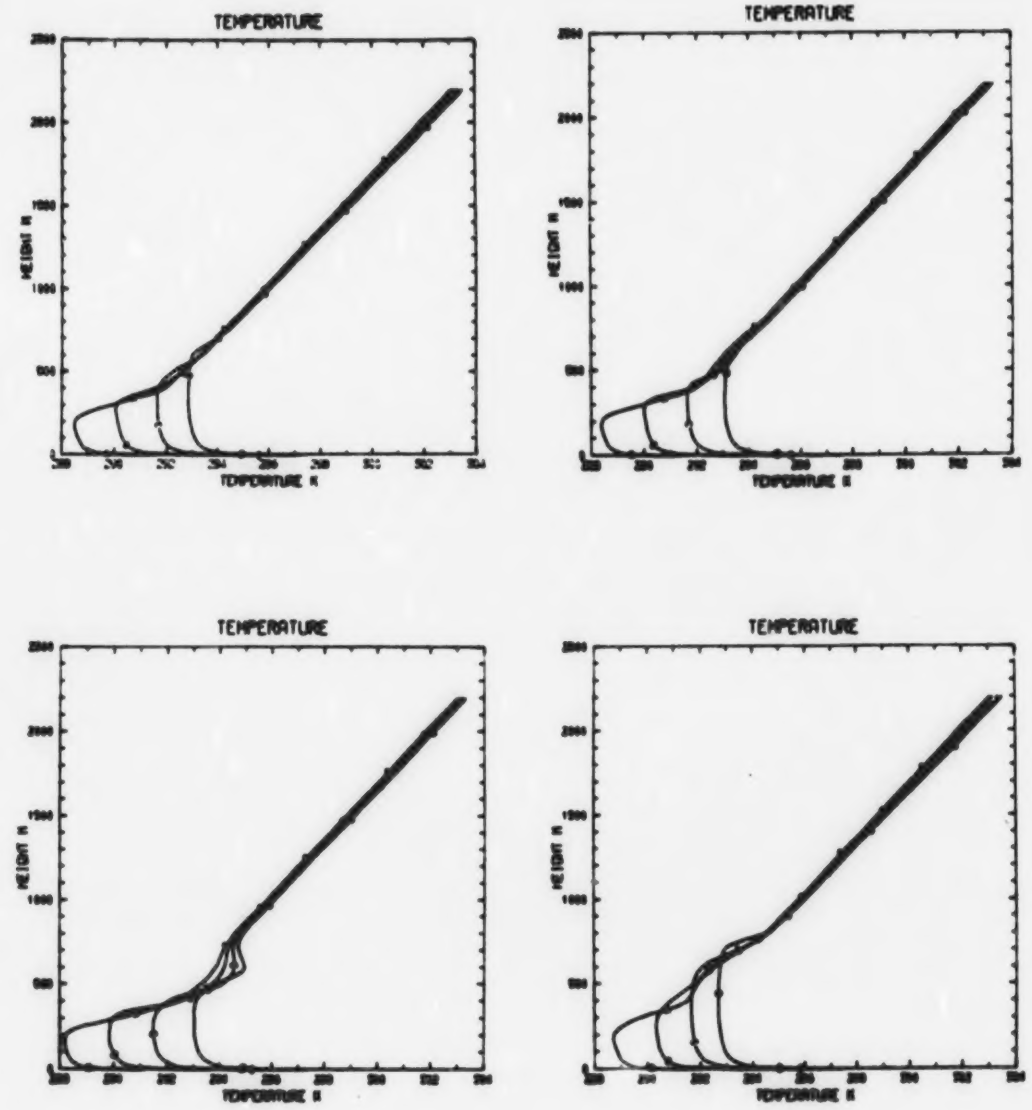

Figure 7.15 Potential Temperature Profiles for Time 09:00 to 12:00. Elevated Pollutant Layer at 300 m (See Figure 7.14 for arrangement).

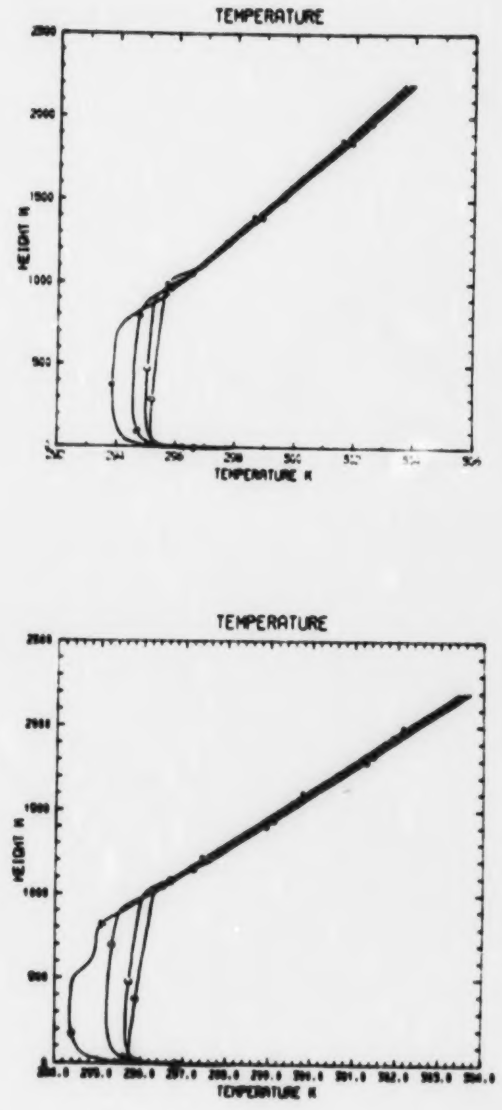

Figure 7.16 Potential Temperature Profiles for Time 13:00 to 16:00. Elevated Pollutant Layer at 300 m (See Figure 7.14 for arrangement).

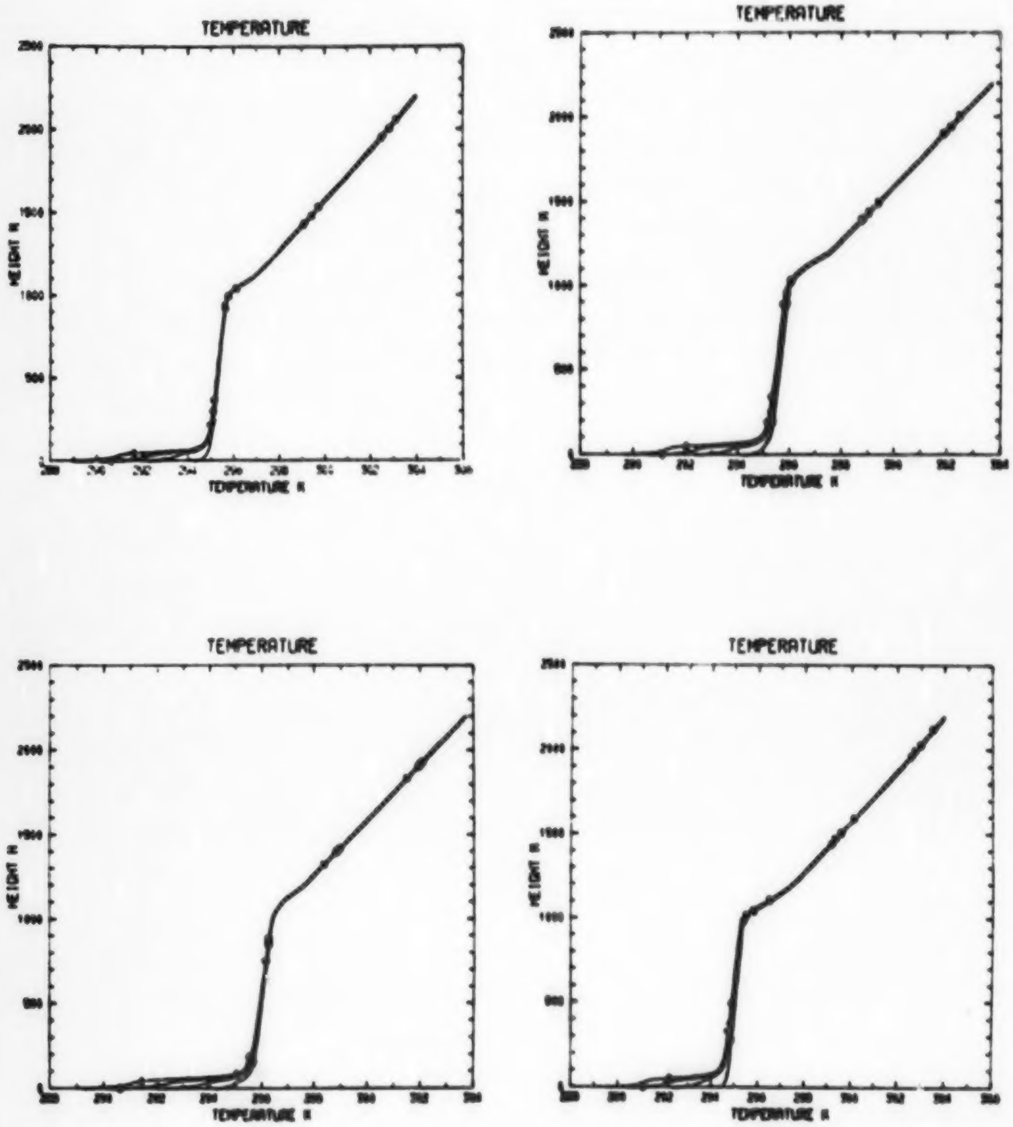

Figure 7.17 Potential Temperature Profiles for Time 17:00 to 20:00. Elevated Pollutant Layer at 300 m (See Figure 7.14 for arrangement).

(non-participating pollutants) show the usual development with the nocturnally established inversion being eroded away as the mixed layer grows during the day. The surface starts cooling in about 10 hours and a surface inversion is re-established. The results of simulation TP show the cooling effect of pollutants which participate only in the thermal spectrum. The cooling is quite pronounced within 4 hours, and the mixed layer grows rapidly as the stable layer above it is cooled. At the same time the thermal participation of the pollutants creates a sharp inversion (~2 K) at the top of the mixed layer. This strong inversion tends to slow down the growth of the mixed layer. The formation of this inversion has been predicted in theoretical studies by Atwater (1970) and Bergstrom and Viskanta (1972). Observations (Bornstein, 1968; Rouse, et al., 1974) of elevated inversions over industrial areas lend some validity to this theoretical prediction.

Simulation SP (aerosol participation only) shows the effects of aerosol heating. In about 8 hours the heating leads to the formation of a highly stable layer at a height of around 400 meters. The layer above the stable layer is marked by a negative potential temperature gradient. It is evident from Figure 7.15 that the sharp temperature gradient caused by aerosol heating effectively impedes the growth of the mixed layer. It is only after 9 hours that the mixed layer is able to penetrate the inversion, and the growth thereafter is relatively rapid as the layer above is unstable.

The results of simulation P (participation by aerosols and gases) show the opposing effects of gases and aerosols. The heating caused by aerosols is counteracted to a certain extent by the cooling induced by the gaseous pollutants. Figure 7.15 shows that the pollutant layer heating up at the bottom and cooling at the top. The stabilizing effect of heating prevents the mixed layer from growing as rapidly as in the case when there is no pollutant participation. Once the mixed layer penetrates the inversion it grows at a rate comparable with that of simulation NP.

Tables 7.12 and 7.13 compare the thermal and solar fluxes at the surface for simulations P, NP, SP and TP. As expected, solar

Table 7.12 Comparison of Thermal Fluxes (in W/m^2) at the Surface (Elevated layer at 300 m)

	Thermal Fluxes			
Time	NP	P	SP	TP
06:00	292.8	314.3	292.8	314.4
07:00	293.9	315.1	293.3	315.8
08:00	299.1	319.8	297.9	320.9
09:00	305.7	326.3	304.2	327.6
10:00	312.9	333.6	311.4	334.8
11:00	320.2	341.3	319.0	342.3
12:00	326.8	349.0	326.5	348.8
13:00	331.8	355.2	332.7	353.9
14:00	335.4	358.9	337.0	357.5
15:00	337.2	360.7	338.5	359.5
16:00	337.4	360.8	338.4	359.7
17:00	336.0	359.1	336.7	358.2
18:00	332.7	355.7	333.2	355.0
19:00	327.7	351.1	328.3	350.1
20:00	324.0	347.7	324.5	347.0
21:00	321.1	345.1	321.5	344.4
22:00	318.5	342.9	318.9	342.3
23:00	316.5	341.2	316.8	340.6
00:00	314.8	339.7	315.1	339.0
01:00	313.3	338.3	313.6	337.7
02:00	311.9	337.1	312.2	336.5
03:00	310.6	336.0	310.9	335.4
04:00	309.4	335.0	309.6	334.4

Table 7.13 Comparison of Solar Fluxes (in W/m^2) at Surface (Elevated Layer at 300 m)

	Solar Fluxes			
Time	NP	P	SP	TP
06:00	70.5	56.3	56.3	70.5
07:00	257.6	200.6	200.6	257.6
08:00	402.9	365.5	365.5	402.8
09:00	550.4	518.7	518.8	550.3
10:00	665.9	640.6	640.7	665.7
11:00	738.5	717.8	718.0	738.3
12:00	762.1	742.9	743.3	761.8
13:00	734.9	713.9	714.3	734.5
14:00	659.5	634.0	634.4	659.1
15:00	543.0	511.3	511.7	542.7
16:00	396.3	359.3	359.6	396.0
17:00	233.5	197.2	197.4	233.3
18:00	69.7	55.9	55.9	69.7

participation by pollutants decreases the solar flux at the surface by about 20% at large zenith angles (06:00) and by about 4% around solar noon. The average solar attenuation of about 12% is consistent with measurements made by Rouse, et al. (1973) in Hamilton, Ontario. Thermal participation by pollutants increases the downward thermal flux by about 10%. It is noticed that around noon the solar attenuation is of the same magnitude as that of the decrease in the thermal flux; this indicates that cooling caused by pollutants might be compensated to a degree by pollutant induced heating. The thermal fluxes of simulation P (solar and thermal participation) are slightly larger than those of simulation TP (thermal participation only). This is to be expected as the increase in the atmospheric temperature caused by solar heating is accompanied by an increase in thermal fluxes.

Table 7.14 presents the potential temperatures at 1 m for the simulations. During the first 6 hours after sunset, the effects of the reduction in the surface solar flux dominate over those of absorption of solar radiation in the surface layer thus reducing the temperature at 1 m for the simulations with solar participation. At 13:00 hours the effects of solar heating become evident with the temperature at 1 m becoming higher in the simulations with solar participation (P, SP) than that in the simulation with non-participating pollutants. This temperature excess is about 0.1 C on an average over the period of simulation. It is interesting to note that the beginning of the solar heating is accompanied by the increase in the surface aerosol concentration from the background value of 50 $\mu g / m^3$ to 130 $\mu g / m^3$. It is seen from Table 7.15 that absorption of solar radiation in the surface layer also affects the surface temperature. Although the solar flux reaching the surface is reduced by about 15% for simulation SP, the surface temperature is 0.1 C higher during the major portion of the period of simulation. The complex physical processes responsible for this seemingly anomalous temperature excess have already been described in Section 7.3.

Table 7.14 Comparison of Potential Temperatures (in K) at 1 m (Elevated layer at 300 m)

Time	Potential Temperature			
	NP	P	SP	TP
06:00	283.57	283.75	283.38	283.92
07:00	285.55	285.43	285.00	285.97
08:00	288.10	287.89	287.50	288.49
09:00	290.62	290.44	290.07	290.97
10:00	292.85	292.73	292.38	293.14
11:00	294.66	294.67	294.35	294.82
12:00	295.93	296.08	295.91	295.93
13:00	296.63	296.84	296.89	296.60
14:00	296.80	297.00	297.12	296.78
15:00	296.48	296.64	296.68	296.47
16:00	295.66	295.76	295.77	295.66
17:00	294.36	294.41	294.37	294.40
18:00	292.47	292.69	292.56	292.62
19:00	290.60	291.08	290.70	290.95
20:00	289.50	290.10	289.60	289.99
21:00	288.61	289.28	288.71	289.11
22:00	287.80	288.68	287.88	288.55
23:00	287.19	288.16	287.28	288.03
00:00	286.64	287.69	286.73	287.57
01:00	286.14	287.28	296.23	287.15
02:00	285.68	286.90	285.76	286.78
03:00	285.23	286.55	285.30	286.43
04:00	284.80	286.23	284.87	286.11

Table 7.15 Comparison of Surface Temperatures (in K) of Simulation with Non-participating (NP) Pollutants and Simulation with Solar Participation (SP) only (Elevated Layer at 300 m)

	Temperature	
Time	NP	SP
07:00	285.76	285.12
09:00	291.75	291.09
11:00	296.23	295.88
15:00	297.18	297.17
17:00	294.14	294.10
19:00	289.95	290.02
21:00	288.10	288.19
23:00	286.81	286.90
01:00	285.81	285.89
03:00	284.93	284.99
05:00	284.12	284.17
07:00	288.06	287.44
09:00	295.43	294.93
11:00	299.36	299.53
13:00	300.16	300.39
15:00	299.15	299.24
17:00	296.20	296.40
19:00	292.05	292.22
21:00	290.21	290.38
23:00	288.89	289.05
01:00	287.82	287.96
03:00	286.84	286.95

Figures 7.18 to 7.21 show the effect of radiative participation of pollutants on pollutant dispersal. During the first four hours, the pollutant layer is unaffected as the mixed layer has not yet grown high enough to disperse the pollutants. During the following 4 hours, the effect of pollutants is evident from the different rates of pollutant dispersal as shown in Figure 7.19. Thermal participation by increasing the initial rate of mixed layer growth is conducive to pollutant dispersal while solar participation decreases the rate at which pollutants diffuse away from the pollutant layer. At the end of 8 hours after the beginning of the simulation, the surface pollutant concentration is 180 $\mu g / m^3$ for no participation, 170 $\mu gm/m^3$ for thermal and solar participation, 135 $\mu g / m^3$ for solar participation only, and 200 $\mu g / m^3$ for thermal participation only. From Figure 7.20, it can be seen that solar participation can slow down pollutant dispersal even after 9 hours. Once the mixed layer penetrates the inversion created by solar heating, pollutants are mixed rapidly, and radiative participation becomes unimportant.

Figure 7.22 shows the effect of radiative participation on the growth of the mixed layer. It is seen that the largest mixed layer heights (1300 m) occur for the simulations in which there is solar participation. An explanation for this apparent anomaly is fairly simple. Solar heating creates a sharp inversion at the height of the aerosol layer; at the same time the layer above the inversion is destabilized. Initially, the inversion created by solar heating inhibits the growth of the mixed layer, but once the mixed layer penetrates the inversion its growth is relatively more rapid than for the other simulations as the layer above the inversion is unstable. The effects of the destabilizing influence of solar heating are evident on the second day when the mixed layer growth is greatest (1420 m) for the simulations with solar participation. Cooling induced by gaseous pollutants helps the growth of the mixed layer as evidenced by the larger mixed layer heights for the simulations with thermal participation.

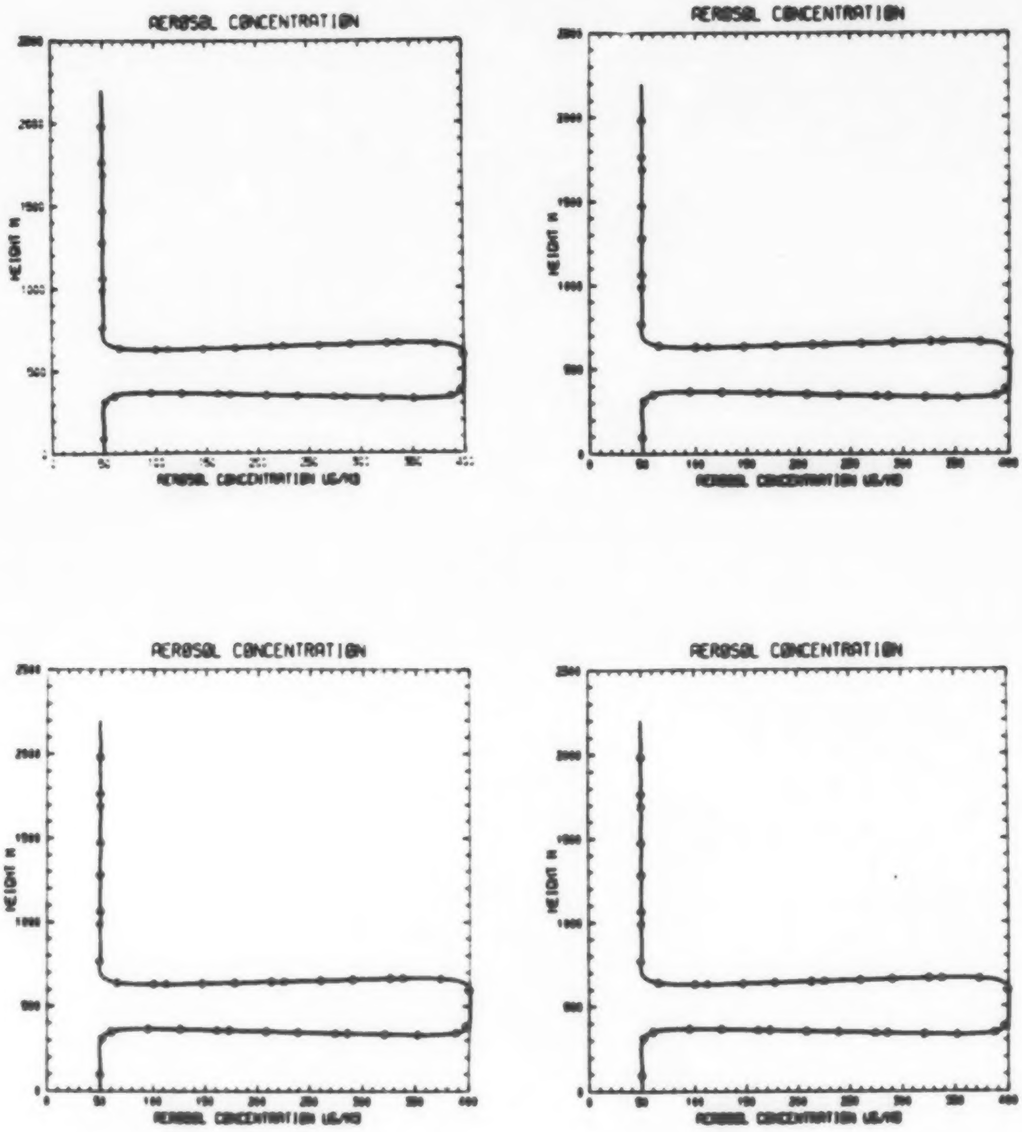

Figure 7.18 Aerosol Concentration Profiles for Time 05:00 to 08:00. Top Left is Simulation NP, Top Right is Simulation P, Bottom Left is Simulation SP, and Bottom Right is Simulation TP. Elevated Pollutant Layer at 300 m.

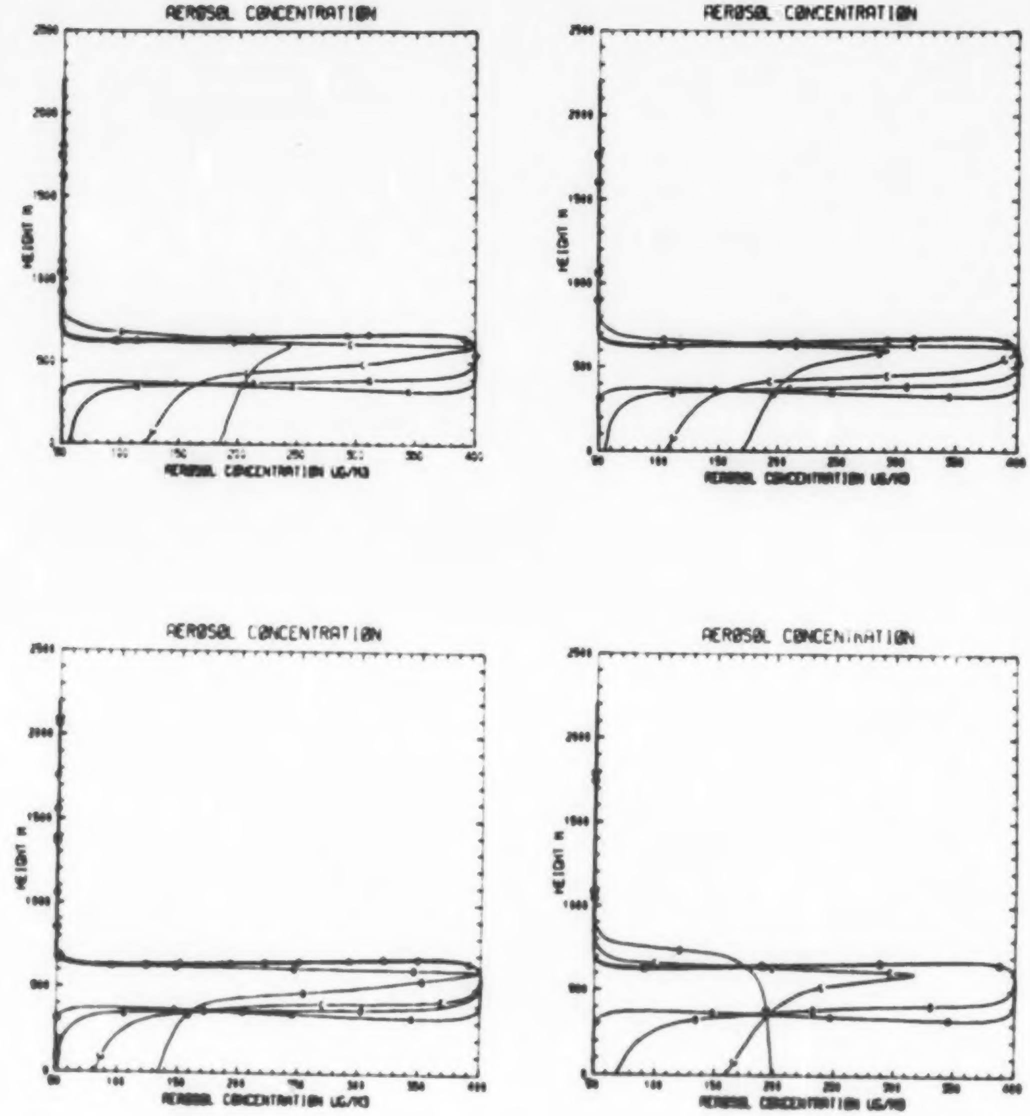

Figure 7.19 Aerosol Concentration Profiles for Time 09:00 to 12:00. Elevated Pollutant Layer at 300 m (See Figure 7.18 for arrangement).

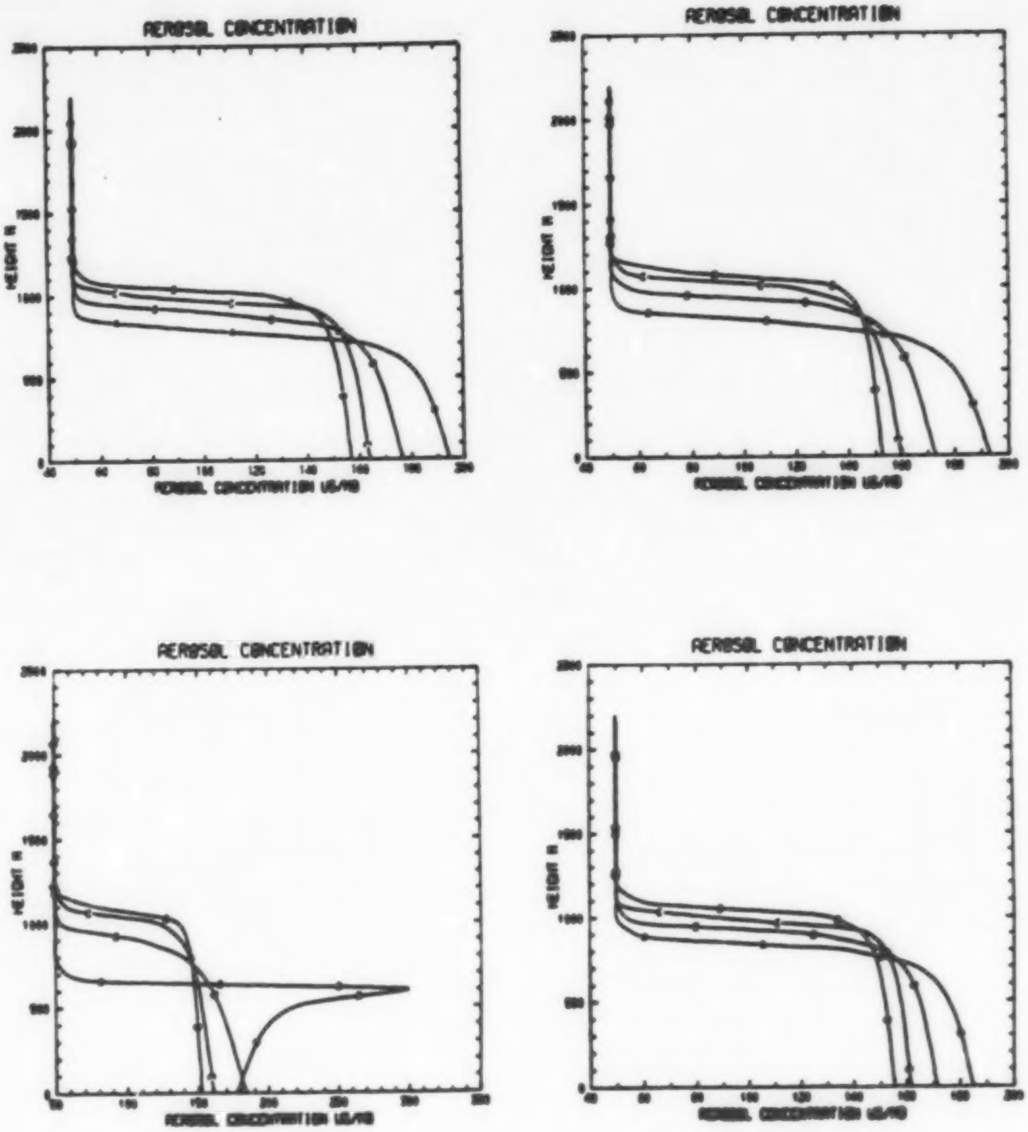

Figure 7.20 Aerosol Concentration Profiles for Time 13:00 to 16:00. Elevated Pollutant Layer at 300 m (See Figure 7.18 for arrangement).

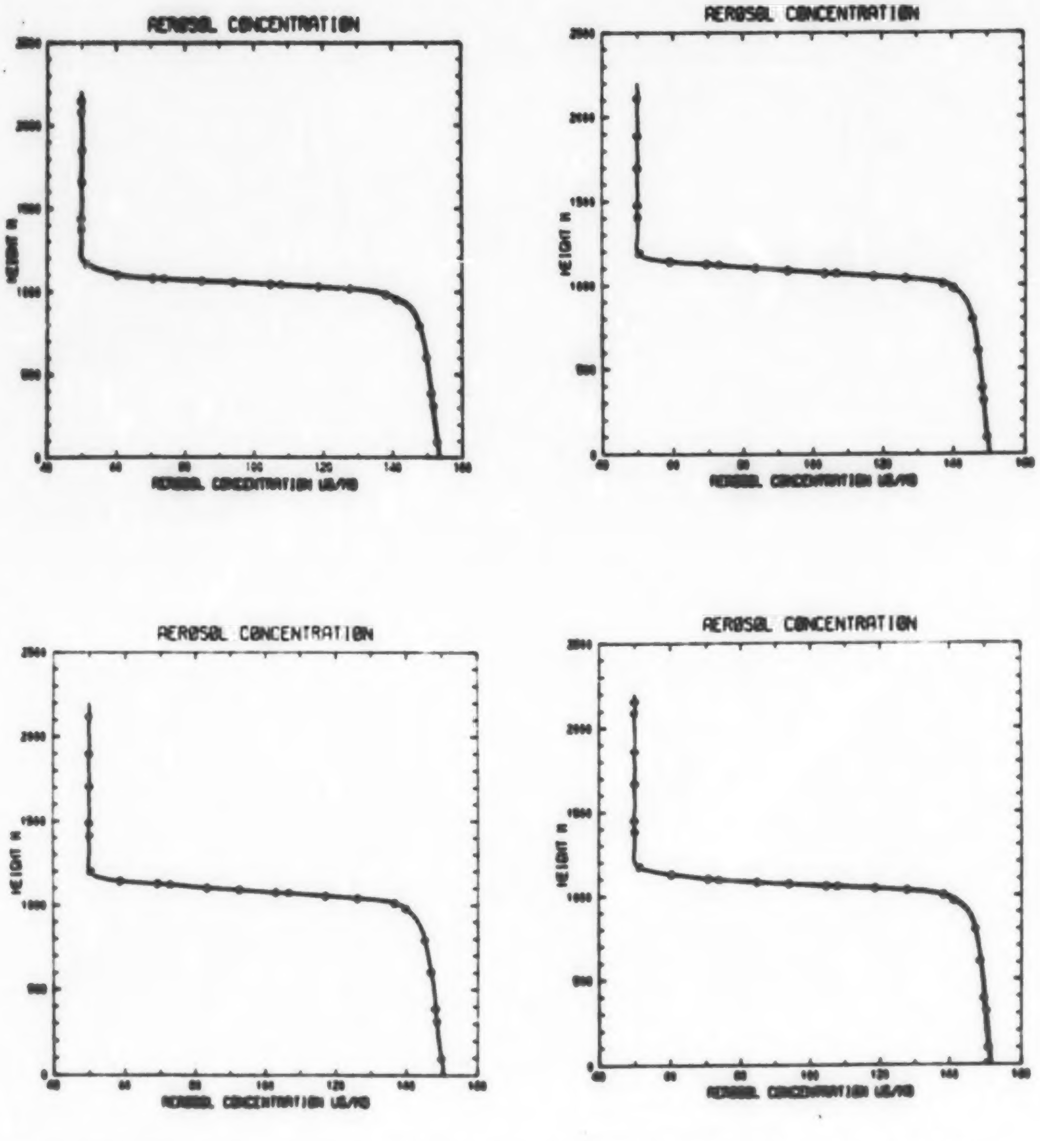

Figure 7.21 Aerosol Concentration Profiles for Time 17:00 to 20:00. Elevated Pollutant Layer at 300 m (See Figure 7.18 for arrangement).

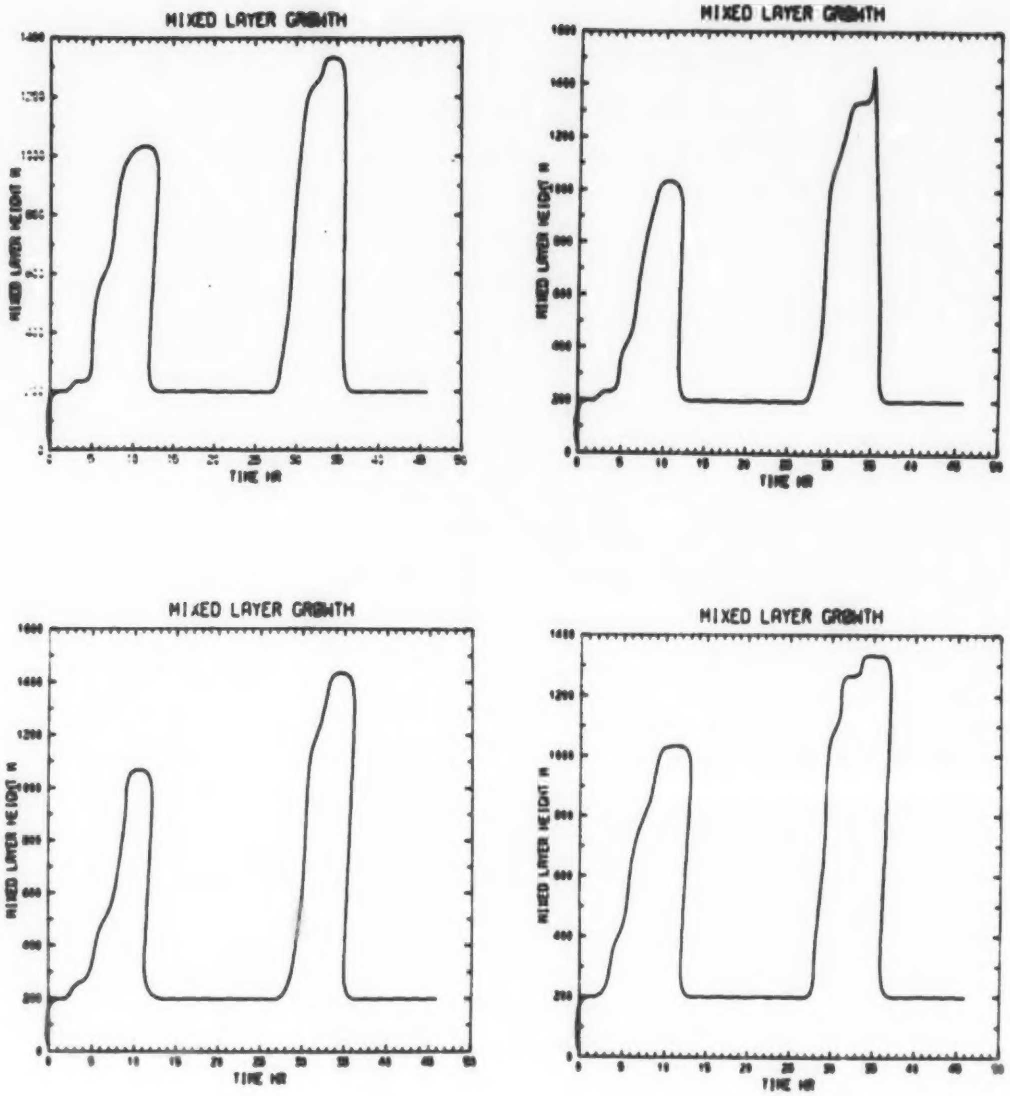

Figure 7.22 Variation of Mixed Layer Height with Time Elevated Pollutant Layer at 300 m. Top Left is Simulation NP, Top Right is Simulation P, Bottom Left is Simulation SP, and Bottom Right is Simulation TP.

7.5 Effect of Changing the Height of the Elevated Pollutant Layer

A second set of simulations was performed to determine the effect of the height of elevated pollutant layer on thermal structure and pollutant dispersal. The lower edge of the pollutant layer was located at 600 m. Figures 7.23 to 7.30 illustrate the variation of the temperature and concentration profiles over a period of 16 hours. The results indicate the same trends as those of the first set of simulations. However, as the greater height of the pollutant layer allowed the pollutant induced heating and cooling to proceed over a longer period of time, the inversions formed were considerably sharper as indicated in Figure 7.24. It is seen from Figure 7.25 that the inversion created by solar heating is large enough to prevent the growth of the mixed layer beyond the height of the pollutant layer. The effect of the creation of this "lid" on pollutant dispersal is evident in Figures 7.29 and 7.30.

The simulations can be better understood by examining the variables presented in Tables 7.16 to 7.19. Radiative participation by aerosols and gases increases the temperature at 1 m. The temperature excess is about 0.2 C during the day and reaches a maximum of 1.5 C at 03:00 of the second day. It is noted that the temperature excess produced by thermal participation alone is slightly higher than that with thermal and solar participation during the first four hours of simulation. This indicates that initially the effects of the decrease in the solar flux at the surface offset those of solar heating and the increase in downward thermal radiation. With solar participation alone, the temperature at 1 m is slightly lower (~0.6 C) than that with no participation during the first 16 hours of simulation. An examination of Table 7.16 shows that the lower surface concentrations (pollutant dispersal is impeded by solar heating) allows the effects of surface solar flux reduction to dominate over those of solar heating during the first 16 hours leading to the decrease in the temperature at 1 m. However, as

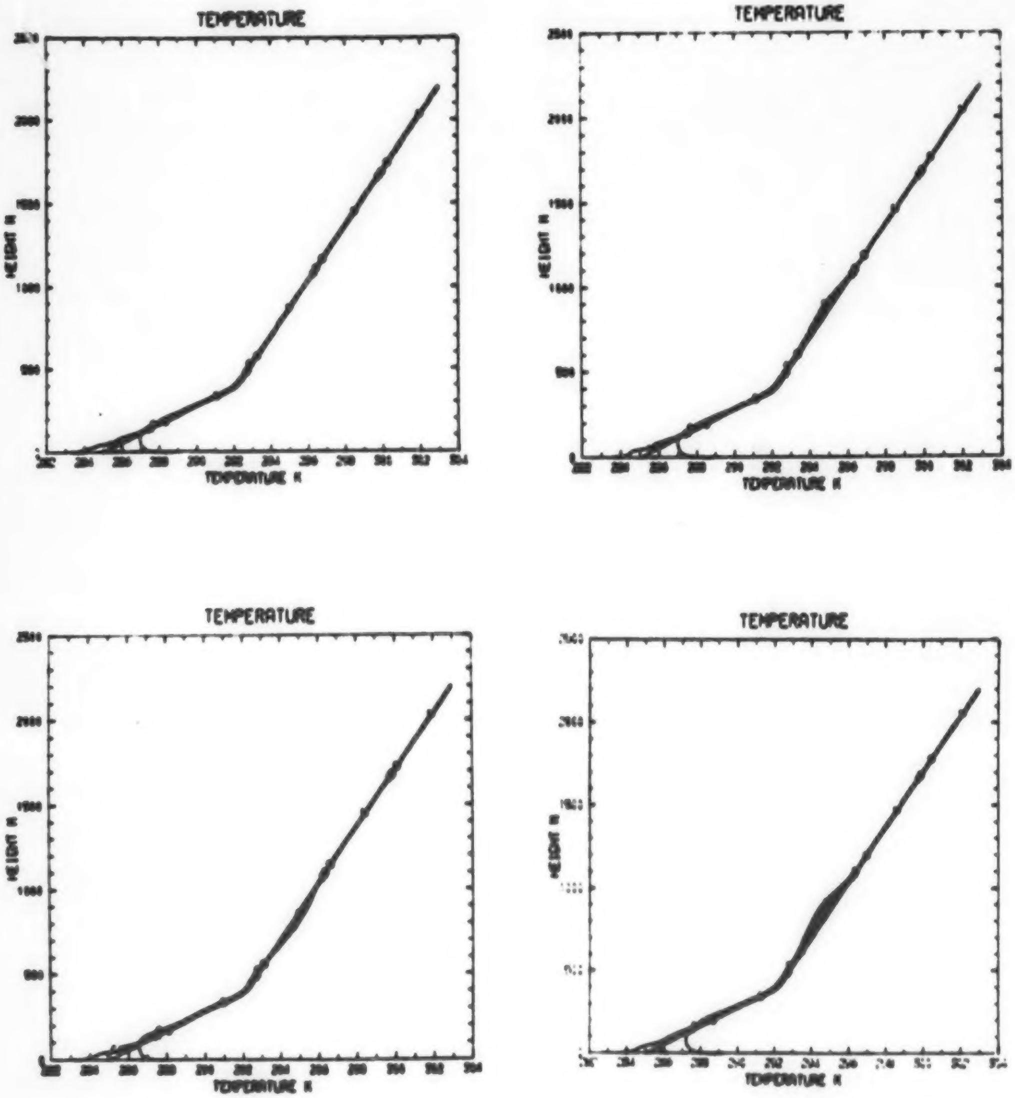

Figure 7.23 Potential Temperature Profiles for Time 05:00 to 08:00. Top Left is Simulation NP, Top Right is Simulation P, Bottom Left is Simulation SP, and Bottom Right is Simulation TP. Elevated Pollutant Layer at 600 m.

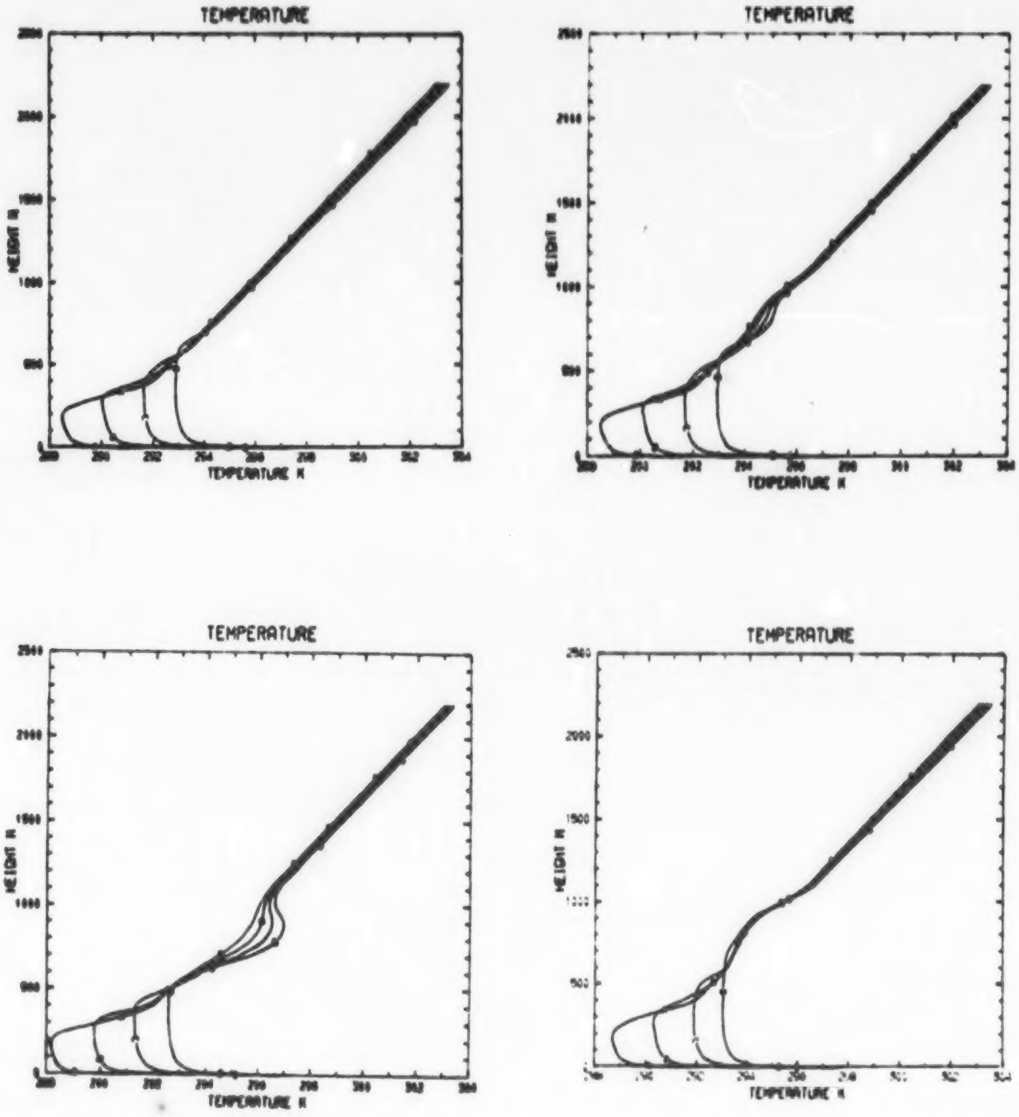

Figure 7.24 Potential Temperature Profiles for Time 09:00 to 12:00. Elevated Pollutant Layer at 600 m (See Figure 7.23 for arrangement).

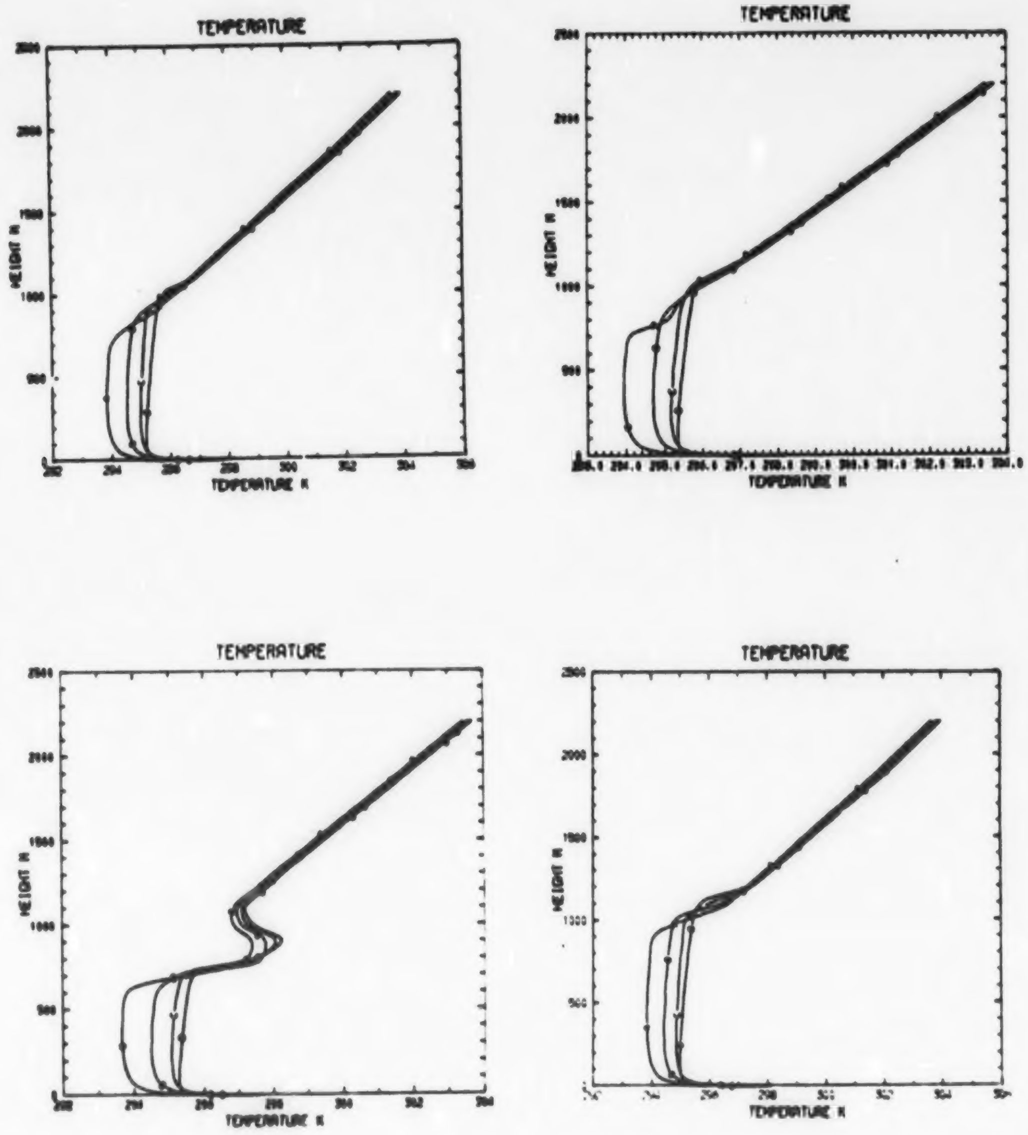

Figure 7.25 Potential Temperature Profiles for Time 13:00 to 16:00. Elevated Pollutant Layer at 600 m (See Figure 7.23 for arrangement).

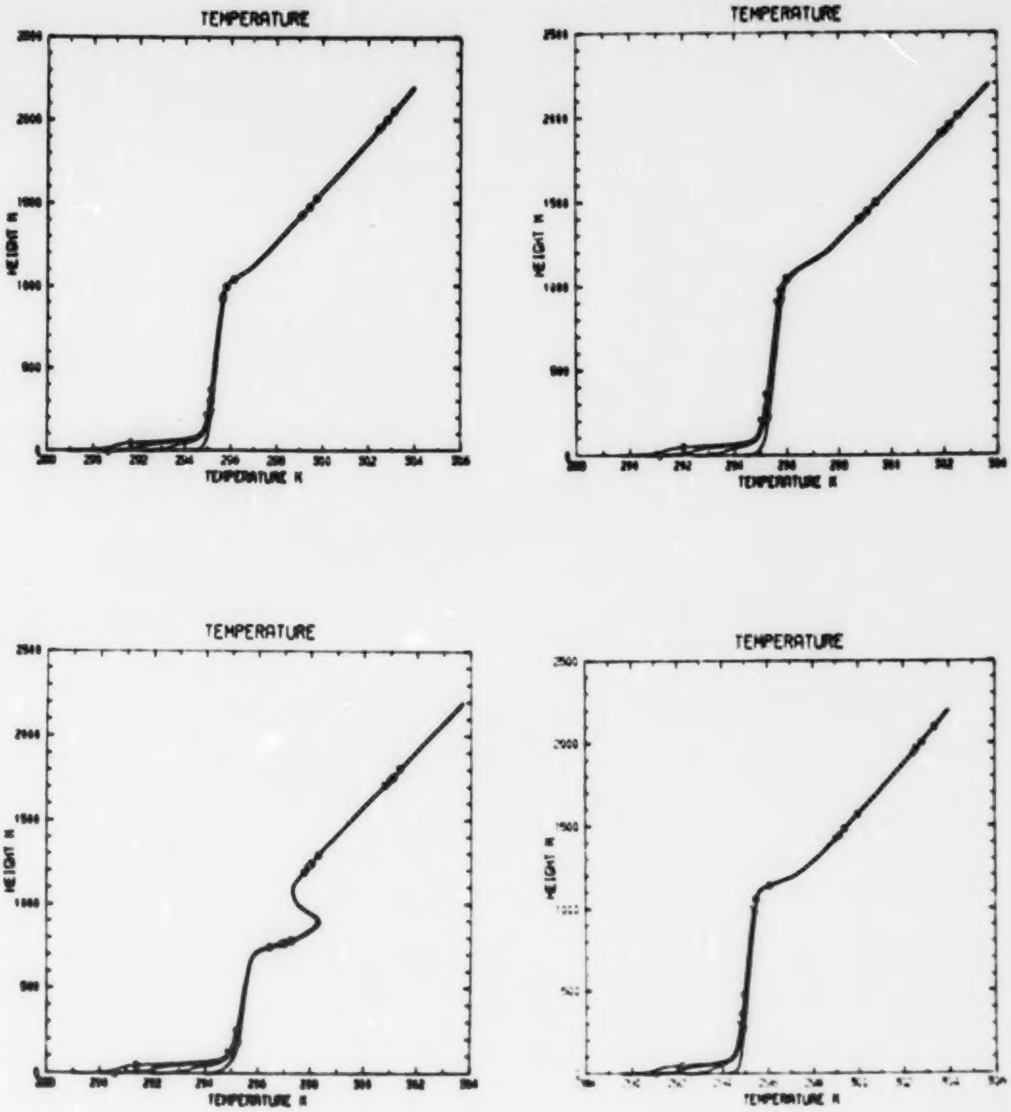

Figure 7.26 Potential Temperature Profiles for Time 17:00 to 20:00. Elevated Pollutant Layer at 600 m (See Figure 7.23 for arrangement).

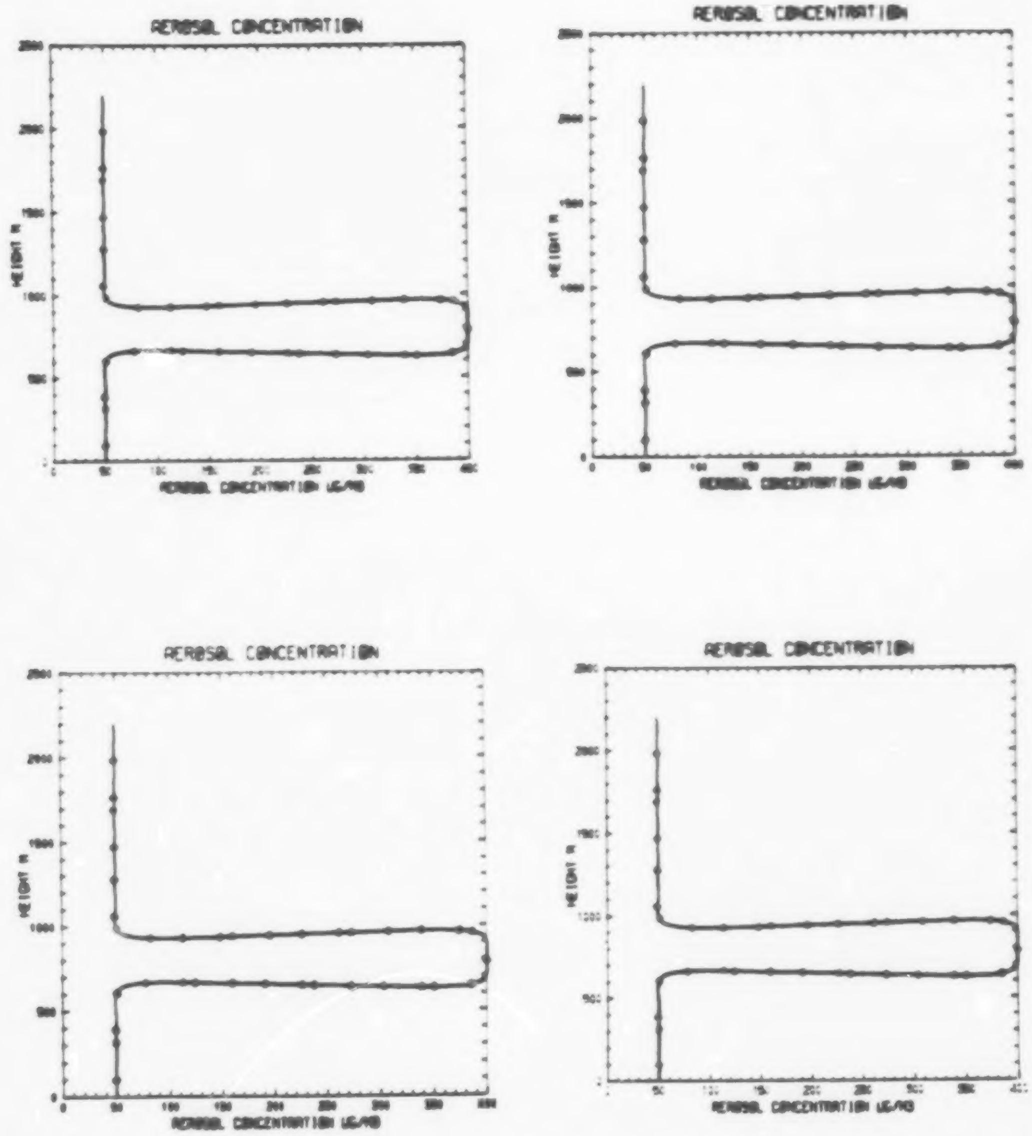

Figure 7.27 Aerosol Concentration Profiles for Time 05:00 to 08:00. Top Left is Simulation NP, Top Right is Simulation P, Bottom Left is Simulation SP, and Bottom Right is Simulation TP. Elevated Pollutant Layer at 600 m.

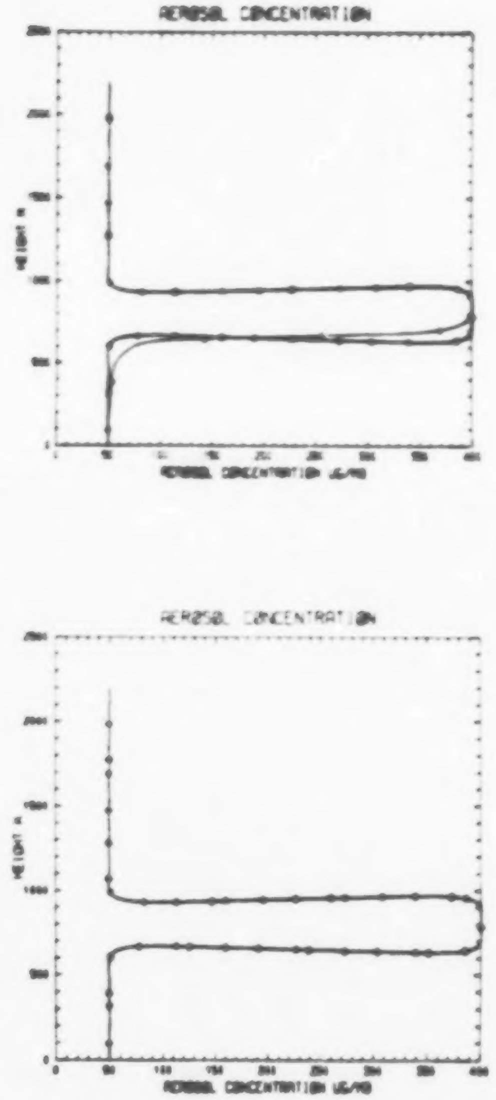

Figure 7.28 Aerosol Concentration Profiles for Time 09:00 to 12:00. Elevated Pollutant Layer at 600 m (See Figure 7.27 for arrangement).

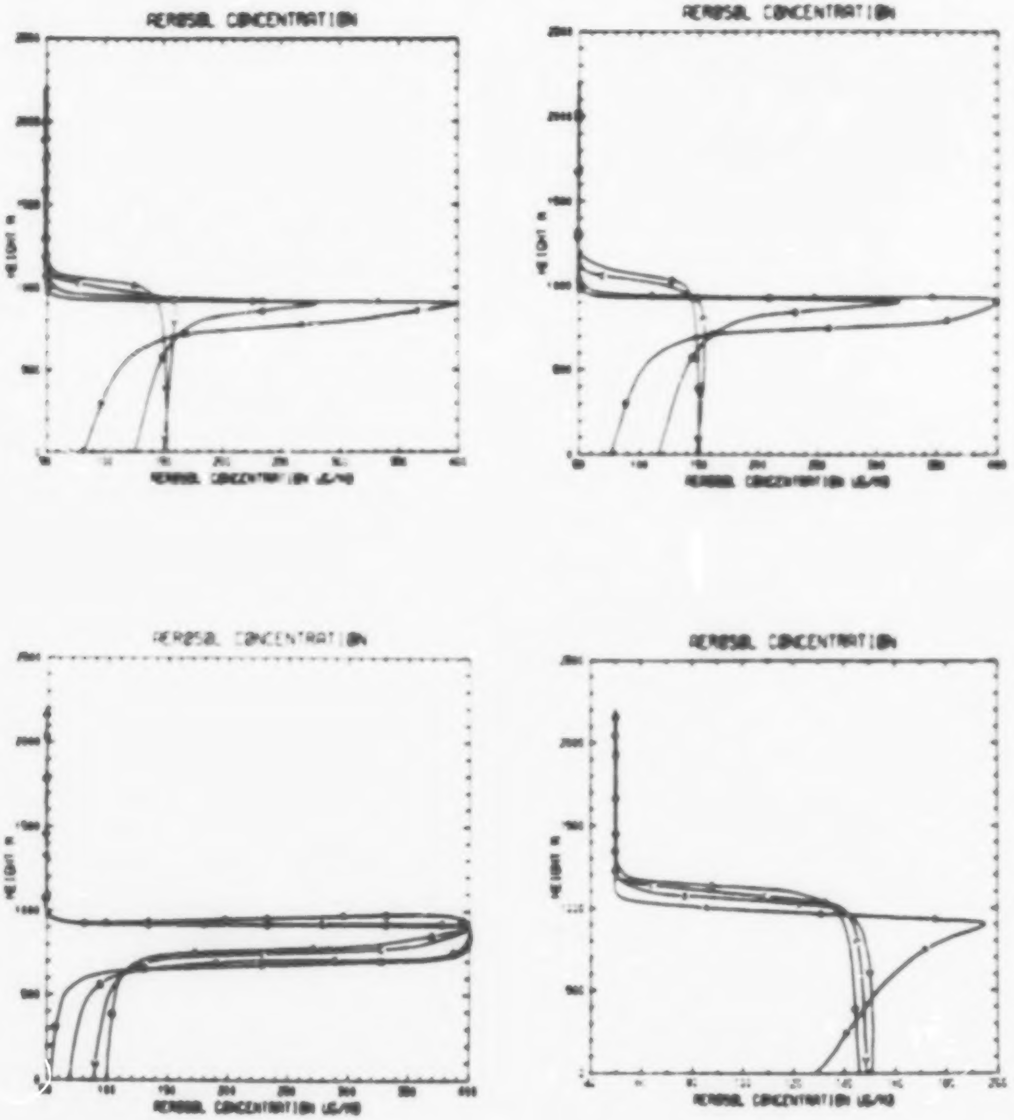

Figure 7.29 Aerosol Concentration Profiles for Time 13:00 to 16:00. Elevated Pollutant Layer at 600 m (See Figure 7.27 for arrangement).

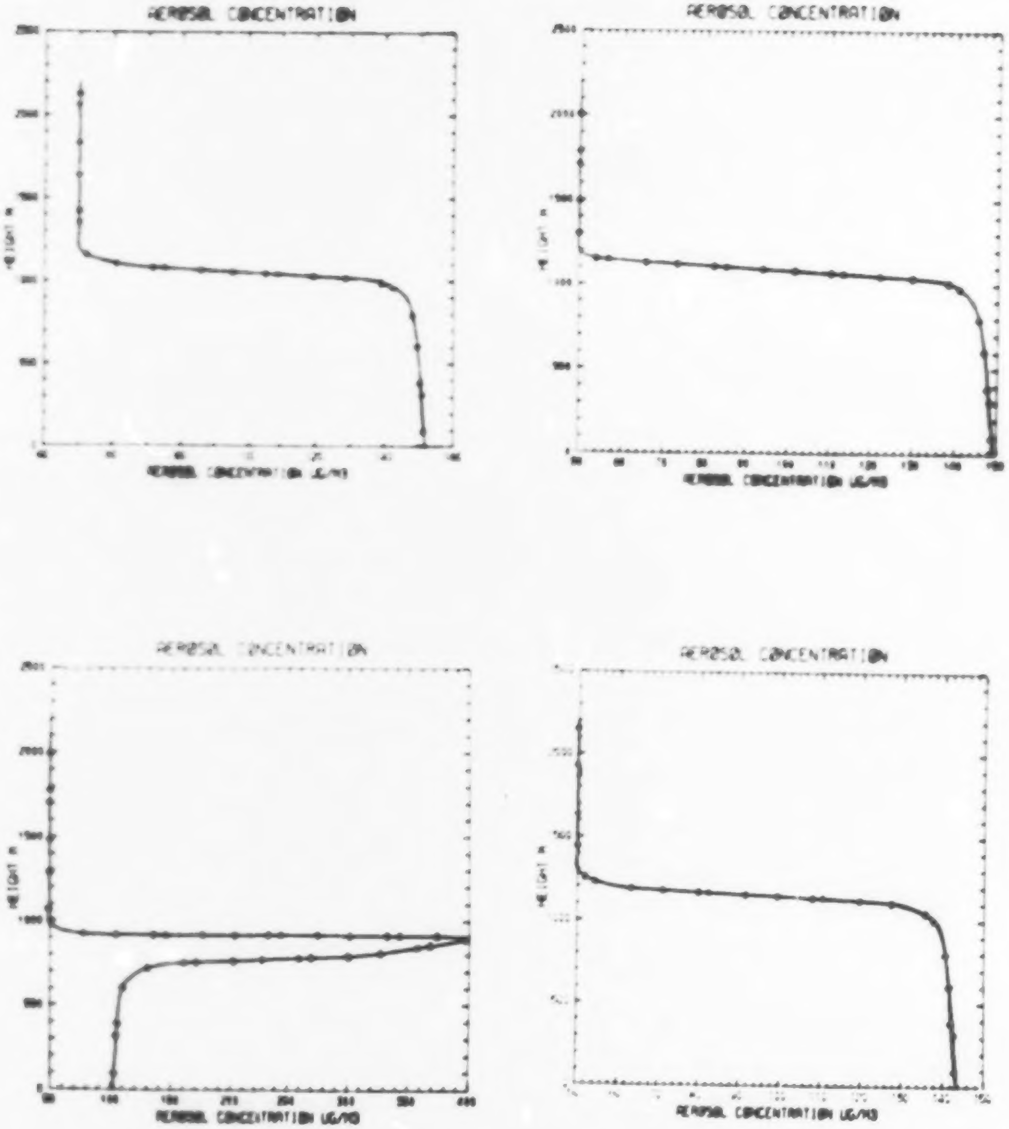

Figure 7.30 Aerosol Concentration Profiles for Time 17:00 to 20:00. Elevated Pollutant Layer at 600 m (See Figure 7.27 for arrangement).

Table 7.16 Comparison of Temperatures (in K) at 1 m (Elevated Layer at 600 m)

Time	Temperature			
	NP	P	SP	TP
07:00	285.55	285.65	285.00	285.95
09:00	290.62	290.69	290.07	290.97
11:00	294.66	294.78	294.23	294.99
13:00	296.63	296.80	296.36	296.78
15:00	296.48	296.68	296.37	296.52
17:00	294.36	294.50	294.18	294.43
19:00	290.60	291.09	290.60	290.97
21:00	288.61	289.25	288.53	289.19
23:00	287.19	288.16	287.28	288.03
01:00	286.14	287.27	286.23	287.15
03:00	285.24	286.55	285.27	286.42
05:00	284.41	285.93	284.43	285.81
07:00	287.79	288.91	287.25	289.10
09:00	294.40	295.00	293.92	295.06
11:00	298.04	298.33	298.04	298.05
13:00	299.04	299.29	299.49	299.00
15:00	298.60	298.82	299.29	298.52
17:00	296.46	296.63	297.10	296.47
19:00	292.72	293.29	293.44	293.09
21:00	290.72	291.50	291.47	291.30
23:00	289.27	290.33	290.00	290.15
01:00	288.17	289.42	288.74	289.26
02:00	287.16	288.67	287.66	288.52

soon as the surface concentration reaches 102.7 $\mu g/m^3$ solar heating becomes more significant and the temperature at 1 m is heated above that of the simulation with no radiative participation. This temperature excess reaches a maximum of about 0.5 C at 03:00 of the second day. The temperature increase is caused to a smaller extent by the increased downward thermal radiation emitted by the atmosphere which is warmer due to solar heating by aerosols.

Tables 7.17 and 7.18 list the thermal and solar fluxes absorbed at the surface for the simulations. As expected, pollutant participation increases the downward thermal flux. Solar heating also contributes to this increase by heating the atmosphere. The maximum downward thermal radiation excess is around 25 W/m^2 (7%) and occurs at 21:00 of the second day. Solar fluxes are reduced by aerosol participation. The maximum reduction occurs at large zenith angles (17:00) and is about 90 W/m^2 (30%). The small differences between the solar fluxes of simulations P and SP are caused by variation of the water vapor path length. It is noted that the reduction of pollutant dispersal by solar participation alone leads to relatively large local heating rates.

Table 7.19 shows the effect of radiative participation by pollutants on pollutant dispersal. It is seen that initially solar heating due to aerosols slows pollutant dispersal from the elevated layer as indicated by the lower surface concentrations for the simulations with solar participation. The concentrations of simulation P show that cooling induced by the gaseous pollutant helps the mixed layer penetrate the sharp inversion created by solar heating due to aerosols. Once the mixed layer penetrates the inversion its growth is more rapid than for the other simulations because the region above the inversion is unstable. The more rapid growth and consequently the higher final mixed layer thickness is indicated by the lowest value (125.7 $\mu g/m^3$) of surface concentration at 03:00 of the second day. It is interesting to note that the greatest surface (1 m) aerosol concentration occurs for the simulation in which aerosols are the only participants. An explanation for this

Table 7.17 Comparison of Solar Fluxes (in W/m^2) at Surface (Elevated Layer at 600 m)

	Solar Fluxes			
Time	NP	P	SP	TP
07:00	237.6	200.6	200.6	237.6
09:00	550.4	518.7	518.8	550.3
11:00	738.5	717.9	718.0	738.3
13:00	734.9	714.2	714.3	734.5
15:00	543.0	511.5	511.7	542.7
17:00	233.5	197.3	197.3	233.3
19:00	0	0	0	0
21:00	0	0	0	0
23:00	0	0	0	0
01:00	0	0	0	0
03:00	0	0	0	0
05:00	0	0	0	0
07:00	233.5	197.6	197.6	233.3
09:00	540.0	509.0	509.2	539.3
11:00	725.2	704.8	704.9	724.0
13:00	722.2	701.6	701.8	721.0
15:00	534.1	502.9	503.2	533.2
17:00	229.8	194.0	194.5	229.5
19:00	0	0	0	0
21:00	0	0	0	0
23:00	0	0	0	0
01:00	0	0	0	0
03:00	0	0	0	0

Table 7.18 Comparison of Thermal Fluxes (in W/m^2) at Surface (Elevated Layer at 600 m)

Time	Thermal Fluxes			
	NP	P	SP	TP
07:00	294.0	314.9	293.3	315.3
09:00	305.7	326.5	304.1	327.2
11:00	320.3	334.3	318.7	341.9
13:00	331.8	353.4	330.7	353.4
15:00	337.2	360.5	337.1	359.5
17:00	336.0	359.2	336.0	358.2
19:00	327.7	351.1	327.6	350.1
21:00	321.1	345.1	321.0	344.4
23:00	316.5	341.2	316.5	340.5
01:00	313.3	338.3	313.4	337.7
03:00	310.6	336.0	310.5	335.4
05:00	308.2	333.0	308.0	333.4
07:00	311.6	337.0	310.6	336.8
09:00	329.0	353.3	327.4	353.3
11:00	344.3	368.5	343.8	367.2
13:00	351.6	375.6	353.3	374.1
15:00	354.7	378.8	358.1	377.4
17:00	352.3	376.2	355.8	375.0
19:00	343.3	367.6	346.3	366.4
21:00	336.2	361.2	338.9	360.3
23:00	331.2	357.0	334.0	356.1
01:00	327.7	353.9	330.0	353.1
03:00	324.6	351.4	326.6	350.6

Table 7.19 Comparison of Aerosol Concentrations (in $\mu g/m^3$) at 1 m (Elevated Layer at 600 m)

	Aerosol Concentrations			
Time	NP	P	SP	TP
07:00	50.0	50.0	50.0	50.0
09:00	50.0	50.0	50.0	50.0
11:00	50.0	50.0	50.0	50.0
13:00	81.7	76.3	53.4	128.4
15:00	149.7	147.7	87.7	149.0
17:00	152.0	149.3	102.6	143.8
18:00	151.7	149.0	102.7	143.3
21:00	151.7	149.0	102.7	143.3
23:00	151.7	149.0	102.7	143.3
01:00	151.7	149.0	102.7	143.3
03:00	151.7	149.0	102.7	143.3
05:00	151.7	149.0	102.8	143.3
07:00	151.7	149.0	102.8	143.3
09:00	141.4	149.0	103.0	143.1
11:00	150.8	147.9	104.1	142.2
13:00	144.9	138.6	133.4	136.8
15:00	134.4	129.3	133.6	129.9
17:00	130.2	125.8	141.5	126.6
19:00	130.1	125.7	141.5	136.4
21:00	130.1	125.7	141.5	136.4
23:00	130.1	125.7	141.5	136.4
01:00	130.1	125.7	141.5	136.4
03:00	130.1	125.7	141.6	136.4

can be found by examining the effect of solar heating on the height of the mixed layer. Solar heating does inhibit dispersal as indicated by the lower surface pollutant concentrations till 11:00 of the second day. At the same time the sharp inversion induced by solar energy absorption prevents the vertical expansion of the mixed layer. Thus, the pollutants which are allowed to disperse over a smaller vertical extent reach higher concentrations at the surface.

Figure 7.31 illustrates the effect of radiative participation on the growth of the mixed layer. It is evident that the height of the elevated pollutant layer determines the effect of solar heating. When the pollutant layer is at 600 m solar heating proceeds over a longer period of time and the inversion formed is large enough to limit the growth of the mixed layer. The mixed layer is not able to penetrate the inversion and does not grow beyond 820 m. It can be seen that cooling induced by gaseous pollutants helps the mixed layer to grow. This effect is evident in the simulation in which there is thermal and solar participation. While the mixed layer is not able to penetrate the solar heating induced inversion when aerosols are the only radiative participants, it does so with the assistance of gaseous cooling. As the layer above the inversion is unstable the mixed layer grows to a height of 1420 m, the largest value for the simulations.

It is clear from the simulations described that aerosols lead to a surface layer temperature increase by absorbing solar radiation in the surface layer of the boundary layer. Thus, this warming effect is dependent on the presence of fairly large aerosol concentrations near the surface. This line of reasoning indicates that aerosols would cause cooling if they are distributed well above the surface layer. To test this hypothesis a simulation was performed with the aerosol layer located at 1200 m. Only solar participation was allowed to prevent the dispersal of pollutants from the layer. Table 7.20 compares the solar fluxes and the temperature at 1 m against those for the simulation with no radiative participation. The small reduction in the solar radiation during the second day

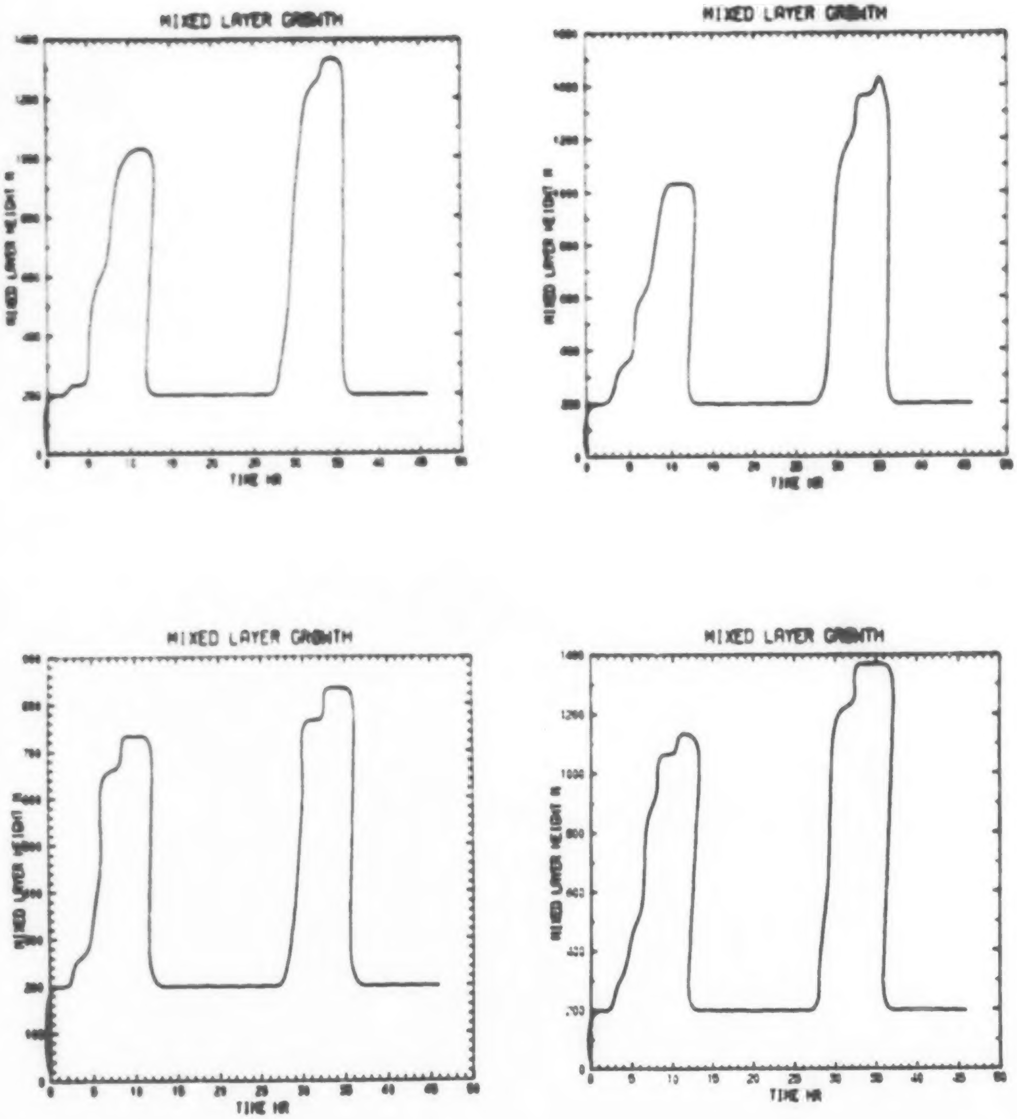

Figure 7.31 Variation of Mixed Layer Height with Time. Elevated Pollutant Layer at 600 m. Top Left is Simulation NP, Top Right is Simulation P, Bottom Left is Simulation SP, and Bottom Right is Simulation TP.

Table 7.20 Comparison of Solar Fluxes (in W/m^2) and Temperature (in K) at 1 m (Elevated Layer at 1200 m)

Time	Solar Flux		Temperature	
	NP	P	NP	P
07:00	374.6	200.3	285.54	284.70
09:00	550.4	515.8	290.62	289.80
11:00	738.5	712.3	294.66	293.95
13:00	734.9	708.4	296.63	296.01
15:00	543.0	508.3	296.48	295.76
17:00	233.5	196.9	294.36	293.42
19:00	0	0	290.60	289.71
21:00	0	0	288.61	287.68
23:00	0	0	287.19	286.21
01:00	0	0	286.14	285.10
03:00	0	0	285.23	284.08
05:00	0	0	284.41	283.18
07:00	233.5	197.6	287.79	285.98
09:00	540.0	505.6	294.40	292.79
11:00	725.2	698.7	298.04	296.97
13:00	722.2	695.5	299.04	298.09
15:00	534.1	499.6	298.60	297.63
17:00	229.8	193.9	296.46	295.32
19:00	0	0	292.72	291.64
21:00	0	0	290.73	289.64
23:00	0	0	289.27	288.15
01:00	0	0	288.17	286.93
03:00	0	0	287.16	285.84

is caused by the increased amount of water vapor in the boundary layer. It is interesting to note that solar attenuation leads to a surface layer temperature decrease of about 1.2 C during the second day.

7.6 Effect of Changing Aerosol Properties

Recent studies (Mitchell, 1971; Russell and Grams, 1975) show that tropospheric aerosols cause cooling or heating of the earth-boundary layer system depending upon their properties. As the properties of aerosols are not well known, it is not possible to draw definite conclusions about their effects. In order to gain some understanding of the importance of aerosol properties, aerosol parameters such as single scattering albedo and forward scattering factor were varied in a number of simulations. The aerosol extinction coefficient was chosen so that the maximum aerosol optical thickness of the boundary layer was around 0.14, a value which is consistent with measurements made by Herman, et al. (1971). They placed the mean aerosol optical thickness of the atmosphere around 0.1.

Some of the most important simulations are listed in Table 7.21 and some selected results are presented in Tables 7.22 and 7.23. Aerosol participation decreases the temperature at 1 m in all the simulations during the first 26 hours. This indicates that during this period the absorption of solar radiation in the surface layer is not significant enough to offset the effect of the reduction of solar flux at the surface. Around 11:00 of the second day of simulation the aerosol optical thickness is about 0.1 and the effects of solar heating become evident. The results of simulations 2 and 4 show that the surface air layer is about 0.1 C warmer during the remaining 20 hours. This result indicates that very slightly absorbing aerosols ($\omega = 0.9$) can cause warming of the surface layer. The predominantly scattering albedo of 0.99 of simulation 3 and the small forward scattering factor of 0.5 ($b = 0.5$) of simulation 5 lead to a decrease in the temperature of the surface air layer. The temperature deficit reaches a maximum of about 1.23 C at 07:00 of

Table 7.21 Summary of Simulations Performed to Study the Effect of Aerosol Property Variation; $r_s = 0.2$, $H = 0.1$

Simulation No.	Parameters Characterizing Radiative Participation
1	No radiative participation
2	Aerosol participation; $\omega = 0.8$, $f = 0.85$ $\beta_{ex} = 5 \times 10^{-7}$ m^2/µg
3	Aerosol participation; $\omega = 0.99$, $f = 0.85$, $\beta_{ex} = 5 \times 10^{-7}$ m^2/µg
4	Aerosol participation; $\omega = 0.90$, $f = 0.85$, $\beta_{ex} = 5 \times 10^{-7}$ m^2/µg
5	Aerosol participation; $\omega = 0.90$, $f = 0.5$, $\beta_{ex} = 5 \times 10^{-7}$ m^2/µg

Table 7.22 Comparison of Temperatures at 1 m to Study the Effect of Aerosol Parameter Variation

Time	Temperature (K)				
	1	2	3	4	5
07:00	285.54	285.33	285.12	285.37	285.29
09:00	290.62	290.46	290.30	290.50	290.30
11:00	294.66	294.59	294.44	294.64	294.38
13:00	296.63	296.63	296.49	296.67	296.36
15:00	296.48	296.48	296.32	296.50	296.18
17:00	294.36	294.27	294.06	294.29	294.00
19:00	290.60	290.59	290.16	290.61	290.38
22:00	288.61	288.60	288.09	288.61	288.41
23:00	287.19	287.19	286.56	287.20	287.03
01:00	286.14	286.15	285.43	286.15	285.99
03:00	285.23	285.23	284.41	285.24	285.08
05:00	284.41	284.41	283.49	294.41	284.26
07:00	287.79	287.27	286.53	287.34	287.01
09:00	294.40	294.29	293.79	294.34	293.67
11:00	298.04	298.23	298.87	298.22	298.60
13:00	299.04	299.28	298.90	299.25	298.57
15:00	298.60	298.82	298.39	298.76	298.08
17:00	296.46	296.65	296.05	296.50	295.95
19:00	292.72	292.91	292.18	292.79	292.33
21:00	290.73	290.92	290.13	290.82	290.40
23:00	289.27	289.48	288.58	289.38	289.01
01:00	288.17	288.33	287.36	288.25	287.82
03:00	287.16	287.29	286.25	287.22	286.88

Table 7.23 Comparison of Solar Fluxes at Surface to Study the Effect of Aerosol Parameter Variation

Time	Solar Flux (W/m²)				
	1	2	3	4	5
07:00	237.6	223.8	228.4	226.2	220.7
09:00	550.4	537.5	542.6	541.7	527.7
11:00	738.5	727.5	732.7	733.0	712.2
13:00	734.9	722.0	728.5	728.3	704.8
15:00	543.0	523.7	532.1	529.8	510.1
17:00	233.5	209.5	217.5	214.0	214.6
19:00	0	0	0	0	0
21:00	0	0	0	0	0
23:00	0	0	0	0	0
01:00	0	0	0	0	0
03:00	0	0	0	0	0
05:00	0	0	0	0	0
07:00	233.5	198.6	210.9	205.3	191.8
09:00	540.0	504.9	522.9	516.1	482.5
11:00	725.2	695.0	715.4	708.9	661.6
13:00	722.2	690.0	711.7	704.6	655.3
15:00	534.1	492.7	514.0	505.7	467.7
17:00	229.8	187.2	202.4	195.4	179.2
19:00	0	0	0	0	0
21:00	0	0	0	0	0
23:00	0	0	0	0	0
01:00	0	0	0	0	0
03:00	0	0	0	0	0

the second day for simulation 3. For simulation 5 the maximum temperature decrease is about 0.8 C at 07:00 of the second day. The lower temperature deficit of simulation 5 is associated with the lower single scattering albedo of 0.9.

The effects of radiative participation of pollutant layers on the total energy balance of the earth-boundary layer system is reflected in the variation of the effective albedo of the system. Figures 7.32 and 7.33 show the effect of aerosol property variation on the system albedo. The effective albedo with no radiative participation is lower than the surface albedo of 0.2 because of the water vapor absorption of solar energy in the boundary layer. Figure 7.32 illustrates the sensitivity of the earth-boundary layer albedo to the forward scattering factor. Aerosols with forward scattering factors of 0.5 and 0.7 lead to cooling of the earth boundary layer system. Aerosols with a forward scattering factor of 0.9 lower the albedo below the albedo with no participation during the major portion of the period of solar irradiation. Thus, the thermal effect is clearly one of warming. At this point it is appropriate to recall the physical meaning of the forward scattering factor. The forward scattering factor represents the fraction of the incident solar energy scattered in the forward direction. Thus, a small forward scattering factor is associated with large back-scattering. This explains the results presented in Figure 7.32.

Figure 7.33 illustrates the effects of aerosol single scattering albedo on the effective system reflectance. It is seen that aerosols with a single scattering albedo as high as 0.99 can cause warming of the earth-boundary layer system during a short period around noon. This heating effect is associated with the large forward scattering factor of 0.85. The radiation scattered predominantly in the forward direction is absorbed by water vapor and to a much smaller extent by aerosols, thus causing the warming. It is noted that water vapor absorption becomes important at small zenith angles around noon when the smaller water vapor path length above the boundary layer allows greater solar absorption in the boundary layer. As water vapor

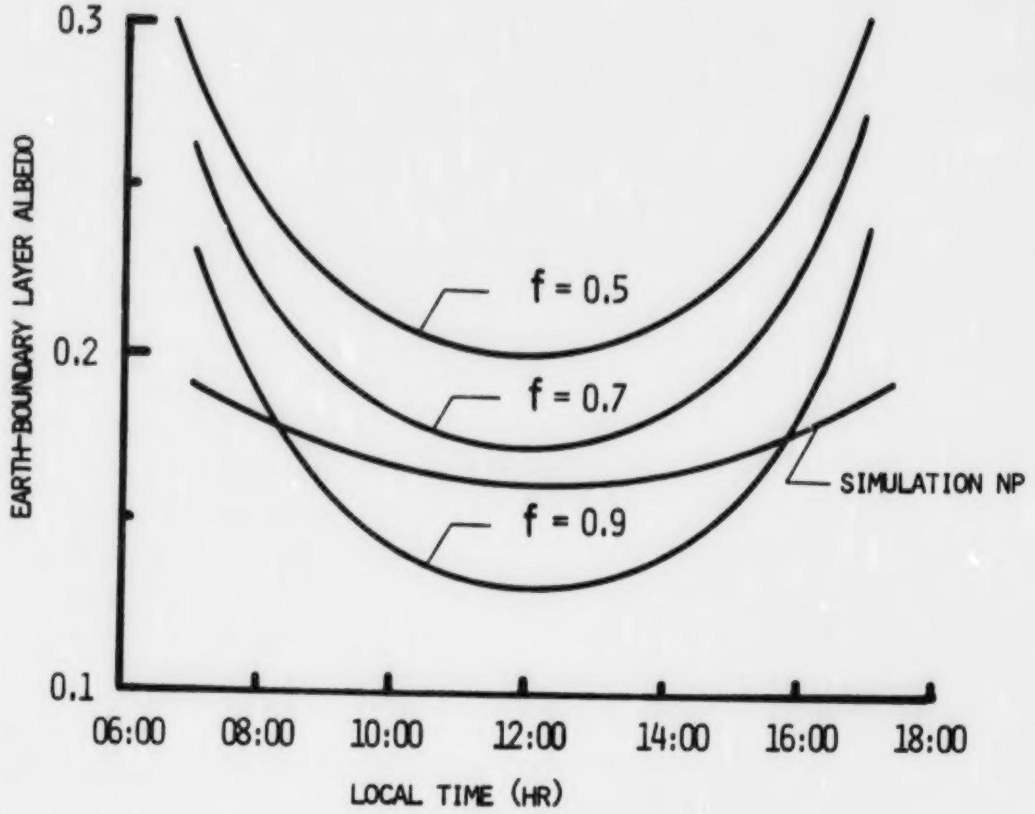

Figure 7.32 Effect of Forward Scattering Factor on Earth-Boundary Layer Albedo of Second Day. $\beta_{ex} = 5 \times 10^{-7}$ m²/μg, ω = 0.9

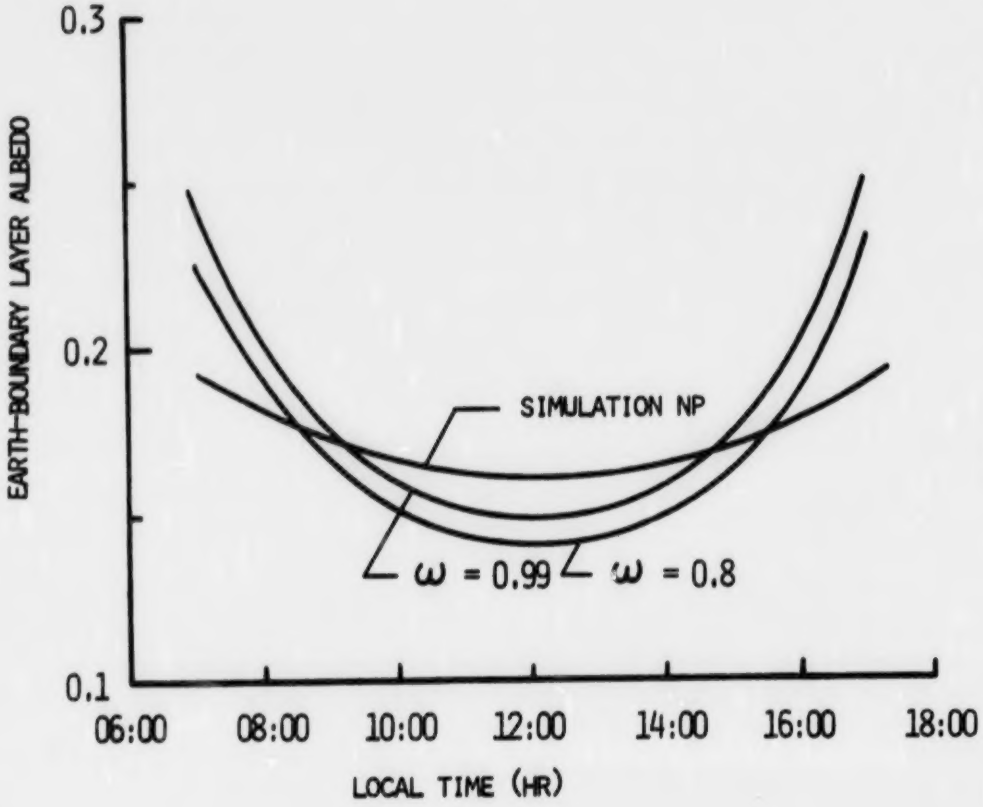

Figure 7.33 Effect of Single Scattering Albedo on Earth-Boundary Layer Albedo of Second Day. $\beta_{ex} = 5 \times 10^{-7}$ m²/μg, f = 0.85

absorbs proportionately larger amounts of solar energy above the surface than near the earth's surface, the overall warming effect is not evident at the surface. This explains the temperature deficit of the surface layer for simulation 3.

7.7 Effect of Choice of Gaseous Pollutant

As the choice of ammonia as a representative pollutant may be criticized as unduly restrictive, a simulation was performed using methane. Methane is produced by bacterial action in swamps, marshes and sewage. It abosrbs strongly in a band centered at 7.6 μm, and it is representative of a typical hydrocarbon pollutant. The emissivity of methane was derived from the wide band correlations presented by Tien (1968). The results of the simulation with methane showed that the effects of radiative participation by methane were extremely small at the concentrations (~200 $\mu g/m^3$) predicted by the numerical model. The temperature at 1 m was increased by a maximum of 0.1 C, and the effect on pollutant dispersal was negligible.

VIII. RESULTS AND DISCUSSION: TWO-DIMENSIONAL MODEL

8.1 Introduction

This chapter discusses the results of the simulations performed with the two-dimensional model. At the outset it should be stated that the model is in the process of development and as such the results to be presented are to be considered preliminary. The construction of the one-dimensional model and the simulations performed with it represented the first stage of an ongoing research. The preliminary one-dimensional simulations were conducted to test the radiation and turbulence models developed in this study, and additional simulations provided valuable understanding of the effects of radiative participation of pollutants on thermal structure and pollutant dispersal. The second phase of the research study consisted of the incorporation of the radiation and turbulence models into a two-dimensional transport model. Several problems were encountered in the process and some of them have not yet been resolved. An attempt to incorporate the turbulent kinetic energy model into the transport model resulted in the numerical scheme becoming unstable. Thus, it was necessary (for the time being) to adopt a simpler model for turbulence. Specifically, the O'Brien cubic profile (O'Brien, 1970) for diffusivity was utilized. Sasamori (1970) and Bornstein (1972) have developed relatively successful P.B.L. models based on the O'Brien profile. In using the O'Brien diffusivity model, the height of the planetary boundary layer was allowed to vary with time. This modification represents an improvement over the versions of the O'Brien model used by Sasamori (1970) and Bronstein (1972) both of whom fixed the height of the boundary layer. As the mixed layer height varies considerably (by a factor of five) over the course of a day, it is unrealistic to assume a constant boundary layer height. It should be emphasized that the instability problem associated with the turbulent kinetic energy model is under investigation. Possible solutions include an improved numerical scheme and/or improved procedures to finite difference the non-linear production and dissipation terms in the turbulent kinetic energy equation.

The effects of radiative participation on vertical stability have already been discussed in the preceding chapter. The complex feedback mechanisms associated with the development of the thermal structure in the boundary layer have been examined in some detail, and will not be emphasized in the discussion of the results presented in this chapter. As the two-dimensional model is still in the process of development, the discussion of the results of the simulations will be brief in comparison with that of the one-dimensional model. It is felt that a more detailed examination is not warranted at this stage of the research program.

The major emphasis of this chapter will be laid on the two important effects of urbanization, the heat island effect and the temperature "crossover" effect. These two effects associated with the rural-urban system have been studied extensively (Bornstein, 1968, 1972; Olfe and Lee, 1971; Oke and East, 1971; Oke and Maxwell, 1975) both theoretically and observationally. Although it has been suggested (Bornstein, 1968; Rouse, et al., 1974) that radiative participation by pollutants could contribute to these effects, there have been relatively few theoretical studies (Atwater, 1971, 1972, 1974, 1975; Bergstrom and Viskanta, 1973; Viskanta, Johnson and Bergstrom 1975) which have investigated this possible role of pollutants. Atwater (1974, 1975) using a two-dimensional model concludes that pollutants are only a minor factor in the formation of the urban heat island. His results also indicate that pollutants have minimal influences on the vertical thermal structure. However, the more recent results of Viskanta, Bergstrom and Johnson (1975) which are based on a more sophisticated radiation model indicate that pollutants can have a significant effect on the urban heat island. As there is a general lack of consensus on the radiative effects of pollutants on urban-rural temperature differences, it is hoped that the results of the simulations presented in this chapter will throw some light on the controversial topic.

The secondary objective of the simulations was to investigate the relative importance of urban parameters in determining the heat island. As pollutants are responsible for radiative effects, it was interesting to study the changes induced by pollutant participation on their own dispersal. A list of the simulations performed is given in Table 8.1.

Table 8.1 List of Two-Dimensional Simulations (see Table 8.2 for other Urban-Rural Parameters)

Reference	Radiative Participation	Change in Urban Parameter	Change in Rural Parameter
N	No participation	—	—
P	Thermal & Solar	—	—
SP	Solar only	—	—
TP	Thermal Only	—	—
1	Thermal & Solar	—	$H = 0.05$
2	Thermal & Solar	$z_0 = 2$m, $H = 0.01$	—
3	Thermal & Solar	$H = 0.01$	—
4	Thermal & Solar	$H = 0.01$, $u_* = 0.2$ m/s	—

8.2 Initial Conditions and Surface Parameters

The urban-rural system was assumed to extend 30 km in the horizontal direction and 2 km in the vertical direction. The city itself was taken to be 15 km long and the adjoining rural areas on each side of the city were assumed to be 7.5 km in horizontal extent (Columbus, Ohio, is about 20 km square). As the planetary boundary layer does not extend much beyond 1.5 km (Lettau and Davidson, 1957) for the conditions chosen for the simulations, the value of 2 km for the vertical extent of the system serves as an upper limit for the boundary layer height.

Sixteen uniformly spaced grid points were used in the horizontal direction (x-axis). The first 5 grid points represented the rural area, the next 6 represented the urban area, and the remaining 5 were situated in the rural area. Variable grid spacing was used in the vertical direction. In particular, the smallest spacing was used near the surface to provide good resolution (see Table 8.2).

The surface parameters used in the simulations were based on values suggested by Pandolfo, et al. (1971) and Oke (1975) and are presented in Table 8.2. It was assumed that there was no variation in soil properties but they were different in rural and urban areas. Thus, heat island effects are produced primarily by the differences in evaporation rates and heat production between the urban and rural areas.

The temperature field was initialized with a profile typical of early morning conditions in O'Neill, Nebraska (Lettau and Davidson, 1957). The nocturnally established inversion extended to 300 m and had a gradient of 18×10^{-3} c/km. The stable layer above the inversion had a gradient of 8×10^{-3} c/km. The initial velocity field was assumed to be uniform in the horizontal direction, and the vertical profile was given by,

$$u(x,z) = v(x,z) = u_* \ln((z + z_i)/z_i)/\kappa \qquad (8.2.1)$$

where

$$u_* = 0.1 \text{ m/s}, \; z_i = 0.1 \text{ m} \qquad (8.2.2)$$

and κ is the von Karman constant. The maximum velocity predicted by Eq. (8.2.1) was 2.48 m/s at the top of the atmospheric layer. As this study was intended to be comparative, it was felt that there was no necessity to initialize the temperature and velocity fields with field data.

As in the one-dimensional simulations, the pollutant sources were assumed to be elevated. They were placed at a height of 100 m along the urban area. It is noted that the source strength is taken to be

Table 8.2 Grid Spacing, Surface Parameters and Pollutant Parameters

a) Grid System

Horizontal grid spacing $\Delta x = 2000$ m
Beginning of rural area: $x = 0$

j	1	2	3	4	5	6	7	8	9	10
z(m)	0	1.0	5.0	15.0	30.0	50.0	100.0	200.0	300.0	400.0

j	11	12	13	14	15	16	17	18	19	20
z(m)	500.0	600.0	700.0	800.0	1000.0	1200.0	1400.0	1600.0	1800.0	2000.0

b) Surface Parameters for Urban Rural System

Parameter	Rural	Urban
Surface Albedo, r_s	0.25	0.15
Surface Emissivity, ε_t	1.00	1.00
Halstead Moisture Parameter, H	0.10	0.05
Soil Conductivity, k_s, W/m C	2.0	2.0
Soil Diffusivity, α_s, m^2/s	1.28×10^{-6}	1.28×10^{-6}
Surface Roughness, z_o, m	0.1	1.0
Artificial Heat Production, $\dot{H}_p$, W/m^2s	0	40
Pollutant Source Strength, $\dot{S}_{C_n}$, $\mu g/m^3 s$	0	0.5

c) Pollutant Parameters

Gas: NH_3 (Ammonia)
Aerosol Properties:
$\omega = 0.9$, $f = 0.85$, $\beta_{ex} = 10^{-6}\ m^2/\mu g$

ten times that used in the one-dimensional simulations. This was necessary because advection reduced the pollutant concentrations to relatively small values (80 $\mu g/m^3$). The source strength was increased in order to generate pollutant path lengths large enough to produce radiative effects.

The horizontal diffusivity K_x was taken to be 100 m^2/s. The main influence of the introduction of horizontal diffusion was that of increasing the stability of the numerical scheme. Increasing the value of the horizontal diffusivity did not affect the velocity and temperature fields to an appreciable extent. This is to be expected as the horizontal gradients of the variables are relatively small. The pollutant concentration fields were affected to a greater extent as the gradients near the boundaries of the urban-rural system were quite large. It was felt that a detailed investigation of horizontal diffusion effects was not warranted from the point of view of this study. It should be mentioned that Lamb and Neiburger (1970) used horizontal diffusivities as high as 800 m^2/s without noticing significant changes in their results. Lee and Olfe (1974) have investigated the effects of very large horizontal diffusivities and conclude that the results of calculations with diffusivities as large as 10^4 m^2/s are similar to those of zero prescribed horizontal diffusivities except that vertical velocities and peak crossover temperatures are reduced by about 40 percent.

The simulations were performed for summer conditions identical to those of the one-dimensional simulations. The choice of summer conditions was based on the observation that stagnating high pressure centers which cause pollution episodes are associated more frequently with summer.

8.3 Effect of Pollutants on Thermal and Solar Fluxes

As the solar and thermal fluxes incident on the air-soil interface determine the surface tempeature, it is instructive to examine the effects of radiative participation by pollutants on these fluxes. Table 8.3 lists the solar and thermal fluxes at the surface in the

Table 8.3a Comparison of Incident Thermal and Solar Fluxes at the Surface (in W/m^2) for Simulations P and NP at x = 16 km (urban area)

Time	Thermal Fluxes			Solar Fluxes		
	NP	P	P-NP	NP	P	P-NP
05:30	302.2	337.7	35.5	--		
07:30	303.5	359.0	55.5	421.8	370.6	-51.2
09:30	315.2	375.8	60.6	784.8	742.4	-42.4
11:30	327.2	391.3	64.1	963.8	932.4	-31.4
13:30	336.1	400.7	64.6	899.0	863.6	-35.4
15:30	338.6	400.3	61.7	613.6	565.0	-48.6
17:30	334.9	394.9	60.0	207.9	165.2	-42.7
19:30	325.0	388.2	63.2			
21:30	318.9	381.3	62.4			
23:30	314.5	374.7	59.9			
01:30	310.9	370.3	59.4			
03:30	307.9	367.6	59.7			
05:30	305.2	365.8	60.6			

Table 8.3b Comparison of Total Radiation (Solar + Thermal) at x = 16 km for Simulations P and NP Total Radiation in (W/m^2)

Time	NP	P	P-NP (%)
07:30	725.3	729.6	0.59
09:30	1064.0	1118.2	4.40
11:30	1291.0	1323.7	2.50
13:30	1235.1	1264.3	2.30
15:30	952.2	965.3	1.30
17:30	542.8	560.1	3.10

urban area (x = 16 km) for simulations P and NP. It is seen that radiative participation increases the downward thermal fluxes substantially. The average increase is about 20%. Solar fluxes are reduced by aerosols; the reduction is largest at large zenith angles in the early morning and late evening. The maximum decrease is about 21% at 17:30, and the reduction is only 3.2% at 11:30. It is interesting to note that the increase in thermal fluxes is always greater than the decrease in solar fluxes. This indicates that under the conditions being investigated radiative participation increases the total radiative energy incident on the surface. These results are consistent with recent observations made by Rouse, et al. (1973). They made simultaneous measurements of global solar and incoming thermal (longwave) radiation at roof-top sites in a heavily polluted zone and relatively clean control sites in and around Hamilton, Ontario. Their measurements (27 March 1972) showed the solar flux at the surface to be reduced by about 4% at noon and 21% in the early morning (07:00) by pollutants. Thermal fluxes in the industrial area were about 25% larger than those in the control sites. During the day, the total radiation (solar plus thermal) received at the surface was slightly larger for the industrial area. Specifically, at noon the increase was about 2%, a value which agrees very well with that predicted in this study. It is realized that a meaningful comparison between the fluxes predicted in this study and those observed cannot be made without a knowledge of the pollutant concentrations in the area in which the observations were made. Solar flux measurements in combination with information about the aerosol concentration profiles (and aerosol properties) are not readily available. Thus, it is not possible to test the validity of the radiation model by comparing predictions with field data. However, the type of comparisons made in this section do show that the predicted trends are consistent with observations.

Table 8.4 lists the solar and thermal fluxes in the rural area (x = 0). It is seen that the background pollutant concentration (50 $\mu g/m^3$) leads to an increase in the downward thermal flux by as much as 13% at 05:30 of the second day. The solar fluxes are affected

Table 8.4 Comparison of Incident Thermal and Solar Fluxes at the Surface (in W/m^2) for Simulations P and NP at x = 0 km (Upwind Rural Area)

Time	Thermal Fluxes			Solar Fluxes		
	NP	P	P-NP	NP	P	P-NP
05:30	302.2	337.7	35.5			
07:30	301.9	338.0	36.1	422.6	396.6	-26.0
09:30	313.3	349.4	36.1	786.2	770.0	-16.2
11:30	324.7	361.4	36.7	965.6	956.2	- 9.4
13:30	333.6	370.7	37.1	900.8	888.8	-12.0
15:30	336.6	373.7	37.1	614.8	593.1	-21.7
17:30	333.2	370.2	37.0	208.3	184.5	-23.8
19:30	323.5	361.0	37.5			
21:30	317.3	355.7	38.4			
23:30	312.9	351.5	38.6			
01:30	309.3	348.1	38.8			
03:30	306.2	345.1	38.9			
05:30	303.4	342.5	39.1			

Table 8.5 Comparison of Incident Thermal and Solar Fluxes at the Surface (in W/m^2) in Urban and Upwind Rural Areas for Simulation P

Time	Thermal Fluxes			Solar Fluxes		
	x = 0 km	x = 16 km	ΔF_t^- (0)	x = 0 km	x = 16 km	ΔF_s^- (0)
05:30	337.7	337.7	0			
07:30	338.0	359.0	21.0	396.6	370.6	-26.0
09:30	349.4	375.8	26.4	770.0	742.4	-27.6
11:30	361.4	391.3	29.9	956.2	932.4	-23.8
13:30	370.7	400.7	30.0	888.8	863.6	-25.2
15:30	373.7	400.3	26.6	593.1	565.0	-28.1
17:30	370.2	394.9	24.7	184.5	165.2	-19.3
19:30	361.0	388.2	27.2			
21:30	355.7	381.3	25.6			
23:30	351.5	374.7	23.2			
01:30	348.1	370.3	22.2			
03:30	345.1	367.6	22.5			
05:30	342.5	365.8	23.3			

to a smaller extent. Aerosol participation leads to a reduction of the surface solar flux by about 2% on an average. As in the urban area, the increase in thermal flux more than compensates for the reduction in solar flux at the surface.

Table 8.5 compares the solar and thermal fluxes at the surface in the rural and urban areas for simulation P. It is seen that the difference in the thermal fluxes between the rural and urban areas is not as great as the increase in thermal radiation caused by the background pollutant concentration of 50 $\mu g/m^3$. This shows that a large increase in pollutant concentration over the urban area is not accompanied by a proportional increase in the downward thermal flux. Thus, relatively small pollutant concentrations (50 $\mu g/m^3$) can cause thermal effects comparable in magnitude to those caused by much higher pollutant concentrations (~300 $\mu g/m^3$ over a height of 800 m in the urban area). The average thermal flux excess of the urban area is about 7%. The solar fluxes show a greater difference between the urban and rural area than the decrease associated with the background aerosol concentration of 50 $\mu g/m^3$. The average difference is less than 10%.

An analysis of the surface solar and thermal fluxes predicted in this study shows that pollutants generally increase (2%) the total radiation reaching the surface during the day. Thus, one can expect radiative participation by pollutants to increase the surface temperature even during daytime. At night, the radiative effect is unequivocally that of warming of the surface temperature, as the downward thermal fluxes are increased by as much as 20% by pollutant participation. A secondary conclusion of the analyses is that an increase in aerosol concentration (for the conditions investigated) has a greater effect on the solar flux than that produced by an equal increase in gaseous pollutants (thermally participating) on the thermal flux.

8.4 Effect of Radiative Participation on the Surface Temperatures of the Urban-Rural System

The major emphasis of this section will be on pollutant induced changes of surface temperature variation both in the rural as well as the urban areas. Effects related to the differences in the thermal structures of the rural and urban areas such as the heat island effect and the crossover effect will be treated in later sections.

Figures 8.1 to 8.4 illustrate the potential temperature isopleths at four selected times for the simulation with non-participating pollutants as well as the simulation with participating (solar and thermal) pollutants. Figure 8.2 shows the development of the mixed layer during the daytime. From about 400 m at 11:30, the mixed layer grows to a height of about 1000 m at 15:30. The formation of the nocturnal surface based inversion is clear in Figure 8.3 which illustrates the evolution of the temperature field during the evening and early morning hours. Although details of the differences between the participating and non-participating simulations cannot be seen very easily, overall differences are clearly discernible. It is noted that participation by pollutants increases the temperature of the surface layer. This warming effect is quite small during the day while during the nighttime hours the temperature excess near the surface is about 1 C as can be seen in Figure 8.4. The explanation for this warming influence of pollutants has already been given in Chapter 7 and need not be repeated here.

Figure 8.5 illustrates the effect of radiative participation by pollutants on the surface temperature variation at the center of the city (x = 16 km). It is seen that the results show trends similar to those of the one-dimensional simulations. However, there is one major difference. With solar participation only the surface temperature is lower than that for the simulation with no participation. This finding is not consistent with that of the one-dimensional simulations, and it illustrates the importance of surface parameters in determining the effect of pollutants on the surface temperature.

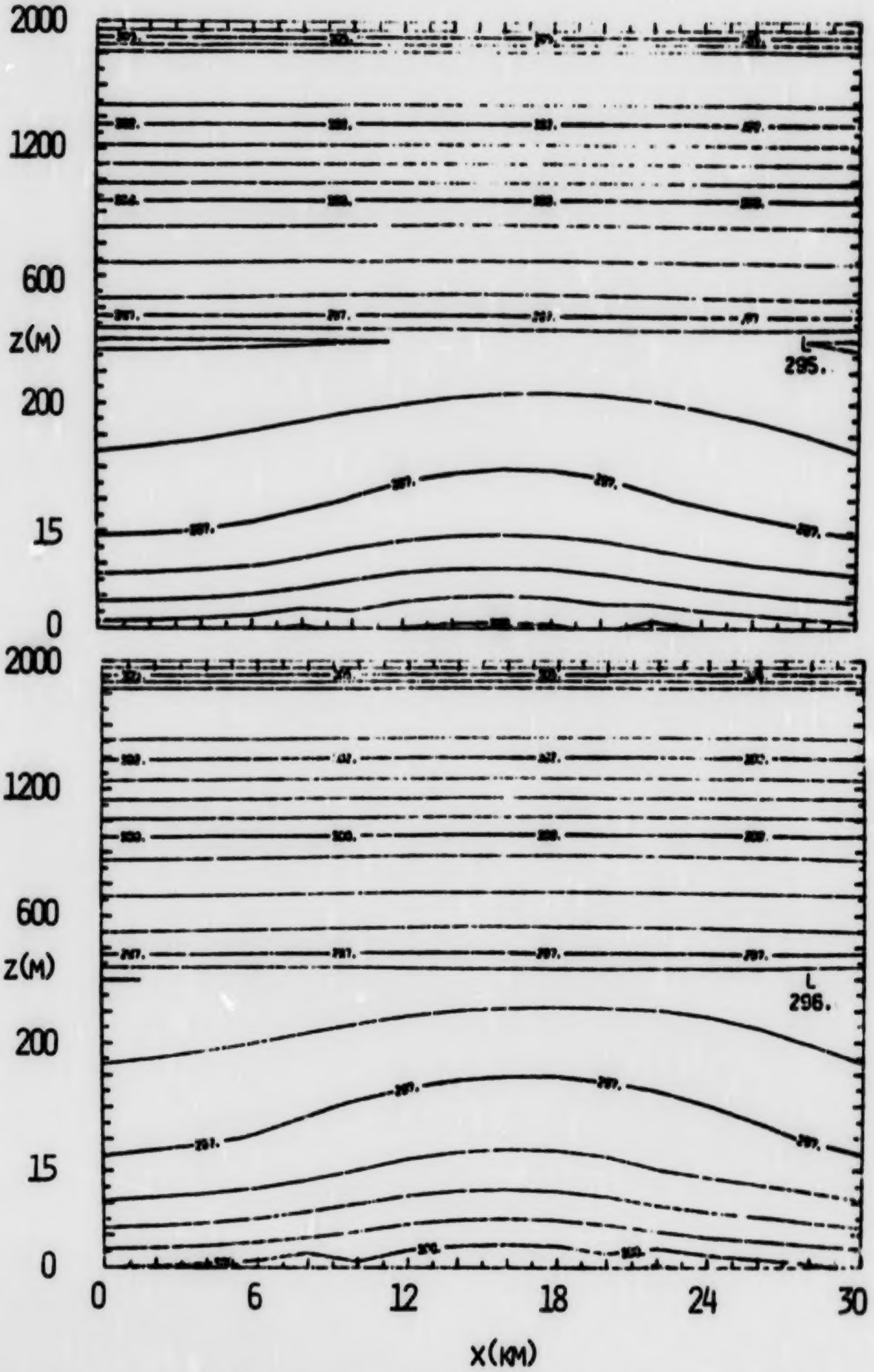

Figure 8.1 Potential Temperature Isopleths at Time = 11:30 Hrs. Top is Non-Participating, Botton is Participating; (for details of grid system see Table 8.2)

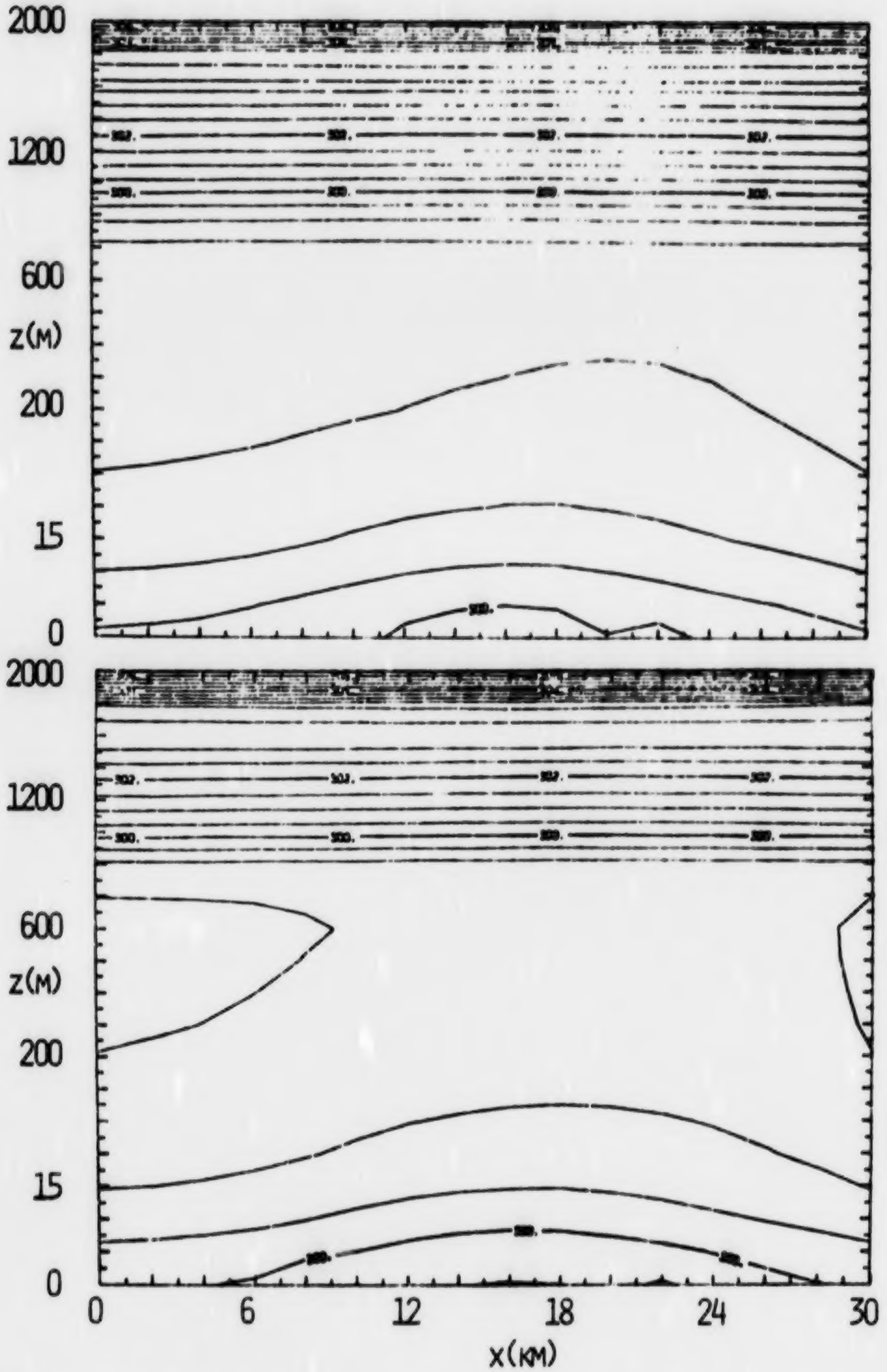

Figure 8.2 Potential Temperature Isopleths at Time = 15:30 Hrs; (See Figure 8.1 for arrangement)

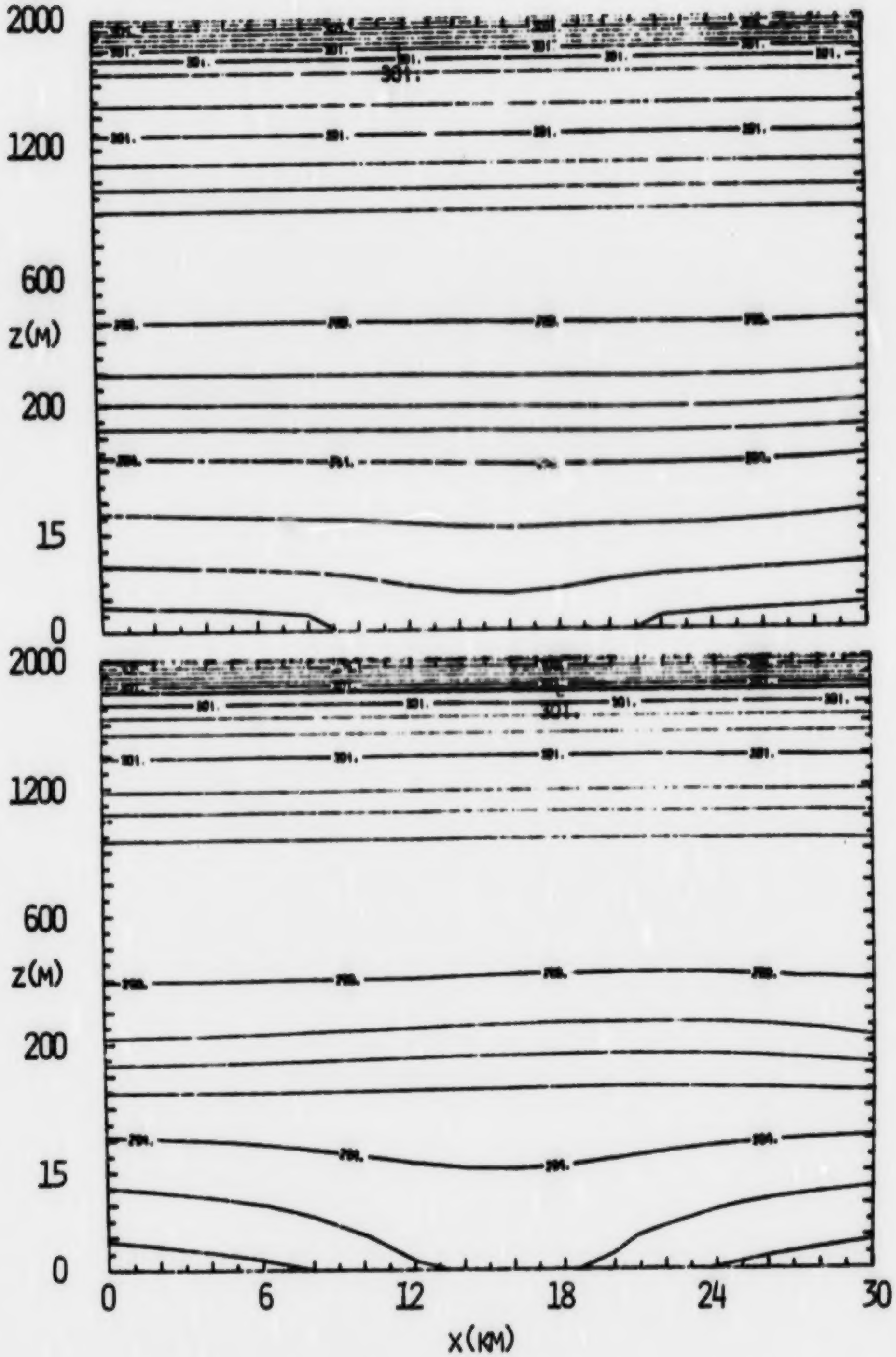

Figure 8.3 Potential Temperature Isopleths at Time = 21:30 Hrs; (See Figure 8.1 for arrangement)

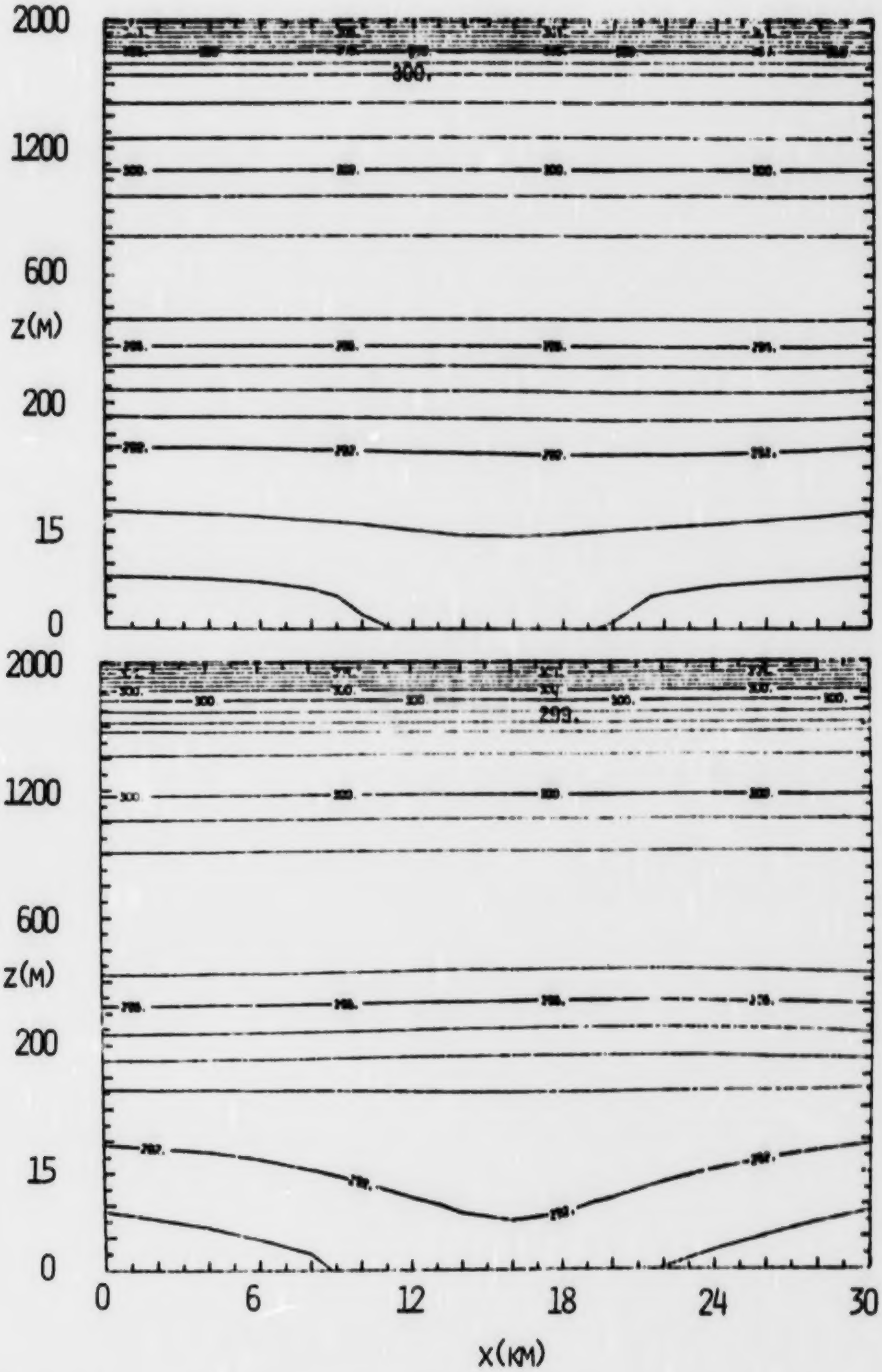

Figure 8.4 Potential Temperature Isopleths at Time = 01:30 Hrs; (See Figure 8.1 for arrangement)

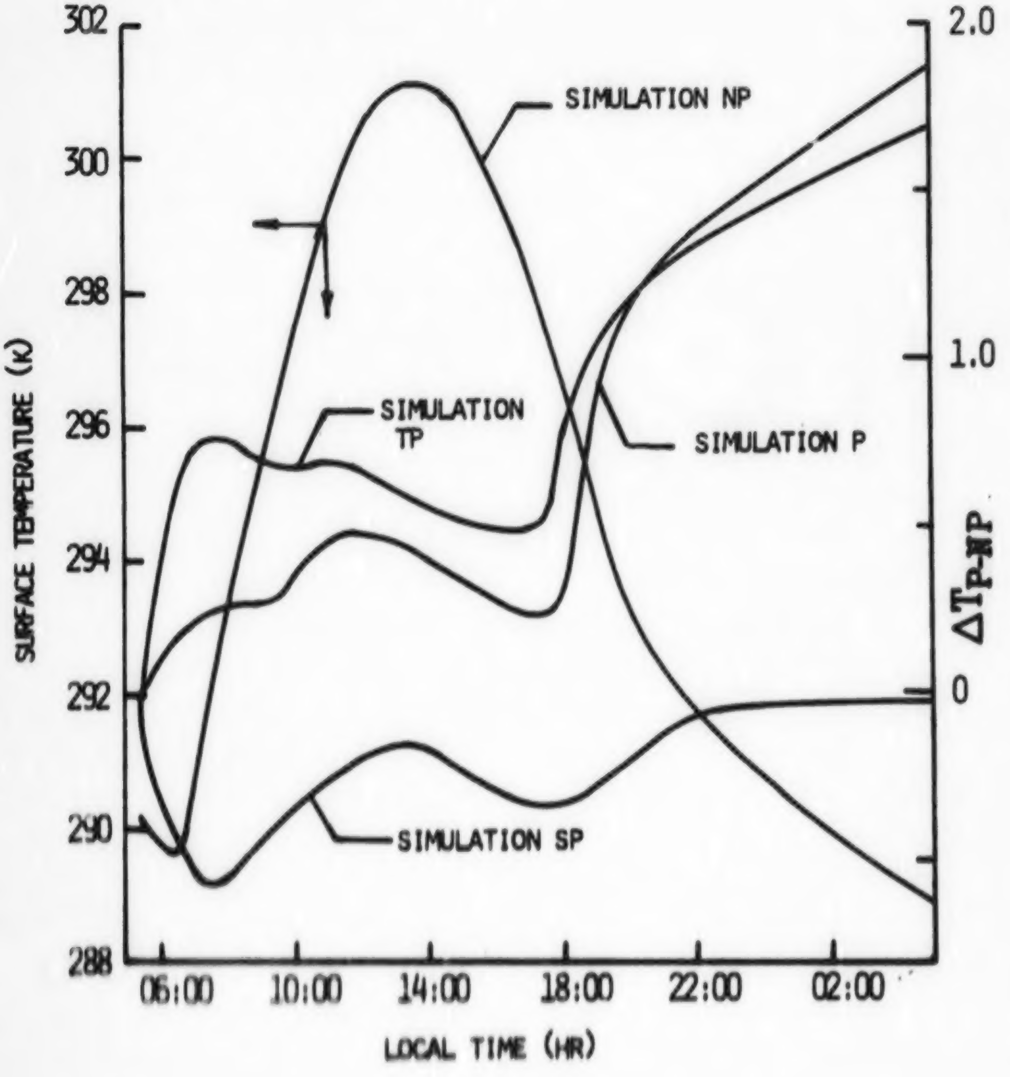

Figure 8.5 Comparison of Surface Temperature Difference Between Participating and Non-Participating Simulations at Center of City

As the urban moisture was relatively low (H = 0.05) the surface temperature was sensitive to the reduction in solar flux at the surface caused by aerosol participation. It is noted that the temperature deficit is the greatest at large zenith angles and reaches a minimum around noon. This is to be expected as the largest solar attenuation occurs around sunrise and sunset. During the daytime hours (05:00 to 17:00) the surface temperature for simulation TP is higher than that of simulation P because the effect of the increase in downward thermal radiation due to thermal participation by pollutants is reduced by the attenuation of solar flux at the surface by aerosols in simulation P. The maximum daytime temperature increase caused by thermal participation is about 0.5 C at 07:30 while the maximum surface temperature difference between simulations TP and P is about 0.3 C at 07:30. During the late evening and early morning hours, the surface temperature of simulation P becomes higher than that of simulation TP, and the temperature excess reaches a value of about 0.1 C at 05:00 of the second day. It is seen that radiative participation by pollutants causes a surface temperature increase of about 1.8 C at 05:00 of the second day.

Figure 8.6 illustrates the effect of radiative participation on the surface temperature variation at the beginning of the rural area (x = 0). It is seen that the relatively small pollutant concentrations of the rural area (50 $\mu g/m^3$) can cause surface temperature changes which are comparable in magnitude to those caused by much higher concentrations (400 $\mu g/m^3$) at the urban center. This underscores the nature of radiative effects, in particular absorption which is not proportional to the pollutant concentration (optical thickness)--the incremental absorption of radiation becomes smaller as the optical depth increases. It is noted from Figure 8.6 that the maximum temperature excess caused by pollutants is about 1.0 C at 05:00 of the second day.

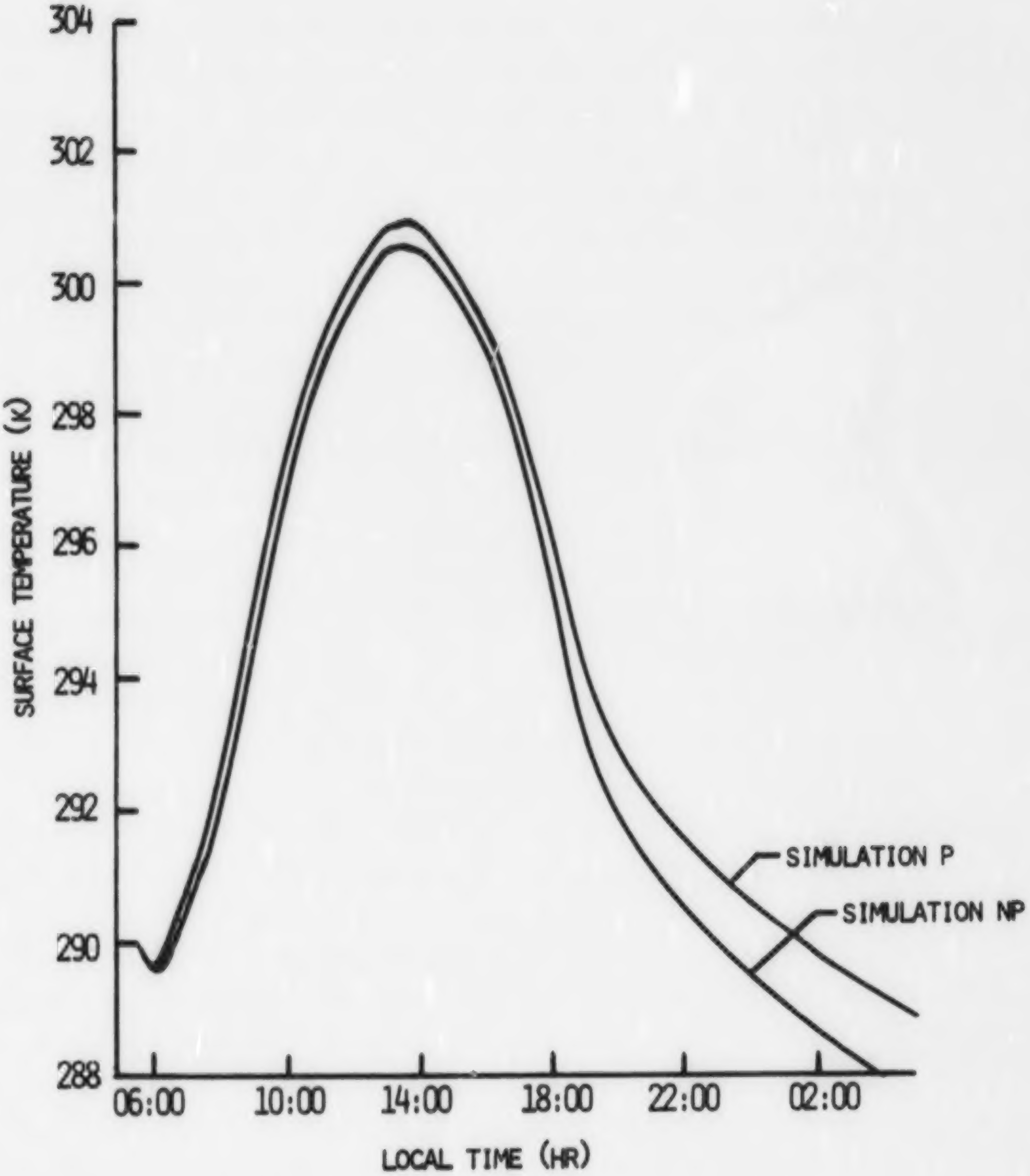

Figure 8.6 Surface Temperature Variation at x = 0 (Rural Beginning)

8.5 Effect of Radiative Participation by Pollutants on the Vertical Potential Temperature Profile

Figures 8.7 to 8.9 show the effect of radiative participation by pollutants on the vertical potential temperature profiles at the urban center. It is seen from Figure 8.7 that while the surface temperature is reduced by solar participation, the temperature of the boundary layer is increased by the heating associated with the absorption of solar energy. Solar heating is also responsible for the higher temperatures below 400 m for simulation P than for simulation TP. Above 400 m, the effects of radiative cooling predominate as indicated by the temperature deficits of the simulations with thermal participation.

The potential temperature difference profiles for 21:30 hours and 03:30 hours (2nd day) show trends similar to those of 11:30 hours. In the absence of solar irradiation, the effects of solar heating of the daytime hours become very small as seen in Figures 8.8 and 8.9 (solar participation only). For simulation SP the temperatures are smaller than those of simulation NP below 400 m and warmer above. The effects of solar heating are confined to heights above 400 m because at large zenith angles (around sunset) most of the solar absorption occurs in the upper part of the boundary layer.

It is seen that thermal participation by pollutants causes cooling of the boundary layer above 400 m, and the resultant temperature deficit increases during the night and early morning hours. At the same time, the increase in downward thermal radiation caused by radiative participation leads to warming at heights below 400 m. This warming effect is greater for simulation P than for simulation TP due to the higher temperatures caused by daytime solar heating.

The rural (x = 0) potential temperature difference profiles are illustrated in Figures 8.10 and 8.11. An examination of Figure 8.10 shows that at 11:30 the predominant effect of solar participation is one of reducing the solar flux at the surface (see Table 8.5). Background aerosols (50 $\mu g/m^3$) do not cause sufficient solar heating to

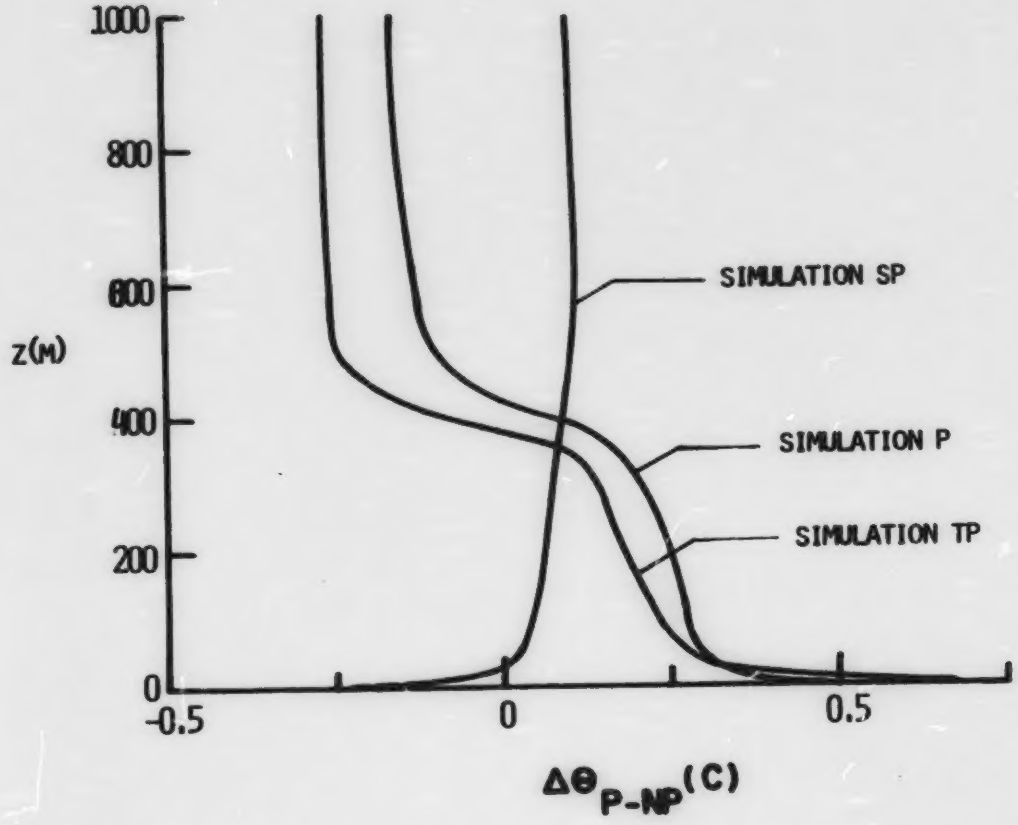

Figure 8.7 Difference Between Temperature Profiles at Center of City (x = 16 Km) for Participating and Non-Participating Simulations (Time = 11:30, 1st Day)

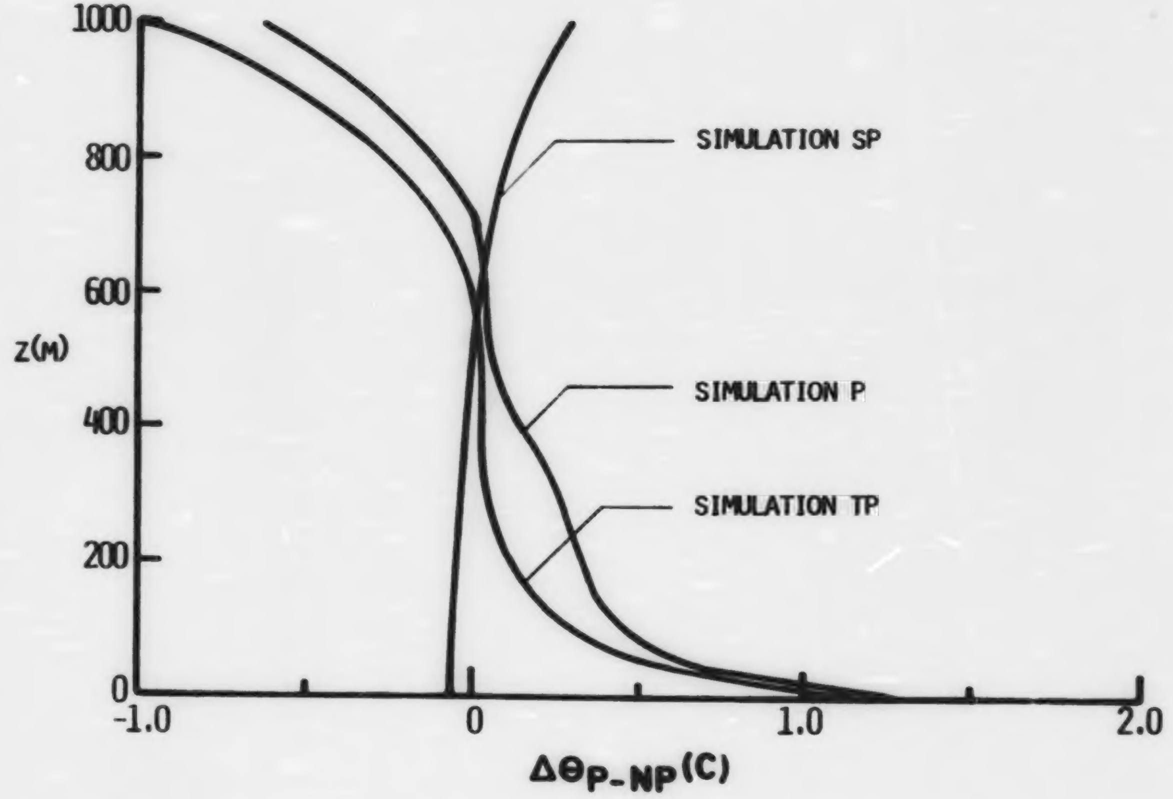

Figure 8.8 Difference Between Temperature Profiles at Center of City (x = 16 Km) for Participating and Non-Participating Simulations (Time = 21:30, 1st Day)

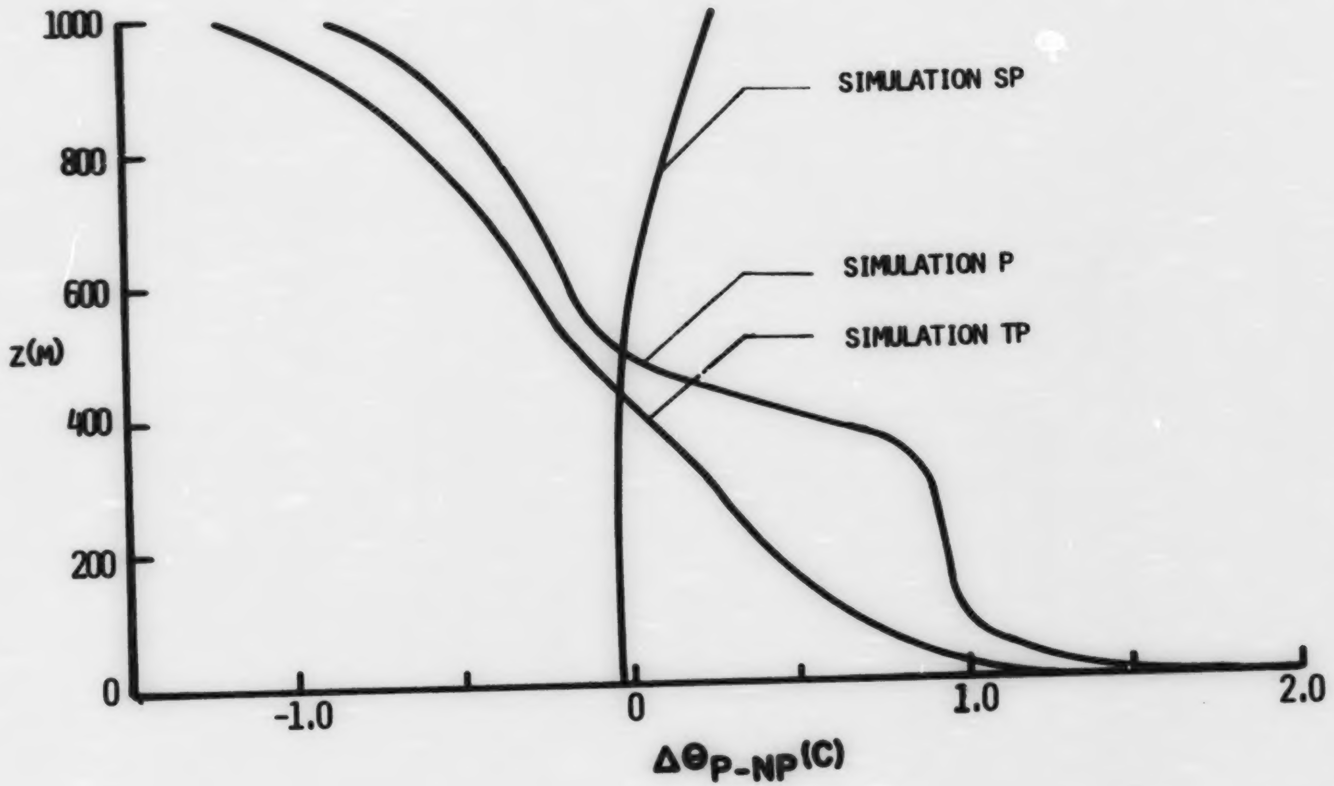

Figure 8.9 Difference Between Temperature Profiles at Center of City (x = 16 Km) for Participating and Non-Participating Simulations (Time = 03:30, 2nd Day)

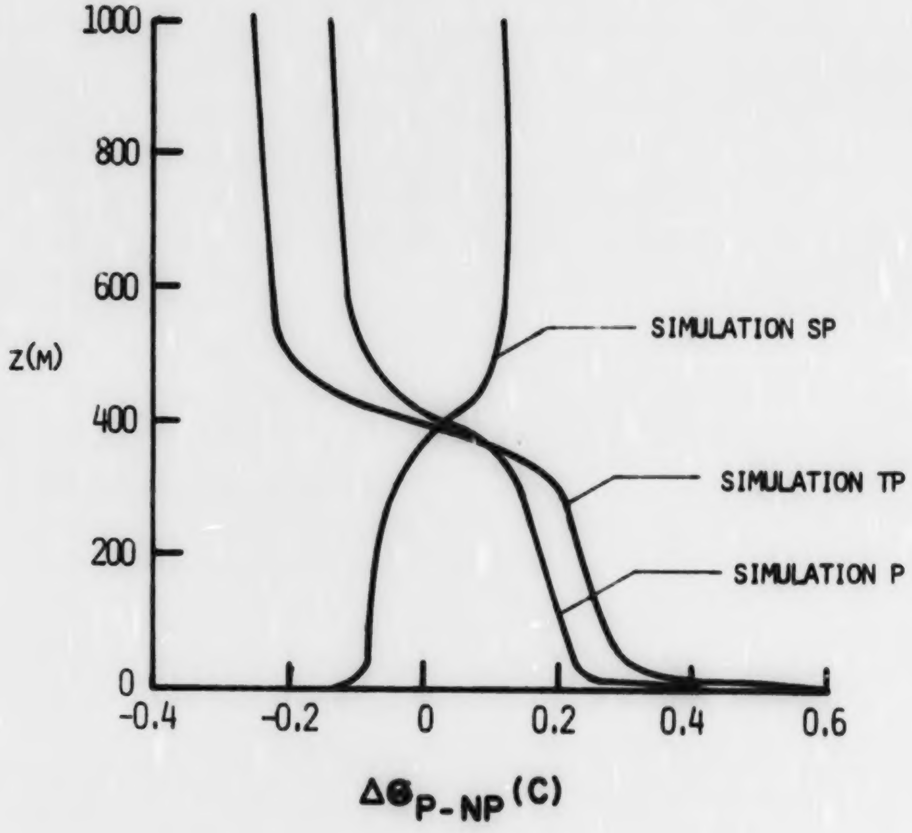

Figure 8.10 Difference Between Temperature Profiles at x = 0 for Participating and Non-Participating Simulations (Time = 11:30, 1st Day)

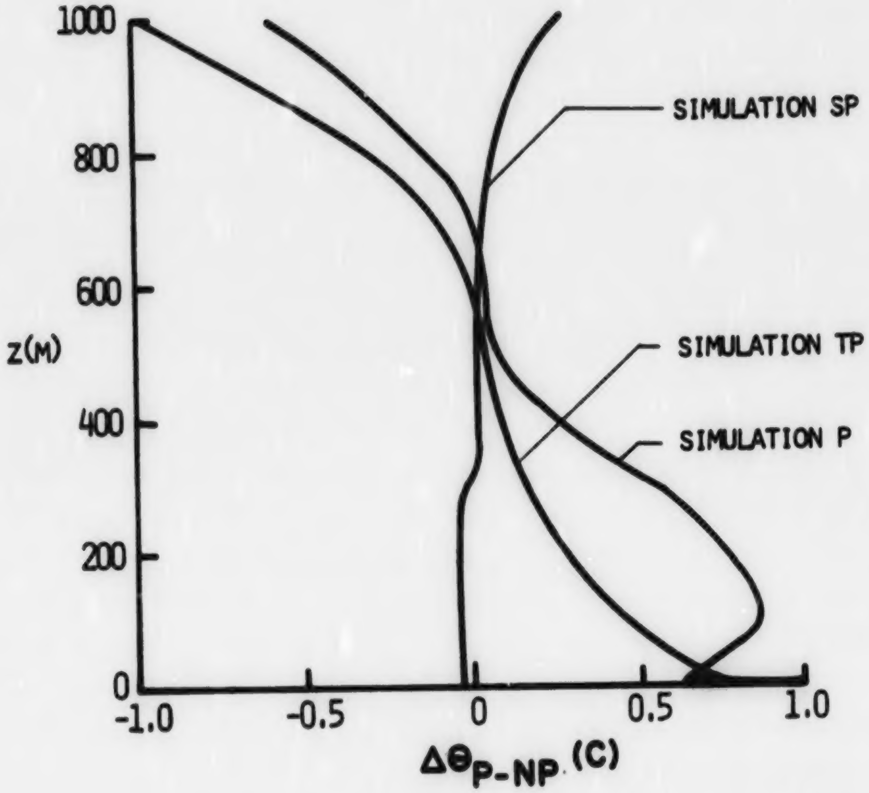

Figure 8.11 Difference Between Temperature Profiles at x = 0 for Participating and Non-Participating Simulations (Time = 21:30, 1st Day)

offset the effect of the reduction in solar flux at the surface. This explains the cooler temperatures at heights below 400 m for simulation SP. Solar heating in the upper part of the boundary layer does lead to warming in simulation SP. The temperatures below 400 m are higher for simulation TP than those of simulation P because of the minor role played by solar heating. However, by 21:30 (see Figure 8.9) the effects of solar heating become more significant as indicated by the higher temperatures below 400 m for simulation P than those of simulation TP. The higher temperatures are caused by the increased downward thermal radiation from the atmosphere heated by solar radiation during the day. The negative values of $\Delta\theta_{u-r}$ above 400 m for simulations P and TP are associated with radiative cooling due to gaseous pollutants.

8.6 Effect of Radiative Participation on the "Crossover" Effect

It is recalled that the temperature crossover effect is associated with the existence of lower temperatures around 400 m over the city (Bornstein, 1968; Davidson, 1967). Below 400 m city temperatures are generally higher than those over the countryside. Two physical mechanisms have been suggested to explain the "crossover" effect. Lee and Olfe (1974) believe that the effect is caused by the lifting of stable air over the city. This suggested mechanism can be better understood by considering the energy equation. Since the maximum temperatures occur around the center of the city, horizontal advection of energy is relatively small in the region. As the "crossover" effect occurs in regions where turbulent diffusion is negligible, the energy equation can be written as

$$\frac{\partial\theta}{\partial t} = -w\,\frac{\partial\theta}{\partial z} \qquad (8.5.1)$$

It should be pointed out that the simplified form of the energy equation has been used only to emphasize the dominant energy transfer processes in the region in which the "crossover" effect is expected to occur. It is seen from Eq. (8.5.1) that local cooling occurs ($\partial\theta/\partial t < 0$) when the vertical velocity w is directed upwards in a stably stratified region ($\partial\theta/\partial z > 0$). It is clear that these conditions are satisfied over a city. As stably stratified air is advected over a city the wind velocity is decreased by the rough city and the resulting upward motion causes cooling ("crossover" effect) in the elevated stable region which has not yet been affected by surface generated turbulence. From the preceding argument it is clear that the postulated mechanism for the crossover effect is dependent on two-dimensional (or three-dimensional) effects.

Lee and Olfe (1974) have conducted numerical experiments to test the hypothesis presented in the previous paragraph. Using a constant eddy diffusivity model they obtained crossover temperatures as large as 0.7 C. However, their calculations using a formula relating the eddy diffusivity to the local shear and stability did not yield much temperature crossover because the eddy diffusivity oscillated rapidly with altitude. Bornstein's (1972) results based on a more sophisticated numerical model do not show the crossover effect.

The second suggested mechanism for the crossover effect is radiative cooling due to pollutants. Using one-dimensional models, Atwater (1971) and Bergstrom and Viskanta (1973) have shown that radiative cooling by pollutants can induce the temperature crossover. However, by definition, the temperature crossover is a two-dimensional effect as it compares rural and urban temperature profiles. It is not possible to explain the crossover effect in terms of the radiative cooling in the urban area without considering the cooling induced by the background pollutants in the rural area. In fact, recent two-dimensional calculations by Atwater (1975) show that the crossover effect cannot be explained in terms of radiative cooling.

It should be pointed out that the prediction of the effect in a numerical experiment is dependent on the particular turbulence model used. It is probable that Bornstein (1972) did not obtain the temperature crossover because he did not account for the variation of the planetary boundary layer height. His assumed constant mixed layer height of 1050 m gave rise to relatively large diffusivities in the upper part of the boundary layer. The turbulent heating associated with these diffusivities offset the cooling induced by the lifting of stable air. It is also possible that Bornstein did not predict the "crossover" effect because he did not account for radiation transfer.

The urban temperature excess profiles obtained in this study are shown in Figures 8.12 to 8.14. It is seen from Figure 8.12 that the temperature crossover occurs even in the simulation with no radiative participation. The maximum temperature deficit occurs at the top of the mixed layer which is around 500 m thick at 11:30. The magnitude of the temperature crossover is about 0.2 C which is smaller than that predicted by Lee and Olfe (1974) but it agrees favorably with the observations made by Bornstein (1968) over New York.

The effects of radiative participation on the daytime temperature crossover are small. Thermal participation increases the crossover effect while solar participation decreases it slightly. Radiative participation has more noticeable effects during the late evening and early morning hours. It is noted from Figure 8.11 that at 21:30 no temperature crossover occurs for the simulation with no radiative participation. It is also interesting to notice that solar heating during the day has a considerable influence on the magnitude of the temperature crossover at night. The maximum crossover of 0.25 C occurs for the simulation with solar as well as thermal participation. This indicates that while solar participation (in combination with thermal participation) heats up the urban and rural boundary layers to the same extent (see Figure 8.11) during the day, the higher pollutant concentrations over the urban area lead to greater cooling over the urban area than over the rural area during the night. As cooling is the only radiative effect in the simulation with thermal participation only, the temperature crossover effect is smaller than that of the simulation with solar and thermal participation. It is seen that the maximum crossover occurs around 150 m.

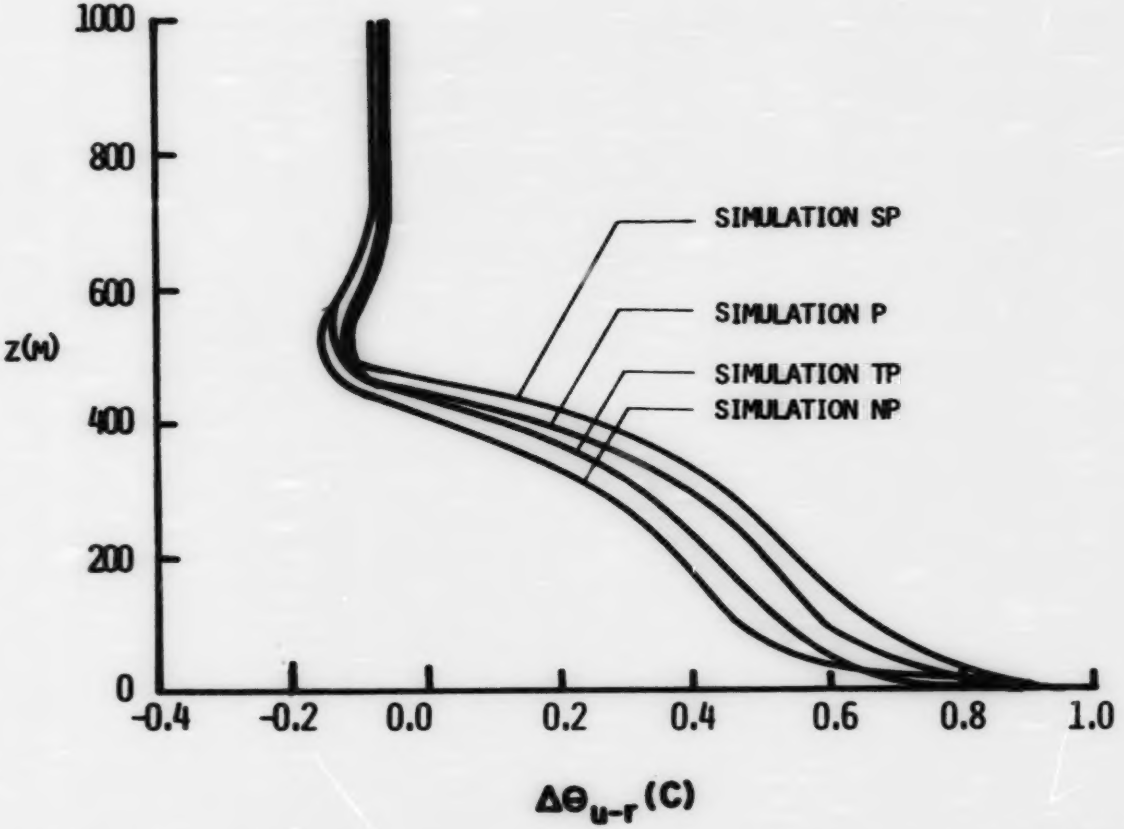

Figure 6.12 Difference Between Temperature Profiles of Urban Center and Rural Beginning for Participating and Non-Participating Simulations (Time = 11:30, 1st Day)

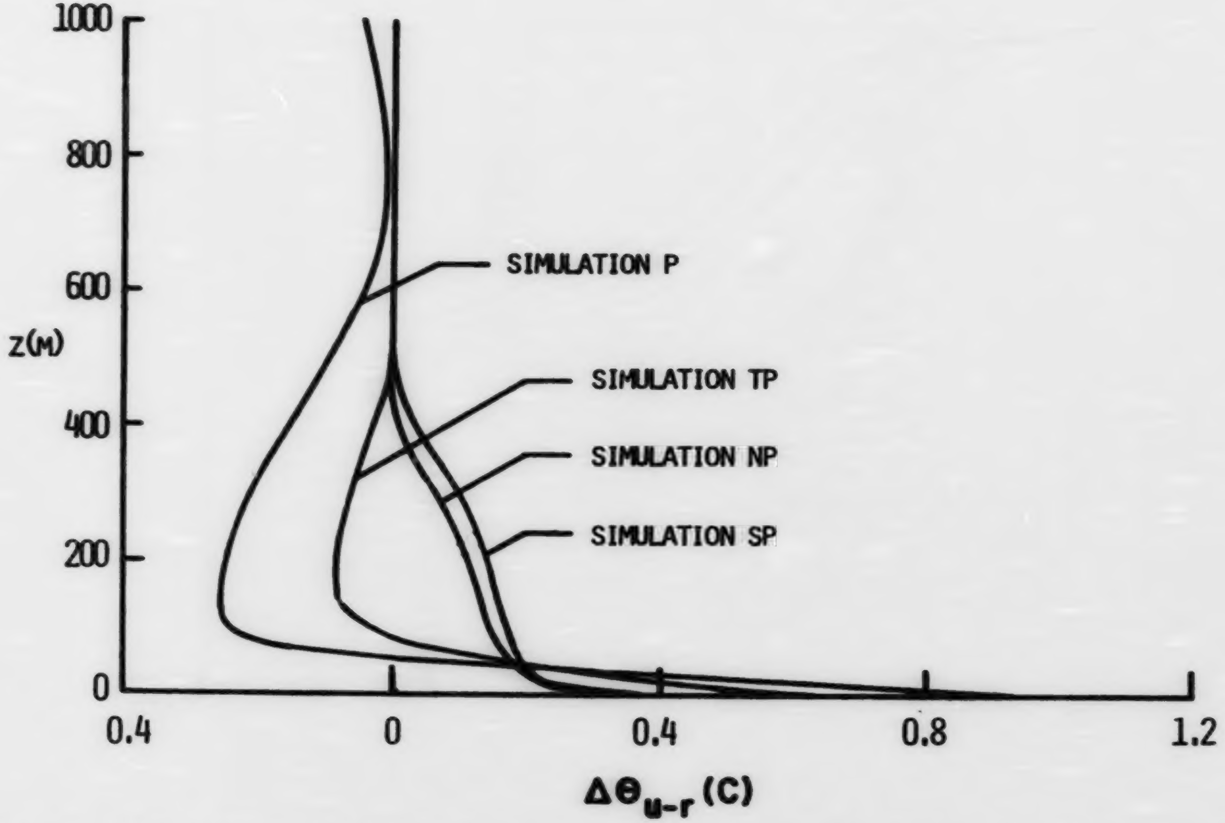

Figure 8.13 Difference Between Temperature Profiles of Urban Center and Rural Beginning for Participating and Non-Participating Simulations (Time = 21:30, 1st Day)

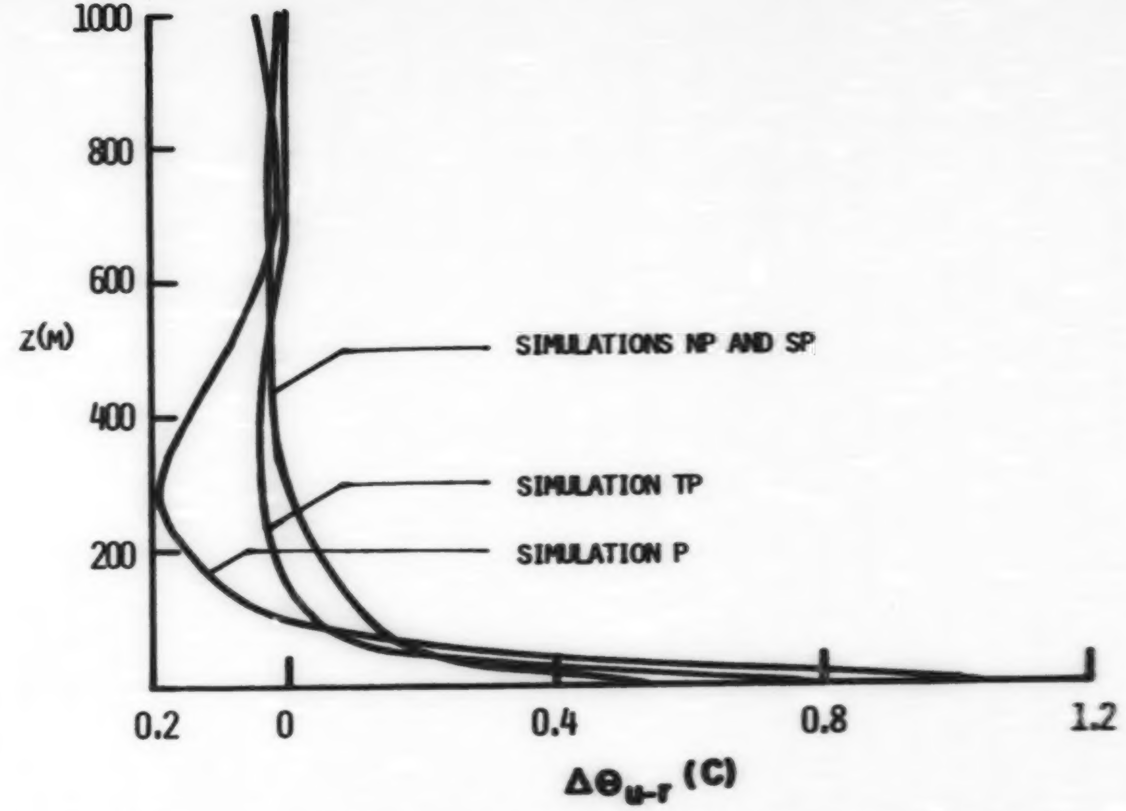

Figure 8.14 Difference Between Temperature Profiles of Urban Center and Rural Beginning for Participating and Non-Participating Simulations (Time = 03:30, 2nd Day)

The results presented in Figure 8.14 show trends similar to that of Figure 8.13. At 03:30 (second day) the temperature excess profile of simulation SP differs little from that of simulation NP. A very small temperature crossover (~0.04 C) is noticed in the simulation with no participation. The maximum temperature crossover occurs for simulation P at a height of 300 m.

The temperature crossover of less than a degree predicted in this study agrees fairly well with recent observations made by Clarke and McElroy (1974) over Columbus, Ohio, and St. Louis, Missouri. The measurements made over Columbus, Ohio, are of particular interest as the city size assumed in this study is comparable to that of Columbus. The evening temperature profiles (September 20, 1968; March 22, 1969) show temperature crossovers of about 0.4 C which is consistent with the predictions of this study.

8.7 The Urban Heat Island and the Effects of Radiative Participation

It is recalled that theoretical studies (Myrup, 1969; McElroy, 1971; Atwater, 1972) show that the urban heat island is caused primarily by the differences in the surface parameters between the rural and urban areas. Also, it is possible to produce the heat island in a numerical experiment by varying any one of the surface parameters in isolation. In view of this it is necessary to discuss the surface parameters used in this study in relation to their role in creating the urban surface temperature excess. During the daytime hours, the heat island is created primarily by the difference in evaporation rates between the urban (H = 0.05) and rural (H = 0.1) areas, while during the night the assumed anthropogenic heat production ($\dot{H}_p = 40\ \mathrm{W/m^2}$) in the urban area is the major cause of the urban temperature excess. The heat production term also contributes to the daytime heat island. The higher roughness length ($z_0 = 1.0$ m) of the urban area tends to decrease the heat island effect during the day by increasing the upward turbulent heat flux at the surface. At night, when the turbulent heat flux is directed downwards, the increased urban roughness reenforces the heat island. The lower solar albedo of the urban area (r_s = 0.15) as compared to that of the rural area (r_s = 0.25) also contributes to the daytime heat island.

Figure 8.15 shows the variation of the urban surface temperature excess as a function of time. It is seen that the temperature excess is about 0.6 C during the day, and increases very sharply to about 1.1 C at 18:00. The heat island shows a small increase during the night and reaches a maximum of 1.2 C at 06:00 of the second day (no radiative participation). This variation of the heat island intensity is consistent with experimental observations made by Oke and Maxwell (1974) over Montreal and Vancouver, Canada. However, the nighttime heat island intensity was considerably smaller than the values observed typically. A possible explanation for this is the neglect of soil property variation along the urban area in this study. The difference in the soil heat capacities between the urban and rural areas is believed to be the primary cause of the heat island during the summer months (Peterson, 1969). Again, however, little observational evidence is available to substantiate or refute this proposition.

It is seen from Figure 8.15 that radiative participation by pollutants affects the heat island intensity to an appreciable extent. Thermal participation increases the daytime temperature excess by about 0.1 C and the nighttime heat island intensity by as much as 0.3 C (25%). Solar participation decreases the urban temperature excess by less than 0.1 C during the day. These trends can be explained in terms of pollutant induced changes of the thermal and solar fluxes at the surface. The higher pollutant concentrations over the urban area lead to a greater increase of downward thermal radiation (see Table 8.5) as compared to that over the rural area. This explains the increase in the heat island intensity due to thermal participation. Solar participation on the other hand decreases the solar flux reaching the surface (see Tables 8.3 and 8.4). This reduction is accompanied by a decrease in the surface temperature. It is noted that the urban temperature excess is the largest for the

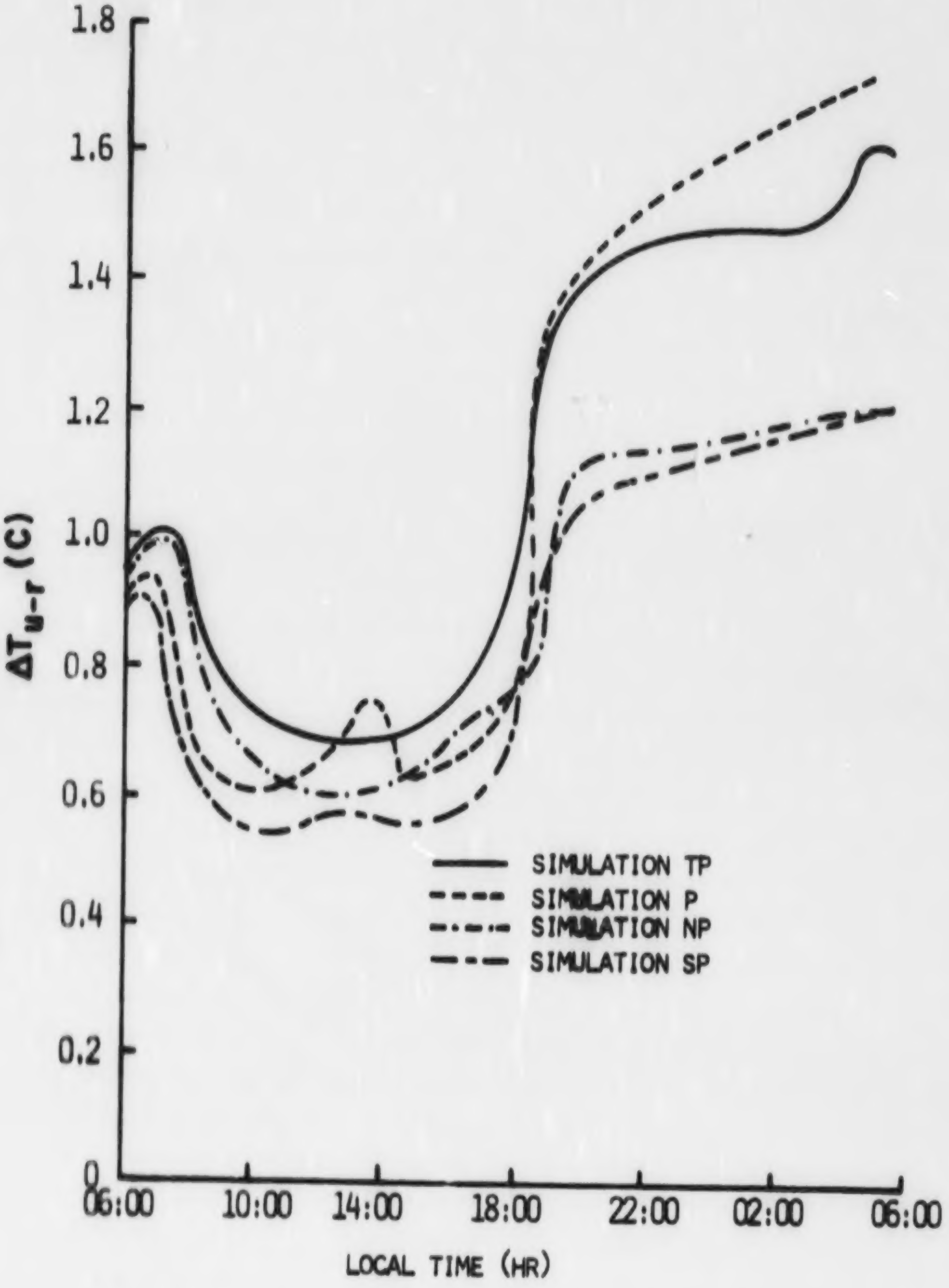

Figure 8.15 Effect of Radiative Participation on the Urban Heat Island Effect

simulation with both solar and thermal participation. This is to be expected as the atmosphere is warmer in simulation P than in simulation TP due to solar heating during the day.

Figures 8.16 and 8.17 show the results of a very limited number of simulations performed to investigate the relative importance of surface parameters in producing the heat island. It is evident from Figure 8.14 that the daytime urban temperature excess is caused primarily by the differences in the moisture parameters between the rural and urban area. When the urban moisture parameter is increased to that of the rural area, the daytime heat island intensity becomes negative and reaches a minimum of -1.5 C at 12:30 (Figure 8.16). The negative heat island is caused by the increased upward turbulent fluxes in the city which leads to a cooling in the urban area relative to the rural surroundings. This result has been observed experimentally (Mitchell, 1961) and has also been predicted theoretically by Nappo (1972). Nappo concludes from his study that negative heat islands could occur when a city is surrounded by desert, or when a city with much vegetation and water is surrounded by farmland. He offers Albuquerque, New Mexico, and Minneapolis, Minnesota, as possible examples of such situations.

Figure 8.17 shows the effect of decreasing the urban moisture parameter. It is seen that the reduced evaporation in the urban area leads to a heat island intensity of 4.5 C. It is also noted that the maximum temperature excess occurs during the day instead of the night. Although this situation has not been observed experimentally it has been predicted in theoretical studies (Myrup, 1969; Tag, 1969).

Two numerical experiments were conducted to study the effect of varying the urban roughness length and the initial velocity on the heat island intensity. The results are presented in Figure 8.17. It is seen that increasing the roughness to twice its previous value decreases the maximum daytime heat island by about 1.5 C. This reduction of heat island intensity is caused by the increase in the upward turbulent flux at the surface. The second numerical experiment was performed after increasing the initial velocity to twice its

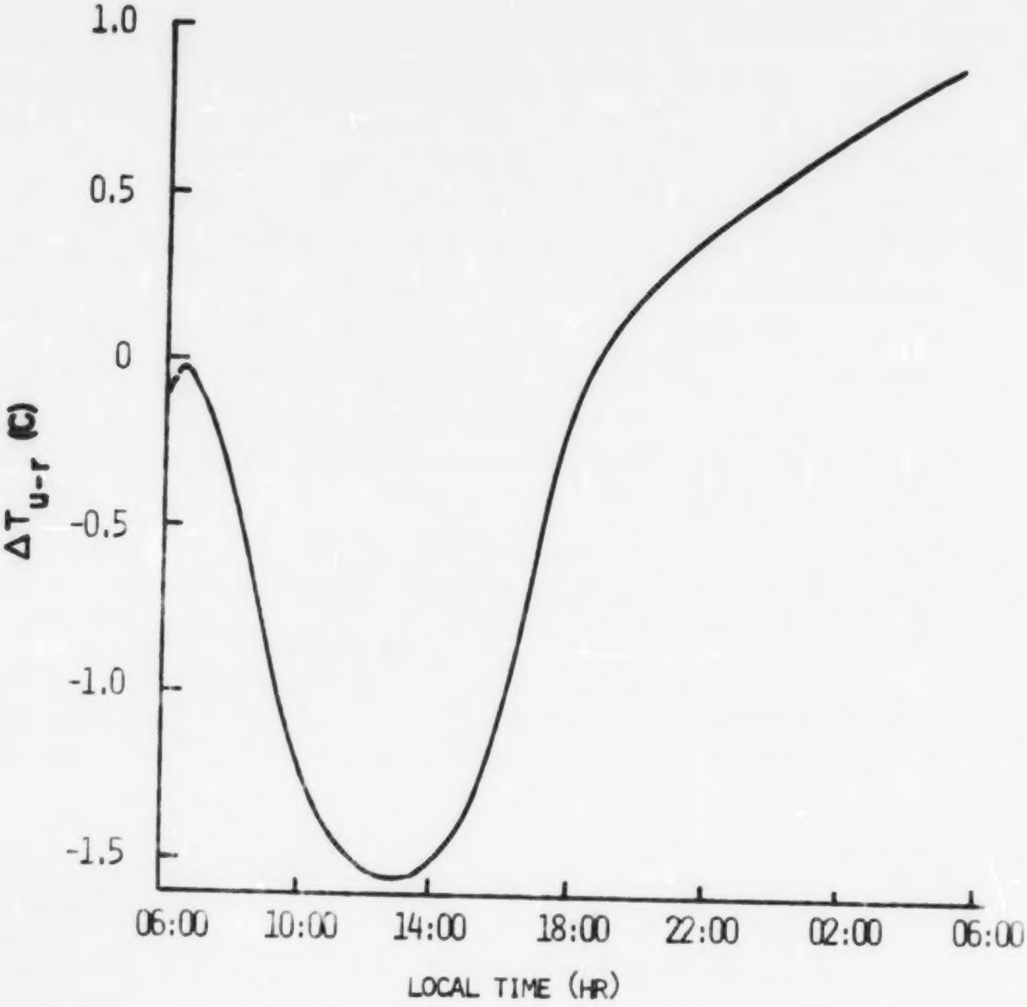

Figure 8.16 Negative Heat Island Created by City. H (urban) = 0.05, H (rural) = 0.05. No Moisture Parameter Variation

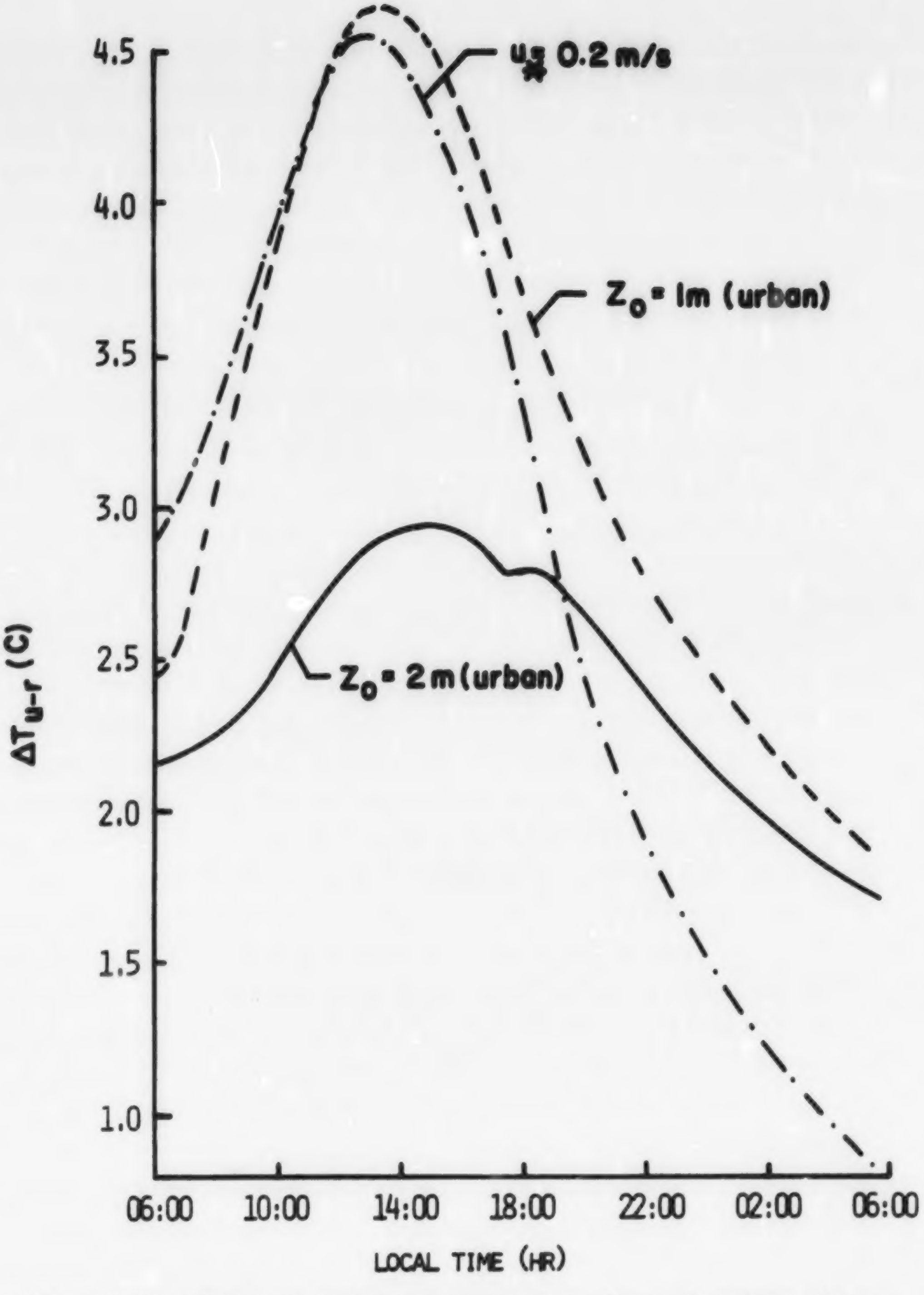

Figure 8.17 Effect of Surface Parameters on the Heat Island Effect. H (urban) = 0.01, H (rural) = 0.1

previous value (u_* was increased from 0.1 to 0.2 m/s). The daytime heat island is not reduced appreciably because the evaporation rates in the rural and urban areas are increased to the same extent, and their difference which determines the heat island intensity during the day is not altered significantly. However, the nighttime heat island is reduced by about 1.5 C at 06:00 of the second day. This decrease in the urban temperature excess with the increase in the wind velocity is consistent with trends of observations (Oke, 1973).

8.8 Pollutant Distributions in the Urban-Rural System

Before discussing the effects of pollutants on pollutant dispersal it is useful to examine the pollutant concentration profiles in the urban and rural areas. Only aerosol concentrations are presented as the concentrations of the gaseous pollutant were assumed to be identical to those of aerosols. The lack of data on pollutant emission did not warrant an accounting of the difference between the emission rates of gases and aerosols. The assumption of equal aerosol and gas concentrations allowed a reduction of the total numerical effort as it was only necessary to calculate the aerosol concentrations. Figures 8.18 and 8.19 illustrate the development of vertical aerosol concentration profiles in the urban region (x = 16 km) and in the downwind rural area (x = 24 km). The effect of the strong elevated source at 100 m is evident in the urban concentration profiles. The concentration reaches a maximum at the source height and decreases gradually to the background value of 50 $\mu g/m^3$ at the top of the mixed layer. The shape of the concentration profile around the source is roughly Gaussian during the day as well as the night. The daytime concentrations in the rural area are almost uniform through most of the mixed layer and decrease quite sharply to the background value at the top of the mixed layer. This predicted shape of the rural concentration profiles is consistent with observations (Edinger, 1973). However, the urban concentration profiles (especially at 15:30, 1st Day) are not well mixed. This indicates that the effects of the assumed source are larger than those observed. It should be recalled, however, that a

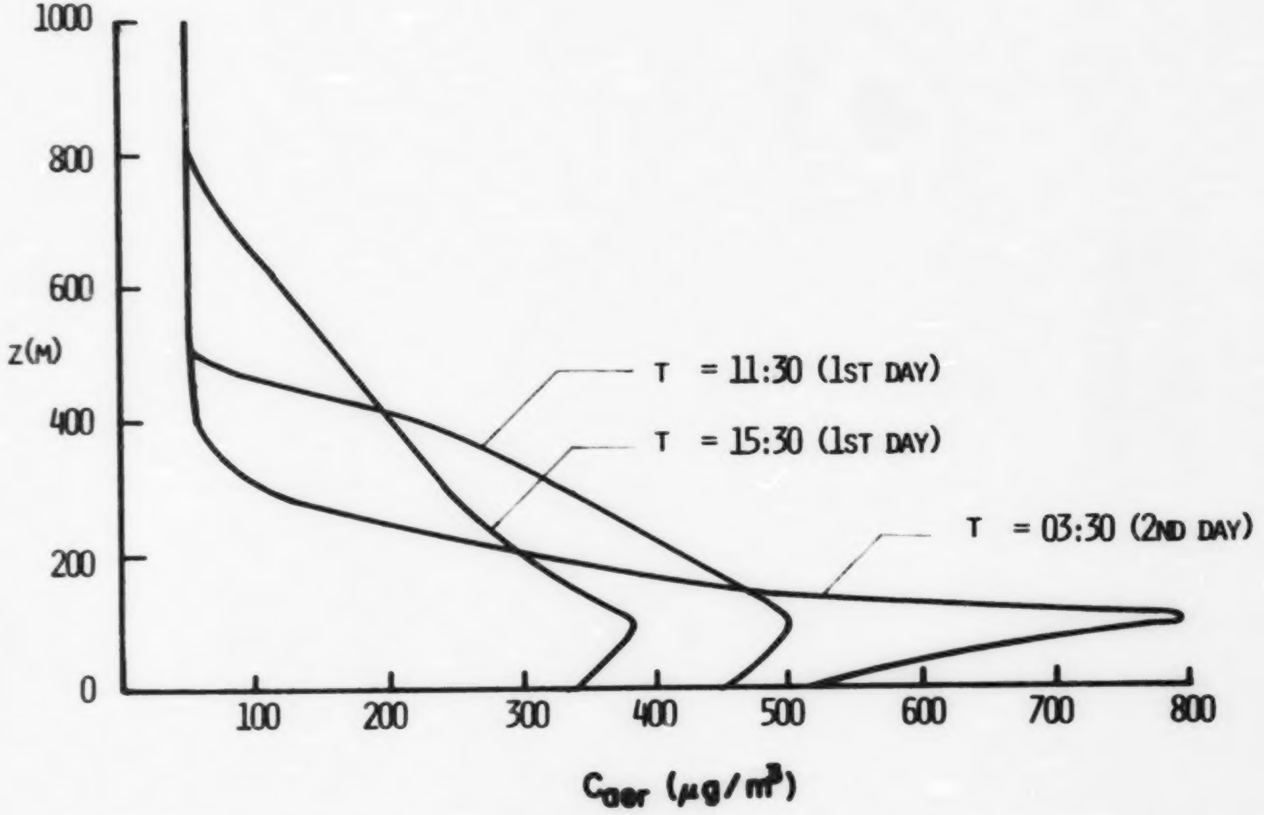

Figure 8.13 Aerosol Vertical Concentration Profiles at Center of City (x = 16 Km) for Simulation NP; (The gradients at z = 0 are zero)

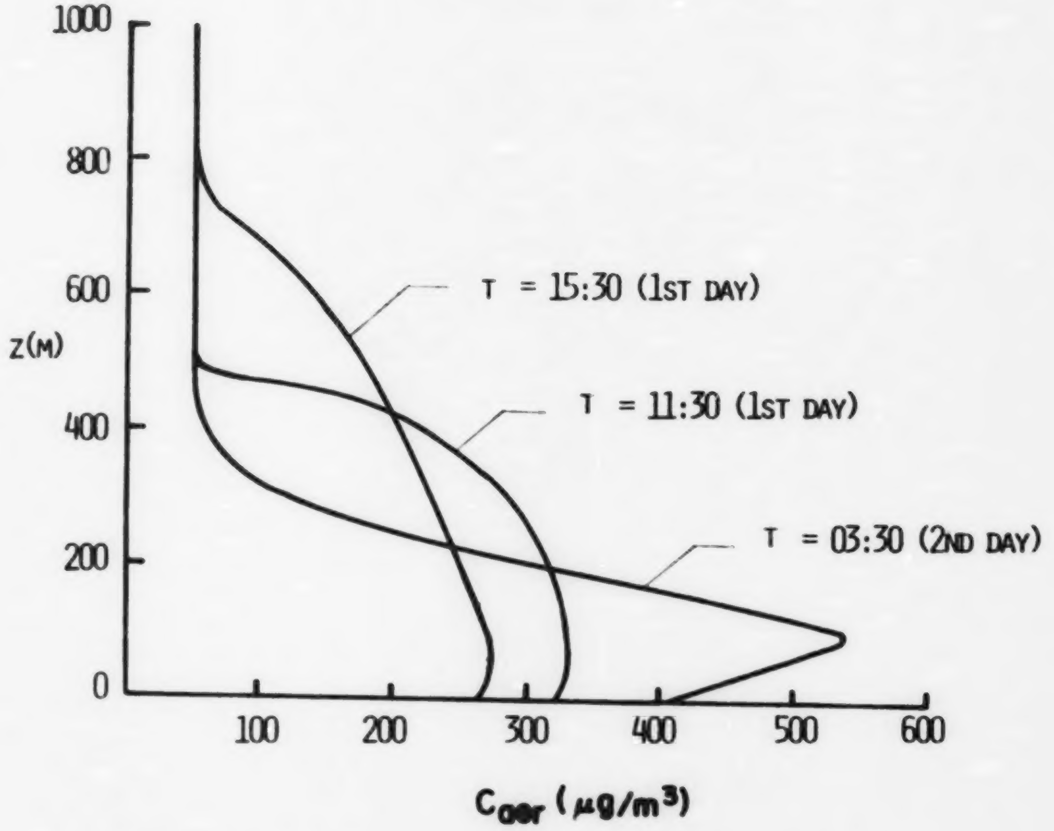

Figure 8.19 Aerosol Vertical Concentration Profiles at Downwind of City ($x = 24$ Km) for Simulation NP; (The gradients at $z = 0$ are zero)

relatively large source strength was used to highlight radiative effects.

It is seen from Figures 8.18 and 8.19 that the maximum pollutant concentrations occur during the late evening (see Table 8.3 also) and early morning hours. The best time for pollutant dispersion is in the afternoon (~15:30). It is clear from the concentration profiles that the mixed layer height is an important parameter in determining the concentration levels. At 11:30 (1st Day) the mixed layer is around 500 m and the average aerosol concentration in the rural boundary layer (see Figure 8.17) is about 300 $\mu g/m^3$. It is seen that the subsequent expansion of the mixed layer is accompanied by a decrease in the average aerosol concentration. At 16:00 (1st Day) the mixed layer has grown to 800 m and the average aerosol concentration has decreased to a value of around 200 $\mu g/m^3$. During the night, the mixed layer decreases in height, and pollutant concentrations increase due to limited vertical mixing. The relatively large concentrations at the source during the night are the result of pollutants being injected into a stable atmosphere (see Tables 8.5 and 8.6).

The variation of aerosol concentrations at the surface and at the source are illustrated in Figure 8.20. As the simulation is started in the early morning (05:30) the pollutants build up rapidly in the shallow boundary layer (400 m). By about 06:30 the concentration at the source has exceeded 700 $\mu g/m^3$ while the concentration at the surface (1 m) has reached a value of about 420 $\mu g/m^3$. Soon after sunrise, the mixed layer starts growing, and the aerosol concentration at the source starts decreasing. Till about 10:00 the surface concentration increases as pollutants from the source diffuse towards the surface. The height, h_c, at which the concentration reaches the background value of 50 $\mu g/m^3$ ($\pm$ 2 $\mu g/m^3$) is also shown in Figure 8.20 in order to explain the concentration variation. The mixed layer height defined with respect to the potential temperature gradient is about 100 m less than h_c at any given time. It is seen from Figure 8.20 that the aerosol concentrations at the source as well as the surface start decreasing at almost the same rate around 10:00. This

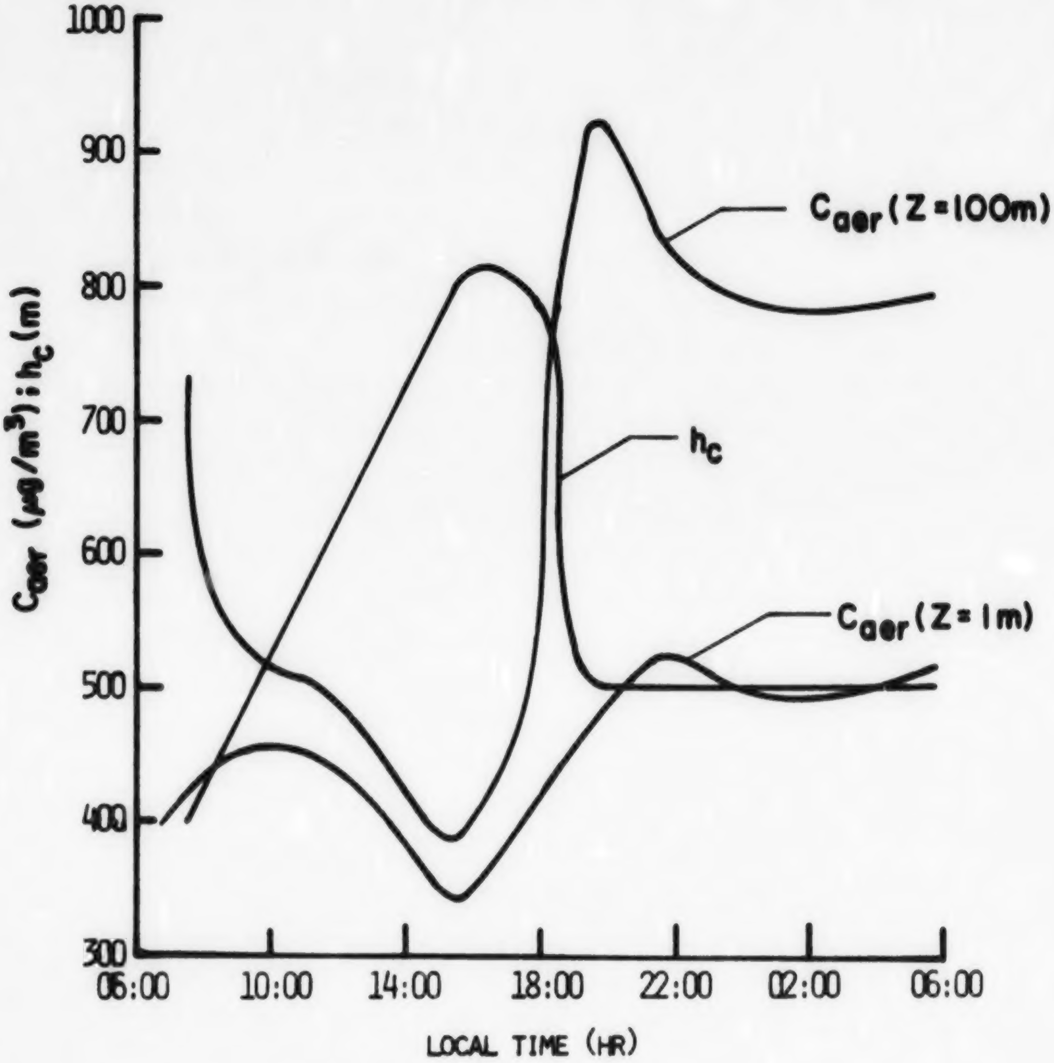

Figure 8.20 Variation of Aerosol Concentration with Time at x = 16 Km for Simulation NP

indicates effective vertical mixing which accompanies the growth of h_c. At 16:00 hrs, h_c reaches a maximum height of about 800 m, and the surface and source concentrations reach their minimum values of 340 μg/m³ and 385 μg/m³, respectively. At 17:00 hrs h_c starts decreasing quite rapidly as the boundary layer becomes stable.

It is seen that the pollutants left in the atmosphere as the mixed layer collapses are transported (diffused and advected) away horizontally. This rapid dispersion of pollutants above the mixed layer is caused by the imposition of periodic boundary conditions in the horizontal direction. As there are no data on the residence time of pollutants above the mixed layer, it is not possible to make any statements about this seemingly unrealistic feature of the model. However, a simple estimate based on the assumption that pollutants above the mixed layer are removed only by horizontal advection indicates that the residence time above the urban-rural system cannot be much greater than 4 hours.

As expected, the collapse of h_c around 17:00 hours is accompanied by sharp increases in the aerosol concentrations at the source as well as the surface. These increases are the result of pollutants building up in the stable shallow evening boundary layer. It is seen that the pollutant concentrations reach a maximum (local) around 19:00 hours, and then level off during the early morning hours. This "overshooting" of the pollutant concentrations above the nocturnal level is caused by the initial difference between the time scales of pollutant buildup and pollutant dispersion by advection and diffusion. The smallest difference between the source and surface concentrations is about 45 μg/m³ and occurs around 14:00 hours when vertical dispersion is most effective. The maximum difference of 300 μg/m³ occurs in the stable conditions of the nocturnal boundary layer.
It is interesting to note that the pollutant concentration variations at the source and surface are similar except that there is a time lag of about 1 hour between the changes at the source and those at the surface. This time lag is to be expected as the distance between the source and surface represents a capacitance for the flow of pollutants.

The results of this section are in reasonable agreement with observations (Edinger, 1973). However, they also illustrate the limitations of the model. It is seen that the elevated source over the urban area has an unrealistically large effect on the shape of the concentration profiles. This feature is attributed to one or both of the following reasons. The assumed source strength may have been too large. Secondly, the O'Brien diffusivity model which does not reflect local stability of the boundary layer cannot represent the intense vertical mixing in the "mixed" layer. Consequently, the daytime boundary layer is predicted to be less well mixed than observations indicate it to be.

8.9 Effect of Radiative Participation by Pollutants on Pollutant Dispersal

Before presenting the results of this section, it is instructive to examine the physical processes through which radiative participation by pollutants affects pollutant dispersal. While radiative participation by pollutants affects the potential temperature directly through the radiative flux term in the energy equation, it modifies the pollutant concentration only indirectly through the turbulent eddy diffusivity (diffusion term in the species equation). The eddy diffusivity is a function of the potential temperature and velocity gradients as well as the mixing length. By modifying the potential temperature and velocity (through eddy diffusivity) gradients, radiative participation alters the eddy diffusivity which in turn affects the pollutant concentration. Thus, it is clear that an understanding of the effect of radiative participation on pollutant dispersal is dependent on the modeling of turbulence. The implication of this will be discussed in detail in a later paragraph.

In the light of the preceding discussion it is appropriate to examine the eddy diffusivity formulation of the two-dimensional model in relation to radiative effects. In the equilibrium layer, the eddy diffusivity is a function of the local temperature and velocity gradients. Thus, it can be expected that pollutant induced changes in these gradients will be accompanied by changes in pollutant concentrations in the equilibrium layer (50 m thick). In the transition layer, eddy diffusivities are specified by the O'Brien cubic profile which does not allow local stability to affect the eddy diffusivity. As the shape of the O'Brien profile is determined by the turbulence characteristics of the equilibrium layer, changes in the transition layer eddy diffusivities only reflect changes in the eddy diffusivities in the 50 m layer adjacent to the earth's surface. Thus, potential temperature modification caused by pollutants does not affect the pollutant concentration locally. This limitation of the model is especially serious from the point of view of stability changes induced by solar heating. As solar energy is absorbed mostly above the equilibrium layer, this model cannot be expected to be sensitive to the stabilizing action of solar heating. As the stability of the equilibrium layer is controlled to a large extent by the surface temperature, a high correlation between changes of surface temperatures and changes of pollutant concentrations can be expected. A higher surface temperature would imply a decrease in the stability of the boundary layer. This would mean better vertical mixing which in turn would lead to more effective horizontal advection. Thus, a warming of the surface temperature can be expected to be accompanied by a decrease in the vertical pollutant mass loading. It is felt that this discussion will help to provide better understanding of the results of this section.

This study assumed that the concentrations of aerosols were identical to those of the gaseous pollutant (NH_3). This allows the combination of aerosol and gaseous pollutant to be treated as a single pollutant which participates radiatively in the thermal as well as the solar spectrum. It is recalled that aerosols participate only in the solar spectrum, and the gaseous pollutant participates only in the thermal spectrum.

Tables 8.6 and 8.7 show the effect of radiative participation by pollutants on pollutant dispersal. As expected the warming effect

Table 8.6 Comparison of Aerosol Concentrations (in μg/m³) at z = 1 m and z = 100 m at x = 16 km for Simulations P and NP

Time	z = 1 m			z = 100 m		
	NP	P	P-NP	NP	P	P-NP
05:30	50.0	50.0	0	50.0	50.0	0
07:30	420.2	430.7	10.5	732.4	705.0	-27.4
09:30	455.3	450.1	- 5.2	518.6	513.3	- 5.3
11:30	446.1	446.7	- 0.6	503.6	503.5	- 0.1
13:30	392.7	375.5	-17.2	433.3	414.8	-18.5
15:30	337.9	321.8	-16.1	384.3	366.0	-18.3
17:30	398.4	380.3	-18.1	537.9	511.3	-26.6
19:30	472.3	499.0	26.7	932.2	829.2	-103.0
21:30	524.6	523.0	- 1.6	839.5	744.6	-94.9
23:30	502.5	477.4	-25.1	793.9	686.0	-107.9
01:30	491.7	451.1	-40.6	780.6	723.3	-57.3
03:30	497.6	461.0	-36.6	785.6	726.7	-58.9
05:30	514.0	481.5	-32.5	793.6	737.2	-56.4

Table 8.7 Comparison of Aerosol Concentrations (in $\mu g/m^3$) at $z = 1$ m and $z = 100$ m at $x = 24$ km for Simulations P and NP

Time	z = 1 m			z = 100 m		
	NP	P	P-NP	NP	P	P-NP
05:30	50.0	50.0	0	50.0	50.0	0
07:30	318.5	322.1	3.6	475.8	467.8	- 8.0
09:30	334.5	330.3	- 4.2	346.5	341.7	- 4.8
11:30	319.4	317.8	- 1.6	329.5	327.5	- 2.0
13:30	290.2	280.9	- 9.3	295.1	285.7	- 9.4
15:30	262.6	251.2	-11.4	269.0	259.1	- 9.9
17:30	300.4	291.5	- 8.9	363.3	343.0	-20.0
19:30	373.6	343.4	-30.2	609.0	602.1	- 6.9
21:30	427.5	404.1	-23.4	596.4	566.1	-30.3
23:30	417.0	389.0	-28.0	579.2	546.8	-32.4
01:30	407.2	376.6	-30.6	569.4	562.6	- 6.8
03:30	404.2	377.3	-26.9	563.4	558.2	- 5.2
05:30	406.5	382.6	-23.9	555.6	549.0	- 6.6

of pollutants on the surface temperature leads to a reduction in the pollutant concentrations in the boundary layer. As explained before, this decrease of pollutant concentrations is the result of the decrease in the surface layer stability (see Table 8.8) when pollutants are radiatively participating. It is noted from Table 8.6 that the reduction of pollutant concentrations is smaller during the day than during the night. This is to be expected as pollutants cause a greater surface temperature increase during the night than during the day. At the surface, the daytime decrease of aerosol concentration is about 4.8% at 15:30, and the reduction during the night is as large as 8.2% at 01:30. The effects of radiative participation on concentrations in the vicinity of the source are almost of the same magnitude (percentage) as those on surface concentrations. The concentration reduction due to pollutants at 100 m is about 4.8% at 15:30 and about 13.5% at 23:30. It is noted that pollutant induced changes in the concentrations are smaller in the rural area than in the urban area. The maximum reduction of surface concentration in the rural area is about 7.5% at 01:30 as compared to 8.2% in the urban area. At the urban source height (no source in rural area) of 100 m the reduction in pollutant concentration is only 5.5% at 23:30. Clearly the larger decrease of 13.5% (107.9 $\mu g/m^3$) in the urban area is caused by the presence of the pollutant source.

As changes in pollutant concentrations are a direct result of changes in eddy diffusivities it is necessary to examine the effect of radiative participation by pollutants on eddy diffusivity profiles. Table 8.8 compares eddy diffusivities at selected heights for simulations P and JUP. It is seen that radiative participation has a noticeable influence on the eddy diffusivities at 1 m. The maximum pollutant caused increase is about 14.8% (0.04 m^2/s) at 23:30. At the source height of 100 m the increase is as large as 63% at 19:30. It is not surprising to note that the period (19:30 to 05:30) of the largest changes in diffusivities is also the time interval during which the pollutant concentration are altered the greatest.

Table 8.8 Comparison of Eddy Diffusivities (in m^2/s) at $z = 1$ m and $z = 100$ m for Simulations P and NP at $x = 16$ km

Time	z = 1 m			z = 100 m		
	NP	P	P-NP	NP	P	P-NP
05:30	0.61	0.61	0	1.12	1.12	0
07:30	0.26	0.27	0.01	3.35	3.91	0.56
09:30	0.39	0.39	0	19.38	20.05	0.67
11:30	0.42	0.42	0	24.47	25.04	0.57
13:30	0.45	0.45	0	26.46	27.32	0.86
15:30	0.43	0.43	0	22.59	23.35	0.76
17:30	0.38	0.34	-0.04	8.84	9.48	0.64
19:30	0.24	0.28	0.04	1.83	2.99	1.16
21:30	0.27	0.31	0.04	2.52	3.65	1.13
23:30	0.27	0.31	0.04	2.68	3.73	1.05
01:30	0.27	0.28	0.01	2.73	2.87	0.14
03:30	0.27	0.28	0.01	2.81	3.00	0.19
05:30	0.27	0.28	0.01	2.98	3.25	0.27

As the shape of the O'Brien diffusivity profile in the transition layer is determined by turbulence characteristics of the equilibrium layer, it is interesting to examine the effects of radiative participation by pollutants on the stability of the surface layer as reflected in the eddy diffusivities of the transition layer. Table 8.9 compares the eddy diffusivity profiles at two selected times for simulations P and NP. It is seen that the pollutant induced increase in eddy diffusivity of about 1.6% at 30 m (13:30) is magnified to 8.3% at 200 m in the transition layer. The increase becomes as large as 103% at 500 m during daytime (13:30). At 21:30, the change of 39.0% caused by pollutants at 30 m in the equilibrium layer is reflected as a 39% increase at 200 m in the transition layer. The analysis of this paragraph indicates that the effect of radiative participation by pollutants on pollutant dispersal should be viewed in the light of the limitations of the particular turbulence being used.

It is clear from the preceding discussion that in this study it is not possible to draw any firm conclusions on the effects of pollutants on pollutant dispersal in the transition layer. As the stability of the surface layer is controlled to a large extent by the surface temperature, the only important radiative effect of pollutants from the point of view of pollutant dispersal is that of warming or cooling of the surface temperature. It is obvious that this statement has important implications. With a turbulence model which does not predict the eddy diffusivities realistically in the transition layer, it is not possible to make definitive recommendations regarding the inclusion of radiation transfer in Air Quality Simulation Models.

It is necessary to reemphasize the importance of the turbulence model in determining the effects of radiative transfer on pollutant dispersal. The effects of radiative participation are largely dependent on the sensitivity of the eddy diffusivity formulation to local stability changes caused by radiative heating or cooling. Thus, surface layer based eddy diffusivity formulations such as those used by Bornstein (1972) and Estoque (1973) cannot be expected to react to

Table 8.9 Comparison of Eddy Diffusivities (in m^2/s) at $x = 16$ km for Simulations NP and P

Height (m)	Time = 13:30			Time = 21:30		
	NP	P	P-NP	NP	P	P-NP
1	0.45	0.45	0.00	0.27	0.32	0.05
5	1.17	1.19	0.02	0.63	0.74	0.11
15	3.45	3.50	0.05	1.21	1.69	0.48
30	7.32	7.44	0.12	1.91	2.67	0.76
50	13.67	13.93	0.26	2.23	3.10	0.87
100	26.46	27.32	0.86	2.68	3.73	1.05
200	36.34	39.37	3.03	2.12	2.95	0.83
300	31.36	36.79	5.43	0.76	1.06	0.30
400	18.79	25.66	6.87	0.00	0.00	0.00
500	5.91	12.00	6.09	0.00	0.00	0.00
600	0.00	1.87	1.87	0.00	0.00	0.00

pollutant caused changes in the transition layer. On the other hand, the model suggested by Pandolfo (1966) is extremely sensitive to local stability. Bergstrom and Viskanta (1973) and Atwater (1974) using Pandolfo's model conclude from their studies that radiative participation can change pollutant concentrations at the ground by as much as 20%. It is clear that this relatively large change is tied to the turbulence model used. As atmospheric turbulence is still incompletely understood, it is not always possible to examine critically the validity of the assumptions on which a particular turbulence model is based. Clearly, conclusions regarding the effects of pollutants on pollutant dispersal have to be qualified with statements about the turbulence model used.

REFERENCES

Atwater, M. A.: 1966, "Comparison of Numerical Methods for Computing Radiative Temperature Changes in the Atmospheric Boundary Layer," J. Appl. Meteor. 5, 824-831.

Atwater, M. A.: 1970, "Investigation of the Radiation Balance for Polluted Layers of the Urban Environment," Ph.D. Thesis submitted to New York University, 116 pp.

Atwater, M. A.: 1971, "Radiative Effects of Pollutants on the Atmospheric Boundary Layer," J. Atmos. Sci. 28, 1367-1373.

Atwater, M. A.: 1972, "Thermal Effects of Urbanization and Industrialization in the Boundary Layer: A Numerical Study," Boundary Layer Meteorology 3, 229-245.

Atwater, M. A.: 1974, "Thermal Changes Induced by Pollutants for Different Climatic Regions," in Symposium on Atmospheric Diffusion and Air Pollution.

Atwater, M. A.: 1975, "Thermal Changes Induced by Urbanization and Pollutants," J. Appl. Meteor. 14, 1061-1071.

Bergstrom, R. W.: 1971, "Predictions of the Spectral Absorption and Extinction Coefficients of an Urban Air Pollution Aerosol Model," Atmospheric Environment 6, 247-258.

Bergstrom, R. W., and Viskanta, R.: 1972, "Theoretical Study of the Thermal Structure and Dispersion in Polluted Urban Atmospheres," Heat Transfer Laboratory Report, School of Mechanical Engineering, Purdue University.

Bergstrom, R. W., and Viskanta, R.: 1973, "Modeling the Effects of Gaseous and Particulate Pollutants in the Urban Atmosphere. Part I: Thermal Structure," J. Appl. Meteor. 12, 901-912.

Bergstrom, R. W., and Viskanta, R.: 1973, "Spherical Harmonics Approximation for Radiative Transfer in Polluted Atmospheres," presented at the AIAA 8th Thermophysics Conference, July 16-18, Palm Springs, California.

Blackadar, A. K.: 1962, "The Vertical Distribution of Wind and Turbulent Exchange in a Neutral Atmosphere," J. Geophys. Res. 67, 3095-3102.

Bornstein, R. D.: 1968, "Observations of the Urban Heat Island Effect in New York City," J. Appl. Meteor. 7, 575-582.

Bornstein, R. D.: 1972, "Two-dimensional Non-steady Numerical Simulations of Nighttime Flow of a Stable Planetary Boundary Layer over a Rough Warm City," Ph.D. Thesis presented to New York University, School of Engineering and Science

Bowne, N. E., and Ball, J. T.: 1970, "Observational Comparison of Rural and Urban Boundary Layer Turbulence," J. Appl. Meteorol. 9, 862-873.

Businger, J. A., Wyngaard, J. C., Izumi, Y., and Bradley, E. F.: 1971, "Flux-profile Relationships in the Atmospheric Surface Layer," J. Atmos. Sci. 28, 181-189.

Businger, J. A.: 1972, "Turbulent Transfer in the Atmospheric Surface Layer," Workshop in Micrometeorology, D. A. Haugen, Ed., American Meteorological Society, Boston, pp. 67-100.

Businger, J. A., and Arya, S. P.: 1974, "Height of the Mixed Layer in the Stably Stratified Planetary Boundary Layer," Advances in Geophysics, Volume 18A, F. N. Frenkiel and R. E. Munn, Eds., Academic Press, New York, pp. 73-109.

Brooks, D. L.: 1950, "A Tabular Method for the Computation of Temperature Change by Infrared Radiation in the Free Atmosphere," J. Meteor. 7, 313-321.

Bray, J. R., Sanger, J. E., and Archer, A. L.: 1966, "The Visible Albedo of Surfaces in Central Minnesota," Ecology 47, 524-531.

Breslau, N., and Dave, J. V.: 1973, "Effect of Aerosols on the Transfer of Solar Energy through Realistic Model Atmospheres, Parts I and II," J. Appl. Meteor. 12, 601-619.

Canosa, J., and Penafiel, H. R.: 1973, "A Direct Solution of the Radiative Transfer Equation. Application to Rayleigh and Mie Atmospheres," J. Quant. Spectros. Radiat. Transfer 13, 21-39.

Carson, D. J.: 1973, "The Development of a Dry Inversion-capped Convectively Unstable Boundary Layer," Quart. J. Roy. Meteorol. Soc. 99, 450-467.

Cebeci, T., and Smith, A. M. O.: 1974, Analysis of Turbulent Boundary Layers, Academic Press, New York, 404 pp.

Cess, R. D., and Tiwari, S. N.: 1972, "Infrared Radiative Energy Transfer in Gases," in Advances in Heat Transfer, J. P. Hartnett and T. F. Irvine, Eds., Academic Press, New York, 229-283.

Chan, S. H., and Tien, C. L.: 1969, "Total Band Absorptance of Non-Isothermal Infrared Radiating Gases," J. Quant. Spectrosc. Radiat. Transfer 9, 1261-1271.

Chan, S. H., and Tien, C. L.: 1971, "Infrared Radiation Properties of Sulfur Dioxide," J. Heat Transfer 93, 172-178.

Chandler, T. J.: 1961, "Surface Effects of Leicester's Heat-Island," E. Midland Geographer 15, 32.

Chandler, T. J.: 1962, "London's Urban Climate," Geog. J. 127, 279-302.

Chandler, T. J.: 1965, The Climate of London, London, Hutchinson and Co., 292 pp.

Chandrasekhar, S.: 1960, Radiative Transfer, Dover Publications, Inc., New York, 393 pp.

Chu, C. M., and Churchill, S. W.: 1955, "Numerical Solution of Problems in Multiple Scattering of Electromagnetic Radiation," J. Phys. Chem. 59, 855-863.

Clarke, J. F.: 1969, "Nocturnal Urban Boundary Layer over Cincinnati, Ohio, Mo. Wea. Rev. 97, 582-589.

Clarke, J. F., and McElroy, J. L.: 1974, "Effects of Ambient Meteorology and Urban Morphological Features on the Vertical Temperature Structure over Cities," Presented at APCA Annual Meeting, Denver, Colorado.

Clarke, R. H., Dyer, A. J., Brook, R. R., Reid, D. G., and Troup, A. J.: 1971, The Wangara Experiment, Boundary Layer Data. Tech. Paper No. 19, Div. Meteor. Phys., CSIRO, Australia.

Coakley, J. A. Jr., and Chylek, P.: 1975, "The Two-Stream Approximation in Radiative Transfer: Including the Angle of the Incident Radiation," J. Atmos. Sci. 32, 409-418.

Cole, H. S., and Lyons, W. A.: 1972, "The Impact of the Great Lakes on the Air Quality of Urban Shoreline Areas," Proc. 15th Conf. Great Lakes Research, Internat. Assoc. Greak Lakes Res., 436-463.

Craig, C. D. and Lowry, W. P.: 1972, "Reflections on the Urban Albedo," Conference on the Urban Environment and Second Conference on Biometeorology, Philadelphia, October 31-November 2, 159-164.

Deardorff, J. W.: 1967, "Empirical Dependence of the Eddy Coefficient for Heat upon Stability above the Lowest 50 m," J. Appl. Meteorol. 6, 631-643.

Deardorff, J. W.: 1972a, "Numerical Investigation of Neutral and Unstable Planetary Boundary Layers," J. Atmos. Sic. 29, 91-115.

Deardorff, J. W.: 1972b, "Parameterization of the Planetary Boundary Layer for Use in General Circulation Models," Mon. Wea. Rev. 100, 93-106.

Deardorff, J. W.: 1974, "Three-dimensional Numerical Modeling of the Planetary Boundary Layer," Workshop in Micrometeorology, D. A. Haugen, Ed., American Meteorological Society, Boston, pp. 271-309.

Deardorff, J. W.: 1974a, "Three-Dimensional Numerical Study of the Height and Mean Structure of a Heated Planetary Boundary Layer," Boundary-Layer Meteorol. 7, 81-106.

Deardorff, J. W.: 1974b, "Three Dimensional Numerical Study of Turbulence in an Entraining Mixed Layer," Boundary Layer Meteorol. 7, 199-226.

Delage, Y.: 1974, "A Numerical Study of the Nocturnal Atmospheric Boundary Layer," Quart. J. R. Met. Soc. 90, 136-146.

Donaldson, C. duP.: 1973, "Construction of a Dynamic Model of the Production of Atmospheric Turbulence and the Dispersal of Atmospheric Pollutants," Workshop in Micrometeorology, D. A. Haugen, Ed., American Meteorological Society, Boston, pp. 313-390.

Duckworth, F. A., and Sandberg, J. S.: 1954, "The Effect on Cities upon Horizontal and Vertical Temperature Gradients," Bull. Amer. Meteor. Soc. 35, 198-207.

Eagleson, P. S.: 1970, Dynamic Hydrology, McGraw-Hill Book Co., Inc., New York.

Edwards, D. K., and Menard, W. A.: 1964a, "Comparison of Models for Correlation of Total Band Absorption," Appl. Opt. 3, 621-625.

Edwards, D. K., and Menard, W. A.: 1964b, "Correlations for Absorption by Methane and Carbon Dioxide Gases," Appl. Opt. 3, 847-852.

Edwards, D. K., Glassen, L. K., Hauser, W. C., and Tuchscher, J. S.: 1966, "Radiation Heat Transfer in Nonisothermal Nongray Gases," ASME Paper No. 66-WA/HT-25.

Edwards, D. K., and Morizumi, S. J.: 1970, "Scaling of Vibration-Rotation Band Parameters for Nonhomogeneous Gas Radiation," J. Quant. Spectrosc. Radiat. Transfer 10, 175-188.

Edinger, J. G.: 1973, "Vertical Distribution of Photochemical Smog in the Los Angeles Basin," Environ. Sci. Tech 1, 247-252.

Elliott, W. P., and Stevens, D. W.: 1961, "A Numerical Method for Computing Radiative Temperature Changes near the Earth's Surface," GRD Res. Note, No. 69, L. G. Hanscom Field, Bedford, Mass., 21 pp.

Elliott, W. P.: 1964, "The Height Variation of Vertical Heat Flux Near the Ground," Quart. J. Roy. Meteor. Soc. 90, 260-265.

Ensor, D. S., Porch, W. M., Pilat, J. J., and Charlson, R. J.: 1971, "Influence of the Atmospheric Aerosol on Albedo, J. Appl. Meteor. 10, 1303-1306.

Estoque, M. A.: 1963, "A Numerical Model of the Atmospheric Boundary Layer," J. Geophys. Res. 68, 1103-1113.

Estoque, M. A., and Bhumralkar, C. N.: 1969, "Flow over a Localized Heat Source," Mon. Wea. Rev. 97, 850-859.

Estoque, M. A.: 1972, "Numerical Modeling of the Planetary Boundary Layer," Workshop in Micrometeorology, D. A. Haugen, Ed., American Meteorological Society, Boston, pp. 217-270.

Fedyayevskiy, K. K.: 1936, Trudy Ts AGI, Nos. 282 and 316.

Fox, D. G., and Lilly, D. K.: 1972, "Numerical Simulation of Turbulent Flows," Reviews of Geophysics and Space Phsyics, 10, 51-72.

France, W. L., and Williams, D.: 1966, "Total Absorptance of Ammonia in the Infrared," J. Opt. Soc. Am. 56, 70-74.

Fuggle, R. F., and Oke, T. R.: 1968, "Infrared Flux Divergence and the Urban Heat Island," Presented at W. M. O. Symposium on Urban Climates and Building Climatology, Brussels, Belgium.

Goody, R. M.: 1964, Atmospheric Radiation: I, Theoretical Basis, Oxford University Press, 436 pp.

Goody, R. M., and Belton, M. J. S.: 1967, "Radiative Relaxation Times for Mars," Planet. Space Sci. 15, 247-256.

Hansen, J. E., and Pollack, J. B.: 1970, "Near-infrared Light Scattering by Terrestrial Clouds," J. Atmos. Sci. 27, 265-281.

Halstead, M. R., Richman, R., Covey, W., and Merrman, J.: 1957, "A Preliminary Report on the Design of a Computer for Micrometeorology," J. Meteor. 14, 308-325.

Herman, B. M., Browning, S. R., and Curran, R. J.: 1971, "The Effect of Atmospheric Aerosols on Scattered Sunlight," J. Atmos. Sci. 28, 419-428.

Howard, L.: 1833, The Climate of London Deduced from Meteorological Observations Made in the Metropolis and at Various Places around it, 2nd Ed., 3 vols., J. and A. Arch, London.

I.A.M.A.P., Radiation Commission: 1974, "Standard Procedures to Compute Atmospheric Radiative Transfer in a Scattering Atmosphere."

Jurica, G. M.: 1970, "Radiative Flux Densities and Heating Rates in the Atmosphere using Pressure-and-Temperature-Dependent Emissivities," Ph.D. Thesis, Physics, Meteorology, University of Arizona, 192 pp.

Kaimal, J. C., Wyngaard, J. C., Haugen, D. A., Izumi, Y., Cote, O. R., and Caughey, S. J.: 1975, "Turbulence Structure in a Convective Boundary Layer," to be submitted for publication.

Kalmykov, V. G., Sherstyuk, A. N., and Shulgina, T. V.: 1975, "The Mixing Length in a Wall Boundary Layer," Fluid Mechanics, Soviet Research 4, 66-69.

Kondratyev, K. Ya.: 1969, Radiation in the Atmosphere, Academic Press, New York.

Kondratyev, K. Ya.: 1972, "Radiation Processes in the Atmosphere," World Meteorological Organization Publication No. 209, Geneva.

Kondratyev, K. Ya.: 1973, "The Complete Atmospheric Energetics Experiment," Global Atmospheric Research Program (GAPP), GARP Publications Series No. 12, ICSU-WMO, Geneva.

Kondratyev, K. Ya., Vassilyev, O. B., Grishechkin, and Ivlev, L. S.: 1974, "Spectral Radiative Flux Divergence and Its Variability in the Troposphere in the 0.4-2.4-μ Region, Applied Optics 13, 478-486.

Kratzer, P. A.: 1956, Das Stadtklima Die Wissenshaft, Vol. 90, Braunschwerg, Friedr. Vieweg S Sohn, 184 pp.

Kuhn, P. M.: 1963, "Radiometersonde Observations of Infrared Flux Emissivity of Water Vapour," J. Appl. Meteor. 2, 368.

Lacis, A. A., and Hansen, J. E.: 1974, "A Parameterization for the Absorption of Solar Radiation in the Earth's Atmosphere," J. Atmos. Sci. 31, 118-133.

Lamb, R. G., and Neiburger, M.: 1970, "Mathematical Model of the Diffusion and Reactions of Pollutants Emitted over an Urban Area," Project Clean Air Research Reports 4, University of California, Los Angeles.

Landsberg, H. E.: 1970, "Man-made Climate Changes," Science 170, 1265-1274.

Launder, B. E., and Spalding, D. B.: 1972, Lectures in Mathematical Models of Turbulence, Academic Press, London and New York.

Leahey, D. M., and Friend, J. P.: 1971, "A Model for Predicting the Depth of the Mixed Layer over an Urban Heat Island with Applications to New York City," J. Appl. Meteor. 10, 1162-1173.

Leckner, B.: 1972, "Spectral and Total Emissivity of Water Vapor and Carbon Dioxide," Combustion and Flame 19, 33-48.

Lee, R. L., and Olfe, D. B.: 1974, "Numerical Calculations of Temperature Profiles over an Urban Heat Island," Boundary Layer Meteorology 7, 39-52.

Lenschow, D. H.: 1974, "Model of the Heihgt Variation of the Turbulence Kinetic Energy Budget in the Unstable Planetary Boundary Layer," J. Atmos. Sci. 31, 465-474.

Lettau, H. H., and Davidson, B.: 1957, Exploring the Atmosphere's First Mile, Vol. 2, New York, Pergamon Press, 201 pp.

Lettau, H. H.: 1962, "Theoretical Wind Spirals in the Boundary Layer of a Barotropic Atmosphere," Beitr. Phys. Atmos. 35, 195-212.

Lettau, H. H., and Dabberdt, W. F.: 1970, "Variangular Wind Spirals," Boundary Layer Meteor. 1, 64-79.

Lilly, D. K.: 1965, "On the Computational Stability of Numerical Solutions of Time-Dependent Non-Linear Geophysical Fluid Dynamics Problems," Mon. Wea. Rev. 93, 11-26.

Ludwig, C. B., Bartle, R., and Griggs, M.: 1969, "Study of Air Pollutant Detection by Remote Sensors," NASA Contractor Report, No. CR-1380.

Ludwig, F. L.: 1970, "Urban Air Temperatures and Their Relation to Extra-urban Meteorological Measurements, Amer. Soc. Heat. Refrig. Air-Condit. Engin., Document SF-70-9, 40-45.

Lumley, J. L., and Panofsky, H. A.: 1964, The Structure of Atmospheric Turbulence, Interscience Publishers, New York, 239 pp.

Lumley, J. L., and Khauch-Nouri, B.: 1974, "Computational Modeling of Turbulent Transport," Advances in Geophysics, Volume 18A, F. N. Frankiel and R. E. Munn, Eds., Academic Press, New York, pp. 169-192.

Lykosov, V. N.: 1972, "Unsteady State in the Planetary Boundary Layer of the Atmosphere," Izv. Atmos. Ocean. Phys. 8, 85-91.

Manabe, S.: 1969, "Climate and the Ocean Circulation, I. The Atmospheric Circulation and the Hydrology of the Earth's Surface," Monthly Weather Rev. 97, 739-805.

Marchuk, G. I.: 1965, "A Theoretical Weather-Forecasting Model," Doklady of the Academy of the Sciences of the U.S.S.R. 55, 10-12.

McCormick, R. A., and Ludwig, J. H.: 1967, "Climate Modification by Atmospheric Aerosols," Science 156, 1358-1359.

McClatchey, R. A., Fenn, R. W., Selby, J. E. A., Volz, F. E., and Garing, J. S.: 1972, Optical Properties of the Atmosphere, Third Edition, AFCRL-72-0497, Environmental Research Papers, No. 411, 108 pp.

McElroy, J. L.: 1971, "An Experimental and Numerical Investigation of the Nocturnal Heat Island over Columbus, Ohio," Ph.D. Thesis, Dept. of Met., Pennsylvania State University.

McPherson, R. D.: 1968, "A Three-dimensional Numerical Study of the Texas Coast Sea Breeze," Ph.D. Thesis, The University of Texas, Austin, Texas.

Mellor, G. L., and Herring, H. J.: 1973, "A Survey of Mean Turbulent Field Closure Models," AIAA J. 11, 590-599.

Mellor, G. L., and Yamada, T.: 1974, "A Hierarchy of Turbulence Closure Models for Planetary Boundary Layers," Submitted for publication.

Melgarego, J. W., and Deardorff, J. W.: 1974, "Stability Functions for the Boundary-Layer Resistance Laws Based upon Boundary-Layer Heights," J. Atmos. Sci. 31, 1324-1333.

Mitchell, J. M., Jr.: 1961, "The Temperatures of Cities," Weatherwise 14, 224-229.

Mitchell, J. M., Jr.: 1971, "The Effect of Atmospheric Aerosols on Climate with Special References to Temperature Near the Earth's Surface," J. Appl. Meteor. 10, 703-714.

Monin, A. S. and Yaglom, A. M.: 1971, Statistical Fluid Mechanics: Mechanics of Turbulence, Vol. 1, The M.I.T. Press, Cambridge, Mass., 769 pp.

Munn, R. E., and Stewart, I. M.: 1967, "The Use of Meteorological Towers in Urban Air Pollution Programs, J. Air Pollution Control Assoc. 17, 98-101.

Myrup, L. O.: 1969, "A Numerical Model of the Urban Heat Island," J. Appl. Met. 8, 908-918.

Nappo, C. J. Jr.: 1972, "A Numerical Study of the Urban Heat Island," Conference on Urban Environment and Second Conference on Biometeorology, American Meteorological Society, Oct. 31-Nov. 2, Philadelphia, Pennsylvania.

O'Brien, J.: 1970, "On the Vertical Structure of the Eddy Exchange Coefficient in the Planetary Boundary Layer," J. Atmos. Sci. 27, 1213-1215.

Ohmstede, W. D., and Appleby, J. F.: 1964, "Numerical Solution of the Distribution of Wind and Turbulence in the Planetary Boundary Layer," Meteor. Res. Note No. 8, DA Task 1-A-0-11001-B-021-08 USAAERDAAMET-5-64, 43 pp.

Olfe, D. B., and Lee, R. L.: 1971, "Linearized Calculations of Urban Heat Island Convection Effects," J. Atmos. Sci. 28, 1374-1388.

Oke, T. R., and East, C.: 1971, "The Urban Boundary Layer in Montreal," Boundary Layer Meteor. 1, 411-437.

Oke, T. K.: 1972, "City Size and the Urban Heat Island," Conference on Urban Environment and Second Conference on Biometeorology, American Meteorological Society, Oct. 31-Nov. 2, Philadelphia, Pennsylvania.

Oke, T. K.: 1972, "City Size and the Urban Heat Island," Conf. Urban Environment, Philadelphia, Pa., November 1972, 144-146.

Oke, T. R., and Fuggle, R. F.: 1972, "Comparison of Urban/Rural Counter and Net Radiation at Night," Boundary Layer Meteorology 2, 290-308.

Oke, T. R., and Maxwell, G. B.: 1975, "Urban Heat Island Dynamics in Montreal and Vancouver," Atmospheric Environment 9, 191-200.

Oke, T. R.: 1973, "City Size and the Urban Heat Island," Atmospheric Environment 7, 769-779.

Oke, T. R.: 1975, "A Review of Urban Climatology, 1968-1972," Report Department of Geography, University of British Columbia.

Orszag, S. A., and Patterson, Jr., G. S.: 1972, "Numerical Simulation of Turbulence," in Lecture Notes in Physics, 12, Statistical Models and Turbulence (Springer-Verlag, New York), pp. 127-147.

Orlanski, I., Ross, B. B., and Polinsky, L. J.: 1974, "Diurnal Variation of the Planetary Boundary Layer in a Mesoscale Model," J. Atmos. Sci. 31, 965-989.

Paily, P. P., Macagno, E. O., and Kennedy, J. F.: 1974, Winter-Regime Surface Heat Loss from Heated Streams, IIHR Report No. 155, Institute of Hydraulic Research, The University of Iowa, 137 pp.

Pandolfo, J. P.: 1966, "Wind and Temperature Profiles for Constant-Flux Boundary Layers in Lapse Conditions with a Variable Eddy Conductivity to Eddy Viscosity Ratio," J. Atmos. Sci. 23, 495

Pandolfo, J. P., Atwater, M. A., and Anderson, G. E.: 1971, "Prediction of Numerical Models of Transport and Diffusion in an Urban Boundary Layer," Sponspor Contract No. CPA 70-62, CEM Contract No. 4082, The Center for Environment of Man, Inc., Hartford, Conn.

Pandolfo, J. P.: 1971, "Numerical Experiments with Alternative Boundary Layer Formulations using Bomex Data," Boundary Layer Meteor. 1, 277-289.

Penner, S. S.: 1959, *Quantitative Molecular Spectroscopy and Gas Emissivities*, Addison-Wesley, Massachusetts, 587 pp.

Peterson, C. M., Paulus, H. J., and Foley, G. H.: 1969, "The Number-Size Distribution of Atmospheric Particles During Temperature Inversions," Journal of the Air Pollution Control Association 19, 795-801.

Peterson, J. T.: 1969, *The Climate of Cities: A Survey of Recent Literature*, National Air Pollution Control Administration Publication No. AP-59, 48 pp.

Pitts, E.: 1954, "The Application of Radiative Transfer Theory to Scattering Effects in Unexposed Photographic Emulsions," Proc. Phys. Soc. 67, 105-119.

Philip, J. R.: 1957, "Evaporation, and Moisture and Heat Field in the Soil," J. Meteor. 14, 354-366.

Potter, J. F.: 1970, "The Delta Function Approximation in Radiative Transfer Theory," J. Atmos. Sci. 27, 943-949.

Rasool, S. I., and Schneider, S. H.: 1971, "Atmospheric Carbon Dioxide and Aerosols: Effects of Large Increases on Global Climate," Science 173, 138-141.

Reck, R. A.: 1974, "Influence of Surface Albedo on the Changes in the Atmospheric Radiation Balance Due to Aerosols," Atmospheric Environment 8, 823-833.

Reynolds, W. C.: 1974b, "Computation of Turbulent Flows," AIAA paper, No. 74-556.

Reynolds, W. C.: 1974a, "Recent Advances in the Computation of Turbulent Flows," Advances in Chemical Engineering, Vol. 9, T. B. Drew, et al., Eds., Academic Press, New York, 193-246.

Roache, P. J.: 1972, Computational Fluid Dynamics, Hermosa Publishers, Albuquerque, N. M., 434 pp.

Roberts, P. J. W., Roth, P. M., and Nelson, C. L.: 1971, "Development of a Simulation Model for Estimating Ground Level Concentrations of Photochemical Pollutants," Report 7 SAI-6, Systems Applications, Inc., Beverly Hills, California 90212

Rodgers, C. D., and Walshaw, C. D.: 1966, "The Computation of Infrared Cooling Rate in Planetary Atmospheres," Quart. J. R. Met. Soc. 92, 67-92.

Rodgers, C. D.: 1966, "The Use of Emissivity in Atmospheric Radiation Calculations," Quart. J. R. Met. Soc. 93, 43-54.

Romanova, L. M.: 1962, "I. The Solution of the Radiative Transfer Equation for the Case when the Indictrix of Scattering Greatly Differs from the Spherical One," Opt. Spek. 13, 429-435.

Rosenberg von, D. U.: 1969, Methods for the Numerical Solutions of Partial Differential Equations, American Elsevier Publishing Co., Inc., New York.

Rossby, C. G., and Montgomery, R. B.: 1935, "The Layer of Frictional Influence in Wind and Ocean Currents," M.I.T. papers, No. 3, 101 pp.

Rouse, W. R., Noad, D., and McCutcheon, J.: 1973, "Radiation, Temperature and Atmospheric Emissivities in a Polluted Urban Atmosphere at Hamilton, Ontario," J. Appl. Meteorol. 12, 798-807.

Russell, P. B., and Grams, G. W.: 1975, "Application of Soil Dust Optical Properties in Analytical Models of Climate Change," J. Appl. Meteorol. 14, 1037-1043.

Sasamori, T.: 1968, "The Radiative Cooling Calculation for Application to General Circulation Experiments," J. Appl. Meteor. 7, 721-729.

Sasamori, T.: 1970, "A Numerical Study of Atmospheric and Soil Boundary Layers," J. ATmos. Sci. 27, 1122-1137.

Sagan, C., and Pollack, J. B.: 1967, "Anisotropic Non-conservative Scattering and the Clouds of Venus," J. Geophys. Res. 72, 469-477.

Sherstyuk, A. N.: 1969, Reports at Scientific and Technical Conference on the Current Results of Research and Design Work for 1968-1969, MEI Press.

Shekter, F. N.: 1950, "Calculation of Thermal Radiative Fluxes in the Atmosphere," Trudy GGO No. 22, 84-86.

Sheppard, P. A.: 1958, "The Effect of Pollution on Radiation in the Atmosphere," Int'l J. Air Poll. 1, 31-43.

Shir, C. C., and Bornstein, R. D.: 1974, "The Eddy Exchange Coefficients in the Numerical Modeling of the Planetary Boundary Layer: Problems and an Alternative Approach," to be published.

Spalding, D. B.: 1969, "The Prediction of Two-Dimensional Steady Turbulent Flows," Imperial College, Heat Transfer Section Rep. EF/TN/A/16.

Spiegel, E. A., and Veronis, G.: 1960, "On the Boussinesq Approximation for a Compressible Fluid," Astrophys. J. 131, 442-447.

Summers, P. W.: 1966, "The Seasonal Weekly and Daily Cycles of Atmospheric Smoke Content in Central Montreal," J. Air Poll. Contr. Asso. 16, 432-438.

Tag, P. M.: 1969, "Surface Temperatures in an Urban Atmosphere," Part I, Rep 15, NSF Grant GA-3956, The Penna. State Univ.

Taylor, P. A.: 1974, "Urban Meteorological Modeling--Some Relevant Studies," Advances in Geophysics, Volume 18B, F. N. Frankiel and R. E. Munn, Eds., Academic Press, New York, pp. 173-185.

Tien, C. L., and Lowder, J. E.: 1966, "A Correlation for Total Band Absorptance of Radiating Gases," Int. J. Heat Mass Transfer 9, 698-701.

Tien, C. L.: 1968, "Thermal Radiation Properties of Gases," in Advances in Heat Transfer, J. P. Hartnett and T. F. Irvine, Jr., Eds., Academic Press, New York, 253-324.

Tien, C. L.: 1973, "Band and Total Emissivity of Ammonia," Int. J. Heat Mass Transfer 16, 856-857.

Telford, J. W., and Warner, J.: 1964, "Fluxes of Heat and Vapor in the Lower Atmosphere from Aircraft Observations," J. Atmos. Sci. 21, 539-548.

Tennekes, H. and Lumley, J. L.: 1972, A First Course in Turbulence, The M.I.T. Press (Cambridge, Mass.), 300 pp.

Tennekes, H.: 1973, "A Model for the Dynamics of the Inversion Above a Convective Boundary Layer," J. Atmos. Sci. 30, 558-567.

Tennekes, H.: 1974, "The Atmospheric Boundary Layer," Physics Today 27, 52-63.

Tennekes, H., and Ulden, van A. P.: 1974, "Short-Term Forecasts of Temperature and Mixing Height on Sunny Days," Symposium on Atmospheric Diffusion and Air Pollution, Santa Barbara, Calif., 35-40.

Tuvari, S. N.: 1975, "Band Models and Correlations for Infrared Radiation," AIAA Paper, No. 75-699.

Wagner, N. K., and Yu, T.: 1972, "Heat Island Formation: A Numerical Experiment," Preprints of papers presented at Conference on Urban Environment and Second Conference on Biometeorology, 83-88.

Walsh, T. E.: 1969, "Infrared Absorptance of Ammonia--20 to 35 Microns," J. Opt. Soc. Am. 59, 261-267.

Wang, W., and Domoto, G. A.: 1974, "The Radiative Effect of Aerosols in the Earth's Atmosphere," J. Appl. Meteor. 5, 521-534.

Webb, E. K.: 1970, "Profile Relationships: The Log-linear Range, and Extension to Strong Stability," Quart. J. Roy. Meteor. Soc. 96, 67-80.

Wu, S. S.: 1965, "A Study of Heat Transfer Coefficients in the Lowest 400 Meters of the Atmosphere," J. Geophys. Res. 70, 1801-1808.

Wyngaard, J. C., Cote, O. R., and Rao, K. S.: 1974, 'Modeling the Atmospheric Boundary Layer," Advances in Geophysics, Volume 18A, F. N. Frankiel and R. E. Munn, Eds., Academic Press, New York, pp. 193-211.

Viskanta, R.: 1966, "Radiation Transfer and Interaction of Convection with Radiation Heat Transfer," in Advances in Heat Transfer, J. P. Hartnett and I. F. Irvine, Jr., Eds., Academic Press, New York, 176-248.

Viskanta, R., Johnson, R. O., and Bergstrom, Jr., R. W.: 1975, "Effect of Urbanization on the Thermal Structure in the Atmosphere," presented at the Conference on Metropolitan Urban Environment, Syracuse, New York, 25-29 August.

Zdunkowski, W. G., and McQuage, N. D.: 1972, "Short-term Effects of Aerosols on the Layer Near the Ground in a Cloudless Atmosphere," Tellus 3, 237-254.

APPENDIX A

Calculation of Directly Transmitted and Diffuse Solar Radiation at the Top of the Atmospheric Layer

This study utilized a combination of empirical procedures summarized by Paily, et al. (1974) to calculate the direct and diffuse solar fluxes at the top of the atmospheric layer being studied. The method is given below for convenience.

The solar altitude α is the angle in the vertical plane between the sun's rays and the horizontal. The zenith angle μ is the complement of α. Using spherical trigonometry μ can be written as

$$\mu = \cos^{-1} [\sin\phi \sin\delta + \cos\phi \cos\delta \cos h] \quad (A.1)$$

where ϕ is geographic latitude in radians, δ is declination of the sun in radians, and h is local hour-angle of the sun in radians.

An approximate relation to obtain δ is given by

$$\delta = (23.45\ \pi/180) \cos[(2\pi/365)(172 - D)] \quad (A.2)$$

where δ is in radians and D is the number of the day in a year with D = 1 for January 1 and D = 365 for December 31.

The attenuation of solar radiation is represented by three coefficients which are functions of the optical air mass, the moisture content of the atmosphere and the dust content of the atmosphere.

The directly transmitted solar radiation S_t at an arbitrary height in the atmosphere is given by

$$S_t = S_0(a'' - d) \quad (A.3)$$

where S_0 is the solar radiation at the top of atmosphere, a" is the coefficient which accounts for attenuation for scattering and absorption by gases and d is the atmospheric dust depletion coefficient. These coefficients are expressed by the relations

$$a'' = \exp\{m[-(0.465 + 0.130w)][0.179 + 0.421 \exp(0.721\, m)]\} \quad (A.4)$$

and

$$d = 1 - 0.99^{m} \quad (A.5)$$

The optical air mass m is given by the following equations:

$$m = m_o(p_a/p_o) \quad (A.6a)$$

$$m_o = [\cos\mu + a(\alpha + b)^{-c}]^{-1} \quad (A.6b)$$

where m_o is the optical air mass at sea level where the barometric pressure is p_o, μ is the zenith angle, and p_a is the barometric pressure at the altitude at which the solar fluxes are being computed. The constants a, b, and c have the values:

$$a = 0.15 \quad (A.7a)$$

$$b = 3.885 \quad (A.7b)$$

$$c = 1.253 \quad (A.7c)$$

The term w in Eq. (A.4) is the precipitable water vapor content in cm above the altitude at which solar fluxes are being computed.

Assuming that half of the scattered radiation reaches the altitude being considered, the diffuse solar radiation S_d can be written as

$$S_d = S_o[0.5(1 - a') + 0.5d] \quad (A.8)$$

where a' is a coefficient which accounts for attenuation by scattering only and is given by

$$a' = \exp\{m[-(0.465 + 0.134w)][0.129 + 0.171 \exp(0.880m)]\} \quad (A.9)$$